A Two-Stage Runoff Detention Model for a Green Roof

Gianni Michael Vesuviano

A thesis submitted in part fulfilment of the requirements for the

degree of Doctor of Philosophy in Civil Engineering

Department of Civil and Structural Engineering

February 2014

Declaration

I declare that no portion of the work contained in this thesis has been submitted in support of an application for another degree or qualification of this or any other university or other institute of learning. The work has been my own except where indicated. All quotations have been distinguished by quotation marks and the sources acknowledged.

Abstract

Urbanization has caused an increase in per-event stormwater runoff volumes. Existing combined sewer systems are becoming less able to take in storm runoff without overflowing, which may cause flooding and water quality issues. Sustainable drainage systems (SUDS) are structures and practices intended to reduce the volume and rate of a site's runoff to pre-development levels. Green roofs, not requiring exclusive land use, can be easily integrated into dense urban areas. However, their hydrological behaviour requires further understanding.

A generic tool was created for routing detained rainwater through separately-modelled substrate and drainage layer components of a green roof. Components were monitored in isolation, in purpose-built rainfall simulators, under laboratory conditions. Configuration variables (e.g. roof slope) were varied and their effects on runoff response assessed. Nonlinear storage routing methods were used to fit modelled to monitored runoff profiles, by optimizing routing parameters. The sensitivity of these parameters to test variables was assessed, greatly reducing the number of individual values required for modelling either layer.

The runoff response of a two-layered green roof system at field capacity was tested under laboratory conditions. The substrate model, in series with the drainage layer model, was parameterized for the two-layered system, and time-series runoff predictions and observations were compared. The model produced consistently accurate results. This model was re-parameterized for three monitored test beds in Sheffield, UK, using estimated parameter values for the three untested system configurations. The model was found to be fit for purpose, approaching laboratory accuracy in the best cases. Peak flow predictions were improved by allowing limited runoff to occur before a roof's water content completely reached field capacity. Further work should extend the model's applicability to long time-series, through improved evapotranspiration modelling. Further laboratory observations of individual roof components are desirable, to increase the range of modellable green roof configurations.

Table of Contents

List of Figures

List of Tables

List of Abbreviations

ADWP	Antecedent Dry Weather Period
ANOVA	Analysis of Variance
ASCE	American Society of Civil Engineers
BBC	British Broadcasting Corporation
BMP	Best Management Practices
BS	British Standard

BSI	British Standards Institution
CEH	Centre for Ecology and Hydrology
CIRIA	Construction Industry Resources and Information Association
CSO	Combined Sewer Overflow
DEFRA	Department for the Environment, Food and Rural Affairs
DIN	Deutsches Institut für Normung
EN	European Standard
FBB	Fachvereinigung Bauwerksbegrünung e.V.
FLL	Forschungsgesellschaft Landschaftsentwicklung Landschaftsbau
HDPE	High-Density Polyethylene
IGRA	International Green Roof Association
ISO	International Organization for Standardization
LECA	Light Expanded Clay Aggregate
LID	Low-Impact Development
LSD	(Fisher's) Least Significant Difference
MCS	Marie Curie Substrate
MWHC	Maximum Water Holding Capacity (Field Capacity)
NERC	Natural Environment Research Council
NSE	Nash-Sutcliffe Efficiency
SUDS/SuDS	Sustainable Drainage Systems or Sustainable Urban Drainage Systems
SWMM	Storm Water Management Model
USEPA	United States Environmental Protection Agency
WaPUG	Wastewater Planning Users Group

List of Symbols

A	Drainage/catchment area (context-sensitive)
a	Scale parameter (nonlinear storage routing)
b	Exponent parameter (nonlinear storage routing)
BP	Breakpoint (modified full green roof model)
CU	Christiansen's coefficient of uniformity
d	Pipe diameter
$delay$	Monitoring time delay parameter (all storage routing methods)
E	Evaporation depth
e	Evaporation depth per time-step
F	Cumulative infiltration depth
f	Infiltration rate
g	Gravitational acceleration (9.807 ms^{-2})
H	Total head

h	Water flow depth
I	Inflow rate (equivalent to rainfall rate in substrate model)
K	Travel time (Muskingum routing)
K	Hydraulic conductivity
K_R	Relative hydraulic conductivity
K_S	Saturated hydraulic conductivity
K_U	Unsaturated hydraulic conductivity
L	Drainage length
L	Substrate depth
l	Pore connectivity
N	Length of sewer in feet per foot of drop (Hawksley's formula)
n	Roughness coefficient (Manning's equation)
n	Pore-size distribution index (Hydrus-1D)
PS	Pump speed
Q	Outflow rate (equivalent to runoff rate in drainage layer model)
R^2	Pearson's coefficient of determination
R_t^2	Young's coefficient of determination
S	Storage depth (all storage routing methods)
S_f	Friction slope
S_o	Channel bed slope
S_P	Prism storage (Muskingum routing)
S_R	Roof slope
S_W	Wedge storage (Muskingum routing)
t	Time
t_{50}	Cumulative median-to-median delay
U	Unit hydrograph
U_i	Ordinate i of unit hydrograph
u	Velocity in horizontal direction
W	Width of routing surface
x	Distance in horizontal direction
x	Weighting coefficient (Muskingum routing)
z	Distance in vertical direction
α	Inverse of air-entry value (Hydrus-1D)
θ	Water content of porous medium
θ_{Field}	Field capacity
θ_R	Residual water content
θ_S	Saturated water content
ψ	Wetting front soil suction head

1   Introduction

1.1   Background

Urbanization has resulted in the covering of permeable land, which can absorb water, with impermeable surfaces, which cannot. Traditional drainage systems have attempted to divert excess rainwater away from urban areas as quickly as possible. However, as urban areas increase in size and population, old sewer systems are becoming less able to perform this task successfully. Consequently, many sewer systems in the UK become overwhelmed during large storm events, failing to accept and transport urban runoff at the same rate at which it is created. As many old sewers carry wastewater in combination with rainwater, combined sewer overflows occur, in which the excess volume is spilled from the sewer system directly into a natural body of water, without treatment. There are an estimated 20,000 combined sewer overflow outlets in the UK, which not only release untreated waste water and urban runoff into rivers, lakes and the ocean, but also provide entrance points for disease to spread via the sewer network. The ecological and public health implications of this are significant.

Sustainable drainage systems (SUDS), whose main principles are also referred to low-impact development (LID) or best management practices (BMPs) in the USA and Canada, aim to reduce the quantity of urban runoff while improving its quality and providing amenity value in an integrated approach. This is in contrast to conventional piped drainage systems, which are mostly concerned with limiting the quantity of urban runoff, while improving quality through treatment in large centralized structures, and only considering amenity value indirectly, if at all. SUDS attempt to mimic natural drainage by: encouraging infiltration to the ground, which reduces the volume of surface runoff from a site; storing water temporarily, which limits the rate of surface runoff; and conveying water slowly, which further limits the rate of surface runoff and allows suspended solids to settle. The objective of many SUDS is to reduce a site's runoff rate and volume to its pre-development levels under a design storm of a given duration and return period. Consequently, in the event that runoff from a site drained by a SUD system enters a combined sewer system off-site, the use of SUDS on-site greatly reduces the storm loading on the combined sewer system, reducing the severity of storm-induced combined sewer overflows or potentially avoiding them altogether. SUDS aim to keep as much surface runoff above ground as possible. This eliminates the concern associated with the spread of disease through underground sewer networks and allows many SUDS components to act as habitats or public amenities.

SUDS are currently required for most new developments in Scotland, and will be required for most new developments in England and Wales from April 2014. Developers will always be aiming for the highest possible returns on their investments, and so will probably aim to reduce the land area given to SUDS in most developments, preferring instead to maximize saleable or

rentable floor area. This will be especially likely in city centres, where land is most expensive. However, this is exactly where SUDS are most required, due to the prevalence of combined sewer systems and the high density of connections to the sewer system.

Green roofs are increasingly viewed as a device to be deployed within the context of sustainable drainage systems, acting to reduce the instance and severity of pluvial flooding in urban areas. Green roofs retain and detain (delay) the runoff of rainwater in situations where conventional roofs would not, reducing the volume and rate of water entering local sewer systems. They also provide many other benefits, such as sorption of airborne particles, reduction of the urban heat island effect and habitat provision. To developers, the obvious attraction of green roofs over other SUDS devices is that green roofs are installed on the roofs of buildings, normally otherwise unusable pieces of land that always exist, regardless of how many usable floors are underneath. In the event that building owners in the UK may be charged in future for their contribution to urban runoff (as is already the case in some countries and municipalities), green roofs may also become financially attractive as retrofit projects to existing buildings. However, to date, uptake of green roofs in the UK has been slow outside of London and Sheffield. This may be related to perceived construction difficulties (e.g. root damage to the structure and the consequences of failed waterproofing), a lack of national standards, a current lack of incentive, a limited supply of existing UK projects on which to base new-development green roofs, and a lack of general understanding of the hydrological behaviour of green roofs and how they should be modelled in urban drainage systems.

The hydrological behaviour of a green roof in response to a rainfall event may be separated into two elements. Retention refers to the deficit between roof runoff and incident rainfall, as a result of water storage in the system. Capacity for retention is increased between storms by the evapotranspiration of held water, but is ultimately finite. Detention refers to the attenuative effects, caused by routing of water through the green roof system, that result in a reduced peak rate of runoff relative to rainfall and a lag time between a depth of rainfall landing on the roof and the same depth emerging as runoff. This thesis specifically focuses on modelling the detention effect; the retention effect is the subject of parallel research, conducted by others.

1.2 Aims and Objectives

The overall aim of this thesis is to improve the understanding of how green roofs function in a rainfall event and to propose a model for that behaviour. This will improve the confidence with which green roof runoff response can be predicted in drainage design, and ultimately should assist in the uptake of green roofs in construction. Specifically, the main objective of this thesis is to observe, characterize and model the effect of runoff detention in a roof at field capacity. The runoff detention model is intended to be generically applicable to as many existing and proposed

green roof system designs as is possible. This is achieved by proposing separate and generic hydrological sub-models for two main components that contribute to detention in a green roof – the substrate layer and the drainage layer. The selected models produce time-series runoff curves, which are of use to drainage engineers attempting to model green roofs as part of a catchment-scale drainage network. By calibrating and verifying the substrate and drainage layer models separately, and testing the effects of controlled variations in component configuration on runoff response, a range of green roof system designs may be modelled.

In summary, the detailed methodology of the research will be to:

- Conduct a review of available literature and existing research to identify suitable modelling methods for the time-series runoff of water from a green roof drainage layer and a green roof substrate, separately.

- Devise and conduct an experimental programme to test the effects, with respect to runoff detention, of controlled variations in the configuration of drainage layers (e.g. by varying roof slope) and substrates (e.g. by varying substrate depth), separately.

- Parameterize the chosen modelling methods to best fit the experimentally-derived results.

- Analyze the statistical significance of each major test variable and genericize the modelling parameter values as far as is justified and useful.

- Combine the drainage layer and substrate models in series, and use model parameter values determined from previous testing of individual roof layers to evaluate the applicability of this combined two-stage model in predicting the runoff response of two-layered green roof test installations.

A timeline of work completed and outputs published/disseminated is presented at the end of Chapter 1.

1.3   Thesis Structure and Content

This thesis contains eight chapters and three appendices. Chapter 1 contains a brief background on what problem justifies the undertaking of the work contained within this thesis and what purpose this work serves.

Chapter 2 contains a literature review, briefly covering the history of urban drainage up to the conventional combined systems still common throughout the urbanized world. Sustainable drainage systems (SUDS), and their advantages over conventional systems, are presented. Green roofs, and their history, benefits and design are introduced, along with city, region and country-

level policy encouraging their uptake in sustainable development. Two of the main sub-components of a typical modern green roof (substrate layer and drainage layer) are considered individually, for their design, function and any existing research devoted specifically to them. Hydrological modelling methods are categorized according to their potential to model the processes occurring within each layer, and evaluated for their suitability and practicality.

Chapter 3 contains a study of the performance of a monitored small-scale green roof test bed located in Sheffield, UK. The performance of this test bed is compared to other long-term monitoring studies at multiple temporal scales. Storms with high return period are identified and an attempt is made to model various performance metrics as functions of storm, weather and climatic characteristics, using simple and multiple linear regression analysis. The high level of inconsistency between monitored and modelled performance gives a strong indication that no parametric regression method has adequate predictive capability. This chapter provides further justification for the development of a process-based modelling method.

Chapter 4 explains the experimental setup for the experimental programmes related to each of the two stages of the green roof model. This consists of a description of all equipment used during the experimental programme, calibration procedures, modifications made and the test programmes to be conducted.

Chapters 5 and 6 contain the results and discussion relating to the experimental programme concerning the drainage layer (with and without underlying protection mat) and substrate layer of a green roof, respectively. Both chapters follow a similar structure. An overview of detention performance is given, followed by a comparison of the selected hydrological models' ability to accurately generate time-series runoff profiles for the tested components and configurations. The parameterization of the successful modelling methods is simplified and genericized in stages, by removing dependence on statistically insignificant configuration variables. The corresponding loss of accuracy at each stage is evaluated to find an optimal trade-off point between accuracy and general applicability.

Chapter 7 combines the most suitable modelling method for the substrate in series with the most suitable modelling method for the drainage layer, and validates this two-stage model against a test system consisting of a substrate layer, particle filter, drainage layer and protection mat. The modelled runoff profiles are compared to monitored runoff profiles for goodness-of-fit. This validation is extended to time-series rainfall-runoff profiles recorded from three unplanted, monitored test beds located in Sheffield, UK.

Chapter 8 contains the main conclusions that can be drawn from the analysis and evaluation contained in Chapters 3, 5, 6 and 7. A discussion of the conclusions is presented, relating to the

initial aims and objectives of this thesis, and recommendations are made for further work, building on the work already conducted and presented.

Appendix A contains a full report on an experimental programme, aimed at determining the rate of storage recharge within the drainage layer between storm events, which was ultimately not considered worthwhile to pursue beyond preliminary stages. This report discusses the initial motivation for conducting the experiments, the experimental setup, results of the preliminary experiments, the conclusions drawn, recommendations for improvement and recommendations for complementary further experiments.

Appendix B contains examples of Matlab scripts used in Chapters 5, 6 and 7

Appendix C contains a full derivation of the adaptation of nonlinear storage routing to incorporate Manning's *n*. This is referred to in Chapter 5.

1.4   Publications

As of January 2014, a total of three published journal papers and six conference presentations, five given by the thesis author, have resulted from work contained in or related to this thesis. Two further journal papers are intended to result from this work. References for all research outputs are presented below, in chapter order.

Chapter 3

Stovin V, Vesuviano G, Kasmin H (2012) The hydrological performance of a green roof test bed under UK climatic conditions, *Journal of Hydrology* 414-5, 148-161.

Vesuviano G, Stovin V (2011) The hydrological performance of a green roof test bed under UK climatic conditions. *SUDSnet/CIWEM National and International Conference*, Dundee, 11-12th May 2011.

Chapter 5

Vesuviano G, Stovin V (2013) A generic hydrological model for a green roof drainage layer. *Water Science and Technology* 68 (4), 769-775.

Vesuviano G, Stovin V (2012) A generic hydrological model for a green roof drainage layer. *9th International Conference on Urban Drainage Modelling*, Belgrade, 4-6th September 2012.

Vesuviano G (2011) A hydrological runoff model for a green roof drainage layer. *1st National Green Roof Student Conference*, Sheffield, 16-17th May 2011.

Chapter 6

Yio MHN, Stovin V, Werdin J, Vesuviano G (2013) Experimental analysis of green roof substrate detention characteristics. *Water Science and Technology* 68(4), 1477-1486.

Yio MHN, Stovin V, Werdin J, Vesuviano G (2012) Experimental analysis of green roof substrate detention characteristics. *9th International Conference on Urban Drainage Modelling*, Belgrade, 4-6th September 2012.

It should be noted that both of these publications relate to re-analysis of a substrate experimental programme conducted in 2010 by the lead author, Yio. The substrate experimental programme conducted in Chapter 6 builds upon the work conducted by Yio, but does not re-use any of its data. It should be noted that, in the two publications, the runoff delay introduced by the substrate is evaluated relative to the delay introduced by the test apparatus, which includes a standard green roof filter layer. In Chapter 6, the substrate runoff delay is evaluated relative to the rainfall profile. However, modelling in both publications, and in Chapter 6 of this thesis, uses rainfall profile as the input and monitored runoff profile as the output to be matched i.e. runoff is modelled relative to rainfall, rather than relative to rainfall after accounting for the routing effects of the test apparatus.

Chapter 7

Vesuviano G (2013) A green roof runoff detention model. *Marie-Curie IAPP 'Green Roof Systems' Project, The Green Roof Research Conference*, Sheffield, 18-19th March 2013.

Vesuviano G, Sonnenwald F, Stovin V (2013) A two-stage storage routing model for green roof runoff detention. *8th International Conference Novatech: Planning & Technologies for Sustainable Urban Water Management*, Lyon, 23-27th June 2013.

The second-listed conference presentation has been selected by the Novatech Committee for recommendation to the journal *Water Science and Technology* and, as of January 2014, is in press as:

Vesuviano G, Sonnenwald F, Stovin V (in press) A two-stage storage routing model for green roof runoff detention. *Water Science and Technology*.

A journal paper, discussing the application of the model to modelling the runoff performance of the Hadfield test beds (Section 7.4 of this thesis) is, as of January 2014, under review for publication in *Hydrological Processes* as:

Vesuviano G, Stovin V, Berretta C. Field validation of a generalized green roof runoff model.

	2009	2010	2011	2012	2013

Literature review (Chapter 2)

Upward flux experiments (Appendix B)

Transfer report

Mappin test bed re-analysis (Chapter 3)

Large rainfall simulator evaluation (Chapter 4)

Large rainfall simulator modification & calibration (Chapter 4)

Drainage layer experimental programme (Chapter 5)

Drainage layer analysis (Chapter 5)

Small rainfall simulator calibration (Chapter 4)

Substrate experimental programme (Chapter 6)

System modelling of test roof (Chapter 7)

Thesis writing

Substrate analysis (Chapter 6)

System modelling of Hadfield roofs (Chapter 7)

Thesis corrections

Journal of Hydrology

Green Roof Student Conference

SUDSnet/CIWEM

UDM (Vesuviano & Stovin)

UDM (Yio *et al.*)

Water Science & Technology (Vesuviano & Stovin)

Water Science & Technology (Yio *et al.*)

Novatech

Marie Curie IAPP Green Roof Systems

Hydrological Processes (Vesuviano *et al.*)

Water Science & Technology (Vesuviano *et al.*)

2 Literature Review

2.1 Chapter Overview

This chapter covers a brief history of urban drainage, including its purpose and evolution towards the conventional urban drainage structures built in many developed countries throughout the 19th and 20th centuries. Concerns surrounding conventional drainage systems are discussed and Sustainable Urban Drainage Systems (SUDS) introduced as an alternative to mitigate these concerns. Green roofs, and the many purposes for which they have been built, are examined, culminating in an analysis of the modern green roof from the perspective of an engineered SUDS component. Two specific layers of the modern engineered green roof, the substrate and the drainage layer, are examined in detail. Existing hydrological research involving green roofs, or specific layers thereof, is evaluated, identifying areas upon which the research presented in this thesis builds. This chapter concludes with a study of potential hydrological modelling methods for the individual substrate and drainage layers, identifying most appropriate in relation to the experimental programmes proposed in Chapter 4.

2.2 Urban Drainage

2.2.1 Historical Urban Drainage

The issue of storm water runoff first arose in Bronze Age settlements as humans began to replace large areas of permeable surface with contiguous areas of impermeable buildings and roads. Surviving examples of Bronze Age urban drainage systems can be found in settlements built by the Indus Valley, Mesopotamian, Persian and Minoan civilizations, among many others (Burian & Edwards, 2002). The Neolithic dwellings of Skara Brae each feature a "cell" – a small room containing a drainage-type connection running towards the sea (Childe *et al.*, 1931). These cells may have functioned as indoor toilets, in a village occupied prior to the advent of the Bronze Age in that region of the world.

Among the Bronze Age civilizations, different preferences for combined or separate storm and waste water systems can be seen. The Indus Valley civilization, for example, conveyed storm water through open channels in streets. Individual houses made waste water connections to these same channels, after first passing the waste water through a sump to settle solids.

In contrast, the Persian and Mesopotamian civilizations maintained separate systems for the conveyance of storm and waste water. The Persians enacted laws to keep urban runoff pure and, consequently, collected and used urban runoff as a source of potable water. Rainwater harvesting was common in both civilizations.

The Minoan Palace at Knossos, Crete, contains a highly engineered, complex waste water drainage system, which partially survives today. It was built both above and below ground, and includes runoff routing channels, conduits and even catchment basins for attenuation. In parallel, a fully-enclosed sanitation drainage system conveyed waste water from toilets and bathtubs, discharging it to the sea at a considerable distance from the palace (Lyrintzis & Angelakis, 2006).

The Roman civilization is known to have engaged in an extensive programme of building works throughout its Empire. The largest Roman sewer, the *Cloaca Maxima*, was built in the 6th Century BC by Etruscan engineers, initially as an open channel. Its purpose was to control the flow of a stream passing near to the Roman Forum, which had been built on artificially-raised land at risk of erosion (Hopkins, 2004). The Romans covered the channel by vaulting no earlier than the start of the 2nd Century BC. Once covered, the *Cloaca Maxima* became the main line of a combined sewer system, draining water from the public baths, fountains, and other public buildings and amenities, together with storm water runoff received from tributary tunnels and channels. Direct connection of homes to the sewer system began around 100 AD in Rome. The Roman sewer system was copied in other Roman settlements, such as Eboracum (York), where a section is still in use today.

Following the decline of the Roman Empire, most cities reduced considerably in population, resulting in the abandonment of their urban drainage systems. In Mediæval Europe, the importance of urban drainage was significantly reduced as people lived near to large bodies of water and both urban and waste runoff discharged directly into these nearby water bodies. Toilet waste was typically fed to pigs and toilet flushing technology was forgotten, reducing the need for waste water drainage. The few drainage systems that were in use at this time usually consisted of open channels in roads. These were built primarily for storm runoff, but were often used for, and blocked by, kitchen wastes (Kirby & Laurson, 1932). To combat this problem, the channels were covered throughout the late Middle Ages, a notable example being the Beltway Sewer in Paris. As a result of the population expansions around the 16th century, cesspools, treating waste separately, became widespread as a means of preventing further blockages of the covered storm water channels. Towards the end of this century, King Henry VIII wrote an edict requiring each household to keep clean the sewer passing by its dwelling and created the Commission of Sewers to enforce these rules (Gayman, 1996).

2.2.2 Modern Urban Drainage

Throughout the late 19th and early 20th century in the UK, sanitary waste and stagnant water became recognized as sources of disease. The cesspools that had been introduced in the late Middle Ages began to be replaced by the direct plumbing of sources of waste water into new

city-wide sewer systems. The first modern sewer system was built in Hamburg, Germany, from 1843 onwards. Following the Great Stink of 1858, a new combined sewer system designed by the chief engineer of the Metropolitan Board of Works, Joseph Bazalgette, was built in London from 1859 onwards, to transport combined storm and waste water to the Thames estuary downstream of the city. Social reformer and commissioner of the Metropolitan Commission of Sewers, Sir Edwin Chadwick, proposed for the separation of the storm and waste water networks, but was overruled on cost and complexity considerations (Butler & Davies, 2004). It was during the design process of these new sewer systems that engineering calculations, rather than accumulated trial-and-error, became the method by which sewer networks were designed. Hawksley's formula, used by Bazalgette to size pipes in the comprehensive sewer system of London, is given below.

$$\log d = \frac{3 \log A + \log N + 6.8}{10} \qquad \textbf{Equation 2.1}$$

Where d is pipe diameter in inches, A is drainage area in acres and N is length of sewer in feet per foot of drop (Burian & Edwards, 2002).

These city-wide sewer systems were gradually copied in other British, European and US cities throughout the late 19th century. They were most frequently built to transport waste water in combination with surface runoff drained from buildings and urban streets, a design decision that continued in the UK until the mid-1960s (Water UK, 2009). Most new buildings (and extensions to existing buildings) built since then use separate systems for removing waste water and storm water. However, as many of the old sewers have not been replaced, the vast majority of the current sewer network in the UK is still combined (Ashley *et al.*, 2007). The comprehensive sewer system of London was originally designed to contain and transport a storm event of one-quarter inch (6.35 mm) depth in addition to waste water. Since then, the population of London has more than doubled, placing increasing waste water demands on the combined sewer system. Furthermore, individual storm events with depths greater than 6.35 mm are not uncommon; the one-in-one-year, 60-minute storm for every part of the UK is deeper than this (NERC, 1975), and storms with longer durations and/or greater return periods are automatically larger still. Although the capacity of the sewer network has been periodically upgraded, it is still possible for it to be exceeded; in London, capacity exceedence is now a greater-than-weekly occurrence (Thames Water, 2011). To avoid situations in which there is simply no spare capacity for excess storm water to enter into an urban sewer, the UK's combined sewer network is fitted with more than 20,000 combined sewer overflow (CSO) outfalls which act as a fail-safe if the capacity of a sewer in a particular area is exceeded. They are essentially pipes that discharge combined untreated sewage and storm water directly into rivers, lakes or the ocean, preventing the sewage

from re-emerging on the local streets, but polluting the area around the outfall with bacteria, viruses, heavy metals, polycyclic aromatic hydrocarbons and other toxic materials. These pollutants can seriously compromise fisheries, shellfisheries, bathing and recreational water use, resulting in fish and shellfish becoming poisoned, public health problems, and aesthetic visual and odour problems (Water UK, 2009). Over 500 CSOs are known to be located near beaches listed in the Marine Conservation Society's Good Beach Guide (BBC, 2009).

As a result of further population growth in the UK, coupled with general increases in per-person water usage, many combined sewer systems that are adequate during dry weather periods do not have sufficient capacity to cope during storms. As CSO outfalls must, by law, only discharge as a result of rain or snow melt (they may not discharge strictly waste water), one very obvious method of reducing the incidence and severity of CSOs is to reduce the volume of runoff resulting from precipitation.

2.3   Sustainable Urban Drainage Systems (SUDS)

Sustainable Drainage Systems, sometimes referred to as Sustainable Urban Drainage Systems (SuDS and SUDS are used interchangeably for the former), are defined by CIRIA as:

> "*A sequence of management practices and control structures designed to drain surface water in a more sustainable fashion than some conventional techniques.*" (CIRIA, 2012a).

They are designed to reduce the quantity of runoff, improve the quality of runoff, and provide amenity and biodiversity benefits, such as public space or additional habitat, in an integrated approach (Figure 2.1). This is in contrast to conventional drainage systems, which are primarily concerned with reducing the quantity of runoff through the use of pipe networks, improving the quality of mixed runoff-sanitary waste by treatment in large centralized structures, and only considering biodiversity and amenity value indirectly, if at all. The main principles of SUDS are referred to as BMPs (best management practices) and LID (low-impact development) in both the USA and Canada.

SUDS offer many benefits over conventional surface water drainage processes. Encouraging rainwater to soak into the ground as it lands recharges groundwater and reduces both the likelihood of flooding, and the volume of the floods which do occur. Reducing the volume of surface runoff reduces the volume of rainwater that could enter a combined sewer system as a result of rain, reducing both the risk of CSOs and the load on water treatment structures. Keeping surface runoff above ground wherever possible allows SUDS components to be designed as habitats for wildlife and public amenities. Many SUDS devices treat pollution present in surface water by settlement and bioremediation, improving the water quality. The use of certain
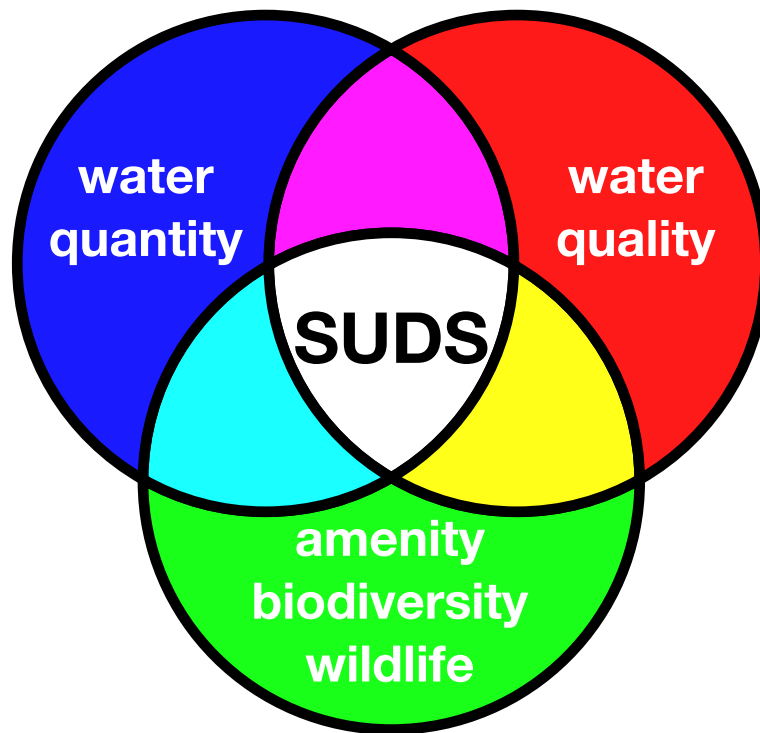
Figure 2.1 – The SUDS triangle.

SUDS structures, such as ponds, detention basins and wetlands, may reduce the urban heat island effect through evapotranspiration and reduced building density. Separating surface runoff from sewers can reduce the number of routes through which vermin are able to enter sewer pipes, reducing the spread of disease.

The SUDS sequence is made up of distinct and ordered elements, referred to as the management or treatment train (Figure 2.2). The first element in this sequence is prevention. Prevention is not a physical component, but is the recognition that minimizing surface runoff reduces the need for subsequent drainage and treatment structures. Examples of prevention techniques include rainwater harvesting, in which rain is collected and used for activities that do not require potable water e.g. flushing toilets and watering plants; general maintenance and cleaning of roads and other surfaces, to prevent the accumulation of pollutants and their subsequent mobilization during a storm; disconnection, in which roof runoff is directed over adjacent undeveloped land or gardens, avoiding any kind of engineered drainage system altogether; and education, such as informing the public of the negative consequences associated with disposing of chemicals in drains. Successful education also reduces the negative consequences of any CSO event that does occur, as the quantity of dangerous materials in the sewer is reduced. It is worth noting that in certain cases e.g. flushing toilets or washing clothes in a washing machine, harvesting and re-using rainwater on-site may simply act to transfer the re-used volume of storm water to the foul sewer system or delay its entry to the combined sewer system. However, this is still more sustainable and less energy intensive than the traditional approach of using potable water for
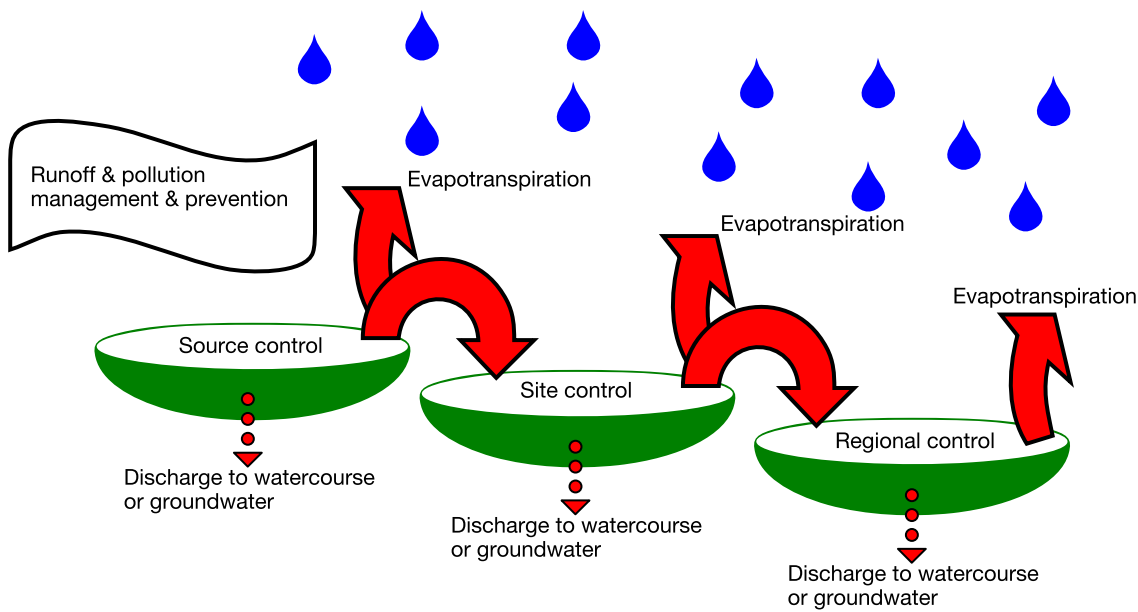
Figure 2.2 – The SUDS treatment train (based on a previous version of CIRIA, 2012b. Now offline).

these tasks. In addition, temporarily detaining storm water on-site and releasing it to the sewer system after use, reduces or eliminates the peak storm loading on a drainage system, greatly reducing or eliminating the possibility of that event causing a CSO.

Following prevention in the SUDS management train are source, site and regional controls. The primary difference between these three controls is their proximity to the source of runoff. Source controls treat runoff at its source, by allowing infiltration of rain water where it lands. Runoff that cannot be infiltrated at source is conveyed, preferably above ground, to site and/or regional controls, which treat surface runoff from several sub-catchments. The surface water management train advocates returning runoff to the natural drainage system as soon as possible. However, certain site and regional controls, particularly ponds, may be mandated for the settlement and degradation of pollutants over an extended time period, before the runoff is discharged to a watercourse. Industrial sites, commercial depots and large residential areas are those for which ponds are usually necessitated.

Aside from prevention, CIRIA categorizes SUDS components according to their storm water management processes. Seven categories are defined (CIRIA, 2012c), with some components falling into more than one category:

1. Source controls – These are SUDS components which attenuate and treat rain water where it lands. Source controls generally aim to infiltrate smaller storms (up to 5-10 mm) in their entirety; site and regional controls are used for further treatment and attenuation of larger storms. Examples of source controls include green roofs, infiltration trenches, permeable

paving and rainwater harvesting. Green roofs are discussed at length in Sections 2.4, 2.5 and 2.6, while infiltration trenches and permeable paving are discussed in SUDS category 4; rainwater harvesting has been discussed previously.

2. Conveyance channels – In the event that source controls alone are insufficient to contain a storm event, overland flow routes are required to convey flood water to SUDS components further down the treatment train. As well as conveying runoff to later-stage SUDS components, swales and well-designed hard channels can be used to provide attenuation and treatment of surface runoff as a stage in their own right. As runoff passes through a swale, it is filtered and slowed by the vegetation. If the runoff flow velocity in the swale is too high, gradual erosion of the channel bed is likely; dams are included as required to slow the runoff; this also has the effect of attenuation. Swales and other vegetated conveyance channels can be used to provide habitats and public open space. Maintenance is required to remove litter and cut any vegetation that may cause turbulence, as failure to do so may lead to erosion at lower velocities. Hard channels will not erode under turbulent flow, can be planted to provide water treatment and may allow solids to settle if properly designed. A hard channel requires less land than an equivalent swale, as it can be built with vertical sides, whereas the swale requires additional area for gently sloping sides. However, the swale can allow infiltration and provide for greater biodiversity.

3. Filtration devices – The purpose of filtration components is to remove sediment from surface runoff, trapping it either on plants, in soil/aggregate or on geotextiles. Filter strips are gently sloping grassy depressions whose purpose is to allow silt to settle so that it does not interfere with drainage components further down the treatment train. Filter trenches are shallow excavations filled with gravel. These provide hydraulic control and filter pollutants. Bioretention areas are gently sloping vegetated depressions with subsurface layers of specially-engineered soil and sand designed to filter pollutants commonly found on highways. The topography of filter strips and bioretention areas makes them suitable for temporary storage of runoff, while the nature of the surface and subsurface layers may allow infiltration if the ground is suitable. Regular maintenance is required for all filtration devices, as the potential for gradual clogging is high.

4. Infiltration devices – These components enhance the ability of the ground to store and drain water, thereby encouraging water passing through them to soak into the ground and return to the water table. Soakaways and filter drains are common infiltration devices consisting of a trench filled with a volume of permeable material. The maximum reduction in runoff quantity is equal to the storage volume of the component, given by the volume of the trench multiplied by the void ratio of the permeable fill. Runoff quality is improved as

the permeable fill traps sediment. Infiltration to the exposed earth takes place at the base and sides of the trench. The rate at which water is infiltrated is determined by the permeability of the surrounding soil; till, rock, clay and clayey soils are unsuitable for infiltration. Other SUDS components may route their runoff to a filter drain, discharging into the trench through a perforated pipe buried in the permeable fill.

Permeable paving is a type of infiltration device in which the top surface consists of paving materials: either porous asphalt or impermeable slabs laid in a way that includes gaps for rainwater to pass through. These systems can be used for almost any hard landscape due to the wide variety of permeable surfaces available, including block paving, asphalt, gravel and plastic-reinforced grass. Swales, basins and ponds, if they are not lined, can fulfil infiltration as secondary functions. Basins can provide amenity value as playing fields and recreational areas during dry periods, only temporarily becoming infiltration and storage devices for short periods after storm events.

5. Retention and detention structures – These are large-scale water storage systems, used as site or regional controls. They receive runoff from SUDS components further up the treatment train, operating optimally when flows are managed and silt has been pre-settled. Basins are detention structures, hence are dry except for a short time period during and following storm events. Their purpose is to attenuate the peak rate of runoff resulting from a rainfall event. The temporary storage of rainwater in a detention basin allows for sedimentation and some bioremediation to take place. Ponds contain a permanent pool of water that increases in volume as a result of a storm event before gradually returning to its original volume after the end of the storm. Pollutants are treated by settlement of suspended solids, bioremediation and adsorption by the plants or soil. In contrast to basins, the typical residence time of a quantity of water moving from a pond's inlet to its outlet may be as long as two or three weeks. Basins and ponds can both be used for recreational purposes. However, ponds provide a greater variety of natural habitats, whereas basins generally have a greater public amenity value, due to the perceived health and safety risks often associated with permanent ponds.

Geocellular storage is a type of extended detention device, consisting of a large underground void supported by a sparse matrix of hard plastic. A device to limit the rate of discharge is included at the outlet; this ensures attenuation. If the storage volume is lined, the void acts as a storage tank. If the storage volume is unlined, it may allow infiltration in addition to storage and attenuation. However, geocellular storage devices cannot be considered SUDS components, except as part of a treatment train, since they provide no treatment or amenity value themselves. The plastic matrix is also liable to block

if sediment and solids are not settled before runoff enters the device. Furthermore, any blockages that do occur are difficult to remove, as the component is situated entirely underground.

6. Wetlands – These permanent bodies of water are more densely vegetated and shallower than ponds. Where required, wetlands should be the final element in a treatment train, with all necessary attenuation and sedimentation occurring before runoff enters the wetland. By controlling the rate of inflow to the wetland, residence times for runoff can be greatly increased. This allows for the biological breakdown of oils, settlement of suspended solids, adsorption of pollutants and consumption of dissolved nutrients by the plants, over weeks. Wetlands deliver high biodiversity value and can deliver high amenity value. However, because the unique advantage of the wetland is its high level of biological treatment processes, shallow water is required throughout to ensure a sufficient supply of oxygen and low rates of inflow are required to ensure long residence times. Hence, provision for attenuation of peak flows must be delivered by upstream components.

7. Control structures – These are purpose-designed inlets to and outlets from SUDS components which limit flow rates. They are often necessary, as many SUDS components do not function as intended under high flow velocities; rapid flow in a swale, for example, will not allow significant settling of suspended solids and may cause erosion of the channel bed. Common control structures include weirs, throttle pipes, orifice plates and vortex controls. Head-discharge relationships may be easily calculated for weirs, throttle pipes and orifice plates, while empirically-determined manufacturers' relationships are used for vortex controls. Weirs and orifice plates are both flat, whereas throttle pipes and vortex controls both involve a significant dimension in the flow direction. An orifice plate can be thought of as a pipe with a length in the order of millimetres, as flow is limited in both cases by a head of water building up above the flow route. Blocking is a significant concern for both throttle pipes and orifice plates, as there may not be an emergency bypass for flow if a blockage alters the head-discharge relationship to the point where water will overtop out of the SUDS component. This is not a problem for weirs, as water is free to flow over the top of a weir plate if its weir notch is blocked. However, this is not the intended design function of the weir and therefore may be a cause for significant concern. Vortex controls consist of a pipe with a specially-shaped volute intake which, at higher inflow rates, generates a vortex of air along the centre of the pipe, only allowing water to flow around the periphery of the pipe. Vortex controls may be preferred over simple throttle pipes, as the central vortex of air causes a larger diameter of pipe to be required for the same limiting flow rate. Consequently, blockages are less likely.

As all flow control structures affect the rate, but not total volume, of runoff, sufficient detention storage capacity must exist directly behind them. Attention must be given to ensuring that flow control components do not block; regular maintenance may be required as a preventative measure. Good design, such as covering inlets and outlets with cobbles to prevent the accumulation of material at the flow control, is essential. Inlet controls to SUDS components must be designed to minimize turbulence, as this may cause erosion.

The CIRIA SUDS selection tool (Woods Ballard *et al.*, 2007) specifies the minimum number of treatment levels that are likely to be appropriate for each type of development. Each SUDS component in a treatment train is considered as providing one level of treatment (with a few specific exceptions). Roof runoff, of any kind, is considered in these guidelines to require only one level of treatment. Hence, outflow from a green roof is, by these definitions, generally considered clean and therefore suitable for direct discharge to a watercourse.

SUDS are required, by General Binding Rule 10 of the Water Environment (Controlled Activities) (Scotland) Regulations (2005) for the drainage of all new developments in Scotland completed after April 2006, except those which consist of a single dwelling only or discharge all runoff directly to coastal waters. Schedule 3 of the Flood and Water Management Act (2010), planned to come into force in 2014, will require SUDS for the drainage of all new developments in England and Wales, except those which consist of a single dwelling or which are publicly-maintained roads. Exceptions will also apply to any part of a drainage system which drains a single dwelling, any part of a development which is, or becomes, a publicly-maintained road, and any other single exceptions made by the English Secretary of State (in England only) or the Welsh Ministers (in Wales only).

2.4 Green Roofs

2.4.1 History of Green Roofs

The concept of planting on roofs has been in existence for millennia, in the form of roof gardens and terraces. The Villa of the Mysteries in Pompeii is one well-preserved example of an ancient roof garden. An elevated terrace on three sides of the Villa, held up by a colonnade, still stands today. When Pompeii was inhabited, this terrace held soil on which plants were grown. Ancient roof gardens were built primarily for recreation, so those using planting beds rather than pots can be considered as much older equivalents to modern intensive green roofs in purpose, though not in detailed design or construction.

The sod roofs of North West Europe date back to at least the Viking era and can be considered as old versions of extensive green roofs on a very superficial level. The main parallel between sod

roofs and modern extensive green roofs is, most obviously, that both feature a layer of low-growing, low-maintenance vegetation, supported by a depth of growing medium that is broadly comparable: sod roofs are typically 150 mm thick, around the upper limit for an extensive green roof. However, the simple design of a sod roof, consisting of a thick layer of sod over a sub-layer of birch bark for waterproofing, is completely different from that of a highly engineered modern green roof, as is its purpose – insulation: Modern extensive green roofs are usually assumed to provide no insulation (Anderson, 2006), unless specific insulation components are included in the system design e.g. thick expanded polystyrene drainage layers.

Towards the end of the 19th century, numerous low-cost rental apartment blocks for the families of industrial workers were built all over Germany (Köhler, 2006), the first (albeit unintentional) boom in green roof construction. A layer of gravel, sand and sod was applied to the roofs of these apartment blocks to act as fire protection. Extensive green roof species such as *Sedums*, mosses and grasses colonized the roofs over time.

In 1914, the Moos lake water-treatment plant in Zürich, Switzerland, was built with a roof consisting of a 15-20 cm layer of topsoil, above a 5 cm drainage layer of gravel and sand, over asphalt waterproofing. Over time, a meadow developed from the seeds of local plants that were present in the transported soil. Some of the species present on the roof, such as the green-winged orchid, are now extinct elsewhere in the region. Though not initially designed as a green roof, its construction in discrete layers is very similar to a modern green roof. Its intended purpose, to keep the building cool, is advertised in various items of modern green roof promotional literature as a secondary function to storm water attenuation and retention.

In the late 1920s and 1930s, green roofs were included on houses designed by Modernist architects such as Le Corbusier and Frank Lloyd Wright, for use as private gardens. Le Corbusier's "Five Points Towards a New Architecture", published in 1926, includes roof gardens as the second point: as a recovery of the area consumed by the building; a utilization of ignored flat space; and a rain water detention component (Conrads, 1970). Frank Lloyd Wright's *Fallingwater* house, voted the best all-time work of American architecture by the American Institute of Architects (JHU Gazette, 2004), incorporates a large amount of usable roof space. Over the period from 1936 to 1938, an intensive green roof totalling 6000 m^2 in area was built on the roof of the Derry and Toms building in Kensington, central London, UK. The Roof Gardens, as they are now known, are located 30 metres above street level, contain over 100 species of tree, and were Grade II listed by English Heritage in 1978. Certain trees on the roof are the subject of preservation orders.

2.4.2　Modern Green Roof Design

2.4.2.1　Introduction

Following the seven-grouped classification of SUDS defined by CIRIA and described in Section 2.3, green roofs fall into the source control, filtration device and infiltration device categories; though green roofs do not strictly allow infiltration, their design is similar to that of a soakaway. Modern green roofs consist of a vegetated, permeable volume of growing medium with a high void ratio of up to ~0.5 (Alumasc, 2012a) and a free-draining outlet. Although standard filter drains and permeable paving can be easily incorporated into multi-use open areas, green roofs have the unique property among SUDS of being easily incorporated into new and existing buildings without requiring any additional land. This is especially useful in highly urbanized areas, such as city centres, where there is a lack of existing open space, high land values and a prevalence of combined sewer systems.

2.4.2.2　System Build-Up

A typical system build-up for a modern green roof would be, from bottom to top: A waterproof membrane above the roof deck, followed by a root barrier, thermal insulation (only in inverted roofs, Figure 2.3 (a)), protection/moisture mat (only in non-inverted roofs, Figure 2.3 (b)), drainage layer, filter sheet, a layer of substrate and above this, the plants. Each of these components works together towards the overall purpose of the system. Specially engineered substrates are used to provide highly appropriate pH values, nutrients, porosity and vapour permeability to the specific plants used. A plastic drainage element is widely used to mimic the free-draining rock layer found below the soil in alpine environments. The filter membrane separates the substrate and drainage element, creating an air gap during dry conditions. This provides aeration to the substrate and ensures free drainage is not compromised by roots or washed-in substrate. The protection/moisture mat, if present, is used both to retain moisture and nutrients and to protect the root barrier and waterproof membrane. In an inverted roof, the thermal insulation layer undertakes the role of protection for the root barrier and waterproof membrane. It also shields the waterproofing from temperature extremes, thereby increasing its lifespan, but does not retain nutrients. Diagrams of typical inverted and non-inverted system build-ups are shown in Figure 2.3; the drainage layer and insulation are integrated in (a). Sections 2.5 and 2.6 consider, in detail, the design and purpose of the drainage layer and substrate components of a modern engineered green roof.

2.4.2.3　Categories of Modern Green Roof

Most modern green roofs, following the system build-up given above, can be considered to divide into two categories: intensive and extensive (Figure 2.4). The largest differences between these categories relate to the substrate layer, vegetation layer and maintenance regime.
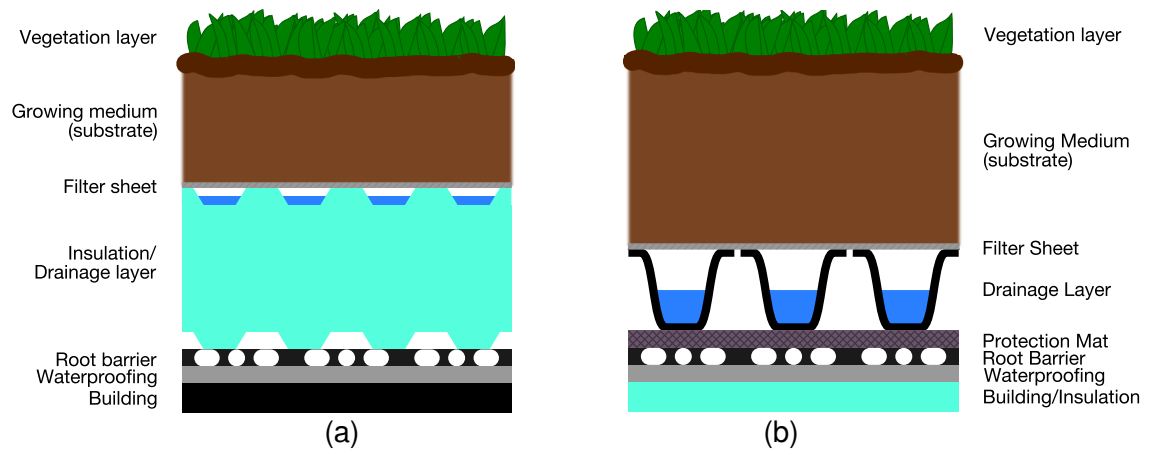
Figure 2.3 – A typical inverted (a) and non-inverted (b) green roof system build-up.

Extensive green roofs feature a substrate layer of low organic content, which is no more than 150 mm deep. Alpine- or rockery-type plants are used for extensive green roofs, as they thrive in poor soils and exposed areas, and can survive long droughts. These characteristics are essential when it is considered that the low substrate depth cannot act as a long-term water reservoir. As the maintenance regime for an extensive green roof is intended to be minimal, replacing dead plants is impractical. To enhance plant survival, the substrates and drainage layers of modern extensive green roofs are designed to mimic the free-drainage and poor soils of rocky alpine areas. An inverted extensive green roof in Esslingen, Germany, is shown in Figure 2.5 (a). The roof uses primarily *Sedum* species and drought-tolerant grasses in 100 mm of substrate, above an expanded polystyrene drainage layer (ZinCo Floratherm WD 180), which provides insulation and water holding capacity.

Bio-diverse roofs are a form of semi-extensive, semi-intensive green roof in which the roof is generally intended to mimic the site of the building or local habitats, pre-development. The design of a bio-diverse roof is intended to meet specific biodiversity objectives, which vary
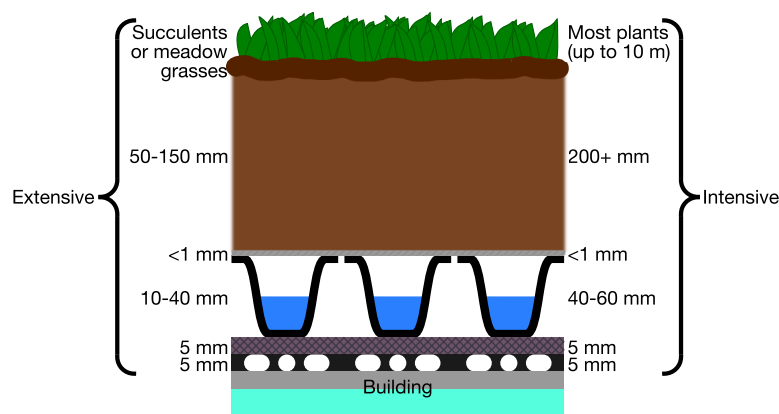
Figure 2.4 – Typical or representative approximate depths of extensive and intensive green roof system layers.

between different cities and countries e.g. complying with a local action plan. A wider variety of plant species and substrate compositions are used, as they must generally match the native or existing species and soil type found at the site. Substrate depths are varied throughout the roof to provide a variety of habitats; the mean depth tends towards the deep end of extensive as locally-native plant species at a site are not necessarily drought tolerant or able to thrive in poor soils.

The substrate layer of an intensive green roof is higher in organic content as compared to an extensive green roof. The increased nutrient level means that intensive green roofs are suitable for a much wider selection of plant species, including trees. The substrate of an intensive green roof may be of any depth greater than 150 mm, the upper limit being imposed by loading on the building below. Under the most suitable conditions, trees of up to 10 metres in height can be supported on an intensive green roof. As the conditions on intensive green roofs are favourable to a much larger selection of plant species than for intensive roofs, regular maintenance is required to remove invasive species and dead specimens. Irrigation may also be required during extended periods without rainfall, as some plants used on intensive green roofs have high water demands e.g. tall trees. Formal gardens, agricultural plots, tennis courts and even a Subaru off-road test track have all been built as intensive green roofs. Figure 2.5 (b) shows a public space on the roof of the Danish National Archive.

Mat-style green roofs are a greatly compressed version of the extensive non-inverted green roof in which a pre-cultivated mat of *Sedum* species is laid over thin filter and drainage layers for a total system depth of 50-60 mm. Some variants of the mat-style green roof consist of only the vegetation and attached thin substrate layers, having no drainage layer or protection/moisture mat; these are rolled out directly over the roof's waterproofing layer. Mat-style green roofs are favoured in applications where extremely light-weight green roofs are required. However, a more regular fertilization regime is necessary than for extensive green roofs, as the thin layer of

Figure 2.5 – Pliensaufriedhof, Esslingen-am-Neckar, Germany (a), Danish National Archive, Copenhagen, Denmark (b).

specially-engineered low density substrate is not capable of storing a great quantity of nutrients. An irrigation regime may also be required, as only a limited quantity of water can be stored and, therefore, made available to plants during any dry period. As a maintenance regime that increases with decreasing substrate depth may seem counter-intuitive, the long-term survival of mat-style roofs in practice is debatable. Some jurisdictions require a minimum substrate depth for a green roof to be legally considered as a green roof (see Section 2.4.3: Policy).

Driveway and walkway green roof systems do not follow the system build-up of extensive, intensive or mat-style green roofs. Instead, they are more similar to permeable paving, consisting of hard slabs covering a permeable granular fill. A drainage layer component is positioned below the granular fill layer to allow the free and rapid movement of percolated water towards a drainage outlet.

2.4.2.4   Benefits of Modern Green Roofs

Research into green roofs as urban habitats began in Germany in the 1950s, the use of thin substrate layers as growing media was investigated in the 1960s and commercially-available modern green roof systems have been produced by some of today's market-leading companies since the 1970s (Dunnett & Kingsbury, 2004). The primary objective of these systems is to reduce roof runoff resulting from storms, though they also provide many other benefits. These most commonly include: mitigation of the urban heat island effect by evaporative cooling (Laberge, 2003; Takebayashi & Moriyama, 2007); provision of habitat (Brenneisen, 2006; Fernandez-Canero & Gonzalez-Redondo, 2010; MacIvor & Lundholm, 2011); thermal buffering of the building, thereby reducing its heating and cooling demands (Palomo Del Barrio, 1998; Kumar & Kaushik, 2005; Sailor, 2008); sorption of airborne particulates (Johnston & Newton, 1993; Tan & Sia, 2005; Currie & Bass, 2008; Yang *et al.*, 2008); consumption of carbon dioxide and production of oxygen by the vegetation (Getter *et al.*, 2009; Li *et al.*, 2010; Hong *et al.*, 2012); sound insulation (Lagström, 2004; Van Renterghem & Botteldooren, 2008); agriculture (Roehr & Laurenz, 2008; Banting *et al.*, 2009; Rowe, 2011); extending the lifespan of the roof membrane (Miller, 2002; Porsche & Köhler, 2003; Kosareo & Ries, 2007); amenity value to occupants and the public (e.g. Namba Parks, in Osaka, Japan, Mountbatten House in Basingstoke, UK and Hundertwasserhaus in Plochingen, Germany – shown in Figure 2.6); an aid to planning consent (see Section 2.4.3: Policy); financial value to developers (Ichihara & Cohen, 2011); and reputational value to the organizations that instigate them (Johnston & Newton, 1993; Dunnett & Kingsbury, 2004). Thermal insulation may also be provided by a layer of air trapped within the vegetation (Peck *et al.*, 1999), though the insulation capacity of green roofs as a whole is disputed (Anderson, 2006) and likely to vary between climates. The document "Guidelines for the Planning, Execution and Upkeep of Green Roof Sites", published in German and English by the Forschungsgesellschaft Landschaftsentwicklung Landschaftsbau e.V. (FLL, 2008), is used in

Figure 2.6 – Hundertwasserhaus, Plochingen, Germany.

many countries, either unmodified or as the basis for country-specific guidelines, for the design of green roof systems and to specify the characteristics of their individual components.

Another secondary benefit, which is essential to the consideration of green roofs as complete and comprehensive SUDS components, is the improvement in water quality that green roofs provide. This is assumed to occur by filtration in the substrate and uptake by the plant roots. However, this viewpoint is controversial. Köhler *et al.* (2002) give evidence strictly in favour, while Berndtsson *et al.* (2009), Gregoire & Clausen (2011) and Carpenter & Kaluvakolanu (2011), all show green roofs to act as a sink of some pollutants and a source of others. Despite this, the total mass of pollutants in runoff was usually found to be reduced, as a result of lower total runoff volumes. Vijayaraghavan *et al.* (2012) take a negative view on the assumption that green roofs improve water quality, but concede that their observed pollutant concentrations were generally below USEPA limits and that some pollutant concentrations in runoff from their control roof also exceeded USEPA guidelines.

One clear disadvantage of green roofs, in relation to many other SUDS components, is that water infiltrated in a green roof does not recharge groundwater levels.

2.4.3 Policy

Two green roof businesses, ZinCo and Optigrün, have both been producing modern green roofs since the 1970s. A third business, Bauder, which started producing green roofs in 1982, is the 2012 leader by market share. All three trade internationally, but all are headquartered in the German state of Baden-Württemberg, as is the International Green Roof Association (IGRA). It is in the German-speaking countries (Germany, Austria and Switzerland) that green roof policy is most advanced. It should be noted that green roofs were in use throughout the German-speaking countries before the introduction of green roof policies, though at a much smaller scale.

In 1985, the city of Linz, Austria, set out its Green Space Plan, introducing legally-binding requirements for green roofs on new buildings (Maurer, 2006). Four years later, a financial incentive of 30% was introduced for green roofs, reduced to 5% in 2005. Currently, green roofs are required on industrial, commercial and mixed use buildings over 500 m^2, residential buildings and extensions to existing buildings over 100 m^2, and all underground structures. The green roof must cover at least 80% of the roof surface and support at least 80 mm of substrate. No green roof is required on roofs pitched at over 20° or on sites with over 60% green space. The main motivation behind green roof policy in Linz has been to counter the reduction in air quality and loss of green spaced that resulted from the rapid expansion of the City's steel and chemical industries in the 1960s and 70s (Maurer, 2006).

The Municipality of Stuttgart, the state capital of Baden-Württemberg, has been the leader of green roof policy in Germany. It has financially assisted in the construction of green roofs since 1986, resulting in over 2,000,000 m^2 of green roofs installed in the region and a further 1,500,000 m^2 in planning as of 2010 (IGRA, 2010). Green roofs were initially made a requirement on flat-roofed industrial buildings in 1989 (Johnston & Newton, 1993) and are now currently required on all roofs pitched at 20° or less, similarly to Linz (IGRA, 2010). However, a main motivation in Stuttgart, in addition to the improvement of air quality, has been to control storm water runoff volumes. This is a main motivation in other German cities as well: A 2004 survey of German municipalities with populations over 10,000, conducted by the Fachvereinigung Bauwerksbegrünung e.V. (FBB), showed that of the 398 municipalities that responded, 201 offered reduced storm water fees to properties with green roofs, 145 had green roof requirements fixed in local development plans and 70 offered direct financial assistance to green roof construction (FBB, 2004; Ngan, 2004).

In the Canton of Basel, Switzerland, green roof systems have been required on all new flat roofs over 100 m^2 since 2002 and two campaigns have provided subsidies for installing them, in 1996-7 and 2005-6 (Kaźmierczak & Carter, 2010). The motivations here are to reduce energy consumption and to replace habitat that has been destroyed by the development. The first motivation can be seen in the funding source for the campaigns: a 5% levy on electricity bills. The second motivation is evident in the City's green roof regulations, which require, on roofs over 500 m^2, the use of "Basel Mix" vegetation, native regional soils and a minimum substrate depth of 100 mm, including mounds of 300 mm depth to provide habitats for invertebrates (Brenneisen, 2004). There is no subsidy or other financial incentive, as green roofs are considered part of the normal costs associated with building in the Canton.

As part of its plan to become fully carbon neutral by 2025, Copenhagen, the capital city of Denmark, adopted a mandatory green roof policy in 2010. The policy requires green roofs on all

new roofs pitched at under 30° and also applies to any roof replacements made using public financial support. The press release accompanying this policy (City of Copenhagen, 2010) states that 200,000 m² of Copenhagen's roofs are green and this policy aims to add 5,000 m² to that total every year, though news outlets have reported the green roof area as 20,000 m². Given that the press release puts the current number of green roofs at "at least 30", it is more likely that the most commonly reported figure of 20,000 m² of green roofs is correct.

Portland and Chicago in the USA, and Toronto in Canada, are considered to be the North American leaders in green roofs. Portland's first modern green roof was installed in 1996 by Tom Liptan, an eco-roof expert working for the Bureau of Environmental Services, on his own garage. A monitoring system was included to compare rainfall to runoff. The favourable results of this private trial led the city to promote eco-roofs as a way of helping to meet its obligations to clean up the Willamette River, by reducing the incidence of CSOs (Lawlor *et al.*, 2006). Green roof policy in Portland is driven by storm water quantity management, countering the urban heat island effect and providing habitats for birds (City of Portland, 2010). Currently, a green roof cover of 70% or greater is required on all new municipal roofs, including roof replacements where practical (City of Portland, 2005). Private developers are encouraged to install green roofs on new buildings as they may earn bonus floor area at a rate which increases with coverage (City of Portland, 2010). Financial incentives are provided by the city for developers and owners to install green roofs that manage storm water (City of Portland Environmental Services, 2011).

Chicago contains over 650,000 m² of green roofs, which is more than half of the total green roof area in the USA (Kamin, 2010), and more than three times greater than Portland's target of 174,000 m² by 2013 (City of Portland Environmental Services, 2011). A semi-extensive green roof of approximately 1,880 m² was added to the City Hall in 2001 to counter the urban heat island effect; monitoring results have shown the green roof areas to be up to 49°C cooler than black roof areas on the same building (Laberge, 2003). Similarly to Portland, developers including green roofs on building proposals in the Central Business District are permitted to increase the number of units on a piece of land. The permit process for these applications is also fast-tracked (Taylor, 2007). Other green roof policy in Chicago includes reduced storm water fees for properties with green roofs, construction grants and a requirement for any development receiving financial assistance from the city (e.g. brownfield redevelopment) to include a green roof (Taylor, 2007). The largest of Chicago's 350+ green roof sites is the 22,200 m² Soldier Field parking garage, completed in 2003.

In 2009, Toronto, Canada, became the first North American city to pass a green roof bylaw, under the authority of section 108 of the City of Toronto Act (City of Toronto, 2006). The list of benefits of green roofs, given in the accompanying information brochure, begins with the

increase in runoff quality and reduction in runoff quantity, before mentioning the urban heat island, improved air quality, amenity value, reduced energy consumption and biodiversity benefits. The bylaw requires a minimum green roof coverage, graded from 20-60%, on all residential and commercial buildings of over 2000 m^2 gross floor area from 31st January 2010 (City of Toronto, 2009). Green roofs were originally required for industrial buildings from 31st January 2011; the bylaw was amended in December 2011 to allow minimum performance specifications for rainwater harvesting and cool roofing to be met by devices and techniques other than green roofs (City of Toronto, 2011). Free exemptions are permitted for residential buildings under 6 floors or 20 m high, or towers of 12 storeys or greater with floor plates under 750 m^2. Developers are also able to individually exempt projects from green roof requirements, for a fee of $200 per square metre to be exempted. The ability for developers to buy their way out of the bylaw's requirements may make it seem weak in comparison to the bylaws of Germany, Austria and Switzerland. However, in the first 20 months after coming into force, over 113,000 m^2 of green roof was planned for construction in Toronto, approximately three times the total area installed prior to 2010 (Green Roofs for Healthy Cities, 2011). An Eco-Roof Incentive Program currently provides $50 per m^2 for green roof retrofit projects on commercial, industrial and institutional buildings, up to a maximum of $100,000. For 2010, funding was also provided to industrial building projects that would not normally require green roofs until 2011.

In the UK, there is no direct mention of green roofs at a national policy level. However, green roofs can help to deliver certain policy objectives, such as the UK Framework Indicators covering bird populations, river quality and air quality (DEFRA, 2010), or the EU Water Framework Directive (2000). Uptake of green roofs in the UK has generally been slow compared to the cities, regions and countries discussed above, often being limited to one-off "flagship" developments and retrofits by enthusiasts. However, local green roof policies in Sheffield and London strongly encourage installation.

As of February 2010, Sheffield contained an estimated total of 120 green roofs. An audit, conducted jointly by The Green Roof Centre, Groundwork and Sheffield City Council, found 48 non-domestic green roofs above 10 m^2, on commercial, industrial, university and local authority buildings, up from only five in 2005, for a total of 25,000 m^2, while also identifying many more domestic and smaller roofs (The Green Roof Centre, 2010). The authors attribute this rapid expansion of green roofing in the city to the introduction of a Green Roofs Policy in 2005 by the city's planning department. Other policy mention of green roofs in Sheffield includes Policy CS64 of the Sheffield Development Framework (Sheffield City Council, 2009) which specifies the acceptable use of green roofs as SUDS techniques to minimize surface water runoff and links with Policy CS67, which requires the use of SUDS on all sites where practicable and sets

maximum rates of surface runoff for different classes of development. A draft version of Sheffield's Designing for Environmental Sustainability Supplementary Planning Document (SPD) expects 80% green roof coverage on all developments above 1,000 m^2 gross internal floorspace or containing more than 15 dwellings (Sheffield City Council, 2010).

In London, Policy 5.11 of the London Plan expects major developments to include roof, wall and site planting where feasible (Greater London Authority, 2011). The motivations for this policy are given as: aiding cooling; sustainable urban drainage; aiding energy efficiency; enhancing biodiversity; accessible roof space; improvements to appearance and resilience of the building; and growing food. Green roofs and/or roof gardens are also cross-referenced in Policy 3.6, covering children and young people's play and informal recreation facilities, Policy 5.3, covering sustainable design and construction, Policy 5.9, covering overheating and cooling, Policy 5.13, covering sustainable drainage, Policy 7.19, covering biodiversity and access to nature, and Policy 7.22 covering land for food. An audit conducted by LivingRoofs in 2010 found 93,712 m^2 of green roofs on 60 buildings in Greater London; a further 15 buildings included green roofs of unknown individual or total size (LivingRoofs, 2010). As with the Sheffield audit, domestic and small green roofs were excluded. Almost two-thirds of the roof area audited was intensive, though these made up less than one-fifth of the total number of roofs. The audit is incomplete and significantly underestimates the level of green roofing in London – both One Bishops Square and The Roof Gardens in Kensington, for example, are excluded; including just these two extra buildings would increase the total measured green roof area in London by 11,400 m^2 or 12%. Kaźmierczak and Carter (2010) state that the total roof area of London greened since 2004 is at least 500,000 m^2.

In Scotland, the Water Environment (Controlled Activities) (Scotland) Regulations (2005) require sustainable drainage for most developments, thereby permitting the use of green roofs as part of a treatment train, but allowing the use of any other source control SUDS device as an alternative. In England and Wales from 2014, Schedule 3 of the Flood and Water Management Act (2010) will also permit, but not explicitly specify, the use of green roofs for the sustainable drainage of most developments, as required by the act.

Modern green roof policy in the UK was originally driven, from the late 1990s, by the desire to replace habitats lost to development, most notably in the case of the Black Redstart and the "brown roofs", initially of London, but now found in other major UK cities. The Black Redstart is a small bird of the Thrush family, whose favoured habitat is small areas of sparsely vegetated rubble or rocky terrain containing vertical structures with many holes and ledges (Greater Manchester Biodiversity Project, 2008). Perhaps unsurprisingly, its UK breeding population was greatly diminished by urban regeneration and the bird became a species protected under

Schedule 1 of the Wildlife and Countryside Act 1981. As an attempt to reverse this population decline, the rocky and sparsely vegetated brownfield sites lost to development were recreated on the roof, achieved by the use of substrates taken from the redeveloped site, spread to a variety of depths and allowed to colonize naturally; the intention of these brown roofs is therefore somewhat similar to that of the bio-diverse roofs of Basel. Comparably, the Green Roof Habitat Action Plan (Rivers *et al.*, 2010), included in the 2010 Sheffield Local Biodiversity Action Plan, contains objectives, targets and actions to increase, maintain and monitor the biodiversity of green roofs in Sheffield.

For further information on green roof policy throughout the world, the report written by Lawlor *et al.* (2006) for the Canada Mortgage and Housing Company is recommended for its global scope and attention to detail. However, some information may be out-of-date, as the report is now seven years old.

2.4.4   Green Roof Performance

2.4.4.1   Field Monitoring Studies

Various studies conducted in many different climates around the world have typically valued the annual retention of extensive green roofs at around 50-80% of total rainfall (Hutchinson *et al.*, 2003; Moran *et al.*, 2004; Bengtsson *et al.*, 2005; Liu & Minor, 2005; Mentens *et al.*, 2006; Getter *et al.*, 2007; Fioretti *et al.*, 2010; Voyde *et al.*, 2010). Notable exceptions are studies conducted by Spolek (2008) in Portland, in the north-west of the USA, and Johnston *et al.* (2004) in Vancouver, in the far south-west of Canada, which both value annual retention at less than 30%. In all annual retention studies, performance is averaged over a long time period; the many factors influencing the retention performance of a green roof at any specific point in time are not taken into account. Antecedent dry weather period, substrate composition, substrate initial moisture content, storm duration and storm intensity are all time-, storm- and spatially-variable factors affecting the depth of rainfall that a green roof is able to retain. In general, the fraction of rainwater that is retained decreases as the storm depth increases, as every green roof has only a finite and limited retention capacity. Conversely, it follows that water retention could approach 100% for small or even reasonably large (20-30 mm) storms under highly advantageous conditions (Stovin *et al.*, 2012; see also Chapter 3 of this thesis). Intensive green roofs could retain even larger storm depths (50 mm or more) under the most favourable conditions, as the approximate maximum retention capacity of a roof is around a quarter of its substrate depth.

Early hydrological research into green roofs mainly focused on determining the annual retention of specific roofs, often buildings (as opposed to purpose-built test rigs). Later, the assessment of retention performance was further divided into season, individual events or categories of event

by depth. Studies which quantify retention performance by event may also quantify other performance metrics, most commonly detention and attenuation. Detention is a figure which quantifies, usually in minutes, the difference between the time at which half of the total depth of a rainfall event has fallen and the time at which the same depth of water is released from the green roof. Attenuation expresses the difference between peak rainfall rate and peak runoff rate, usually as a percentage reduction from one to the other. It is common for the percentage retention associated with one storm to be lower than the percentage attenuation associated with the same storm. Even a green roof with zero retention capacity may have high attenuation performance, as the majority of the attenuation effect results from the slow percolation of water through the substrate. This primarily occurs through pores which are large enough for the effects of gravity to dominate over the effects of capillarity, and hence do not have a capacity for retention. In field monitoring studies, Stovin *et al.* (2012) report a mean per-event retention of 42.7% and a mean per-event attenuation of 59.2% for 21 storms with high return period, while Voyde *et al.* (2010) report a mean of 78% per-event retention and 91% per-event attenuation for all events occurring in a one-year period from 23rd October 2008 to 23rd October 2009. High attenuation performance does, however, imply high detention performance, as greatly-reduced rates of runoff imply relatively shallow cumulative runoff profiles.

Figure 2.7 shows an example rainfall/runoff profile in cumulative (a) and time-series (b) forms. A retention depth of 6.5 mm is shown by the vertical red line on (a), equivalent to 19.9% of the total rainfall depth. A median-to-median detention time, or t_{50}, of 818 minutes is shown by the horizontal red line on (a). Attenuation cannot be clearly shown on a plot of cumulative depth, but can be shown on a time-series rainfall and runoff plot (b) through comparison of the relative heights of the peaks of the rainfall and runoff curves, (vertical red line on (b)).
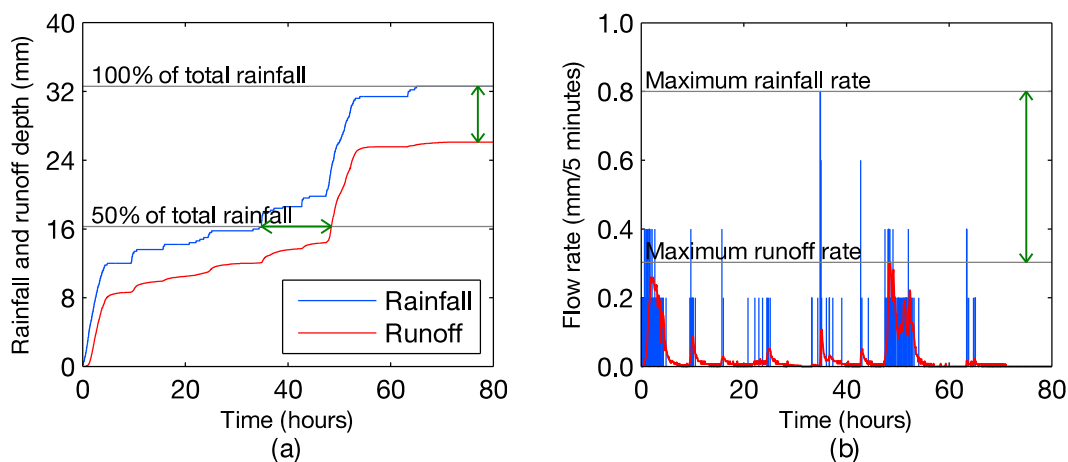
Figure 2.7 – Example cumulative rainfall/runoff profile (a), showing retention depth (vertical green line) ana median-to-median detention time, t_{50} (horizontal green line), and time-series rainfall/runoff profile (b), showing peak flow reduction (vertical green line).

While performance monitoring studies are useful in clearly explaining the hydrological benefits of green roofs to non-specialists, any performance figures associated with one study are dependent upon and inseparable from the system build-up of the roof, the local climate of the area (including microclimatic effects in the immediate vicinity) and, especially in shorter studies, the weather experienced by the green roof over the study period, which may or may not be typical for the area.

2.4.4.2 Coefficient of Discharge/Runoff Reference Value

The simplest and most widespread standardized measures of green roof performance are the coefficient of discharge, C, and run-off reference value, ψ. These measures are related by $C + \psi = 1$. The methodology for calculating either metric can be found in an appendix to "Guidelines for the Planning, Execution and Upkeep of Green Roof Sites" (FLL, 2002). The purpose of both performance measures is to make standardized comparisons of the detention capabilities of different green roof systems possible, by removing many of the inconsistencies associated with field monitoring studies. The methodology specifies one width (1 metre), one gradient (2%) and a choice of only three lengths (2.5, 5 or 10 metres) for the test system, its initial state (field capacity) and constant (laboratory) environmental conditions throughout. To calculate either C or ψ, the test system is first wetted (at an unspecified rainfall rate, though implied to be 1.8 mm/minute due to further instructions) in a rainfall simulator until inflow and outflow rates remain equal over a period of 10 minutes. The system is then left to drain for 24 hours, before a constant block rain of 1.8 mm/minute intensity is applied over 15 minutes. The depth of runoff released from the green roof during the 15-minute rainfall event is divided by the 27 mm depth of rainfall and multiplied by a flow length correction factor (a constant which is specified separately for each of the three permitted rainfall simulator lengths), to give C. The test is then repeated twice more at 24-hour intervals and the mean value taken.

The coefficient of discharge/run-off reference value is simple to obtain for a green roof system and the test procedure is unambiguous. No specialist monitoring equipment is required, as the only measurement taken is the total quantity of runoff at a single time point. Due to its common usage in commercial green roof literature, a value of C can easily be used to compare prototype systems to existing systems. However, each value of C is specific to one green roof system design only, and has no predictive modelling capability. Simply, behaviour of an untested roof cannot be estimated from observations of another similar roof design. As the actual rate of runoff is not recorded at any point in the FLL test, the observations are of limited use to drainage engineers attempting to predict the time-series runoff response to a design storm event. The specification of a single roof slope and rainfall profile in the test procedure also precludes the use of C to predict the runoff response of a green roof installed at any slope other than 2% or under any other rainfall event, including common design storm profiles.

2.4.5 Runoff Modelling

2.4.5.1 Overview

Because of the limitations of field monitoring programmes, in their inability to predict the hydrological behaviour of differently-designed roofs, roofs in other climates or roof response to specific design storm profiles, newer research has in part been directed towards quantifying green roof performance by consideration of the hydrological processes occurring in green roofs. These methods have been adapted from general runoff and flow modelling methods used elsewhere.

The following sub-sections discuss existing research into modelling entire green roof systems. In parallel, the most common runoff modelling methods available, which may or may not be appropriate for hydrological modelling of green roofs, are evaluated. Existing research into green roof systems is discussed in parallel with the principles, assumptions and limitations of the selected modelling methods. Most current hydrological modelling of green roofs has concerned the entire system. However the methods used are equally applicable to the processes occurring in the substrate and drainage layer of the green roof, either separately or combined. They may also be more generically applicable to traditional catchments. It is intended in this thesis to present separate models for the substrate and drainage layers, to allow different system build-ups to be represented by modification and recombination of the models. Methods which are applicable to only one layer are discussed in the sections concerning research into the substrate or drainage layer (2.6.3 and 2.5.4 respectively), along with any existing research using those methods.

Any hydrological models that are selected for the runoff modelling of a green roof, or any of its component parts, should be able to both reproduce existing rainfall and runoff relationships and accurately predict the runoff response to a theoretical rainfall event. Any selected hydrological model should also be appropriate for the component being modelled; it is certainly within the realm of possibility that a model may give superficially good results, but be based on completely wrong interpretations of the underlying processes. The selection of potential hydrological models for the substrate layer is discussed in Section 2.6.3.6. Separately, the selection of potential hydrological models for the drainage layer is discussed in Section 2.5.4.3. It was intended for the two-stage substrate-drainage layer model to be composed of the best tested substrate model in series with the best tested drainage layer model. The selection of sub-models for each of the substrate and drainage layers is therefore discussed at the end of Chapters 5 and 6.

2.4.5.2 Conservation of Volume and Momentum

Central to runoff modelling methods are the principles of conservation of volume and conservation of momentum, though many methods do not apply both together. The equation for hydrologic continuity over a control volume is presented in Equation 2.2:

$$I(t) - Q(t) = \frac{dS}{dt}$$
<div style="text-align: right">**Equation 2.2**</div>

Throughout all modelling discussion in this chapter, the term I will refer exclusively to the input to a model (typically rainfall or inflow) Q will refer exclusively to the output from a model (typically runoff or outflow) S will refer to transiently stored water (with the exception of S_o – bed slope and S_f – friction slope), and t will refer exclusively to time. All terms in Equation 2.2 have dimensions of $[L^3T^{-1}]$.

For a river, it is reasonable to assume conservation of volume, as water is effectively incompressible at the range of typical pressures experienced through a river's depth, water is not created or destroyed, and evaporation to the atmosphere and infiltration through river banks will represent only a tiny fraction of the volume of water contained in a reach. The assumption of negligible evaporation will become more strained for a green roof, as much lower depths of water are considered, though for the particular experimental programmes in this thesis, the amount of evaporation that may take place indoors between closely-spaced tests is also likely to be a small fraction of the total storm depth.

Hydraulic routing methods combine conservation of volume (Equation 2.2) with physical modelling of moving water. Conservation of momentum is often assumed. The Saint Venant equation for conservation of momentum is given in Equation 2.3:

$$\frac{\partial Q}{\partial t} + \frac{d}{dx}\left(\frac{Q^2}{A}\right) + gA\left[\frac{dh}{dx} + \left(S_f - S_o\right)\right] = 0$$
<div style="text-align: right">**Equation 2.3**</div>

where A is hydraulic section, g is gravitational acceleration, h is flow depth, S_f is friction slope and S_o is channel bed slope. Water is a dispersive medium, in which waves of different wavelengths travel at different phase speeds. Momentum cannot automatically be assumed to be conserved in this case. However, conservation of momentum is often assumed in shallow water, which is generally taken to be water whose depth is less than 5% of the wavelength of the modelled waves. This is because dispersion effects are reduced as the wavelength-to-water depth ratio increases, and at ratios of 20:1 or greater, dispersion effects generally become small enough to be ignored. Many of the governing rules for movement of water through a porous medium (e.g. Darcy's Law, discussed in Section 2.6.3.2) are derived from conservation of momentum.

2.4.5.3   Storage Routing

Storage routing methods are based on a re-arrangement of the finite difference form of the volume conservation equation, placing all known parameters on the right side of the equation separately from all unknown parameters on the left side (Equation 2.4):

$$\left(\frac{S_2}{\Delta t} + \frac{Q_2}{2}\right) = \left(\frac{S_1}{\Delta t} + \frac{Q_1}{2}\right) - Q_1 + \left(\frac{I_1 + I_2}{2}\right)$$ **Equation 2.4**

Storage routing methods assume that the rate of outflow from a storage reservoir is related directly, monotonically, consistently and uniquely to the head of water above the point of outflow. Put simply, one volume of water in storage corresponds to only one rate of outflow, which is fixed throughout, and increasing the volume in storage increases the rate of outflow. Hence, even though only the sum of the two unknown parameters on the left side of Equation 2.4 can be directly calculated, separate values of S_2 and Q_2 can still be derived. A table or plot of Q vs. $2S/\Delta t$ can be generated theoretically for any individual storage reservoir as both Q and S are dependent on the geometrical properties of the reservoir and outflow weir. The accuracy of a runoff profile obtained through reservoir routing is linked directly to the accuracy of the theoretical relationship, and errors are propagated through steps. Reservoir routing methods can only be applied in situations where downstream conditions are unable to affect conditions further upstream. It is therefore only applicable where a substantial hydraulic gradient exists (Strelkoff, 1980) e.g. a reservoir spillway. The outlets from both rainfall simulators used during the experimental programmes conducted in this thesis can be considered functionally identical to a reservoir spillway, as it is impossible for flow quantities or effects to propagate back out of the runoff collection barrels.

It is noted that storage routing equations, are normally only used when the stored water has a measurable free surface. In the case of the drainage layer, this means that storage routing is valid for values of h up to the top of the drainage layer, as higher values of h represent water re-entering the substrate from below and the consequent loss of a measurable free surface. However, the in-plane flow capacities of drainage layers are extremely high. ZinCo Floradrain FD 25 at a 2% gradient, for example, has an in-plane flow capacity of 51 litres per minute per metre width (BSI, 2010a). For a five-metre length of drainage layer, 51 litres of inflow per minute is equivalent to a rainfall intensity of 10.2 mm/minute. This is one-third greater than the peak intensity of the 1-in-500 year, 30-minute, 50% summer storm for Sheffield (NERC, 1975) and five times its mean intensity. It is also expected that the substrate layer above would act to attenuate the rate at which rainfall reaches the drainage layer. Due to the relationship between S and Q, storage routing equations are unable to model retention, as $Q > 0$ for all values of $S > 0$. Hence, if any water remains in storage, outflow will occur, depleting the storage, until stored water approaches zero.

Standard storage routing methods have been modified to allow their use in situations where no measurable free surface exists. This is made possible by directly measuring the volume of stored water, S, within a storage reservoir, as the difference between cumulative input volume and

cumulative output volume. Kasmin *et al.* (2010a) and Yio *et al.*(2012) both take this approach, rather than the more usual geometric link via *h*, as both use storage routing in applications where an accurate measurement of *h* is impossible. The choice of hydrological model made by these researchers is unusual, as storage routing methods do not explicitly conserve momentum. Therefore, they are theoretically valid only when a free-surface exists. Nevertheless, the models was demonstrated to predict the recorded runoff with a high level of accuracy, suggesting that the water temporarily detained in substrate pores (i.e. not by capillarity) can be assumed to have a (very small) free surface. Wittenberg (1999) and Vesuviano & Stovin (2012) both considered situations with an obvious free surface, but chose to measure storage via *S* rather than *h*. In both cases, measurement of *h* was deemed impractical in comparison to measurement of *S*.

In most river systems, the relationship between storage and discharge is nonlinear (Tung, 1985). Nonlinearities can be accounted for by including an exponent on either the outflow or storage term. An analysis of flow recession curves obtained from 100 river gauging stations by Wittenberg (1999) demonstrated that the equation $S = aQ^b$ is adequate to describe the relationship between storage and discharge, the mean and standard deviation of *b* being 0.49 and 0.25 respectively. Kasmin *et al.* (2010a) used the same nonlinear method, in its inverse form of $Q = aS^b$, to successfully model the runoff profile of an entire green roof system subjected to individual storms, suggesting a value of 2.0 for *b*, close to the inverse of the mean suggested by Wittenberg (1999).

Any of the variants of storage routing discussed here can be extended to more complex applications and runoff responses by considering multiple storage reservoirs in series (Zimmer & Geiger, 1997; Palla *et al.*, 2012), each with its own parameter values for *a* and *b*. Applied to a green roof, the system may be considered as two reservoirs: a substrate reservoir in series with a drainage layer reservoir. If the hydrological properties of the substrate vary throughout its depth, horizontal slices could be taken through it and each slice treated as one reservoir in a series, however for a well-mixed substrate which is consistent throughout its depth, there is no basis to assume that the hydrological behaviour of the substrate is significantly dependent on depth. Alternatively, different hydrological processes may be modelled by different reservoirs: Palla *et al.* (2012) used two parallel storage reservoirs to model the slow and fast response of the drainage layer, both receiving inflow from the single substrate reservoir.

2.4.5.4 Muskingum Method

The Muskingum method was first developed by McCarthy (1938) from flood control studies of the Muskingum River basin in Ohio, USA. It is based on a finite difference form of the equation for conservation of volume (Equation 2.4), in which total instantaneous storage is expressed as the sum of "prism" and "wedge" storage. For uniform river flow, the volume of water in storage

between two points is given by KQ, where K is the travel time between the two points and Q is the uniform flow rate. This is termed prism storage, S_P, due to the volume of water in uniform flow in a uniform reach taking a prismatic shape. If flow in the river is not uniform, wedge storage, S_W, arises due to the difference between inflow rate at the first point and outflow rate at the second. Wedge storage is given by $Kx(I - Q)$, where x is a dimensionless weighting factor ranging from 0 to 0.5 and all other terms are previously defined. Adding prism and wedge storage together gives the Muskingum equation (Equation 2.5):

$$S = S_P + S_W = K[xI + (1 - x)Q] \qquad \textbf{Equation 2.5}$$

For $x = 0$, $S = KQ$ and the Muskingum equation reduces to that for linear reservoir routing. Substituting Equation 2.5 into the finite difference form of the volume conservation equation gives the Muskingum routing model, which after some rearrangement becomes:

$$Q_2 = \frac{\Delta t - 2Kx}{2K(1 - x) + \Delta t}I_2 + \frac{\Delta t + 2Kx}{2K(1 - x) + \Delta t}I_1 + \frac{2K(1 - x) - \Delta t}{2K(1 - x) + \Delta t}Q_1 \qquad \textbf{Equation 2.6}$$

where all terms are defined previously.

It is clear from Equation 2.6 that the accuracy of the Muskingum routing model depends on the values chosen for K and x. If K and x are not known, they can be calculated by regression analysis, based on a semi- or fully-implicit finite difference rearrangement of the volume conservation equation (Equation 2.4), where Equation 2.5 is used in place of S (Gelegenis & Serrano, 2000). Depending on stability criteria, either scheme may be preferable for any individual case. Both schemes give the same value for K, but the fully-implicit scheme gives an x value that is $\Delta t_{in}/2K$ higher than the semi-implicit scheme. This does mean, however, that an x-value calculated using a traditional semi-implicit scheme can be transferred to a fully-implicit scheme, if doing so would improve the outflow modelling.

In common with storage routing, the Muskingum method is unable to model permanent retention, as the three fractional coefficients on the right side of Equation 2.6 always sum to 1. The Muskingum routing model's stability is greatly dependent on the choice of time step; for stability, $2Kx < \Delta t < 2K(1-x)$ (US Army Corps of Engineers, 1998). This limits the temporal resolution at which the Muskingum method can be used.

The Muskingum method remains popular for routing flood waves in rivers and channels. No published research has attempted to use the method for modelling runoff from green roofs. As it is similar to storage routing, it should be theoretically possible to model green roof runoff using the Muskingum method, though a limited temporal resolution must be used to maintain stability.

2.4.5.5 Unit Hydrograph

A unit hydrograph is a time-series runoff response of a catchment to a spatially- and temporally-uniform rainfall event of an exact duration, usually 10 mm excess precipitation in an hour. Unit hydrograph theory assumes that the catchment's response to longer rainfall events, of varying depths, can be found by discretizing the longer event into a record of consecutive hour-long storms, all of which will most likely produce either more or less than 10 mm of excess precipitation. Each hour's excess precipitation is expressed as a fraction of 10 mm and the unit hydrograph is convolved with this record to give the response of the same catchment to a longer, time-varying rainfall event. All catchments are different, therefore every catchment has a different unit hydrograph. A catchment's slope, surface permeability, vegetation cover, soil type, catchment shape and hydraulic length are some of the many factors that affect the shape of its unit hydrograph. As some factors, such as vegetation cover, are seasonal, a catchment's unit hydrograph is usually averaged from long-term historical data.

The convolution process is represented by the following equation:

$$Q_j = \sum_{j=1}^{N} I_j U_{N-(j-1)} \qquad \textbf{Equation 2.7}$$

where Q_j is the runoff rate at time interval j, I_j is the rainfall depth falling in time interval j and U is the unit hydrograph with ordinates at all time intervals from 1 to N. As Q is typically measured in m^3/s and I is typically measured in mm, U must necessarily take the dimension $10^3 m^2 s^{-1}$.

The unit hydrograph methodology was first proposed and tested by Sherman (1932) using monitored rainfall and streamflow data obtained from watersheds of 1300 to 8000 km^2. Due to the extreme impracticality of monitoring thousands of catchments for sufficient time to develop individual unit hydrographs, Snyder (1938) proposed a triangular synthetic unit hydrograph for catchments with insufficient data records. The synthetic unit hydrograph is defined by three points: peak discharge (U_p), time to peak discharge (T_p) and time base (T_b), which are all estimated from topography. The Soil Conservation Service (United States Department of Agriculture, 1957) smoothed the triangular shape by defining nineteen points which had been derived and averaged from observations of many real small watersheds, to produce a synthetic unit hydrograph intended for generic application to other small watersheds. FEH Supplementary Report No. 1 (Kjeldsen, 2005) introduces a fourth parameter, U_k, to Snyder's synthetic unit hydrograph. This is used to specify the rate of discharge at time $2T_p$ as a fraction of the rate of discharge that would be expected with a triangular unit hydrograph. U_k may vary from 0 to 1, representing all possibilities from a triangle to an infinite time base. It is not allowed to exceed 1, therefore the minimum permitted time base is equal to that of a triangular unit hydrograph.

Runoff predictions made by unit hydrograph methods are less accurate if the storm does not meet assumptions of spatial or temporal uniformity. In typical usage, this may be the result of a real storm moving with time, varying in intensity throughout an hour-long time step or being of varied intensity over the area of the catchment. For a controlled storm in a test chamber, uniformity assumptions are easier to meet and hence the unit hydrograph method will be near its theoretical maximum accuracy. In common with the other generic methods presented, unit hydrographs cannot model retention; the sum of the ordinates is designed to give equality between I and Q. Expected infiltration in a catchment is accounted for by scaling or subtracting from the rainfall record prior to routing with the unit hydrograph.

If rainfall and runoff data are known, a unit hydrograph can be produced from any rainfall-runoff pair by deconvolution. This is the opposite process to convolution and involves deriving the unknown U for a known I and Q. Villarreal and Bengtsson (2005) derived an averaged, 1 mm-in-one-minute unit hydrograph for a green roof test bed, by deconvolution of rainfall-runoff pairs at three constant rainfall intensities and four roof slopes. The unit hydrograph follows the general shape proposed by Kjeldsen (2005), but also features a small rise in runoff rate near the beginning of the falling limb and a second, smaller rise and fall in runoff near the end. This unusual shape may be attributed to noise in the runoff data. The averaged unit hydrograph fitted well to the observed runoff data for constant intensity storms but was also found applicable in tests based on a design storm and two real storms observed in Lund, the Swedish town in which the researchers were based. As the unusually-shaped unit hydrograph was applicable to storms that played no part in its derivation, is likely that the noise in the unit hydrograph profile smoothed out in the convolution with the time-varying rainfall records. However, as a data-based unit hydrograph is applicable only to the catchment for which it is derived, the authors' results are applicable only to a very small (1.54 m^2), very shallow (40 mm) substrate over an unspecified geotextile layer, and are of no use to determining the response of other roofs, beyond showing the validity of the method.

Research published by the author of this thesis (Vesuviano, 2011) suggests that the unit hydrograph approach may not be appropriate to model the processes occurring in profiled board-type green roof drainage layers. It is however noted that the derived unit hydrographs were fitted as exactly as possible to the start of noisy and coarsely-resolved runoff profiles. Instabilities and errors present near the beginning of the time-series runoff profile would then propagate to later time steps, with possible amplification occurring from one step to the next. The runoff data collected in this thesis is of a much finer resolution, both temporally and volumetrically, and exists in smoothed forms. As the design of one particular profiled board is constant, a unit hydrograph derived for one design of drainage board will be generally applicable to all drainage

boards of that design, slope and hydraulic length. It may also be applicable, with minimal loss of accuracy, to other drainage board arrangements of similar surface material, slope and length. However, if a desired roof configuration is between two tested configurations, represented by two different unit hydrographs, the methods for interpolating these to model the desired roof configuration are not well-defined.

2.5   Green Roof Drainage Layer

2.5.1   Design

Sufficient drainage is an essential consideration for green roofs and consequently, the use of drainage layers predates the modern green roof itself. Though they did not intend to produce a green roof at the time, the designers of the Moos lake water-treatment plant understood that if their roof was to carry a layer of soil, a sub-soil drainage layer would be necessary to prevent waterlogging. In modern green roof terminology, the drainage layer used there is referred to as a "granular drainage layer". This is the older of the two commonly-used classes of drainage layers on green roofs. As the name suggests, granular drainage layers consist of large particles such as gravel, pumice or expanded shale, with large voids to allow free movement and rapid drainage of liquid water which has percolated through the substrate. The second and more commonly-used class of drainage layer is the synthetic module-type drainage layer, which originated in the 1970s as an engineered component in the design of the modern green roof. Synthetic drainage layers are formed in hard plastic (high density polyethylene, polypropylene, high impact polystyrene etc.), rubber or expanded polystyrene modules. Four forms of synthetic drainage layer are common (Figure 2.8); each has specific attributes, discussed in more detail in Section 2.5.2, which are advantageous to different roof designs and fulfil secondary functions.

1.   Geocomposite mesh (e.g. Xero Flor XF 108, Colbond Enkadrain ST) – The drainage layer consists of a layer of a non-woven plastic (e.g. polyamide) mesh with loops, containing a very high proportion of large voids through which water is transported with little

| (a) | (b) | (c) | (d) |
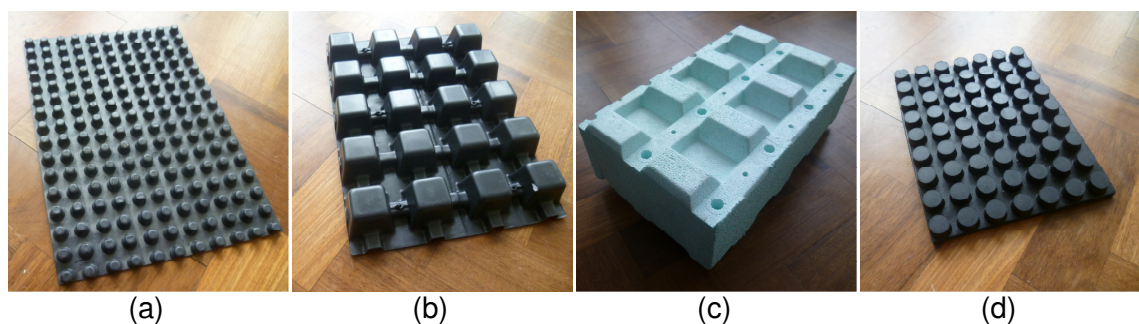
Figure 2.8 – A selection of drainage layers: Type 1 – ZinCo DBV 12 (a), Type 2 – Zinco Stabilodrain SD 30 (b), Type 3 – Zinco Floratherm WD 120-H (c), Type 4 – Zinco Elastodrain EL 202 (d).

resistance. This mesh layer is laminated with filter material to prevent substrate from washing into the drainage layer. Mesh drainage layers can be extremely thin and lightweight, but have a design water holding capacity of zero.

2. Profiled board (e.g. ZinCo Floradrain FD 25, Bauder DSE 20, Lindum Roofdrain 40) – The drainage layer consists of a thin layer of hard plastic moulded into a regular three-dimensional pattern containing cup-like storage receptacles and channels. This gives some models the appearance of egg boxes or blister packs. The top of the drainage layer is bridged by a filter sheet to keep out the overlying substrate. The profiling of the drainage layer is designed to provide a system of channels on the underside which allow free drainage of water, and cups on the top side to store an additional quantity of moisture that has percolated through the substrate, which then transfers back into the substrate via evaporation during dry periods, consequently providing a supply of moisture over a long time period. The highest points on the surface profile usually also feature small holes, which allow water stored below the drainage layer (in a protection/moisture mat) to evaporate into the substrate. Profiled drainage layers can be made in a variety of depths, although some of the deepest do not provide as much moisture storage as would be expected, as they are required to be filled with gravel on the upper side.

3. Expanded polystyrene (e.g. ZinCo Floratherm WD 180, ZinCo Floratec/Floraset FS 75, Axter Drain) – These are deep polystyrene modules with water storage receptacles formed in the upper surface profile. Expanded polystyrene drainage layers may be used for two purposes. First, designs with deep profiled troughs on the upper side may be used on sloped roofs without a filter sheet, to hold substrate in place against shear forces. Second, deeper modules are used to take advantage of the opportunity to provide extra insulation outside of the waterproofing layer when converting an existing roof to a green roof. Expended polystyrene modules are very light and certain models have high water holding capacity in their deeply profiled troughs. However, some models have no water holding capacity and most models require large depths to provide significant insulation capacity; ZinCo Floratherm WD 180 is 180 mm deep, which is deeper than some entire extensive green roof assemblies.

4. Rubber mat (e.g. ZinCo Elastodrain EL 202) – These are rubber sheets with a flat underside and a large number of studs on the upper side. The studs are bridged by a filter sheet to preserve the air gap existing between the studs. Water flows only along the top surface of the sheet, largely unimpeded. Rubber mats are strong enough to be used underneath areas with high traffic and heavy vehicles, including lorries. They are also shallow; Elastodrain EL 202 measures only 19 mm high. However, they are relatively

heavy and their design water storage capacity is zero. As the rubber itself is very tough, and water only flows over the upper surface of the mat, a separate protection/moisture mat is not used underneath these drainage layers. There also exists a type of profiled board bearing physical resemblance to the upper side of a rubber mat drainage layer, with no water storage capacity, little resistance to flow, no flow on the underside and a very small thickness (e.g. Bauder PLT 10, ZinCo DBV 12). These are not intended to compete with rubber mat drainage layers, but rather with geocomposite mesh drainage layers.

Certain experimental green roofs have featured drainage layers consisting of rubber crumbs as a substitute for conventional granular materials (Cabeza, 2012; Vila *et al.*, 2012), due to the ready availability of old car tyres. Rubber crumbs are already used as a replacement aggregate in some drainage applications, though not in green roofs.

2.5.2 Function

The primary function of a green roof drainage layer is to quickly remove excess water from the roof. In order to provide hospitable growing conditions for plants, green roofs are carefully designed to mimic the natural environment of the plants that they support. Extensive green roofs, which usually feature mainly alpine and rockery species, are therefore designed to recreate alpine/rockery-type conditions. In the context of an alpine/rockery environment, the drainage layer emulates the porous rock layer that lies beneath the thin layer of humus.

In addition, a green roof drainage layer may serve various secondary functions. Not all drainage layers serve all possible secondary functions; some are specific to certain designs. The primary and secondary functions of a green roof drainage layer are discussed in more detail below.

2.5.2.1 Removal of Excess Water

This is the primary function of all drainage layers, whether they are granular or synthetic. Proper drainage is important to prevent damage to the roof membrane that could result from continuous contact with water or wet substrate (Dunnett & Kingsbury, 2004), and to prevent waterlogged conditions in which plant roots may rot. Furthermore, the species commonly used on extensive green roofs are drought tolerant and are adapted to thrive in dry conditions. Efficient drainage is essential to mimic the natural environment of these plants, providing the necessary conditions for them to thrive. Due to the requirement for drainage layers to quickly remove excess water, detention times in the drainage layer are generally assumed to be small.

2.5.2.2 Aeration of Substrate

As a result of the air gap present in a drainage layer, the bottom of the substrate layer is always in contact with air. This provides a necessary route by which the substrate is aerated. All drainage layers, both granular and synthetic, serve this secondary function.

2.5.2.3 Storage of Water

Drainage layers with profiled surfaces on the upper side store additional runoff that exceeds the storage capacity of the overlying substrate in cup-like receptacles. Examples include profiled boards such as ZinCo's Floradrain series or Bauder's DSE series, and expanded polystyrene modules such as ZinCo's Floraset series. The drainage layers in each of these series are available in a wide variety of depths: 20/25 mm, 40 mm and 60 mm for both the ZinCo Floradrain and Bauder DSE series. However, the water holding capacity of the deeper drainage layers in a series is not as high as might be expected, as the receptacles are required to be filled with granular media, which occupies some of the volume that would otherwise be available for water storage. The listed water storage capacities of Floradrain FD 25, FD 40 and FD 60 are 3 l/m^2, 4 l/m^2, and 5 l/m^2, respectively, when filled with granular media. The effectiveness of storing water in drainage layers is disputed. Miller (2003a) states that the incorporation of a retention/drainage sheet is frequently an additional unnecessary expense, as many green roof media will retain over 30% water by volume. This is indeed a higher percentage retention than is offered by any commonly-available drainage layer (ZinCo Stabilodrain SD 30 is notable for its maximum capacity of 7.5 mm of water, equivalent to 23% of its height). However, since it is usually necessary to include a drainage layer in a green roof system for functions other than water storage, the storage capacity of one drainage layer can be considered a bonus over the lack of storage capacity of another drainage layer of similar depth.

Because of the matrix of large voids between the particles, the water storage capacity of a purely granular drainage layer is near-zero. Geocomposite mesh and rubber mat-type drainage layers do not feature profiled troughs on their upper surfaces. Hence, the storage capacity of these synthetic drainage layers is near-zero also.

2.5.2.4 Provision of Moisture during Dry Weather Periods

Immediately following a rainfall event, moisture is retained in the substrate. The quantity of moisture in the substrate may be greater than the substrate's field capacity, in which case the excess will drain away soon after the end of the storm. The moisture that remains may be depleted by evaporation and transpiration at a rate typically around 1-2 mm/day, rising to 3 or more mm in summer (Kasmin *et al.*, 2010a). Considering that the substrate of an extensive green roof is able to store a maximum of approximately 20-30 mm of water, this supply will be depleted within the first few days after a typical summer storm. The water retained by the protection/moisture mat and drainage layer is separated from the substrate by an air gap; therefore it cannot be drawn up into the substrate by capillary rise to replenish the moisture lost by evapotranspiration in the substrate. This air gap is also an effective barrier to plant roots, so plants cannot directly access this source of water. The main mechanism by which water is transferred upward from a drainage layer or protection/moisture mat with water holding

capacity, to the substrate, is evaporation, so the rate of depletion is very low (see Appendix A for further information). Consequently, water retained by the drainage layer and protection/moisture mat is available, albeit in more limited quantities, for much longer periods after the end of a rainfall event. This is beneficial to the plants during long droughts.

It is interesting to note that if only the substrate is considered, the two functions of rainfall retention and moisture provision conflict, as a high rate of moisture loss between storms is required to quickly recharge the substrate's retention capacity, but a low rate of moisture loss allows plants to access water for a longer time period after each storm.

2.5.2.5 Root Growth

Granular drainage layers, and synthetic drainage layers with granular infill, may provide additional space for plant root growth. Plant roots are often found extending into granular drainage layers, due to the aerated environment, and relatively stable temperature and moisture conditions (Dunnett & Kingsbury, 2004). Conversely, plant roots very rarely enter other types of synthetic drainage layer, as a continuous void is immediately encountered below the bottom of the substrate layer.

2.5.3 Exclusion of the Drainage Layer

As has been shown above, all drainage layers provide the primary function of removing excess water from the roof and the secondary function of aerating the substrate. Some also perform the secondary functions of storing water, providing that moisture back to the substrate during dry weather periods and providing extra space for root growth. Johnston and Newton, writing for the London Ecology Unit (now the Greater London Authority), state that a roof pitched at 10-15° will drain naturally by gravity, rendering a drainage layer unnecessary (Johnston & Newton, 1993). Considering this advice in the context of the wider benefits offered by the drainage layer, it is not clear how eliminating the drainage layer will provide aeration to the substrate or allow for long-term storage and hence the provision of water during extended droughts. These additional benefits explain the widespread use of drainage layers on green roofs of all roof slopes.

2.5.4 Drainage Layer-Specific Modelling Methods

2.5.4.1 Overview

Though the synthetic green roof drainage layers (particularly the profiled boards) are the most widely used types, their hydrological behaviour is poorly understood. Consequently, the design of profiled board drainage layers has evolved through empirical observation. In fact, as of January 2014, only one article relating specifically to the properties of drainage layers has been published in a peer-reviewed journal (Vesuviano & Stovin, 2013) and this was lead-authored by the author

of this thesis. Two conference papers have been presented on this topic; both were presented by and either written or co-written by the author of this thesis (Vesuviano, 2011; Vesuviano & Stovin, 2012).

Drainage layer-specific modelling methods are those which are appropriate to model the processes occurring in a synthetic drainage layer, but not in the substrate layer. These methods more generally describe the movement of water through an open channel with a free surface. For granular drainage layers, either generic or substrate-specific methods should be used.

2.5.4.2   Spatially-Varied Unsteady Flow

The spatially-varied unsteady flow equations are a kinematic wave approximation to the shallow water equations. They are used to model time-varying water surface profiles resulting from the addition of water to a channel (e.g. simulated rainfall landing on a green roof component). "Spatially-varied" refers to variations in the depth of flow along the considered channel, while "unsteady" refers to variations in depth through time at fixed monitoring points. The 1-D form of the spatially-varied unsteady flow equations, for vertical rainfall, is presented below:

$$\frac{\delta h}{\delta t} + h\frac{\delta u}{\delta x} + u\frac{\delta h}{\delta x} = I$$

Equation 2.8

Equation 2.9

$$\frac{\delta u}{\delta t} + u\frac{\delta u}{\delta x} + g\frac{\delta h}{\delta x} = g(S_o - S_f) - \frac{uI}{h}$$

where h is flow depth, u is spatially-averaged velocity, g is gravitational acceleration, S_o is bed slope and S_f is energy slope. Being based on the shallow water equations, the spatially-varied unsteady flow equations conserve both mass (Equation 2.8) and momentum (Equation 2.9). Excluding a few idealized cases, these equations can only be solved numerically.

By discretizing the drainage layer along its length, the equations can be solved numerically over short distances, allowing the flow profile within the drainage layer to be approximated. The volume of water in each discrete element at each time step can be summed cumulatively and subtracted from the cumulative inflow volume to give the cumulative outflow volume at each time step. The time-series runoff profile can easily be derived from the cumulative profile by evaluating the differential increase in runoff depth over each time step. However, the use of 1-D equations may not be valid, as the shape of the free water surface will be complex for a typical profiled drainage board e.g. ZinCo Floradrain FD 25. 2-D overland flow equations can be used, though these are even more computationally complex than the 1-D equations presented above.

She & Pang (2010) use the SWMM RUNOFF module to model the drainage layer in their comprehensive green roof model. This combines the Unsteady State Continuity Equation

(Equation 2.8) with Manning's Equation, but without the additional use of the Unsteady State Momentum Equation (Equation 2.9), to give a nonlinear routing model. The SWMM RUNOFF equation is presented in Equation 2.10.

$$\frac{dh}{dt} = I(t) - \frac{W}{An}h^{5/3}S_o^{1/2}$$ **Equation 2.10**

where A is plan area of growing medium above drainage layer, $i(t)$ is flow input to drainage layer, n is Manning's roughness coefficient, W width of the routing surface and all other terms are defined previously. In Equation 2.10, the use of S_o, rather than S_f, necessitates that the energy slope and channel bed slope are equal. Strictly, this necessitates uniform flow conditions. However, fine spatial discretization may allow for S_o and S_f to be approximated as equal over each step. The factor of 1.49 shown before W in the SWMM manual (James *et al.*, 2000) is omitted in Equation 2.10, as it reduces to 1 following conversion from imperial to metric units.

A Manning's n of 0.05 is used to describe the roughness of the drainage layer in She & Pang's research (She & Pang, 2010), which, depending on the physical form taken by the drainage layer, could easily be an unrealistic over-estimate e.g. in the case of a smooth plastic profiled board. The drainage layer is not described in that paper or an earlier paper by Hutchinson *et al.* (2003) concerning the same roof.

2.5.4.3   Model Selection

In comparison to the generic methods given in Section 2.4.5, the one method given above for modelling the drainage layer is complex and likely to require high processing power and time. For the drainage layer, nonlinear storage routing and Muskingum routing will both be tested, as both models have precedent of working successfully the field of runoff modelling and neither method requires significant parameterization or processing time. The SWMM RUNOFF equation will be combined with conservation of volume (Equation 2.2) to produce a variation of nonlinear storage routing, in which the exponent parameter is fixed at 5/3 and Manning's n calculated for each drainage layer test. This model will be evaluated as a physically-based method for estimating nonlinear storage routing parameters. The spatially-varied unsteady flow equations will not be tested or validated, except in the indirect form used by SWMM's RUNOFF module, as direct validation would require the generation of an entire surface profile for each time step, greatly over-complicating the modelling of runoff from the drainage layer. Furthermore, it is particularly difficult to imagine how the three-dimensional surface of a profiled board-type drainage layer might be modelled using such a method. Collecting the necessary data for direct validation is considered to be infeasible in the extreme; each cell in a discretized grid representation of the drainage layer would require its own equipment for measuring depth, which would not be permitted to interfere with the flow.

2.6   Green Roof Substrate

2.6.1   History

Being the component in which vegetation is grown, a growing medium has featured on green roofs since antiquity. Throughout history, traditional roof gardens have tended to emulate ground-level gardens in their planting and design. Furthermore, the concept of designed and mass-produced substrates was not introduced until around two decades after the concept of the green roof began to be re-examined in the modern era. Hence, for most of history, substrates have consisted purely of local, readily available soils. Considering traditional, primarily recreational, uses of green roofs, the lack of an engineered substrate would not have been a problem. For insulation purposes, the use of local soils may still be advantageous over the use of substrates, which are assumed to provide no insulation (Anderson, 2006). For roof gardens and camouflaging underground buildings, the fact that local soils naturally support local plants may well have been desirable. An historical exception to the use of purely local soils occurred on the apartment blocks built throughout Germany at the end of the 19th century, in which a mix of sand, gravel and sod was used for the specific purpose of fire protection (Köhler, 2006). With the possible exception of these, traditional green roofs were usually built only as one-offs, for which the increased costs and difficulties associated with the use of the most readily available, rather than the most optimal substrate, would not have been a serious concern. Systematic research into and improvement of the growing medium did not begin until the 1960s, when lighter and shallower alternatives to soil layers were first considered (Dunnett & Kingsbury, 2004). After this standardization, green roofs began to be produced and installed in larger numbers.

2.6.2   Hydrologic Performance and Key Influencing Factors

2.6.2.1   Overview

By mass, the substrate is the most substantial component of a green roof. It is the component in which the majority of retained runoff is stored and it is necessary to support vegetation. Hence, the major concerns for substrate design are: low density, composition matched to vegetation, high volumetric moisture holding capacity and sufficient drainage, matched to vegetation.

When considering green roofs on a continuous scale, from very shallow extensive to very deep intensive, four main substrate properties vary in line with substrate depth. These are: Grain size, from coarse to fine; water retention, from low to high; Air volume, from high to low; and nutrient reserves, from low to high (Alumasc, 2010). The first three of these properties are interrelated, as smaller particles are able to pack more tightly, reducing the air volume. Smaller average grain sizes also result in a higher percentage of the voids in the substrate being sufficiently small to allow water to be held by capillarity. A selection of modern substrates is shown in Figure 2.9.

2.6.2.2   Substrate Composition

Since the development of modern green roofs, a variety of materials has been used or proposed for the substrate. Commercially available substrate mixes generally use crushed brick as the primary base material. Mineral aggregates, compost, coir and clay soil may also be added in lesser quantities, the exact ratios varying between and, to a lesser extent, naturally within different mixes. Other additives, such as crumb rubber (Ristvey *et al.*, 2010), paper ash and clay/sewage sludge (Molineux *et al.*, 2009), and biochar (Beck *et al.*, 2012), are currently largely confined to experimental observation. Pending further research into its suitability, crumb rubber may find itself incorporated into standard green roof system build-ups, due to its low density and the relative sustainability of its source (waste tyres, of which a large surplus exists). Biochar, the production of which is carbon net-negative, may be incorporated into standard intensive green roof substrates in the future. The FLL guidelines set maximum permissible percentages for clay and silt content in substrates (FLL, 2008). In keeping with the expectation that grain size reduces as substrate depth increases, the maximum permissible percentage of clay and silt is set at 20% by mass for intensive green roofs but only 7% by mass for single-course construction extensive green roofs. Permissible granulometric distributions are specified separately for intensive, multiple-course extensive and single-course extensive substrates. The maximum organic content is also specified in the guidelines: from 4-12% by mass, depending on the substrate density and roof classification. Furthermore, the use of mineral aggregates may be restricted by FLL guidelines that specify maximum levels of nitrogen, phosphorus (pentoxide), potassium (oxide) and magnesium. These restrictions also necessarily influence the permissible fertilization regimes of an intensive green roof.

The choice of component materials can be varied to provide favourable conditions to certain species or to prevent certain species from establishing. For example, nutrient-poor substrates will not be an impediment to the growth of *Sedum* species, but will discourage many other species against which the *Sedum* may otherwise have to compete. Increasing the organic content of the roof slightly will allow more species to establish, at the expense of *Sedums*. Increasing the

(a)   (b)   (c)   (d)
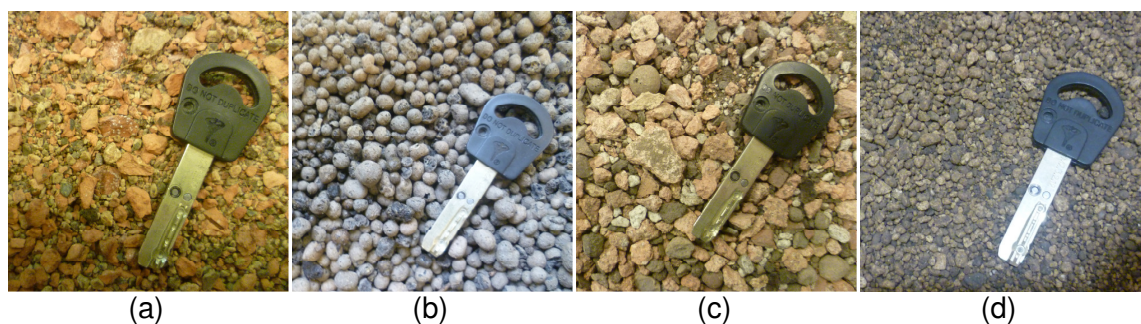
Figure 2.9 – A selection of substrates: Marie Curie substrate mix (a), LECA mix (b), ZinCo Heather with Lavender (c), pumice, a component of many substrates (d).

organic content further may allow a different set of species to thrive, out-competing both *Sedums* and those plants which benefitted from a slight increase in organic content. The conditions on brown roofs are favourable to plant species which inhabit derelict land precisely because substrates which mimic the ground at brownfield sites are used.

2.6.2.3   Depth

As implied in Section 2.4.2, the depth of the substrate can be used to control the plant species establishing on a green roof. Substrate depths of around 80 mm or less are generally only suitable for succulents; most commonly a mix of *Sedum* species is used on these roofs. *Sedums* will thrive in a thin layer of poor soil that would not be able to support most other plant species. Increasing the depth slightly to 100-120 mm will allow meadow grasses to grow, but will not store and supply water in sufficient quantities to allow for the long-term healthy establishment of e.g. lawn grasses. As the depth of substrate is increased further, more and larger species are able to thrive. Conversely, species which can establish themselves successfully on thin substrate layers may find themselves out-competed in deeper substrate layers.

2.6.2.4   Moisture Storage/Retention

FLL guidelines set minimum water storage capacities for green roof substrates: 20% for single-course extensive, 35% for multiple-course extensive and 45% for intensive green roofs (FLL, 2008). A maximum water storage capacity of 65% is also set for all roofs, to prevent waterlogging. All of these values refer to the "field capacity", meaning the amount of water that can be held by the substrate against gravity. This is lower than the saturation capacity, which is the maximum amount of water that can be temporarily held in the substrate before ponding occurs on the surface.

The moisture storage capability of a green roof substrate is dependent on two factors already discussed – composition and depth.

Pore space sizing, a property dependent upon substrate composition, is also a controlling factor on moisture storage in green roofs. If pore spaces are too large, water will drain from these voids under gravity. If pore spaces are too small, plant roots will be unable to provide the necessary suction required to extract the water from the voids. Hence, too-large pore spaces will increase the saturation capacity of a substrate, but reduce its field capacity. Too-small pore spaces will increase a substrate's field capacity, even though the water stored in these pores is inaccessible to plants. The term "permanent wilting point" refers to the storage capacity of a substrate when all of the plant-accessible water is exhausted. Gregory *et al.* (1999) state that the wilting point for silt loam is as high as 9% volumetric water content. However, both intensive and extensive substrates consist primarily of sand and larger particles, which contain, on average, larger pores.

Research conducted on coconut coir dusts by Abad *et al.* (2005) shows that the air volume and field capacity are both controlled almost entirely by the inter-particle pore spacing existing between particles of diameter 0.125 to 1 mm. In this study, the effects of intra-particle pore spacing (i.e. relating to pores on the surface of particles) are not assessed. However, as only one material, coir dust, is used throughout the experimental programme, the effects of intra-particle pore spacing should be relatively constant across all tests. The importance of intra-particle pore spacing upon water holding capacity means that the choice of substrate material can influence the water retention performance of a substrate. Material choice can become important, as maximum and minimum water storage capacities for green roofs are set in the FLL guidelines.

As substrate depth relates linearly to total substrate volume then, assuming no other factors are varied, total volume for moisture storage scales linearly with substrate depth.

2.6.2.5 Detention of Runoff

As well as permanent retention of moisture, the substrate layer can temporarily detain runoff in its network of voids. After the end of a storm, the detained runoff drains away gradually under gravity. Detained runoff is therefore held at a volumetric water content between the substrate's field and saturation capacities. It is this temporary storage volume that allows for significantly reduced peak runoff rates, relative to rainfall rate, even in roofs with no free retention capacity. Following a storm, the rate of runoff can clearly be seen to reduce with time (see time-series runoff profiles in Chapter 6). Fonteno (1993) states that, as volumetric water content in a substrate decreases, water movement is conducted mainly through smaller pores and more tortuous flow paths.

Detention of runoff relates primarily to the ability of a green roof to temporarily hold water at a high volumetric content in its substrate. A long detention period is beneficial from a storm water management perspective, as it corresponds to a low rate of roof runoff. However, the detention period also corresponds to the period over which the substrate's volumetric water content is higher and its volumetric air content is lower than can be sustained in the long-term. Therefore, the detention period, as well as being long enough to reduce peak flows from the roof to a required design specification, must also be short enough to prevent rotting of the plant roots. It should be noted that rotting is not a concern if only retention in the substrate is considered, as the purpose of the maximum water storage capacity (equivalent to field capacity) specifications, given earlier, are to prevent waterlogging under long-term conditions.

2.6.3 Substrate-Specific Modelling Methods

2.6.3.1 Overview

Substrate-specific modelling methods are those which are applicable to the hydrological processes occurring in the substrate, but inapplicable to the hydrological processes occurring in the drainage layer. These methods all describe the movement of water through a porous material. As such, they are equally applicable to granular drainage layers. In all methods, ponding and/or surface runoff will occur if rainfall rate exceeds infiltration rate. However, the permeability of substrates is sufficiently high that neither surface runoff nor ponding should ever occur (Miller, 2003b).

For all equations presented in Section 2.6.3, ψ is defined as wetting front soil suction head, θ is defined as substrate water content and K is defined as hydraulic conductivity, with U and S subscripts referring respectively to unsaturated and saturated. Note that the definition of K used in substrate-specific modelling methods is different from the definition of K used in the Muskingum routing model (Section 2.4.5.4); this usage is consistent with the standard terminologies of the respective methods.

2.6.3.2 Darcy's Law

Darcy's Law is an expression of conservation of momentum that describes the flow of fluid through a porous medium. It was initially determined empirically (Darcy, 1856), and was experimentally verified on numerous occasions before finally being derived theoretically from the Navier-Stokes equations over a century later (Hubbert, 1957). A simplified version of Darcy's Law is used generically to model infiltration to the ground. This equation can be simplified further for green roof substrates, by removing the term accounting for ponded water:

$$f = K_S \left[\frac{\psi + L}{L} \right] \qquad \textbf{Equation 2.11}$$

Where f is infiltration rate and L is the total depth of substrate.

Darcy's Law therefore assumes the rate of infiltration to be constant. If an accurate value for ψ is known, Darcy's Law can be used to determine the runoff time delay introduced by a substrate layer. The runoff profile can be calculated by conservation of mass, relating the volume of rainfall input to the system to the volume of water infiltrated within the depth of the substrate at regular time intervals.

However, as Darcy's Law is applicable only to saturated media, which green roofs substrates very rarely are, it is poorly suited to understanding the hydrological processes occurring in a substrate layer. She & Pang (2010) incorporate Darcy's Law into a comprehensive green roof model, to

calculate infiltration when the substrate is saturated. The comprehensive model includes provision for surface ponding, though this should only be considered a theoretical contingency for a competently designed and maintained green roof. This model, which also includes Green-Ampt infiltration (Section 2.6.3.3), was calibrated against two storm events. One monitored runoff record was fitted well, while peaks in the runoff profile, aside from the single largest, were noticeably overestimated for the other. The model was then verified against a continuous 36-month record of rainfall and monitored runoff from the West Wing of the Hamilton Apartments Building in Portland, Oregon. The absolute error between monitored and modelled runoff was 10%; the authors do not state the sign of this error, though a fifty-day rainfall-monitored runoff-modelled runoff record presented by the authors suggests that monitored runoff was over-estimated, due to the modelled peak runoff rates being noticeably higher than (often double) the monitored runoff peaks.

2.6.3.3   Green-Ampt Infiltration

The Green-Ampt method (Heber Green & Ampt, 1911) generates an infiltration profile over a period of time, accounting for soil suction head, porosity and hydraulic conductivity. It assumes a wetted zone moving downwards through a soil column, with a sharply-defined horizontal boundary between the wetted soil above and the soil at initial water content below. The governing equation is given in Equation 2.12:

$$f(t) = K \left[\frac{\psi \Delta \theta}{F(t)} + 1 \right]$$

Equation 2.12
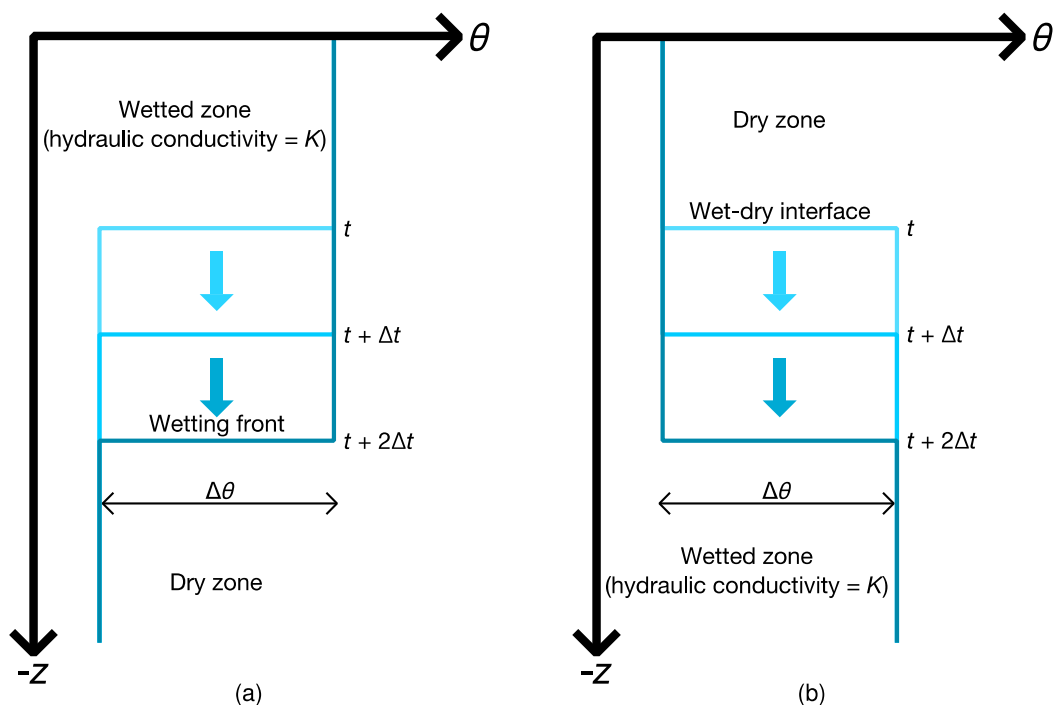
Figure 2.10 – Green-Ampt Infiltration, with advancing (a) and receding (b) wetting front.

where f is infiltration rate at time t, F is cumulative volume infiltrated and unsubscripted K is effective hydraulic conductivity of the wetted zone. A graphical representation of the processes in Green-Ampt Infiltration are given in Figure 2.8.

In contrast to Darcy's Law, the modelled rate of infiltration is not constant. At a time when F becomes equal to the maximum volume that can be held in the substrate layer, runoff will begin to emerge. With appropriate parameter values, the runoff delay introduced by a substrate layer can be determined and, similarly to Darcy's Law, the time-series runoff profile can be generated implicitly from the time-series rainfall and infiltrated water profiles.

The comprehensive model proposed by She & Pang (2010) uses Green-Ampt infiltration to calculate the advancement of a wetting front through a substrate layer when substrate moisture content is below saturation, taking effective hydraulic conductivity K as equal to K_S. This contrasts with the ASCE's recommendation that K be set equal to $K_S/2$ in the absence of more accurate information (American Society of Civil Engineers, 1996).

2.6.3.4 Richards Equation

The Richards Equation was devised in 1931 to model the movement of water in the unsaturated (vadose) zone (Richards, 1931). It is equivalent to Darcy's Law with an added requirement for continuity of volume. In the vertical dimension (z, measured upwards from a surface datum), the governing equation is given by Equation 2.13:

$$\frac{\partial \theta}{\partial t} = \frac{\partial}{\partial z}\left[K(\theta)\left(\frac{\partial \psi}{\partial z} + 1\right)\right]$$

Equation 2.13

where all terms are defined previously.

By substituting $h = \psi + z$ (i.e. hydraulic head equals pressure head plus vertical elevation) and rewriting hydraulic conductivity as the product of saturated and relative conductivities, Equation 2.14 is given:

$$\frac{\partial \theta}{\partial t} = \frac{\partial K_S K_R(h)dH}{\partial z^2}$$

Equation 2.14

Where K_R is relative hydraulic conductivity and H is total head. The Hydrus-1D software package, developed by Šimůnek *et al.* (1998) and published by PC-Progress, numerically solves the one-dimensional Richards equation for saturated-unsaturated water flow in the form given in Equation 2.14. To solve this equation, K_R and θ are required to be expressed as functions of pressure head (Healy, 2010). Relationships between K_R, θ and h can be determined experimentally, but measurements are both expensive and time-consuming (Dane & Topp, 2002). A number of empirical equations exist (e.g. van Genuchten, 1980; Vogel & Císlerová,
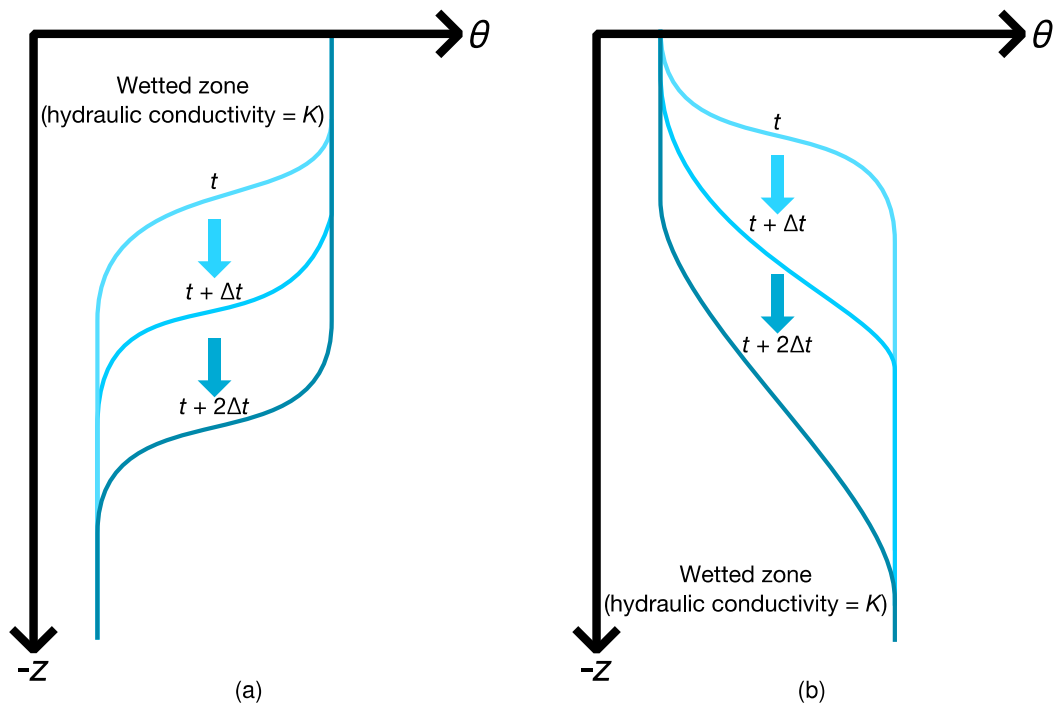
Figure 2.11 – Example soil depth-water content profiles for advancing (a) and receding (b) wetting front, according to Richards Equation.

1988; Kosugi, 1996) to determine these relationships in the absence of experimental data. The van Genuchten (1980) equations for K_R as a function of h and θ as a function of h are given in Equations 2.15 and 2.16.

$$\theta(h) = (\theta_S - \theta_R)[1 + (\alpha h)^n]^{-m} + \theta_R \qquad \textbf{Equation 2.15}$$

$$K_R(h) = \frac{\{1 - (\alpha h)^{n-1}[1 + (\alpha h)^n]^{-m}\}^2}{[1 + (\alpha h)^n]^{m/2}} \qquad \textbf{Equation 2.16}$$

where θ_R and θ_S are residual and saturated soil water contents respectively, α is the inverse of the air-entry value, n is a pore-size distribution index and $m = 1 - 1/n$. These are implemented in Hydrus-1D as the default method for determining values of K_R and θ.

Hydrus-1D can be used to directly generate profiles of time- and depth-varying water content in a block of soil (Figure 2.9), and to model the fluxes through its upper and lower boundaries. By setting appropriate boundary conditions, soil parameters and a time-series record of precipitation, it is possible to model the time-series runoff from a green roof in response to a storm event.

Hilten *et al.* (2008) modelled runoff from Green Roof Blocks, a modular system with 100 mm of substrate (80% expanded slate, 20% worm castings) and no drainage layer, using the software package Hydrus-1D v4.04 (Šimůnek *et al.*, 2008) to numerically solve the Richards equation for

variably saturated media discretized into finite elements. Wilting point, field capacity and density were measured from samples of the substrate. Texture was described as 100% sand to consistently provide model closure; the authors identified that this was not a rigorous description of the substrate texture. Estimates of the substrate's residual and saturated moisture content, and hydraulic conductivity, were estimated by Rosetta Lite (Schaap *et al.*, 2001), a neural network prediction function incorporated into Hydrus-1D. These known and derived parameters were then used to model the time-series runoff profile of the Green Roof Blocks in response to 24-hour SCS Type-II design storms (United States Department of Agriculture, 1992) of 1.27, 2.54, 3.81, 5.08 and 7.93 mm depth. The runoff curves produced were of an unusual shape, generally consisting of a very long delay to the start of runoff, followed by a very steep rise in runoff rate, followed by a close match to the shape of the time-series rainfall profile. Possible reasons for this include the incorrect specification of substrate texture, the extremely small range between specified initial moisture content at 0.1 and field capacity at 0.11, and the model's possible under-estimation of attenuation: the model is known to over-predict total runoff volume. It is also highly questionable that the model reported 1.7 mm retention for the four largest design storms, when the available storage depth at the start of each storm is a 0.01 fraction of the 100 mm substrate depth i.e. 1 mm. The modelling phase was not verified experimentally.

The use of Hydrus-1D was extended by Palla *et al.* (2012) to a 356 m^2 intensive green roof system on the environmental engineering laboratory at the University of Genova. In addition to a 200 mm depth of Vulcaflor intensive substrate (Europomice, 2011a), the modelled green roof system also has a granular drainage layer, consisting of a 200 mm depth of Lapillus (Europomice, 2011b). Both layers were modelled in Hydrus-1D, as both are variably-saturated granular media. The hydraulic parameters required by the infiltration module were either literature referenced from Carsel and Parrish (1988) for similar soil textures (empirical constants α and n) or calibrated from five events (saturated and residual water contents, and saturated hydraulic conductivity). The model, with referenced and calibrated parameters, was applied to calculate time-series runoff from five validation events. For both single- and multi-peaked runoff responses, the model produced acceptable results, quantified by high Nash-Sutcliffe Efficiency (NSE, equivalent to R^2) values. However, NSE was consistently lower for the five validation events (mean 0.788) in comparison to the five calibration events (mean 0.948). Palla's PhD thesis (Palla, 2009a) considers two calibration and two validation events in more detail. Modelled runoff depth was within 1% of recorded runoff depth for both calibration events. However, modelled runoff depth exceeded recorded runoff depth by 8% for both validation events. The peak runoff intensity was also noticeably underestimated (-9.2%) for one of the two calibration events, though it was generally acceptable for both validation events and the other calibration event (absolute error ≤ 3.5%).

The main limitations of the Hydrus-1D models for green roof applications presented in both papers are the requirements for a large number of input parameters, all of which are difficult to quantify accurately and consistently, though Palla *et al.* (2012) demonstrated that it is possible to overcome this model limitation in practice.

2.6.3.5 Other Methods

Yio *et al.* (2012) used a laboratory rainfall simulator to investigate the effects of substrate depth, substrate composition and rainfall rate on runoff detention in a sample of substrate initially at field capacity. Time-series runoff was monitored at a five-second interval and modelled using a nonlinear storage routing equation with an adjustable delay between inflow and outflow. It was found that increasing organic content, through adding either compost or coir to the original substrate mix, increased runoff detention times and reduced peak runoff rates. Similarly, increasing substrate depth resulted in increased runoff detention times and reduced peak runoff rates. However, all of these effects on runoff were proportionally reduced as the rainfall rate was increased. The coefficient of determination, R_t^2, between modelled and monitored runoff exceeded 0.93 for all tested substrate variations. It was hypothesized that the storage routing parameters could be predicted from substrate depth and permeability; this was suggested as further work.

Although this model was produced for a layer of substrate in isolation, nonlinear storage routing is equally applicable to drainage layers, whole green roof systems and many other hydrological situations, such as rivers and reservoirs. Consequently, it should be considered a generic method; it is fully discussed as such in Section 2.4.5.3.

2.6.3.6 Model Selection

The three substrate-specific methods presented above are all relatively complex in comparison to the more generic methods considered in Section 2.4.5. It is clear that the assumption of saturation that Darcy's Law requires will not be met consistently, if at all, throughout the proposed experimental programme, or indeed in any well-designed green roof. The use of both Green-Ampt infiltration and the Richards Equation are justified physically. Time-series runoff profiles can be generated implicitly as the difference between rainfall and infiltration volumes, for both methods. However, the use of the Richards Equation is preferred, due to the relative ease of experimentally obtaining the parameters required for the Richards Equation-based Hydrus-1D model, against obtaining the parameters required for either the Green-Ampt infiltration model or the standard form of the Richards Equation presented in Equation 2.13. Nonlinear reservoir routing, with regards to runoff from the substrate component, will also be tested, as a simple alternative that requires minimal parameterization and processing time.

3   Analysis and Modelling of Green Roof Runoff Response on Multiple Temporal Scales

3.1   Chapter Overview

This chapter presents a re-analysis of a 29-month period of rainfall and runoff data (1/1/2007 – 31/5/2009) collected from a small green roof test bed located on the roof of the department of Civil and Structural Engineering at the University of Sheffield. Performance of the test bed is considered cumulatively, annually, seasonally and per-event, and compared to that of other long-term green roof performance monitoring projects. Significant storms are identified and their easily identifiable characteristics (peak intensity, antecedent dry weather period etc.) quantified. Multiple non-linear regression analyses are performed, attempting to link these characteristic values to a number of easily identifiable metrics of green roof performance (peak rate of runoff, time delay to start of runoff etc.). Climatic factors prior to each storm (total rainfall in preceding 7 days, average temperature over antecedent 24 hours etc.) are identified for each significant storm. Multiple non-linear regression analyses are performed, attempting to link these climatic factors to the same easily identifiable metrics of green roof performance. For both sets of variables, either kept separately or combined into a single set, it is found that the optimal equation derived for each performance metric has generally poor predictive capability and is unable to adequately match the recorded performance data of the green roof test bed. Finally, it is argued that the runoff response of a green roof to a rainfall event can only be adequately understood by considering the hydrological processes that occur in the green roof system during and before the storm.

This work was the basis of a presentation first given by the PhD author at a SUDSnet conference in May 2011 (Vesuviano & Stovin, 2011) and later published in the *Journal of Hydrology* in January 2012 (Stovin *et al.*, 2012). The collection and initial study of the long-term rainfall and runoff data set formed part of the doctoral work of Dr Hartini Kasmin (Kasmin, 2010).

3.2   Motivation

In Chapter 2 (Literature Review), a number of hydrological modelling methods were evaluated for their suitability in modelling green roof and individual layer runoff response. This chapter explores the use of a more generic, non-hydrological method for estimating various aspects of green roof performance in response to significant storm events. By avoiding hydrological theory entirely in favour of simple equations, it is intended that this method may allow specialists and non-specialists alike to estimate the retention and detention performance of a roof in response to a typical design storm, with limited data.

(a)   (b)

Figure 3.1 – The green roof test bed (a) shown in the context of its surroundings (b). The red x on (a) indicates the vantage point from which (b) was taken.

3.3   Experimental Setup

The green roof test bed is located on a roof terrace level above the second floor of the Sir Frederick Mappin Building, near the junction of Broad Lane and Newcastle Street in central Sheffield (53.382469, -1.478123). On the north side of this terrace, the building extends upward for a further three floors. The test bed is positioned approximately ten metres from the north wall, along the south edge of the terrace. The vegetated surface of the test bed is above the level of the terrace's safety parapet. The test bed itself has a length of three metres, width of one metre and is laid at a slope of 1.5°. The green roof system uses standard components in an extensive configuration with no protection mat. The components used are: a ZinCo Floradrain FD 25-E drainage layer infilled with gravel; a ZinCo Systemfilter SF filter sheet; an 80 mm depth of 4-15 mm recycled crushed brick (Zincolit), fines and organic growing medium; and a vegetation layer consisting of various low-growing *Sedum* species. The listed maximum retention capacity of the drainage layer is approximately 3 l/m² (Alumasc, 2012b), equivalent to 3 mm rainfall.

As the test bed is very small in comparison to most green roofs on new developments (which generally cover the majority of the roof area on a large building), it is possible that the recorded durations of runoff detention may be comparatively reduced, as the horizontal distance through the drainage layer that water is required to travel to the roof outlet is shorter. If, however, the detention effects are primarily and overwhelmingly due to the rate at which water percolates through the substrate, then detention performance should not be significantly affected by the test bed's small size. It is worth noting that amateur projects e.g. carports, are generally no longer than a few metres in any dimension and so the small test bed may represent the performance of these well. The retention performance of a green roof depends on the vertical movement through and storage of moisture in the substrate and drainage layers and so should be independent of the length and width of the test roof.

Rainfall at the site is monitored using an Environmental Measures ARG-100 tipping bucket rain gauge with 0.2 mm resolution, located less than a metre from the test bed and also above the level of the safety parapet. Runoff from the green roof system is collected in a tank underneath the test bed, via a sealed gutter at its downstream end. This tank automatically empties at 09:00 every day and at any time that its maximum capacity of approximately 7 mm of runoff is reached. A Druck PTX 1730 pressure transducer is installed in the tank to monitor the depth of runoff collected. During an automatic emptying event, runoff collection cannot be recorded; in this study, it is estimated by linear interpolation of differential runoff depth changes recorded in the time intervals immediately surrounding the emptying event. Output values from both the rain gauge and pressure transducer are sampled at one-minute intervals by a Campbell Scientific CR1000 data logger.

The upper and lower zones of the runoff collection tank are of two different constant cross-sectional areas, joined by a transition zone in which cross-sectional area varies with height. Approximately 0.5 mm of rainfall can be collected in the lower zone, 1.1 mm in the transition zone and 5.2 mm in the upper zone, for a total of 6.8 mm. The resolution of the pressure transducer is approximately 2×10^{-3} mm in the lower zone and 7×10^{-3} mm in the upper zone, increasing from one to the other in the transition zone. As the upper and lower zones are of constant cross-section, a linear relationship between recorded pressure and collected runoff is valid in these zones. The cross-section of the transition zone varies with height and an exponential relationship between recorded pressure and collected runoff is used in the transition zone. The relationship between recorded pressure and collected runoff depth was derived by Dr. Hartini Kasmin as part of her PhD research and is shown in Figure 3.2.

3.4 Data Record Analysis

3.4.1 Overview

The data analyzed in this chapter were collected over a 29-month period, from 1st January 2007 to 31st May 2009. Due to instrumentation malfunctions, pressure transducer data collected from 17th January 2008 to 3rd March 2008, and from 17th March 2008 to 1st April 2008, are not considered in this chapter, nor are they considered in either the SUDSnet conference presentation (Vesuviano & Stovin, 2011) or *Journal of Hydrology* article (Stovin *et al.*, 2012).

3.4.2 Climate and Context

The climate in Sheffield is temperate. From 1981 to 2010 inclusive, the mean annual rainfall was 834.6 mm, the mean wettest month was December (86.7 mm) and the mean driest month May (53.8 mm). The yearly mean temperature ranged from a low of 6.6 to a high of 13.4°C. The highest monthly mean temperatures occurred in July, ranging from 12.7-21.1°C, and the lowest
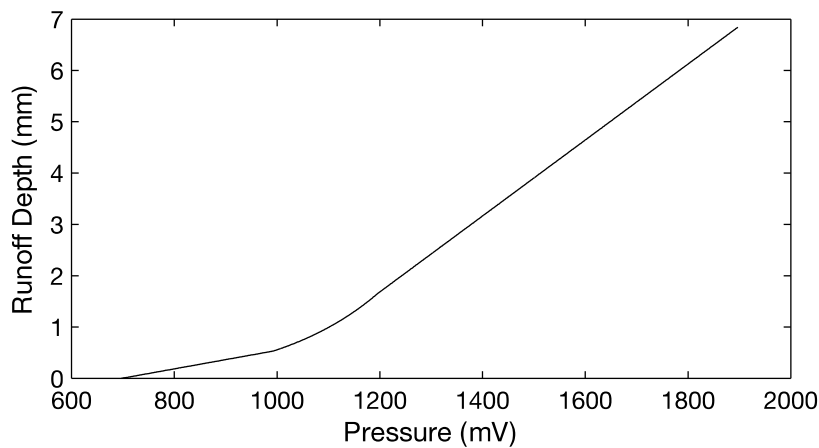
Figure 3.2 – Pressure-runoff depth curve for runoff collection tank.

occurred in January, ranging from 1.9-6.8°C (Met Office, 2008). Snow was, and is, not uncommon in winter.

The 29-month data record cannot be considered "long" in hydrological terms. A brief study is presented here to evaluate the representativeness of the data set with respect to Sheffield's long-term climatic means. Figure 3.3 presents the monthly rainfall totals for the experimental rain gauge alongside the monthly totals recorded by the Met Office at Weston Park and the monthly mean rainfalls recorded by the Weston Park gauge over the period 1981-2010. As the two sites are less than one kilometre apart, any differences in monthly totals are likely to result from effects caused by buildings around the experimental site. Figure 3.3 also plots the monthly totals recorded by the experimental rain gauge as a percentage of the 1981-2010 mean monthly rainfall depths. Overall, the experimental gauge recorded 2042 mm of rainfall, 93.4% of the 2182.9 mm recorded at Weston Park. The Weston Park gauge recorded 9.4% more rainfall than the 1995.5 mm that would be expected over two full years and one January-May period according to the 1981-2010 monthly means. June 2007, in particular, experienced over 300% of the monthly mean rainfall, while July 2007 experienced 199% of the mean. Conversely, total rainfall for each of April, August, September and October 2007 was below 50% of the long-term mean. Summer 2008 was wetter than average, with July experiencing over 150% of the mean monthly rainfall, while the period from October 2008 to April 2009 was consistently drier than average. The overall rainfall record for this period is therefore one of wet summers, dry winters and a notably greater than average total depth.

3.4.3   Cumulative and Annual Analysis

The full, 29-month rainfall record was first considered on a multi-annual basis, relating cumulative rainfall and runoff over the approximately 27-month period for which both records contained usable data. A total of 1892.2 mm of rain fell in this time, of which 933.8 mm was
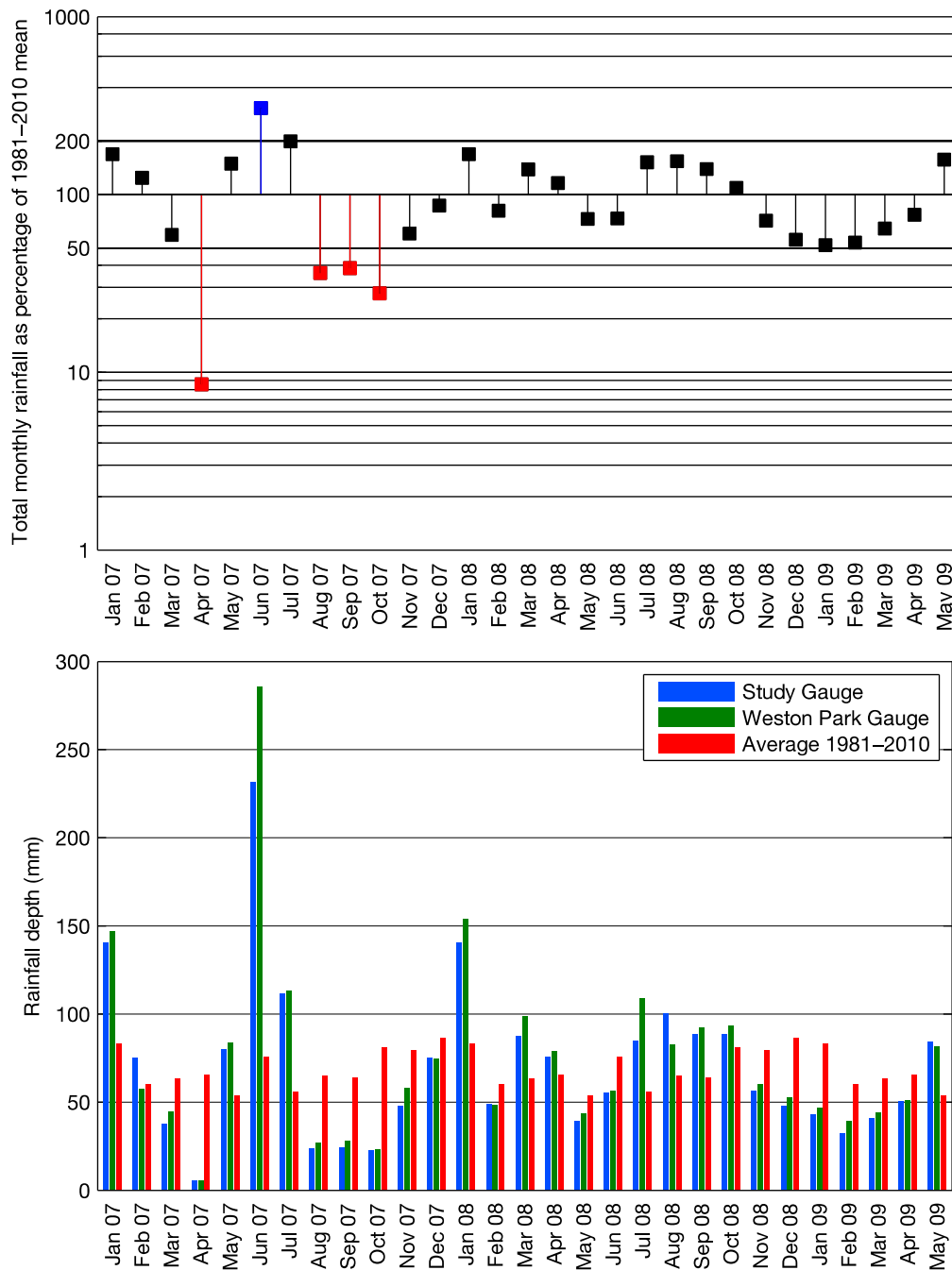
Figure 3.3 – Monthly rainfall totals (adapted from Stovin *et al.*, 2012).

retained and 958.4 mm became runoff. This equates to a cumulative retention of 49.3%, towards the lower end of retention performance quoted in published studies (Section 2.4.4.1). This is probably a consequence of Sheffield's cool and wet climate, in which evapotranspiration rates, even in the height of summer, are moderate. The substrate depth of the test bed is also relatively shallow in comparison to many other experimental configurations, although it is typical of extensive green roof systems. The low observed level of retention could be an underestimate of long-term performance when it is considered that the total rainfall over the monitoring period was approximately 10% above the long-term climatic average.
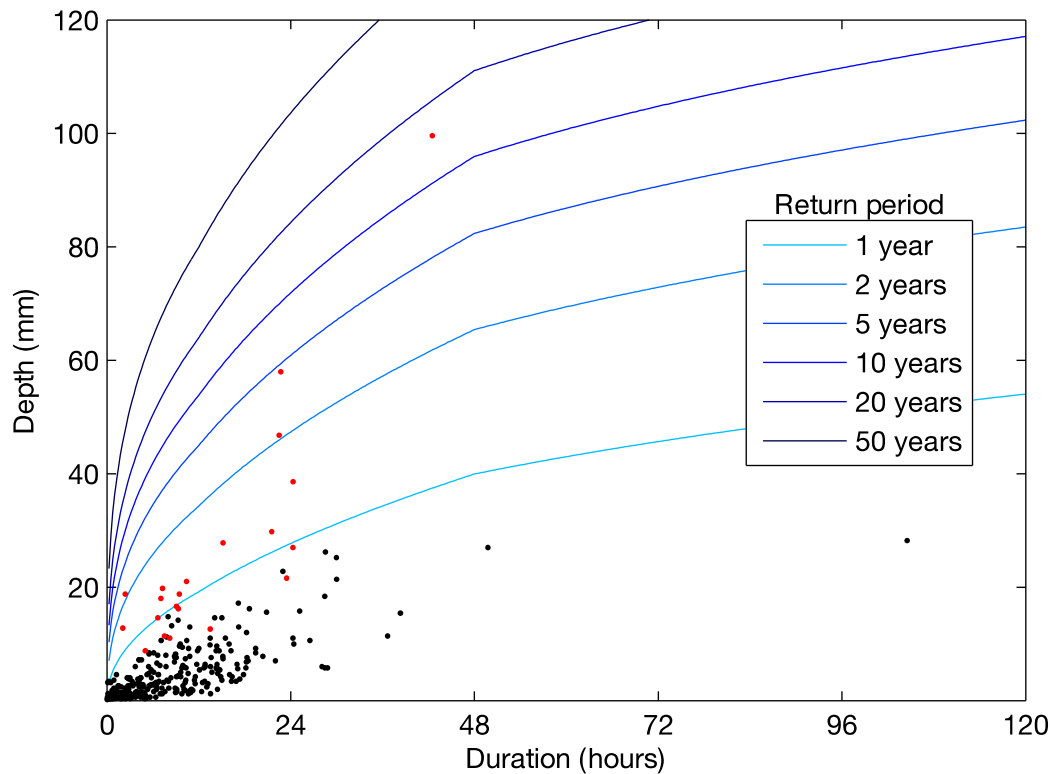
Figure 3.4 – Fully-monitored individual storms, plotted against depth-duration-frequency curves for Sheffield, UK (adapted from) (Stovin *et al.*, 2012).

Considering each year separately, cumulative annual retentions for 2007, 2008 (excluding the dates previously given) and the first five months of 2009 were 43.5%, 51.6% and 62.6% respectively. The total rainfalls for each of these periods were 105.8%, 112.1% and 74.8% of the long-term average. The fact that the cumulative annual retention is lowest for 2007, rather than the wetter 2008, corresponds to the fact that four of the five largest storms of the entire monitoring period occurred in 2007, totalling 226 mm between them. For comparison, the four largest fully-monitored storms of 2008 have a combined depth of 129.8 mm and the four largest storms of January-May 2009 have a combined depth of 69.8 mm. Further discussion of significant storms can be found in Section 3.4.6.

3.4.4   Individual Event Analysis

The rainfall record contains a total of 468 events, all separated by an antecedent dry weather period (ADWP) of six hours or more. This minimum duration of ADWP was used in previous green roof studies by VanWoert *et al.* (2005), Getter *et al.* (2007) and Voyde *et al.* (2010), but other minimum ADWP durations are used elsewhere, 24 hours being common e.g. WaPUG Code of Practice (WaPUG, 2002). The minimum depth of a single rainfall event was equal to the resolution of the rain gauge – 0.2 mm. Of the 468 recorded storm events, 432 occurred while the pressure transducer was working correctly (Figure 3.4) – it is only these storms that were considered in the cumulative, annual and seasonal analyses above, and only these storms that are

considered in the single-event analyses following in this chapter. 173 storms occurred in 2007, 175 in the considered part of 2008 and 84 in the first five months of 2009. The mean and median retention on a per-storm basis were 69.6% and 90.9% respectively, far above the 49.3% cumulative retention over the same time period. This is a consequence of the per-storm figure giving equal weighting to every storm, including the many small storms from which runoff was minimal or zero – more than half of the storms analyzed were of less than 2 mm depth.

200 storms equalled or exceeded a depth of 2 mm. The performance of the roof in response to these "midsize" storms is evaluated separately from the performance in response to storms of less than 2 mm depth, as events of less than 2 mm depth are unlikely to produce runoff from a conventional roof (Voyde *et al.*, 2010). Considering only the 200 storms of depth 2 mm or greater, the mean and median per-event retention reduce to 60.4% and 61.7% respectively, while cumulative retention reduces to 46.9%. This compares poorly with the 78% per-event retention reported by Voyde *et al.* (2010), also for storms of depth 2 mm or more, though for a roof of 20% lower slope (1.2°) and approximately 20% deeper substrate (80 mm + 15 mm reinforced coir). The Sheffield experimental roof's peak runoff reduction of 78.9% for midsize storms also compares poorly with the 91% achieved in the same Voyde *et al.* study, though an almost 80% reduction in peak flow rate is highly significant when considered in isolation. The minimum and maximum retention for either the full or midsize-only set of Sheffield storm events were 0% and 100% respectively.

3.4.5   Cumulative and Individual Event Analysis by Season

Due to the cyclic variation in rainfall, solar radiation and temperature throughout a typical year, it is reasonable to expect the performance of the green roof to vary on a seasonal basis. Hutchinson *et al.* (2003), Mentens *et al.* (2006), Van Seters *et al.* (2007) and Uhl & Schiedt (2008) all present runoff monitoring results which show that retention, as a percentage of total rainfall depth, is higher in the (typically) driest, warmest and sunniest months and significantly reduced in the wettest, coldest and darkest months. However, Voyde *et al.* (2010) found no significant differences in seasonal performance for a 12-month rainfall-runoff monitoring programme conducted in Auckland, New Zealand. This may be due to their strict interpretation of "significant" to mean "statistically significant", a more robust definition that the other authors do not appear to have followed. Despite the seasonal variation in retention performance not strictly being significant in their study, the mean per-event retention was around 95% in summer and around 15-20 percentage points lower in each of autumn, winter and spring.

The 432 fully-monitored storms in this study divide seasonally thus: 126 events in spring (March, April, May) totalling 462.6 mm, 104 events in summer (June, July, August) totalling 607.8 mm, 84 events in autumn (September, October, November) totalling 328.4 mm and 118 events in

winter (December, January, February) totalling 493.4 mm. Due to instrumentation malfunction, and the start and end dates of the monitoring programme, not all seasons are represented equally in this data set. The number of monitored months falling into each season is: spring – 8½, summer – 6, autumn – 6 and winter – 6½. The mean number of individual storms per month on a seasonal basis therefore ranges from 14 in autumn to 18.2 in winter. Cumulative and per-event retention figures for each season are given in Table 3.1.

Interestingly, the retention performance of the roof, both cumulative and per-event, is highest in spring, not summer. This is likely to be explained by the larger average rainfall event depth in summer, as a constant retention depth is a lower percentage of a larger storm. Additionally, the rainfall depth per month in summer is almost double that of spring and the number of rainfall event-hours per month is almost 25% higher. Hence, in the sampled summers, fewer dry periods existed during which storage could be recharged, while a much greater quantity of water was required to be removed: the total rainfall depth over all summer months was 154% of climatic average, while for spring, total rainfall depth was only 90% of climatic average. It is also noted that, by measurement of rainfall depth per month, number of event hours per month and mean rainfall event depth, spring was the driest of the four seasons.

For the same reasons given in the individual event analysis (Section 3.4.4), cumulative retention is lower than per-event retention for each season individually. Both measures of retention are greatly lowered for winter, a season in which evapotranspiration rates (and therefore storage recharge) are usually at their lowest. In terms of rainfall depth per month and mean event depth, winter was the second wettest season, behind summer, while in terms of event hours per month, winter was notably wetter than each of the other three seasons. These are all contributing factors to the poor retention performance of the test bed in winter.

3.4.6   Significant Event Analysis

Over the 29-month monitoring period, 14 storms exceeded the depth-in-duration requirements to be considered a one-in-one year storm for central Sheffield (NERC, 1999). A further eight storms contained a peak intensity period of one, six or twelve hours, which would exceed the same requirements had this period alone occurred as a separate storm. The 22 events selected by these criteria, excluding one which occurred on 20th January 2008 during a period of pressure

Table 3.1 – Seasonal properties of rainfall distribution and retention performance.

Season	Rainfall Depth	Rainfall Depth Per Month	Event Hours Per Month	Mean Event Depth	Cumulative Retention	Per-Event Retention
Spring	462.6 mm	54.4 mm	84.3	3.67 mm	69.0%	84.5%
Summer	607.8 mm	101.3 mm	104.8	5.84 mm	50.7%	79.3%
Autumn	328.4 mm	54.7 mm	102.2	3.91 mm	51.4%	78.9%
Winter	493.4 mm	75.9 mm	126.3	4.18 mm	27.8%	38.6%

transducer malfunction, form the data set of 21 significant storms which are considered in parametric analyses of green roof performance. These storms are highlighted in red on Figure 3.4. It should be noted that, for the eight events failing to qualify entirely as one-in-one-year storms, the complete storm event, and not just the significant part, is considered both here and in the parametric analyses. It is noted here that for two storms, those beginning on 2nd June 2008 and 1st August 2008, runoff was not recorded for the entire duration of the storm. This was a consequence of debris becoming trapped in the solenoid valve of the collection barrel, thereby preventing it from fully closing after a barrel emptying event. A storage routing model, described in Kasmin *et al.* (2010), was fitted to the part of each storm runoff record known to be accurate, and from this a prediction of the entire runoff profile was made. However, as the calculations of values for certain parameters (e.g. peak-to-peak delay) are more dependent on the exact shape of the runoff profile than are the calculations for others (e.g. percentage runoff reduction), the two partly-reconstructed runoff profiles are not considered in any analyses of: cumulative median-to-median delay, peak-to-peak delay, peak runoff rate and peak runoff reduction that result from the effects of hydrological processes occurring within the green roof. A full list of storm, climatic and performance parameters used in the parametric analysis, some of which are referred to in the following paragraphs, is given in Section 3.5.1.

This set of 21 significant storms is heavily biased towards the summer months (June, July, August), with 12 storms occurring in summer and only three in each of the three-month periods representing autumn (September, October, November), winter (December, January, February) and spring (March, April, May). The discarded significant event occurred in the winter. The three storms with the highest return periods all occurred in summer months. The seasonal mean depths of the significant summer, winter and autumn events (Table 3.2) are similar, but all greatly exceed the average depth of the three significant spring events. Mean storm intensity was highest in summer and lowest in winter. Additionally, peak storm intensity was highest in summer and lowest in winter, which is a known and documented characteristic of typical British storms (NERC, 1975). Retention was unsurprisingly lowest in winter, when evapotranspiration rates, and hence the rate of storage capacity recharge, are low. However, retention rates were, on average, higher in spring than summer. This unusual observation has been explained in Section 3.4.5 for the full set of 432 storms, and the same explanations, regarding weather conditions and storm characteristics, also hold true for the subset of 21 significant events. It should be noted that

Table 3.2 – Significant storm characteristics by season.

Season	Events	Mean depth	Mean storm intensity	Peak storm intensity	Percentage Retention
Winter	3	28.9 mm	1.57 mm/hour	15.2 mm/hour	5.65%
Spring	3	18.5 mm	1.64 mm/hour	18.4 mm/hour	76.2%
Summer	12	26.8 mm	2.79 mm/hour	26.2 mm/hour	45.6%
Autumn	3	28.7 mm	1.81 mm/hour	20.8 mm/hour	34.9%

the two largest events (99.6 and 58.0 mm) occurred in the summer and were, respectively, more than triple and approximately double the depth of the largest spring event (29.8 mm). It is important to note that, with a small data set of only 21 events, it cannot be assumed that any of the observations made can be extrapolated.

Of the 21 significant storm events for which rainfall and runoff data are both known, total depth ranges from 8.8 to 99.6 mm, while mean depth is 26.17 mm. Event duration ranges from 123 to 2,549 minutes (42 hours 29 minutes), whilst the mean is exactly 14 hours. Mean storm intensity is 2.31 mm/hour, though only six of the 21 events exceed this value; the mean is pulled to the right of the median value (1.83 mm/hour) by a single storm event of mean intensity 7.83 mm/hour. Peak storm intensity, measured over five minutes, is significantly less skewed; mean and median values are 22.51 and 21.60 mm/hr respectively, while range is 7.2-50.4 mm/hour. The ADWP preceding each storm varies greatly, from the minimum possible value of exactly six hours, up to 199 hours and 14 minutes. The mean value of ADWP (25 hours 56 minutes) is pulled to almost double the median (13 hours 28 minutes) by this single outlier; only one other storm has an ADWP of over 48 hours and only six storms in this data set have an ADWP above the mean value.

For these 21 events, the mean per-event retention is reduced again to 42.7%, cumulative retention is greatly reduced to 29.3% and the peak runoff reduction is reduced to 59.2%. Despite comparing unfavourably with the figures of around 50-80% retention most often quoted for annual performance, the retention performance of this experimental test bed in response to large and/or intense storms is still significant in its own right. Furthermore, the test bed was able to retain over 99.9% of one significant storm and over 98% of another. Additionally, the peak flow reduction was in excess of 95% for both of these storms and one other. The cumulative median-to-median runoff delay took a mean value of 87.7 minutes (for the 19 storms considered in analysis of this parameter). For the largest storm in the data set, this delay was 261 minutes. Even for the four storms with less than 5% retention, the mean value of the cumulative median-to-median delay was 53.9 minutes and the mean value of peak attenuation was 32.5%, indicating that green roofs can still reduce the peak flow into a drainage system, regardless of whether or not any retention takes place.

3.4.7 Conclusions of Data Record Analysis

Runoff from a small-scale green roof of typical extensive build-up was monitored near-continuously from January 2007 to May 2009. Rainfall at the site, in central Sheffield, was also monitored over this time period. The two data records were analyzed and compared at multiple temporal scales. Over the entire monitoring period, 49.3% of cumulative rainfall was retained by the green roof. This is significant, but low in comparison to many other long-term monitoring

studies. Reasons for this include Sheffield's maritime temperate climate and the above average rainfall depth, relative to the long-term climatic average, recorded over the study period. Seasonally, the highest retention was found to occur in spring, rather than summer. This result is linked to the relatively dry springs and relatively wet summers that occurred over the monitoring period. The least retention occurred in winter periods, despite the monitored summers being around a third wetter than the monitored winters, on average. This is due to the difference in storage recharge rates, resulting from evapotranspiration, in the different seasons. Assuming a minimum antecedent dry weather period of six hours, 432 fully-monitored storms could be extracted from the data record. Mean retention per storm event was 69.6%. This greatly exceeds cumulative retention due to the high number of small storms (< 2 mm) that were completely or almost completely retained. Considering only the 200 storms of 2 mm or greater depth, mean retention was 60.4% and mean peak flow reduction was 78.9%. Both of these observations show that the green roof significantly reduces the volume and intensity of runoff, even when small storms are ignored. 21 significant storms, ranging in depth from 8.8 to 99.6 mm and in duration from 123 to 2,549 minutes, were selected by return period criteria for further consideration. Twelve of the significant storms occurred in the six monitored summer months, while only nine occurred in the 21 monitored spring, autumn and winter months combined. Mean per-event retention for these storms was 42.7% and mean peak runoff reduction was 59.2%. This shows that an extensive green roof can greatly reduce the peak flow and total runoff volumes into a drainage system, even for large storms.

3.5 Parametric Modelling of Significant Events

3.5.1 Overview

Five storm characteristics: rainfall duration in hours (D); rainfall depth in mm (P); antecedent dry weather period in hours ($ADWP$); mean storm intensity in mm/hour (i); and peak 5-minute storm intensity in mm/hour (i_P), were identified for the 21 significant storms considered. Four performance metrics: runoff depth in mm (Q), retention depth in mm (S), percentage retention (S_V) and time to start of runoff in minutes (Q_t), were identified by comparison of rainfall and runoff records for the 21 significant storms, while a further four performance metrics: 5-minute peak runoff intensity in mm/hour (Q_P), peak attenuation (A_P) i.e. percentage reduction between i_P and Q_P, peak-to-peak runoff delay in minutes (t_P) and cumulative median-to-median runoff delay in minutes (t_{50}) were identified for only the 19 significant storms with complete monitored runoff records. Five antecedent climatic factors were identified for each storm: precipitation in the 24 hours, 7 days and 14 days preceding the rainfall event (P_D, P_W and P_F respectively), mean temperature over preceding 24 hours (T_D), and mean monthly temperature over the period 1981-2010 (T_L), as recorded by the Met Office at Weston Park, approximately 1 km west of the study

Table 3.3 – Storm event characteristics. Events with ADWP over 24 hours are starred. Dashes indicate return periods below one year.

Event Start dd/mm/yy hh:mm	D (hh:mm)	P (mm)	$ADWP$ (hh:mm)	i (mm/hour)	i_P (mm/hour)	Event	Return period 1-hour	6-hour	12-hour
18/01/07 01:11	24:17	27.0	10:26	1.11	21.6	-	-	>1	>1
20/01/07 19:47	24:18	38.6	9:02	1.59	14.4	1.54	>1	>1	>1
13/05/07 12:34	21:30	29.8	16:04	1.39	12.0	1.20	-	>1	>1
12/06/07 05:38*	2:03	12.8	199:14	6.24	28.8	1.56	>1	n/a	n/a
13/06/07 15:39*	42:29	99.6	31:58	2.34	21.6	15.91	>2	>2	>10
15/06/07 17:54	9:19	16.2	7:46	1.74	12.0	-	>1	>1	n/a
24/06/07 22:12	22:41	58.0	6:00	2.56	28.8	4.73	>1	>2	>5
26/07/07 06:56	13:29	12.6	13:25	0.93	33.6	-	>1	-	-
15/01/08 02:51	10:23	21.0	7:19	2.02	9.6	1.22	-	>1	n/a
28/05/08 14:33	8:11	11.0	6:24	1.34	19.2	-	>1	-	n/a
02/06/08 20:40*	23:27	21.6	34:04	0.92	9.6	-	>1	>1	-
26/06/08 13:22	9:05	16.6	21:57	1.83	16.8	-	-	>1	n/a
19/07/08 00:13	5:00	8.8	12:49	1.76	26.4	-	>1	n/a	n/a
31/07/08 10:12*	7:15	19.8	27:22	2.73	48.0	1.39	>2	>1	>1
01/08/08 01:44	2:24	18.8	8:17	7.83	50.4	2.71	>5	n/a	n/a
12/08/08 05:13	7:02	18.0	13:28	2.56	24.0	1.25	>1	>1	n/a
16/08/08 19:05*	9:26	18.8	49:56	1.99	14.4	1.13	>1	>1	n/a
03/09/08 13:43	7:29	11.4	14:31	1.52	28.8	-	>1	-	n/a
05/09/08 04:36	22:29	46.8	14:38	2.08	26.4	2.24	>1	>1	>1
04/10/08 17:19*	15:09	27.8	30:23	1.83	7.2	1.38	-	>1	>1
28/04/09 16:37	6:39	14.6	9:39	2.20	24.0	1.02	>1	>1	n/a
Minimum	**2:03**	**8.8**	**6:00**	**0.92**	**7.2**				
Maximum	**42:29**	**99.6**	**199:14**	**7.83**	**50.4**				
Mean	**14:00**	**26.17**	**25:56**	**2.31**	**22.74**				
Median	**9:26**	**18.8**	**13:28**	**1.83**	**21.6**				

site. Individual parameter values, as well as minimum, maximum, mean and median values, are presented in Table 3.3, Table 3.4 and Table 3.5 for all storm events. It should be noted that, as the parameter values for T_L are not derived from the data record, neither they, nor their minimum, maximum, mean and median values in any way represent the weather conditions prior to a storm event.

From a storm water management perspective, there is a requirement for modelling tools that enable both the total volume and temporal profile of runoff to be predicted in response to an arbitrary or design rainfall. Multiple regression analysis was undertaken to attempt to identify potentially useful equations, capable of predicting green roof performance from storm characteristics or antecedent climatic factors. For all 18 sets of parameters the Shapiro-Wilk test of normality was undertaken, and power or logarithmic transformations were applied as appropriate to maximize the normality of each parameter set. In the case of $ADWP$ and i, no transformation could raise the Shapiro-Wilk significance above 0.05, indicating that normality assumptions were not met for these parameters. Although it may be argued that non-parametric

Table 3.4 – Green roof performance characteristics. Events for which the runoff record was partially reconstructed are starred.

Event Start dd/mm/yy hh:mm	Q (mm)	S (mm)	S_V (%)	Q_t (minutes)	Q_P (mm/hour)	A_P (%)	t_P (minutes)	t_{50} (minutes)
18/01/07 01:11	25.33	1.67	6.18	15	11.28	47.79	7	42.74
20/01/07 19:47	36.75	1.85	4.79	18	11.55	19.81	5	70.22
13/05/07 12:34	9.98	19.82	66.50	262	4.17	65.22	90	198.57
12/06/07 05:38	0.01	12.79	99.95	483	0.02	99.93	103	83.38
13/06/07 15:39	86.48	13.12	13.17	350	15.24	29.43	9	261.32
15/06/07 17:54	16.19	0.01	0.04	9	8.97	25.26	7	39.04
24/06/07 22:12	57.96	0.04	0.07	12	14.92	48.20	4	51.69
26/07/07 06:56	10.06	2.54	20.18	14	13.89	58.67	6	66.64
15/01/08 02:51	19.75	1.25	5.97	9	6.63	30.96	9	41.30
28/05/08 14:33	1.67	9.33	84.79	78	2.52	86.89	44	31.12
02/06/08 20:40*	15.10	6.50	30.09	451				
26/06/08 13:22	0.27	16.33	98.36	359	0.59	96.48	283	181.41
19/07/08 00:13	4.25	4.55	51.66	13	3.39	87.16	35	78.77
31/07/08 10:12	3.15	16.65	84.10	41	13.66	71.54	54	4.50
01/08/08 01:44*	13.30	5.50	29.26	4				
12/08/08 05:13	5.24	12.76	70.89	73	2.41	89.97	77	78.54
16/08/08 19:05	9.46	9.34	49.68	396	10.12	29.70	18	85.03
03/09/08 13:43	1.45	9.95	87.30	218	1.32	95.43	43	121.65
05/09/08 04:36	44.53	2.27	4.84	35	16.72	36.66	-49	54.63
04/10/08 17:19	24.35	3.45	12.40	56	4.80	33.40	12	75.36
28/04/09 16:37	3.32	11.28	77.23	106	6.57	72.62	272	100.39
Minimum	**0.01**	**0.01**	**0.04**	**4**	**0.02**	**19.81**	**-49**	**4.50**
Maximum	**86.48**	**19.82**	**99.95**	**483**	**16.72**	**99.93**	**283**	**261.32**
Mean	**18.51**	**7.67**	**42.74**	**56**	**7.83**	**59.22**	**54.16**	**87.70**
Median	**10.06**	**6.50**	**30.09**	**142.95**	**6.63**	**58.67**	**18**	**75.36**

tests (e.g. Spearman's rho) would be more suitable under such circumstances, they lack the predictive capacity of parametric approaches and hence were not utilized. For all regression analyses, the coefficient of determination (Pearson's R^2) is presented, to indicate correlation strength i.e. the proportion of variability that can be explained by the model. All parameter set transformations and multiple regression analyses were undertaken in SPSS 19. Multiple regression analyses require that all parameters are independent, which is not true for the following parameters: $P = i \times D$; $A_P = 100 \times (1 - Q_P/i_P)$; i is dependent on i_P; P_F contains P_W which contains P_D. Care was taken not to combine dependent parameters within individual multiple regression analyses. It is noted that a parametric modelling approach will not generate a temporal runoff profile directly. However, peak runoff rate, Q_P, some measure of delay (peak-to-peak, t_P, or cumulative median-to-median, t_{50}) and total runoff volume, Q, provide sufficient information to deduce a triangular approximation.

In addition to multiple regression analyses, which fitted green roof performance to multiple transformed storm or climatic descriptors in a purely statistical fashion, single regression

Table 3.5 – Antecedent weather conditions to storm events.

Event Start dd/mm/yy hh:mm	P_D (mm)	P_W (mm)	P_F (mm)	T_D (°C)	T_L (°C)
18/01/07 01:11	3.8	28.6	50.0	7.04	4.32
20/01/07 19:47	4.2	42.8	81.2	9.40	4.32
13/05/07 12:34	2.6	21.6	21.6	11.96	11.77
12/06/07 05:38	0	0	1.4	19.11	14.65
13/06/07 15:39	0	12.8	14.2	17.19	14.65
15/06/07 17:54	59.2	112.4	113.0	11.26	14.65
24/06/07 22:12	3.8	34.0	162.6	14.03	14.65
26/07/07 06:56	6.6	26.2	65.8	15.36	16.89
15/01/08 02:51	1.4	32.8	49.8	7.59	4.32
28/05/08 14:33	7.0	18.4	20.0	10.99	11.77
02/06/08 20:40	0	37.6	37.6	15.52	14.65
26/06/08 13:22	0.4	7.4	10.8	14.67	14.65
19/07/08 00:13	1.4	10.4	41.8	15.57	16.89
31/07/08 10:12	0	4.2	16.8	20.64	16.89
01/08/08 01:44	19.8	24.0	34.4	18.79	16.51
12/08/08 05:13	0.2	11.6	52.4	15.87	16.51
16/08/08 19:05	0	23.4	34.4	15.77	16.51
03/09/08 13:43	0.4	9.0	20.2	13.06	13.99
05/09/08 04:36	0.4	20.8	24.0	12.26	13.99
04/10/08 17:19	0	30.0	31.4	7.07	10.51
28/04/09 16:37	14.2	23.8	26.0	15.24	8.63
Minimum	**0**	**0**	**1.4**	**7.04**	**4.32**
Maximum	**59.2**	**112.4**	**162.6**	**20.64**	**16.89**
Mean	**5.97**	**25.32**	**43.3**	**13.73**	**12.94**
Median	**1.4**	**23.4**	**34.4**	**14.67**	**14.65**

analyses were also undertaken. These relate untransformed single green roof performance metrics to the untransformed single storm characteristics deemed most likely to influence them. The single, untransformed regression analyses were undertaken in Microsoft Excel 2007.

3.5.2 Single Regression Analyses

In an attempt to create and test simple green roof performance rules, for quick implementation by any drainage engineer, without specialist software (or even necessarily understanding), single parameter regressions were undertaken for the following eight parameter set pairs: rainfall depth-runoff depth; rainfall depth-percentage retention; ADWP-retention depth; ADWP-percentage retention; peak storm intensity-peak runoff intensity; peak storm intensity-percentage retention; mean storm intensity-runoff depth; mean storm intensity-percentage retention. The first two parameter set pairs, where rainfall depth is used as a predictor, follow the proposition that the roof's retention capacity is finite, hence runoff will be higher and retention lower for larger storm events. The next two parameter set pairs, using ADWP as a predictor, are based on an assumption that more storage recharge takes place when the dry periods between storms are longer. The last four parameter set pairs, using peak and mean storm intensity as predictors,

follow from the argument that more intense storms are more challenging for the green roof to retain, and attempt to quantify that argument in various ways. Figure 3.5 plots these eight pairs of parameters with their best-fit regression lines. The equations describing the regression lines (solid black) are the simple performance rules. The dotted lines on plots (a) and (e) represent equality between horizontal and vertical axes; a point lying above the dotted line would indicate negative retention or attenuation. Overall, the value of these regression models is low, as evidenced by low coefficients of determination. The only best-fit line which appears to fit well to its data points is that for rainfall depth-runoff depth ($R^2 = 0.9248$), though this is largely due to the effect of four points away from the main cluster. The actual relationship given by the line of best fit: "runoff depth is approximately 8 mm less than rainfall depth" implies a constant retention capacity for the green roof, regardless of the duration of the dry period before a storm and the ambient temperature and direct solar radiation experienced by the roof in that time, and is therefore physically meaningless from an engineering and stormwater management perspective. It is shown in (b) that the depth of water retained by the roof is in no case greater than 20 mm, represented by the curved dotted line on that figure. As this corresponds to approximately 25% of the substrate depth (or 21% of the substrate depth plus 3 mm of storage in the drainage layer), it is assumed that the maximum recorded retention depth of 19.6 mm is at or near the finite upper limit of the green roof's storage capacity. The significance of Figure 3.5 (b), which plots rainfall depth against percentage retention, is much less than that of Figure 3.5 (a), reflecting the fact that a storage depth measured in mm does not change, but that same storage depth measured as a percentage is a variable that depends on the depth of the storm.

Figure 3.5 (c) and (d) do not show any significant link between ADWP and either measure of retention. This is likely due to the fact that evapotranspiration rates vary widely throughout the year; one full day of direct solar radiation in the height of summer could recharge as much storage capacity as one cloudy week in mid-winter. Hence, the total storage recharge occurring in a dry weather period is somewhat unrelated to its duration. ADWP does not take into account the general weather conditions in the days or weeks leading up to an event, only the elapsed time since the previous event occurred. The ADWP measure does not differentiate between a storm of the smallest depth recordable by a rain gauge and a storm of record-breaking depth. In common with many other parameters, the AWDP plots feature a clear outlier: a storm with an antecedent dry weather period of 199 hours. As this event occurred in the summer, and was relatively shallow and of short duration, it is not surprising that it was retained in its entirety.

As the use of 24-hour ADWP is common, consideration was also given to the small group of six events with ADWP in excess of 24 hours. The mean retention of these events was 9.04 mm, 1.37 mm higher than the mean retention of all 21 significant events, while the minimum was
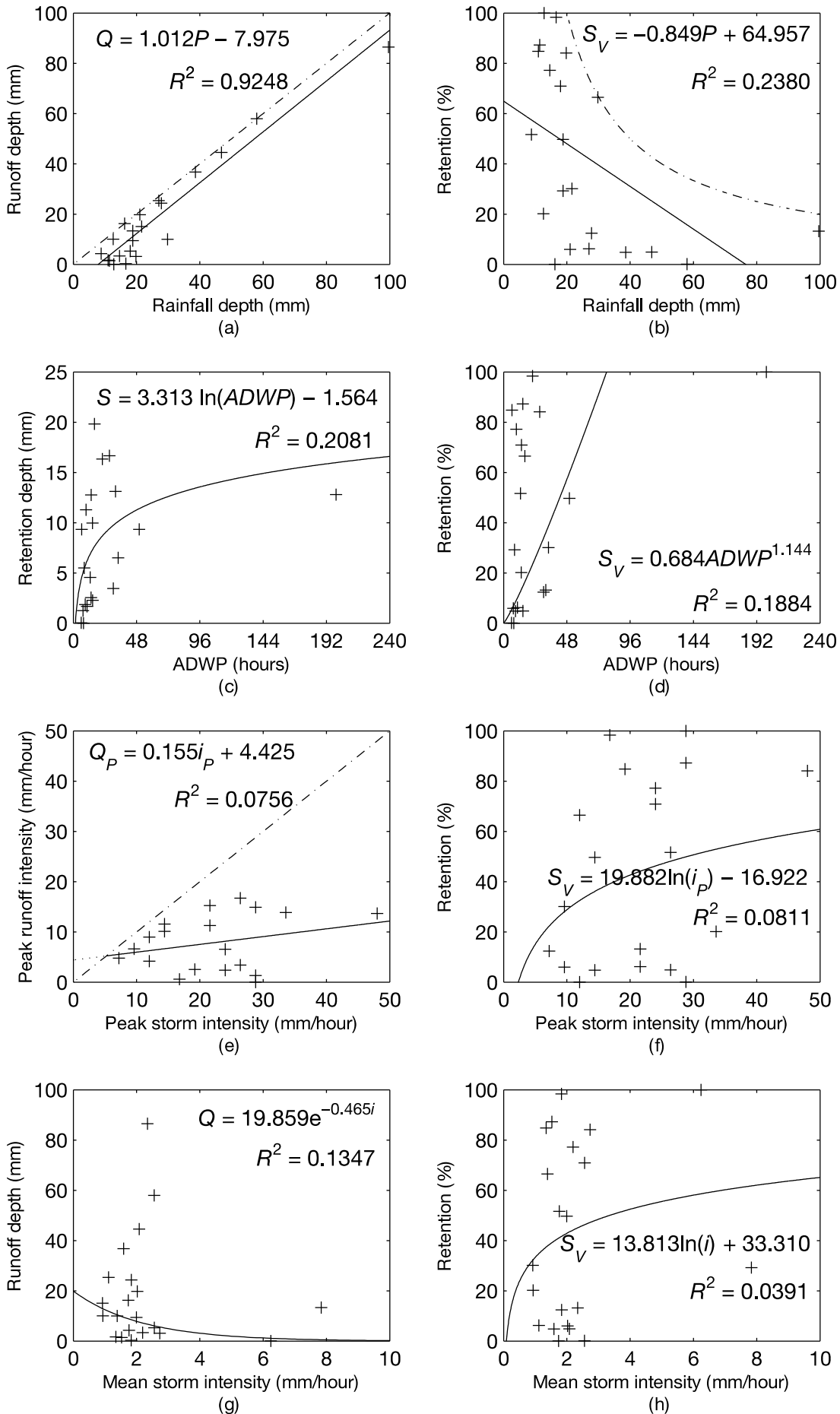
Figure 3.5 – Untransformed single-parameter regressions.

Table 3.6 – Single-parameter equations with transformed variables.

Equation	R^2	Standard Error
$Q^{1/3} = 1.514 \ln P - 2.410$	0.724	0.215, 0.670
${S_V}^{0.43} = -2.173 \ln P + 11.052$	0.329	0.712, 2.222
$S^{0.55} = 0.882 \ln ADWP + 3.130$	0.248	0.352, 0.317
${S_V}^{0.43} = 1.136 \ln ADWP + 4.832$	0.175	0.567 0.510
${Q_P}^{3/5} = 1.089 {i_P}^{1/5} + 1.190$	0.014	2.200, 4.022
${S_V}^{0.43} = 3.421 {i_P}^{1/5} - 1.858$	0.088	2.526, 4.636
$Q^{1/3} = -0.314 \ln i + 2.448$	0.024	0.462, 0.393
${S_V}^{0.43} = 0.690 \ln i + 3.916$	0.025	0.982, 0.835

significantly above zero, at 3.45 mm. While it is not surprising that more retention occurred of events with longer antecedent dry periods, it is noted that the event for which retention depth was greatest had an ADWP of just over 16 hours, highlighting the crudeness of the ADWP measure as a proxy for a roof's initial moisture content at the beginning of a storm event.

The mean storm intensities recorded in this experimental programme are spread over a large range and somewhat negatively skewed. Peak storm intensities are less skewed, with similar values for the mean and median, an almost equal number of storms above and below the median, and a Shapiro-Wilk significance of 0.065 for the untransformed data set. Peak and mean storm intensity are not strongly correlated to each other ($R^2 = 0.3494$). Figure 3.5 (f) to (h) show high levels of scatter and low coefficients of determination for the best fit lines, demonstrating that neither peak nor mean storm intensity can be used to predict the retention performance of this green roof. While it may be intuitive to assume that more intense storms will cause more intense runoff, Figure 3.5 (e) shows that peak storm intensity is not a good predictor of peak runoff intensity. This implies that the attenuation effect of the green roof test bed is very high. Although the correlations shown in Figure 3.5 (g) and (h) are very weak, they are unusual, in that the lines of best fit run opposite to their expected gradients, showing improved performance under more intense storms.

Table 3.6 presents the equivalent equations to those depicted in Figure 3.5, using the transformed forms of the parameters. These equations would normally be expected to be more accurate than the equivalent equations using untransformed statistics, due to all data sets being similarly (i.e. more normally) distributed, and this is generally the case here. However, as the predictive capacity of these equations is still generally poor, and the requirement for transformations of variables moves these equations away from easy-to-understand, easy-to-implement "rule of thumb" territory, they will not be discussed further.

3.5.3 Multiple Regression Analyses

The single-parameter analyses generally produced models with poor predictive capability. It is presumed that the roof's performance, as quantified by any metric, is more likely to depend on a range of independent factors, rather than just one. However, the large number of possible combinations of the ten measured storm and climatic variables, repeated for each of the eight performance metrics, precludes an exhaustive assessment of all combinations. Furthermore, it is not intuitive as to which combinations of storm and climatic variables will produce the most useful models for any particular performance metric. Stepwise linear multiple regression is a repeatable methodology for model evaluation and optimization, subdividing into forward, backward and bi-directional methods. A model created by forward linear multiple regression begins with only one term, a constant. A pool of potential independent variables is defined, and each variable is tested in the model independently of all others. The one variable which has the largest semi-partial squared correlation with the dependent variable is added to the model and its scale constant optimized. This process is repeated with the remaining pool of independent variables until no independent variable meets the minimum significance criterion for entry, as measured by its p-value. If no independent variable in the initial pool meets the minimum significance criterion for entry, then no independent variable can be considered to correlate significantly with the dependent variable. Backward linear multiple regression is the reverse process: the model begins with all proposed independent variables and at each stage, the independent variable which has the lowest semi-partial squared correlation with the dependent variable is removed, until all remaining independent variables meet the minimum significance criterion for inclusion. Bi-directional regression is a more sophisticated regression method. It is similar to forward regression, but after the addition of a new independent variable to a model, any of the terms already in the model may be removed if they are no longer significant.

Increasing the number of predictive terms in a regression analysis will always cause R^2 to increase. Adjusted R^2 is a measure that increases only if the addition of an extra term improves the model more than would be expected by chance. Its value is therefore always equal to or less than the value of R^2 for the same model, and may be negative. Adjusted R^2 is defined as:

$$\bar{R}^2 = R^2 - (1 - R^2)\frac{p}{n - p - 1}$$

Equation 3.1

where p is the number of regressors and n is the size of the data set, which is 21 for most variables, 19 for three of the four statistics requiring exact storm profiles and 18 for t_P, due to one untransformed value being negative and the best transformation being the natural logarithm.

Bi-directional linear multiple regression analyses were performed in IBM SPSS Statistics 19, using a significance (p-value) of 0.05 as the criterion for entry/removal. All possible pools of

independent variables from the group of storm characteristics and the group of weather/climatic factors were proposed as potential regressors, with no mixing between these two groups. As with the single regression analyses, most of the models produced by stepwise multiple regression analyses were of low predictive capability. Table 3.7 presents only those equations with some possible potential to predict the hydrologic behaviour of the green roof test bed (adjusted $R^2 \geq 0.6$).

Some equations, particularly for S and S_V, had adjusted R^2 values between 0.5 and 0.6, which is close to the threshold value for inclusion in Table 3.7. Although the threshold for minimum R^2 is arbitrary, it is set low with general regards to consistent model accuracy. Therefore, as their utility is highly marginal, these equations should not be presented.

Of the many different models proposed for green roof performance, only two meet the minimum threshold for inclusion in this table. As both models are for cumulative runoff depth, it can be concluded that, of the eight green roof performance metrics for which models were proposed, only one, Q, can be accurately and consistently modelled using parametric correlations. Furthermore, no variable was entered into any proposed model for t_{50} (cumulative median delay), indicating no significant link between t_{50} and any proposed independent variables.

In both equations presented in Table 3.7, the independent modelling parameters describe only storm event characteristics i.e. no proposed model based on antecedent weather and long-term climatic factors fits well enough to the recorded green roof data to justify presentation. Both equations given in Table 3.7 show a positive link between runoff depth and rainfall depth, either expressed directly as P, or indirectly as duration D and mean intensity i. Both also show a negative link between runoff depth and ADWP. This is partly to be expected, as a longer ADWP generally corresponds to increased cumulative evapotranspiration. However, the relationship between evapotranspiration and ADWP is greatly variable (see the discussion related to Figure 3.5 (c) and (d)).

Further bi-directional regression analyses were conducted, allowing storm event characteristics and weather/climatic variables to be mixed, provided that all of the proposed regressors in a single pool were independent. Thirteen equations were produced with adjusted $R^2 \geq 0.6$: five for Q, five for S_V, two for A_P and one for Q_P. Table 3.8 presents the best-fitting equation for each of these four performance metrics. Figure 3.6 presents comparisons between recorded and

Table 3.7 – Multiple parameter equations with transformed variables.

Equation	$\bar{R}^2$	Standard Error
$Q^{1/3} = 1.497 \ln P - 0.381 \ln ADWP - 2.506$	0.792	0.182, 0.130, 0.567
$Q^{1/3} = 8.559 D^{1/5} + 1.104 \ln i - 0.378 \ln ADWP - 6.052$	0.803	1.000, 0.256, 0.131, 0.982
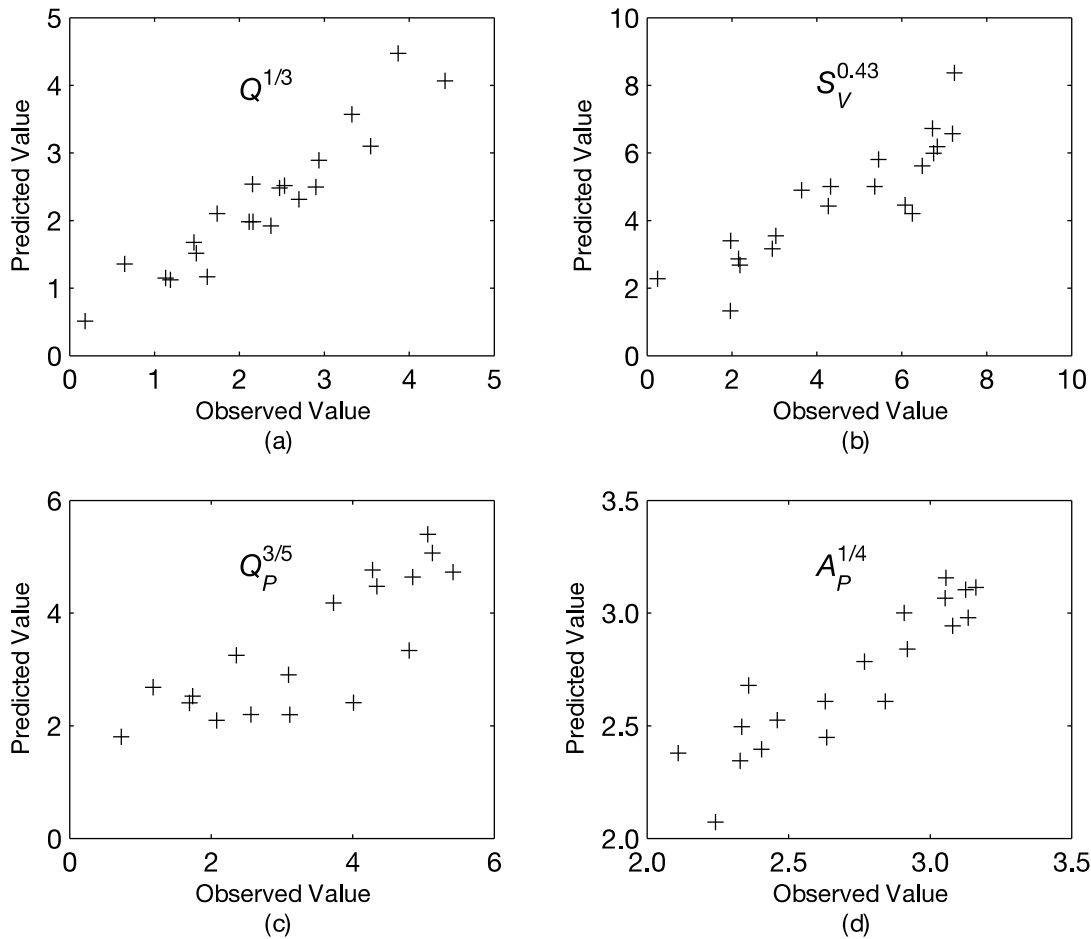
Figure 3.6 – Best-fitting mixed multiple parameter equations.

modelled values using the equations in Table 3.8 for runoff depth, percentage retention, peak runoff rate and peak runoff attenuation.

The first equation in this table takes a similar form to the two equations in Table 3.7. Runoff depth is positively correlated to storm event depth, represented by duration D and mean intensity i. P_F, the total depth of precipitation in the previous fortnight, replaces antecedent dry weather period, increasing the adjusted R^2 in the process. This improvement to the goodness-of-fit strongly suggests that the state of the test bed before a storm event (which influences its performance during a storm event) can be more accurately modelled by taking a more nuanced approach to characterizing the antecedent conditions before a storm; P_F attempts to measure the size and frequency of recent previous storms, while $ADWP$ simply measures the time elapsed since the last event, regardless of its size and the overall weather conditions leading up to it. Though the scalar term before $P_F^{0.3}$ is the smallest, the actual values taken by $P_F^{0.3}$ in the set of significant storms are generally larger than those taken by $\ln(i)$, such that the influence of P_F is around twice the influence of i in that equation. By mean influence, the largest term in this, and each of the other three equations in Table 3.8, is the constant.

Table 3.8 – Best-fitting mixed multiple parameter equations.

Equation	$\bar{R}^2$	Standard Error
$Q^{1/3} = 7.855D^{1/5} + 1.097 \ln i + 0.564P_F{}^{0.3} - 6.924$	0.872	0.823, 0.204, 0.121, 0.824
$S_V{}^{0.43} = -8.922D^{1/5} - 2.164 \ln i - 1.800P_F{}^{0.3} + 0.032T_D{}^{3/2} + 17.066$	0.749	2.468, 0.656, 0.372, 0.015, 2.719
$Q_P{}^{3/5} = 8.249D^{1/5} + 5.130i_P{}^{1/5} + 0.495P_W{}^{0.45} - 15.226$	0.684	1.962, 1.445, 0.164, 3.387
$A_P{}^{1/4} = -0.247 \ln P - 0.185P_W{}^{0.45} - 0.175 \ln ADWP + 4.114$	0.784	0.063, 0.031, 0.061, 0.200

The second equation, for $S_V{}^{0.43}$, depends generally on the same parameters as the equation for $Q^{1/3}$, but negatively. This is not surprising, as runoff and retention are linked to each other and, as one increases, the other decreases. A fourth parameter, $T_D{}^{1.5}$, describing the mean temperature in the 24 hours preceding the significant event, is statistically significant ($p = 0.047$) in determining retention. Physically, this states that more of an event is retained if the weather preceding the event is warmer. This is a reasonable assumption to make, as hotter weather leads to more evapotranspiration and hence more storage recharge in the substrate. The scale parameter of $T_D{}^{1.5}$ is small, suggesting that antecedent temperature only slightly affects percentage retention. However, its exponent is large in relation to transformations performed on other independent variables, so a linear change in temperature results in a greater than linear increase in retention. Applying the equation separately to each of the 21 significant storms reveals that the influence of T_D is of a similar magnitude to the influence of i. As the adjusted R^2 for the second equation in Table 3.8 is relatively high, it is perhaps surprising that the actual depth of retention, in mm, could not be successfully modelled by any proposed combination of parameters. It should be noted that the equation for $S_V{}^{0.43}$ gives a negative value for one event (monitored retention 0.07%, negligible). This cannot be raised to an exponent of (1/0.43), so predicted S_V cannot be calculated for that storm. However, assuming $S_V = 0$ would, in this case, be an accurate prediction.

The equation for $Q_P{}^{3/5}$ takes a similar form to the equation for $Q^{3/5}$, consisting of a constant and three positive predictors. In both cases, the performance statistic to be modelled is correlated positively to transformed rainfall duration and some transformed measure of antecedent rainfall. The dependence on mean storm intensity is replaced by a dependence on peak storm intensity. This may not initially seem surprising as the performance statistic now considers peak, rather than total, runoff. However, the direct linear relationship between peak storm intensity and peak runoff intensity (Figure 3.5 (e)) is particularly poor-fitting, with R^2 below 0.1, and the correlation between the transformed parameters ($i_P{}^{1/5}$ and $Q_P{}^{3/5}$) is even lower with R^2 of just 0.014. Applying the equation separately to each of the 21 significant storms reveals that the i_P term is second only to the constant term in mean influence. In common with the predictive equation for $S_V{}^{0.43}$, one value predicted for $Q_P{}^{3/5}$ was negative and was therefore unable to be raised to the exponent of 5/3

necessary to give a prediction for Q_P. For this event, the recorded value of Q_P was negligible, at 0.02 mm/hour. Again, assuming $Q_P = 0$ would be an accurate prediction in this case.

The fourth equation, for $A_P^{1/4}$, attempts to model time-series peak reduction, similarly to the third equation, for $Q_P^{3/5}$. It is in fact noted in Section 3.5.1 that $A_P = 100 \times (1 - Q_P/i_P)$. The form of the fourth equation in Table 3.8 is greatly different from that of the third equation, especially when the link between Q_P and A_P is considered. This may be in part due to the parameter transformation, but that is unlikely to be the sole or main explanation for the great difference. The equation for $A_P^{1/4}$ is unique in Table 3.8 for being the only equation to show $ADWP$ as a predictor for the performance metric. It is hypothesized earlier in this section that $ADWP$ is too crude a measurement for predictions of this type. The equation for $A_P^{1/4}$ includes, in addition to $ADWP$, a term for P_W, one of the more nuanced alternatives proposed for $AWDP$. The mean magnitude of the P_W term is over five times the mean magnitude of the $ADWP$ term, suggesting that the inclusion of the term for $ADWP$ may result from the rigid application of statistical rules to the multiple liner regression analyses. By the inclusion of P as a predictor variable, the link between peak rainfall intensity and peak runoff intensity is broken, though it is unclear whether a physical link between these two variables existed; they are poorly correlated, either when transformed or untransformed, but have a greater effect on the prediction of $Q_P^{3/5}$ than any other variable.

While, individually, none of the equations contains unexpected predictors, the seemingly random way in which similar parameters (e.g. P and i/D) are included or omitted from interrelated predictions of performance (e.g. Q_P and A_P), suggests that these relationships may be more a product of rigidly-applied statistical rules than physical processes and dependencies. This is further supported by the fact that very few stepwise regression analyses resulted in well-correlated equations.

3.6   Conclusions

The retention performance of a green roof test bed, over 27 months of a 29-month period, was assessed at multiple temporal scales – cumulative, annual, seasonal and individual event. Cumulative retention over the entire period was found to be 49.3%, a relatively low figure which may be attributed to the local maritime temperate climate, the above average total precipitation depth over the monitoring period and, potentially, the depth of the system build-up which, although typical of an extensive roof, is shallow in comparison to roofs monitored in many similar studies. Annual retention was found to be highest for the calendar year with the lowest depth of rainfall. The lowest annual retention figure, however, was for the calendar year containing most of the largest individual storms and not the calendar year with the greatest overall rainfall depth. A seasonal appraisal of retention performance suggested that the greatest

retention occurred in spring, not summer. However, the depth and frequency of storms was noticeably higher in summer than in spring, suggesting that the expected increase in evapotranspiration, hence storage recharge in the roof, over the summer, was insufficient to fully counter the increased depth and frequency of large individual rain events. The retention performance of the green roof on an individual event basis was significantly higher than on a cumulative basis – 69.6% mean, 90.9% median. This is a result of the individual event metric weighting each storm event equally, in contrast to cumulative performance evaluations, which implicitly weight storms according to their depth. More than half of the recorded storm events were of less than 2 mm depth and would therefore be unlikely to generate runoff from a conventional roof. Applying a minimum depth criterion of 2 mm to the consideration of individual storm events reduced the mean and median per-event retention to 60.4% and 61.7% respectively. It is therefore concluded from the annual, seasonal and per-event assessments that the retention performance of a green roof can be greatly affected by individual large storms. It is also apparent that traditional per-event performance statistics, which consider all events with equal weighting, will hide the decrease in retention performance under the largest storms. Even cumulative retention figures may obscure this decrease in performance, provided that the cumulative depth of small storms is major in relation to the cumulative depth of all rainfall over the monitoring period. Overall, it can be seen from the analysis of rainfall and runoff data that a range of performance figures can legitimately be given to evaluate the performance of a single green roof. This originates from the range of ways in which rainfall data can be considered. In particular, retention performance under more important (from a drainage perspective) storms is unlikely to meet the (normally annual) figures reported in most commercial literature, but may still be highly significant in its own right.

A set of 21 significant events with utilizable rainfall and runoff data was identified from the full data set, consisting of all those storms with return period above one year and those whole storms whose peak one, six or twelve-hour period would exceed the same requirement, if taken in isolation. These storms were characterized according to five intrinsic properties. The antecedent weather conditions preceding each storm were characterized by four parameters, with the related mean long-term monthly temperature as a fifth weather/climatic parameter. The green roof's runoff response to each storm was characterized by eight performance metrics, except in the case of two partially-reconstructed runoff records, which were characterized by four. Eight proposed relationships between one intrinsic storm property and one green roof performance metric were tested by evaluating the coefficient of determination (R^2) of the best-fit relationship between the observed values of the performance metric and the estimated values of that metric as derived from a linear predictive equation. In all cases but one, R^2 was less than 0.25. Only the linear relationship between rainfall depth and runoff depth had an apparently high predictive capability,

though the actual best-fit equation generated was physically meaningless from an engineering perspective (approximately, runoff depth equals rainfall depth minus eight millimetres).

The eighteen parameter sets were transformed to increase their normality, and stepwise linear regression, using all possible sets of independent predictor variables, was employed to identify less obvious relationships between green roof performance, and storm properties and/or antecedent weather/climatic conditions. A handful of equations were generated with adjusted R^2 greater than 0.6, though no equation of this quality could be produced for four of the eight performance metrics.

Due to the generally poor quality of even the best-fitting predictive equations, it is concluded that parametric analyses are not consistently valid for modelling the performance of a green roof test bed in response to the most significant storm events. Instead, a generic, process-based model of the movement of water over time within a green roof is likely to provide the most suitable framework for modelling the runoff response of a green roof test bed resulting from a storm event. Chapters 5, 6 and 7 propose and test appropriate modelling methods for the drainage layer, substrate layer and a two-layered system respectively. The corresponding experimental setup and test programmes are discussed in Chapter 4.

4 Experimental Setup

4.1 Chapter Overview

This chapter contains detailed descriptions of the two rainfall simulators used in the testing of green roof substrate and drainage layers. Modifications made to the large simulator are detailed. Calibration tests performed and test programmes for each simulator are given. Reference is made to a third set of experimental equipment, different forms of which were used in two experiments aimed at quantifying moisture fluxes of green roof components during dry weather periods. These experiments did not produce suitably robust results to warrant further discussion outside of Appendix A. A brief section on units of measurement is also included, to aid in understanding of the sections that follow.

4.2 Introduction to Experimental Programme

To create the separate hydrological models for the drainage and substrate components, two separate rainfall simulators were used: one "large" rainfall simulator to test the drainage components and one "small" rainfall simulator to test the substrate. Separate rainfall simulators were required as water percolates vertically through substrates, but flows horizontally along drainage components. Hence, the large rainfall simulator has an impermeable base and a full-width side outlet at its downstream end, whereas the small rainfall simulator has impermeable sides and a full-diameter outlet at the base of the substrate holder. When a storm event occurs over a complete green roof system, the substrate and drainage layer act as components in series, i.e. all water passes first through the substrate, then irreversibly into the drainage layer, then out of the system. Therefore, as all runoff leaves complete systems by horizontal transfer, it is only appropriate to use the large simulator for testing a substrate and drainage component together.

As the shape of the runoff profile is expected to be affected by different physical parameters for the substrate and drainage layer, each rainfall simulator is designed to allow the factors specific to its tested component to be easily altered.

4.3 Units of Measurement

The following text does not use a single unit of measurement to refer to flow rates or intensities, as different units of measurement are more appropriate for different contexts. The intensity of a storm, for example, is commonly written either with units of litres per time interval per unit of area (DIN, 2008; FLL, 2008) or units of depth per time interval (CEH, 1999). When referring to the large rainfall simulator, one particular unit of measurement may be converted to another using Equation 4.1:

$$100 \, \mathrm{l/s} \cdot \mathrm{ha} = 0.6 \, \mathrm{mm/minute} = 3 \, \mathrm{l/minute} \qquad \textbf{Equation 4.1}$$

For the small rainfall simulator, the conversion equation is given by Equation 4.2:

$$100 \, \text{l/s} \cdot \text{ha} = 0.6 \, \text{mm/minute} = 61.072 \, \text{ml/minute} \qquad \textbf{Equation 4.2}$$

In both equations, the third term is not dimensionally consistent with the first two; the equations are only valid as the areas of the rainfall simulators ($5 \, \text{m}^2$ and $0.1018 \, \text{m}^2$ respectively) are incorporated into the conversion factors. As the plan area of the large rainfall simulator is almost 50 times greater than that of the small simulator, the last term in Equation 4.1 is presented in litres per minute, whereas the last term in Equation 4.2 is presented in millilitres per minute.

It is also worth noting that rainfall depth can be related to volume by the simple equation:

$$1 \, \text{l/m}^2 = 1 \, \text{mm} \qquad \textbf{Equation 4.3}$$

The relation given in Equation 4.3 is dimensionally consistent and generically applicable both inside and outside of this thesis.

4.4 Large Rainfall Simulator

4.4.1 Overview

The large rainfall simulator (Figure 4.1) was located in workshop/lab space at the ZinCo GmbH international headquarters which, for the duration of this experimental programme, was located in Unterensingen, Germany. Since summer 2012, the simulator has been operational in a ZinCo warehouse in nearby Kirchheim-unter-Teck. The large rainfall simulator was originally built by ZinCo to determine the coefficients of discharge of various ZinCo green roof systems, following the methodology given in "Guidelines for the Planning, Execution and Upkeep of Green-roof sites" (FLL, 2008). For this reason, its original design copied that of an official FLL rainfall simulator in Geisenheim, Germany. A detailed description of the large rainfall simulator, in its original state, can be found in Section 4.4.2. Following a detailed analysis of the capabilities and limitations of the rainfall simulator, modifications were made to reduce or eliminate any
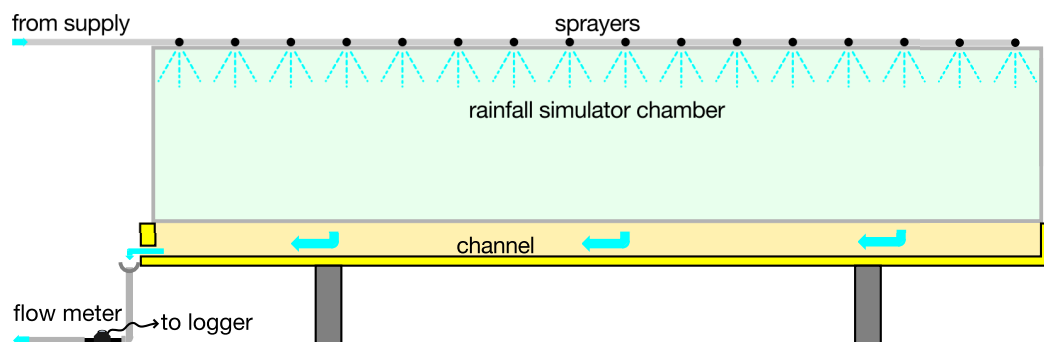
Figure 4.1 – Large rainfall simulator as of October 2010.

shortcomings that would have seriously impacted the quality of the results obtained from the test programme. These modifications are detailed in Section 4.4.3.

4.4.2 Description as of October 2010

The large rainfall simulator consists of the following components: A water control system to control the rate of inflow to the rainfall simulator; a sprayer network for supplying simulated rainfall; a chamber with clear plastic sides and a waterproofed test bed; a gutter and drainpipe to remove water that has passed through the chamber; a nutating disc flow meter on both the water supply system and drainpipe; a data logger to record the outputs of the two flow meters; and a computer connected to the ZinCo fileserver, to permanently store the data records. Each of these components is described in detail below.

The water control system connects the building's water supply to the sprayer network. It consists of, in flow order: an Amiad Filtration Systems filter with 100 micron mesh; a main tap, which is used only to stop and start the flow; a pressure-regulating valve with needle gauge, which is used to monitor and manually control the rate of flow; and a Badger Meter RCDL M25 LCR nutating disk flow meter. The components are connected by plastic pipes of 15 mm diameter. The building's water supply pressure is an unknown of at least 5 bar, but the sprayers that supply simulated rainfall are believed to be damaged by pressures above 3 bar. Measured water pressure and rainfall rate are related quadratically, hence the pressure regulating valve is the means by which rainfall rate is controlled and varied. At a gauge pressure of 3 bar, the rate of inflow is slightly over 18 litres/minute. At the valve's minimum pressure of 0.2 bar, the rate of flow into the sprayer network is slightly under 4 litres/minute; hence, the range of possible rainfall rates varies from 0.8 to 3.6 mm/minute. The Badger Meter records, at 15-second intervals, the total quantity of water that has passed through since its last reset, to a volumetric resolution of 0.1 litres. As the total quantity is sampled at 15-second intervals, the flow rate for each 15-second period can be calculated to the closest 0.4 litres/minute. The output from the Badger Meter was used to adjust the pressure valve in order to find the pressures required to produce all possible even-numbered flow rates in litres/minute; it is from this that the quadratic calibration curve was generated (Figure 4.2)

The sprayer network consists of three parallel 16 mm diameter pipe lines running along the length of the simulator, which are connected to each other and the water control system, by a pipe running perpendicular to their length, at their lowest point. The two outside lines of the sprayer network are both 32 cm to the side of the central line, which is centred relative to the width of the simulator chamber. Each line contains 16 spraying nozzles, spaced at 30 cm intervals, the release rates of which are dependent on the pressure of the water in the network. Due to frictional pressure losses that would be expected along any length of pipe, it is expected
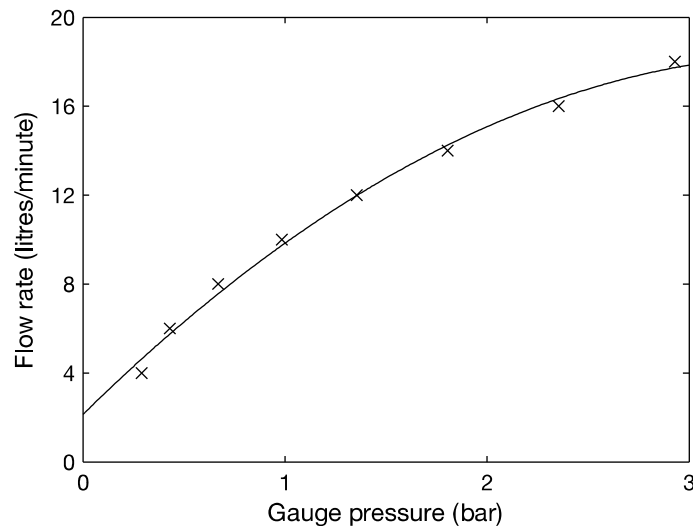
Figure 4.2 – Calibration curve of flow rate vs. gauge pressure for initial dripper network.

that the release rates of the sprayers decrease with distance from the point at which water enters the network. A related concern is that the angle over which water is sprayed is dependent on pressure; higher pressure corresponds to a greater angle of spray. Connected to the perpendicular running pipe is another similarly-dimensioned pipe containing a tap, which runs vertically downward. The tap is normally closed, but at the end of a test, can be opened to quickly drain the sprayer network; this abruptly terminates the release of water from the spraying nozzles. If the drain tap is not opened, water will continue to spray until it can be held in the pipe network by atmospheric pressure; the total volume of excess spray is estimated at between 1.5 and 2.5 litres.

The rainfall simulator chamber consists of a channel base with side walls rising to approximately 300 mm, all made of wood. Green roof systems and components to be tested are placed here. The channel base has a length of slightly over 5 metres and width of slightly over 1 metre. However, as the wood surfaces are covered by a rubbery grey waterproofing sheet, the length and width into which green roof systems and components can be placed are reduced to 5 metres and 1 metre respectively. Above the channel side walls are positioned transparent plastic walls, held together by a metal frame. This frame also supports the sprayer network at a height of approximately 1.1 metres above the channel bed. The walls, frame and sprayer network assembly can be lifted as a single unit, to allow access to the channel base. This is achieved by the use of two cranes, each of which is attached to the frame at approximately one-third of the distance from either end. The slope angle of the simulator chamber is infinitely adjustable, from flat to an unknown maximum greater than 10 degrees. A full-width opening at the downstream end of the chamber allows water that has transferred out of the tested system or component to leave the chamber unimpeded. A 130 mm diameter gutter is attached outside the chamber, running alongside the opening for its full width and transitioning to a 70 mm downpipe at one end.

The downpipe runs vertically to the floor of the workshop, where it turns horizontal and is capped by a reduction fitting, out of which comes a flexible 25 mm diameter pipe. The flexible pipe feeds directly into a Badger Meter RCDL M25 LCR nutating disk meter, configured identically to the previously mentioned Badger flow meter. The 25 mm flexible outlet pipe from the flow meter connects to an expansion fitting, where it joins to another 70 mm rigid drain pipe. This drain pipe carries the water out of the building.

The output from both flow meters is recorded by an Ahlborn Almemo data logger with 256 kb internal solid-state memory. This therefore holds corresponding time-series rainfall and runoff profiles for a test, at a temporal resolution of 15 seconds and a volumetric resolution of 0.1 litres, which together give an equivalent depth resolution of 0.08 mm/minute. The data logger is permanently connected to a desktop computer via RS-232, which is used to provide a greater storage capacity for test runoff records. Downloaded records are saved on the ZinCo fileserver.

In addition to the sprayer network installed as of October 2010, two other interchangeable alternative rainfall distribution systems are present in the lab. One of these consists of 34 spraying nozzles, of the same type as those used in the installed spraying system, arranged in 2 lines of 17, with a dripper spacing of approximately 29 cm along the lines and a line spacing of approximately 38 cm between the lines. The other alternative system consists of 50 one metre-long lines, running across the width of the simulator, at a line spacing of 10 cm. Each of these lines contains either 10 or 11 Netafim button drippers for a total of 516. The nominal flow rate of these drippers is 2.0 l/hour at 1 bar. Their maximum recommended working pressure is 2 bar, though they are known to have been used previously at pressures up to 3 bar.

4.4.3 Modifications

Following a detailed assessment of the capabilities of the rainfall simulator, a number of issues requiring improvement were identified. These were: the volumetric resolution of the existing monitoring equipment, the spatial distribution of the rainfall; the range of available rainfall rates; the fine control of rainfall rates; and the adjustment of drainage length. The processes used to address these issues, as well as the final outcomes, are given below. Figure 4.3 depicts the simulator after all modifications.

A sixth issue was also identified, namely the low impact velocity of the raindrops. The modification programme did not address this issue, primarily due to the extreme impracticalities that would be involved: a fall height of 12 m is required for a drop of 5 mm diameter to reach terminal velocity under gravity (Clarke & Walsh, 2007). The use of high-pressure spraying nozzles, which themselves impart kinetic energy to the simulated rainfall, reduces the required fall height, but is not compatible with the proposed solution for improving the spatial and

temporal distribution of rainfall. For this experimental programme, accurately reproducing drop velocity and kinetic energy is not considered important, as the components exposed to the rainfall are made of rigid polyethylene and polystyrene. Indeed, drops with low energy are considered advantageous for the tests considered in Chapter 5 as the risk of splashing, which would never occur in the drainage layer component of a properly designed full green roof system, is limited. For tests including substrate, the low drop energy reduces the risk of erosion. Overall, all users of the simulator considered the low drop velocity and energy to be less important than the greatly improved spatial and temporal rainfall distribution. Following the end of this experimental programme, further modifications were made to the rainfall control system. These are discussed in Chapter 7.

4.4.3.1   Monitoring Resolution

If the methodology given by the FLL is used to determine the coefficient of discharge of a green roof system, then the minimum required monitoring setup consists of a stopwatch and a large collecting container with volumetric gradation. As the original monitoring setup was capable of measuring varying rates of runoff through time, it is clear that it was already well in excess of the requirements of the simple tests for which the rainfall simulator was initially built. However, the resolution of 0.08 mm/minute was considered too coarse to accurately record the time-series runoff curves that would be generated in this experimental programme, particularly for planned test events with comparably low rates of inflow. As the flow meters measure volume rather than rate, their volumetric resolution can be increased, but at the corresponding expense of temporal resolution. To improve both temporal and volumetric resolution, the outlet monitoring system was replaced with a pressure monitoring arrangement, consisting of a collecting barrel with included pressure transducer. The barrel was made from a length of vertically standing DN 315 drain pipe, with a capped bottom. A Druck PDCR 1830 pressure transducer and its data cable were taped vertically up the internal side wall of the barrel, the tape preventing movement of the cable or transducer during tests. The transducer was configured to record the pressure of the water above it in the barrel at one-second intervals. Above the top of the pressure transducer, a further 0.71 metres of the barrel height was of a constant cylindrical cross-section, giving a
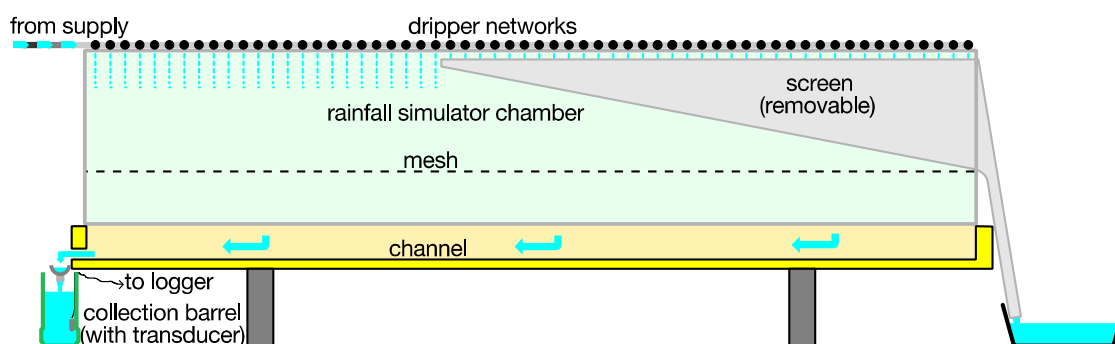
Figure 4.3 – Large rainfall simulator after modifications.

volume of approximately 50 litres for which an increase in collected runoff would be linearly related to an increase in recorded pressure. The minimum stable increase in pressure that could be recorded was equivalent to a volume of approximately 55 ml, or 0.011 mm equivalent rainfall depth, though three equally-spaced "unstable" pressure values also existed between each "stable" value, giving, with some uncertainty, a resolution of approximately 0.0028 mm, less than one thirty-fifth of the lowest test inflow rate proposed in Section 4.4.4.

4.4.3.2   Rainfall Distribution, Range and Control

The sprayer network that was installed at October 2010 could supply a minimum rainfall intensity of 0.8 mm/minute and a maximum rainfall intensity of 3.6 mm/minute. The minimum supplied rainfall rate was considered much too high to realistically simulate water inflow to drainage layer components; the layer of substrate above normally acts to greatly attenuate the intensity of the rainfall. The maximum supplied rainfall rate was also considered to be too low; a request was made from ZinCo that simulation of the 1-in-100 year, 5-minute storm for Stuttgart, an event of uniform 5.2 mm/minute intensity (DIN, 2008), should be possible for planned tests outside of this experimental programme.

The spatial distribution of sprayed water landing on the channel bed was not quantified as part of this research, but it could be seen that most water fell straight down at low pressures. Conversely, much of the water was sprayed against the plastic walls of the simulator chamber at high pressures, where it ran down to the edges of the channel bed. A Masters Student at a local college had previously quantified, for the network installed at October 2010, the spatial distribution of simulated rainfall at the channel bed and found it to be highly uneven.

Specific rainfall rates could not be directly requested. Instead, the required rainfall rate was indirectly requested by manually turning a valve to reduce or increase the water pressure, as measured by a needle gauge positioned before the sprayer network. At the end of a test, rainfall was stopped by closing the main tap. However, simply closing this tap alone did not cause the rainfall to end instantaneously. The drain tap, which was fitted to the sprayer network to allow it to be rapidly emptied, was opened simultaneously with the main tap's closure. This procedure quickly stopped the rain from falling at the end of a test, but left the sprayer network empty of water. Hence, when the main tap was re-opened at the beginning of the next test, an unknown and potentially varying fraction of the supplied water at any given time went towards re-filling the network, until the network was entirely re-filled.

It was therefore concluded that modifications to the experimental setup would be required to increase the available range of rainfall intensities, improve the spatial distribution of rainfall and decrease the uncertainty associated with the control of rainfall intensity. All three of these issues

were addressed by replacing the sprayer network with three new dripper networks and adding a microprocessor control system. The spatial distribution was further improved by adding a steel mesh between the dripper networks and channel bed (discussed separately in Section 4.4.3.4).

The three new dripper networks differed from any of the three existing networks by the use of pressure-compensating Netafim PCJ-LCNL drippers to supply the simulated rainfall. Pressure-compensating drippers are designed to supply water at a constant rate within a certain pressure range; in the case of the drippers used in these networks, this range is 0.7-4.0 bar. These drippers also completely shut-off at pressures of 0.12 bar and below (Netafim, Undated). As the flow rate through the drippers cannot be adjusted, three networks were built to allow three constant flow rates, low, medium and high, and all three networks were mounted side-by-side in the place of the removed sprayer network. In all three new networks, drippers are arranged according to a square grid pattern: $36/m^2$ in the low-flow network and $144/m^2$ in the medium- and high-flow networks. Pipes run parallel to the length of the simulator and the spacing between adjacent pipes is used to control the spacing of drippers across the width of the simulator, according to the square grid pattern. Two different variants of the PCJ-LCNL dripper are used: the low- and medium-flow networks use drippers with a stated flow rate of 0.5 litres per hour, whereas the high-flow network uses drippers with a stated flow rate of 2.0 litres per hour. Hence, the low flow network features 180 drippers to deliver a total of 90 litres per hour (0.3 mm/minute), while the medium- and high-flow networks feature 720 drippers each, delivering 360 and 1440 litres per hour (1.2 and 4.8 mm/minute) respectively. With all three networks running simultaneously, the maximum rainfall rate that can be simulated is 6.3 mm/minute. This is significantly in excess of the 5.2 mm/minute maximum rainfall rate required of any replacement system.

In order to allow for more than the seven rainfall intensities that can be simulated simply by operating one or more dripper networks continuously, the point of inflow to each network is gated by an electromagnetic valve. A Netafim Miracle Plus AC6 microprocessor is connected to each of these valves, thereby allowing a dripper network to approximate a lower rainfall intensity than its continuous flow rate, by opening and closing its associated valve over short time periods. The Miracle Plus controller can store six rainfall events in numbered slots in its internal memory. Each slot has its own numbered output terminal on the front of the controller, which can be physically wired to any valve or combination of valves. Each rainfall event is stored and described by four parameters. The total duration of the event is stored, as a start time and end time in hh:mm format. An "irrigation cycle" is also stored, as two durations in hh:mm:ss format, the first of which controls the duration of a high-voltage signal (causing the valve to open), and the second of which controls the duration of a low-voltage signal (causing the valve to close). If the duration of the irrigation cycle is less than the total duration of the event, then the irrigation

cycle is repeated from the beginning. If the stored end time is not reached, then the irrigation cycle is repeated, in full, until the stored end time has passed. Hence, each event always consists of an integer number of irrigation cycles, and is in general slightly longer than the integer number of minutes between stored start time and stored end time. For example, a cycle lasting 26 seconds will occur exactly 12 times between a specified event start time of 11:48 and end time of 11:53; the event will actually run from 11:48:00 to 11:53:12, ending twelve seconds after the specified end time. If a rainfall event requires that a network is only operated continuously, a continuous operation can be stored in the microprocessor's internal memory by setting the duration of the high-voltage signal equal to the required duration of the entire rainfall event, and setting the duration of the low-voltage signal sufficiently high that only one irrigation cycle can occur between the stored start and end times.

The continuous supply rates of the three systems (0.3, 1.2 and 4.8 mm/minute) are arranged in a geometric series, where each is four times greater than the previous. The purpose of this series, and its starting value of 0.3, is to allow all constant rainfall intensities from 0.1 to 6.3 mm/minute, in steps of 0.1 mm/minute, to be easily programmed using only continuous operation, or irrigation cycles with either a 2:1 or 1:2 ratio of high-to-low voltage duration. It is noted that a network operating at a 1:2 ratio of high-to-low voltage duration supplies rainfall for one-third of the event's total duration and supplies no rainfall for two-thirds of the event's total duration. As the time ratio of rainfall-to-no rainfall is increased, an event becomes less like a continuous rainfall of lower intensity and more like a series of short, isolated storms of the continuous-operation intensity, separated by increasingly large time periods with no rainfall. The 1:2 ratio was chosen as a compromise, allowing a wide range of different rainfall intensities to be programmed with simplicity and produced using an amount of readily-available equipment that was minimal and light enough to be crane-lifted into and supported by the simulator frame.

4.4.3.3   Calibration of the Microprocessor

For this experimental programme, the Netafim Miracle Plus AC6 microprocessor was intended to be used in "irrigation" mode, in which an irrigation cycle, consisting of some time period of rainfall followed by a pause, occurs one or more times over a given total event period. It was planned that any rainfall intensity that would be unavailable through continuous operation of a network (e.g. 0.8 mm/minute) would be simulated by operating a network or combination of networks with a higher continuous rainfall intensity, over a fraction of the event duration. Initially, it was assumed that the required time fraction would scale linearly with the required intensity i.e. dividing the required rainfall intensity by the continuous rainfall intensity of the network(s) to be used would yield the time fraction for which the networks in use should operate over the entire event duration. However, this assumption was quickly found to be incorrect for two reasons. First, rainfall did not immediately stop after the closure of a valve. This was not

surprising, as immediately upon valve closure, the pressure in a network is greater than the 0.12 bar shut-off pressure. Hence, rainfall will continue until the shut-off pressure is no longer exceeded. Second, the microprocessor inserted its own unexpected pause between irrigation cycles which were intended to immediately follow each other. As a simple fractional relationship was clearly unsuitable, a full calibration programme was developed in order to accurately relate rainfall intensity to microprocessor programming.

The first part of the calibration programme determined the duration of the extra pause inserted by the microprocessor and quantified its variability. A short irrigation cycle, of 20 seconds high-voltage followed by 10 seconds low-voltage, was programmed to repeat continuously over a ten-minute test duration. A digital clock, capable of displaying seconds, was kept close to the rainfall simulation system, observed continuously over the course of the test and the time displayed was noted at every voltage state change. This was repeated six times, for a total of 6×10 (nominally programmed) minutes. Next, a cycle of 20 seconds high/20 seconds low was programmed to repeat for 20 minutes. This was repeated twice for a total of 3×20 minutes. Finally, a cycle of 20 seconds high/40 seconds low was programmed to repeat for 60 minutes. Over the 180-minute course of this calibration programme, 217 extra pauses were inserted, once for every change from a low to a high state. The extra pause inserted by the microprocessor was always 8 seconds. There was no variation in this value and no evidence to suggest that, if more accurate time-keeping equipment had been used, this pause would be noticeably less or more than the recorded integer value of 8 seconds i.e. N in Equation 4.4 was always an integer value.

$$\frac{Time\ between\ any\ two\ similar\ state\ changes\ (s)}{8 + cycle\ duration\ (s)} = N \qquad \textbf{Equation 4.4}$$

In Equation 4.4, a "state change" is defined as either a step from high- to low-voltage or a step from low- to high-voltage. "Similarity" between state changes requires that they occur during the same programmed irrigation cycle and the voltage steps in the same direction.

With the pause now accurately quantified, the second part of the calibration programme was to develop a calibration curve for each network for the purpose of relating the effective long-term rainfall rate to the programmed low-voltage duration. Four tests, each of 10 minutes duration, were performed for the medium-flow network, in which the high-voltage duration was fixed at 20 seconds and the low-voltage duration took values of 10, 20, 30 and 40 seconds. The total volume of rainfall released in each test was recorded, to the nearest 0.1 litres, by the Badger Flow Meter. The total volume per test was then plotted against the programmed low-voltage duration; this relationship is shown in Figure 4.4. Otherwise identical tests, with the high-voltage duration now fixed at 10 seconds, were performed separately for each of the three inflow networks, including
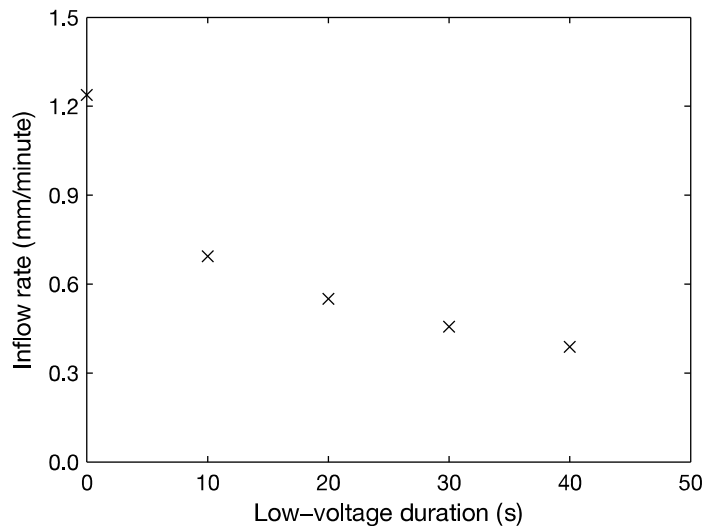
Figure 4.4 – Calibration curve of simulated flow rate vs. low-voltage duration for medium-intensity dripper network.

the medium-flow network. These tests were used to estimate the low-voltage durations required to provide the non-constant flow rates intended for use in the drainage layer experimental programme (0.6 and 2.0 mm/minute). After these low-voltage durations were estimated, all were verified by running the simulator for ten minutes using the derived low-voltage duration values and subsequently reading, from the Badger inflow meter, the total quantity of water delivered.

4.4.3.4 Mesh

As only pressure-compensating drippers are used in these new networks, and each network features only drippers with one stated flow rate, it was assumed during the design stage that the variability of rainfall from each individual dripper in a network would be small, provided that the actual flow rate of each dripper was close to the stated flow rate. However, there was concern that the physical spacing between drippers, especially in the low-flow network, could potentially be large enough to leave significant dry patches at the channel bed, leading to poor spatial variability at smaller scales. In addition, as the drops fall vertically downwards, erosion, directly underneath the drippers, could potentially occur of any substrate being tested. A steel mesh, of 1 mm diameter wire and 3 mm spacing was positioned between the drippers and channel bed, in plane with the slope of the simulator, to randomize the position and size of the drops released by the drippers, thereby improving rainfall distribution and reducing the risks of substrate erosion.

To determine the height at which the mesh should be placed for the most even distribution of rainfall upon a test system, a "uniformity grid" was assembled. This consisted of 196 plastic drinking cups, of approximate rim diameter 71 mm, capacity 225 ml and height 110 mm, glued in a 14 × 14 square grid arrangement to a square metre panel of ZinCo Floradrain FD 25 drainage layer. As the randomizing mesh was proposed as an initial measure, months before the

planning, design and installation of the new networks, the tests described below were performed with the original network of 516 non pressure-compensating drippers.

An empty, nominally identical, removable cup was stacked into each glued cup at the beginning of each test. The grid was placed on the channel bed at the centre of the simulator. A 1.4 × 1 metre sample of the mesh was suspended above the uniformity grid, at an initial height of 35 cm relative to the bottom of the transparent plastic walls, increasing to 55, then 75 cm for the two subsequent tests. The dripper network was operated at a continuous rainfall rate of 1.6 mm/minute for 15 minutes. At the end of each rainfall event, the mass of each removable cup and its contained water was recorded and the results plotted in a square grid matching the arrangement of the cups in the simulator. 11 grams was subtracted from every value to account for the mass of the plastic cups, leaving a map of rainfall distribution for the centre of the simulator, for three different mesh heights. Christiansen's Coefficient of Uniformity (Christiansen, 1942) was assessed separately for each mesh height, taking the m-value to be the mean mass of water in one cup, for each test.

The tests of uniformity showed that the most uniform distribution of rainfall occurred at a mesh height of 35 cm. Uniformity was greatly reduced at a 55 cm mesh height and slightly reduced further at a 75 cm mesh height. However, distribution was not highly uniform at any mesh height. The observation that 516 nominally identical drippers could vary so significantly in practice directly inspired the use of pressure-compensating drippers in the replacement of the rainfall networks. Before the installation of the replacement network, further tests of uniformity were performed using the original network of 516 drippers, positioning the uniformity grid variously at the front, centre and back of the simulator, resting the grid on the channel bed or elevating by either 4 or 11 cm, and using rainfall rates of 0.8 or 4.0 mm/minute. As all original rainfall networks were replaced before the start of the experimental programme, the results of these tests are not discussed further.

After the installation of the three new dripper networks, the spatial uniformity of rainfall was tested for each network separately. A mesh height of 35 cm was used, as the new drippers appeared physically identical in shape to those which they replaced and hence were initially assumed to produce drops with similar characteristics. Due to time constraints, two more uniformity grids, both identical to the first, were assembled to allow simultaneous tests of uniformity at the front, centre and back fifth of the simulator. A 5 × 1 metre mesh, simultaneously covering all three grids, was assembled and used for both these tests and the experimental programme. The rain event in all three tests was of the continuous-operation intensity, and was of the duration required to produce 24 mm of rainfall. The results of these three tests are given in Figure 4.5 and Figure 4.6. The mass of an empty cup was revised to

5 metres

0.88	1.73	0.75	1.93	0.47	2.06	0.69	0.59	1.14	0.60	1.92	0.65	1.33	1.78
0.39	0.86	0.59	1.14	0.68	0.84	1.06	0.62	1.54	0.58	1.84	0.59	1.52	0.83
0.96	0.80	0.98	1.41	0.71	1.09	0.85	0.89	1.15	0.40	2.28	0.28	1.85	0.73
2.25	0.90	0.52	1.91	0.54	0.62	0.41	0.80	1.63	0.62	1.49	0.84	0.88	1.32
0.31	0.70	0.67	1.26	0.63	1.39	0.97	0.98	0.99	1.26	0.64	0.39	0.56	0.52
1.29	1.65	1.08	2.09	0.98	1.45	1.04	0.85	1.83	0.52	3.09	0.47	1.92	0.80
0.52	0.67	0.38	0.68	0.46	0.59	0.49	0.44	0.93	0.49	0.40	0.55	0.74	0.49
1.56	1.39	0.78	3.11	0.79	1.62	1.35	1.41	2.33	0.74	1.93	0.88	1.17	0.82
0.51	0.98	0.37	0.51	0.89	1.11	0.69	0.45	0.79	0.73	1.18	0.84	1.08	0.79
1.39	0.81	0.76	1.75	0.51	1.57	0.52	1.03	1.31	0.64	1.44	0.57	1.13	1.07
1.26	1.34	0.48	1.97	0.34	2.01	0.43	0.64	2.58	0.79	2.10	0.46	1.42	0.92
0.34	0.45	0.50	1.00	0.73	0.61	0.45	0.82	0.74	0.65	0.83	0.63	0.59	0.69
1.87	2.47	0.58	3.26	0.51	3.45	0.85	1.10	2.27	0.59	2.57	0.53	2.10	1.53
0.32	0.60	0.30	1.06	0.36	0.80	0.75	0.45	0.70	0.62	1.14	0.69	1.12	0.34

0.66	0.66	0.62	0.39	0.58	1.00	0.65	1.02	0.44	0.73	0.62	0.88	1.01	1.09
0.51	0.89	0.69	0.68	0.90	0.66	0.89	0.83	0.57	0.61	0.78	0.75	0.78	0.80
0.74	1.00	0.84	0.81	0.87	1.31	1.61	0.68	0.80	0.83	0.98	0.97	1.01	0.78
0.94	0.86	0.99	1.04	1.02	0.85	0.75	0.92	1.08	0.79	1.07	0.97	1.06	1.09
0.72	0.80	0.75	0.88	0.78	0.92	1.33	1.08	0.82	0.63	1.06	0.99	0.80	1.00
0.94	1.34	1.13	1.15	0.94	1.07	1.21	0.87	1.23	1.00	0.88	0.88	1.61	0.79
0.65	1.05	0.74	0.81	1.06	1.05	1.03	1.02	0.97	0.92	1.17	1.57	0.88	0.91
1.01	0.71	0.96	0.89	1.21	0.88	1.22	1.13	1.15	0.78	1.24	1.25	1.55	0.79
0.88	1.06	0.87	1.08	1.02	1.04	1.11	0.99	1.04	0.89	0.94	0.89	1.23	1.00
0.69	0.79	0.85	0.82	0.97	1.05	0.98	0.83	0.87	0.98	0.93	0.72	1.19	1.00
1.14	0.84	0.90	1.29	1.02	1.00	1.03	1.14	0.80	0.87	1.08	0.87	1.36	0.45
1.23	1.07	1.02	0.84	0.70	0.96	1.19	1.03	1.07	0.95	1.08	0.85	1.16	0.77
1.27	0.56	0.84	1.18	0.70	0.94	1.46	1.05	1.10	1.01	1.29	0.82	1.46	0.87
1.44	1.30	0.77	1.22	0.91	0.90	1.06	1.27	0.86	0.80	0.91	1.28	1.27	1.16

4 metres

3 metres

1.31	1.30	0.46	1.37	0.69	1.04	0.71	0.72	1.79	0.80	1.16	0.68	1.67	0.51
0.54	1.20	0.64	1.55	0.61	0.94	0.66	0.57	0.78	0.47	0.81	0.77	1.23	0.41
0.46	0.62	0.34	1.77	0.52	0.91	0.70	1.20	0.75	0.70	1.20	1.17	0.23	0.39
1.70	2.96	0.42	3.08	0.46	2.52	0.59	1.03	2.07	0.52	1.72	0.69	2.24	1.04
0.21	0.38	0.42	1.02	0.34	0.87	0.85	0.93	0.91	0.50	1.32	0.59	0.23	0.11
0.85	2.53	0.90	3.24	0.79	1.31	0.48	0.98	1.77	0.55	3.10	0.59	3.23	0.91
0.34	0.61	0.51	0.77	0.46	1.12	0.96	0.53	0.94	0.41	0.66	0.61	0.27	0.25
0.79	0.79	0.67	1.85	0.64	1.62	0.76	0.59	1.58	0.48	2.73	0.48	2.08	0.96
0.88	1.19	0.42	2.10	0.49	2.03	0.65	0.75	1.35	0.49	1.88	0.51	0.50	1.18
0.33	0.70	0.34	0.78	0.28	0.77	0.58	0.55	0.90	0.61	0.74	0.57	0.75	1.14
1.28	1.90	0.53	4.16	0.61	2.10	0.77	0.96	3.04	0.84	3.62	0.74	0.72	0.67
0.41	0.39	0.24	0.44	0.25	0.72	0.85	0.73	0.78	0.59	0.72	0.62	0.50	0.67
1.92	1.73	0.67	4.38	0.65	1.92	0.65	1.34	1.36	0.80	2.78	0.33	1.34	2.34
0.54	0.55	0.24	0.76	0.46	0.86	0.89	0.43	0.95	0.38	1.18	0.32	0.47	0.39

0.96	1.05	0.95	0.89	1.00	1.15	0.82	1.13	0.81	1.04	0.92	1.16	0.94	1.20
0.52	0.72	0.81	0.79	0.78	1.10	0.82	1.57	0.78	0.99	0.87	1.04	1.07	1.06
0.85	1.32	1.07	0.82	1.01	1.11	0.85	0.85	0.59	1.18	0.85	0.64	0.83	0.93
1.18	0.97	1.37	0.74	0.94	1.32	1.00	1.28	1.21	0.97	1.23	1.38	1.46	1.00
1.25	0.98	1.05	0.85	1.02	1.14	1.12	0.90	0.99	0.81	1.29	0.90	1.04	0.97
0.71	1.25	1.07	0.69	1.18	1.40	1.16	1.45	0.95	0.90	1.24	1.20	1.41	1.24
0.80	1.07	0.97	0.74	0.95	0.96	1.19	0.91	1.02	0.91	0.85	1.30	0.81	1.42
0.71	1.03	0.85	0.98	0.93	1.03	1.05	1.41	0.89	1.11	1.05	0.99	1.55	1.12
0.75	0.75	1.14	0.96	0.89	1.04	1.02	1.00	1.02	0.85	0.95	0.93	1.26	0.64
1.18	0.99	1.15	0.95	1.42	0.84	1.13	1.16	0.94	0.88	1.09	1.02	0.69	0.87
1.04	1.18	1.21	1.14	1.16	1.25	0.97	1.17	0.93	0.91	0.99	1.11	1.73	0.76
1.02	1.17	0.74	1.16	0.97	1.05	0.97	0.91	1.06	0.98	1.19	1.38	1.00	0.95
1.52	0.78	0.81	1.07	0.88	1.00	1.40	1.34	0.89	0.98	1.19	1.45	1.32	1.05
0.50	1.30	0.81	1.47	1.22	1.21	0.81	1.01	0.67	1.20	0.90	0.92	1.12	1.10

2 metres

1 metres

0.27	0.49	0.28	1.26	0.61	1.37	0.83	0.55	1.69	0.47	1.40	0.64	0.77	0.98
0.56	2.21	0.32	3.26	0.50	2.05	1.13	0.53	1.40	0.37	2.30	0.32	1.12	1.00
0.37	0.47	0.33	0.94	0.41	0.78	0.62	0.67	1.23	0.34	0.90	0.43	0.93	1.45
1.92	2.10	0.74	2.68	0.87	1.50	0.62	1.10	2.39	0.59	2.77	0.41	1.45	0.75
0.33	0.50	0.35	0.93	0.41	1.20	0.78	0.44	0.58	0.31	0.61	0.35	0.55	0.74
0.67	2.48	0.69	2.82	0.83	1.16	0.70	0.82	2.79	0.66	3.03	0.97	1.31	1.91
0.37	0.89	0.30	0.85	0.48	1.03	1.33	0.69	0.74	0.61	0.74	0.39	0.56	0.62
0.24	1.81	0.37	1.62	0.64	0.86	1.05	0.45	1.38	0.32	2.21	0.69	0.84	1.15
0.33	2.17	0.54	2.58	0.71	1.98	0.91	0.72	1.76	0.58	1.65	0.84	0.77	0.47
0.47	0.77	0.40	0.69	0.34	0.65	0.44	0.23	0.57	0.43	1.10	0.72	0.45	0.41
0.59	3.00	0.29	3.14	0.53	2.90	0.80	0.69	4.56	0.52	2.62	0.65	1.10	2.09
0.52	0.52	0.34	0.74	0.32	0.70	0.45	0.25	0.55	0.16	0.65	0.28	0.43	0.34
0.52	1.68	0.46	3.15	0.41	2.02	1.55	0.45	4.08	0.21	3.88	0.62	0.81	2.24
0.23	0.93	0.24	1.11	0.28	0.43	0.44	0.27	0.33	0.16	0.17	0.28	0.26	0.28

0.64	0.99	0.86	1.04	1.03	1.08	1.27	1.09	0.85	1.18	1.12	1.27	0.70	1.29
0.50	1.11	0.90	1.03	1.21	1.16	1.05	1.25	1.00	1.23	0.81	0.80	1.44	0.58
1.32	1.19	0.70	0.95	0.82	1.17	0.97	1.11	1.01	0.81	1.19	1.07	0.99	0.70
0.84	1.05	0.88	1.11	0.98	1.12	1.00	1.06	1.08	0.87	1.06	1.18	1.23	0.93
0.81	1.13	1.27	0.98	1.00	1.13	1.27	1.17	1.14	1.05	0.90	1.07	1.20	1.20
0.65	0.79	0.79	1.18	0.80	1.46	0.99	1.24	0.98	1.13	1.21	0.99	1.35	1.04
0.76	1.12	0.97	0.85	1.14	1.09	1.02	1.01	1.13	1.03	1.04	0.94	1.15	0.71
0.69	1.20	1.05	1.13	1.08	1.04	1.05	1.02	0.92	0.96	1.82	0.89	1.48	1.00
0.58	1.00	0.88	0.92	0.98	1.12	1.22	1.08	0.98	0.78	1.00	0.85	1.26	0.75
0.73	0.97	0.86	1.04	1.08	1.12	1.09	1.19	1.14	0.94	1.23	1.26	1.01	0.80
0.72	0.98	0.85	1.28	1.03	1.12	1.22	0.99	1.34	1.00	0.84	0.93	1.08	1.35
1.05	0.71	1.28	0.94	0.94	0.98	1.18	1.03	1.27	1.07	1.17	1.07	1.00	1.27
0.57	0.82	0.86	1.31	0.93	1.18	0.95	0.82	0.71	1.10	0.78	1.10	1.52	1.24
0.71	0.56	0.51	0.59	0.61	0.88	0.47	0.61	0.93	0.79	0.84	1.33	0.65	1.26

0 metres (gutter)

(a)   (b)

Figure 4.5 – Christiansen's coefficient of uniformity tests (CU) for the low-flow (a) and medium-flow (b) replacement dripper networks.

5 metres

0.55	0.58	0.64	0.61	0.65	0.63	0.66	0.67	0.66	0.63	0.69	0.75	0.90	0.47
0.99	0.89	0.85	0.95	0.92	0.95	0.92	0.93	1.00	0.94	0.91	0.84	0.90	0.65
0.87	1.02	0.86	0.98	0.99	1.05	0.99	0.96	1.03	1.00	1.04	0.91	0.96	0.76
1.00	1.14	1.09	1.15	1.00	1.05	1.05	1.05	1.10	1.02	1.09	1.00	1.10	0.81
1.13	1.14	1.23	1.09	0.99	1.03	1.04	1.07	1.06	1.04	1.07	0.98	1.02	0.76
1.03	1.06	1.06	1.02	1.12	1.00	1.03	1.02	1.07	1.02	1.05	0.94	0.95	0.73
0.94	0.99	1.06	1.04	1.10	0.94	1.04	1.07	1.10	1.05	1.07	0.98	1.00	1.03
0.98	1.02	1.07	1.09	1.01	0.98	1.10	1.14	1.26	1.01	1.10	0.99	1.06	0.68
1.28	1.07	1.10	1.10	1.01	0.97	1.04	1.13	1.14	0.95	1.07	0.97	1.01	0.72
1.05	0.97	1.00	1.08	1.02	0.94	0.97	1.07	1.08	0.89	1.05	0.91	0.99	0.72
1.04	0.96	0.92	1.04	0.99	0.96	0.95	1.14	1.09	0.86	1.10	1.01	0.99	0.60
1.13	0.90	0.97	1.02	0.98	0.99	0.95	1.10	1.18	0.96	1.07	0.98	1.08	0.68
1.20	1.17	1.12	1.07	1.02	1.00	1.12	1.17	1.05	1.03	1.06	0.97	1.10	0.74
0.62	1.11	1.11	1.04	1.04	0.98	1.03	1.11	1.03	1.08	0.99	0.98	1.04	0.69

4 metres

3 metres

0.99	1.04	1.02	0.93	0.98	0.90	0.92	1.11	1.13	0.99	0.96	0.99	1.06	0.70
1.44	0.96	1.07	0.96	1.05	1.07	0.88	1.12	1.07	0.98	0.94	0.93	1.03	0.74
1.09	1.10	1.12	1.05	1.01	0.96	0.91	1.16	1.08	0.95	0.94	0.92	0.95	0.65
0.98	1.28	1.22	1.16	1.01	0.95	0.94	1.09	1.14	0.98	1.04	1.19	1.00	0.64
1.20	1.01	1.17	1.13	1.00	0.97	0.96	1.08	1.21	1.02	0.97	1.16	1.11	0.74
0.93	1.18	1.07	1.19	1.02	0.98	1.01	1.07	1.21	1.07	0.90	1.12	1.18	0.77
1.12	0.92	0.94	1.00	0.94	1.03	1.02	1.11	1.07	0.99	0.96	0.95	1.10	0.66
0.94	1.22	0.95	1.06	0.96	1.03	0.96	1.01	1.13	1.01	1.05	1.00	1.12	0.62
0.90	1.02	1.00	1.05	1.00	1.04	0.98	1.05	1.17	0.96	0.92	0.97	0.94	0.61
1.25	1.23	1.05	1.12	1.03	1.00	0.96	1.06	1.22	0.98	0.87	1.02	1.07	0.65
1.09	1.12	1.01	1.02	1.05	0.97	1.00	1.05	1.18	1.15	0.92	1.11	1.07	0.70
1.28	1.01	0.95	1.04	0.95	1.03	0.95	1.04	1.10	1.02	0.97	1.08	1.03	0.74
1.20	1.11	1.00	1.08	0.94	1.05	1.00	1.06	1.05	1.03	1.10	0.97	1.16	0.74
1.23	0.98	1.16	1.07	0.95	1.01	1.08	1.03	1.02	1.06	1.01	0.99	1.14	0.69

2 metres

1 metres

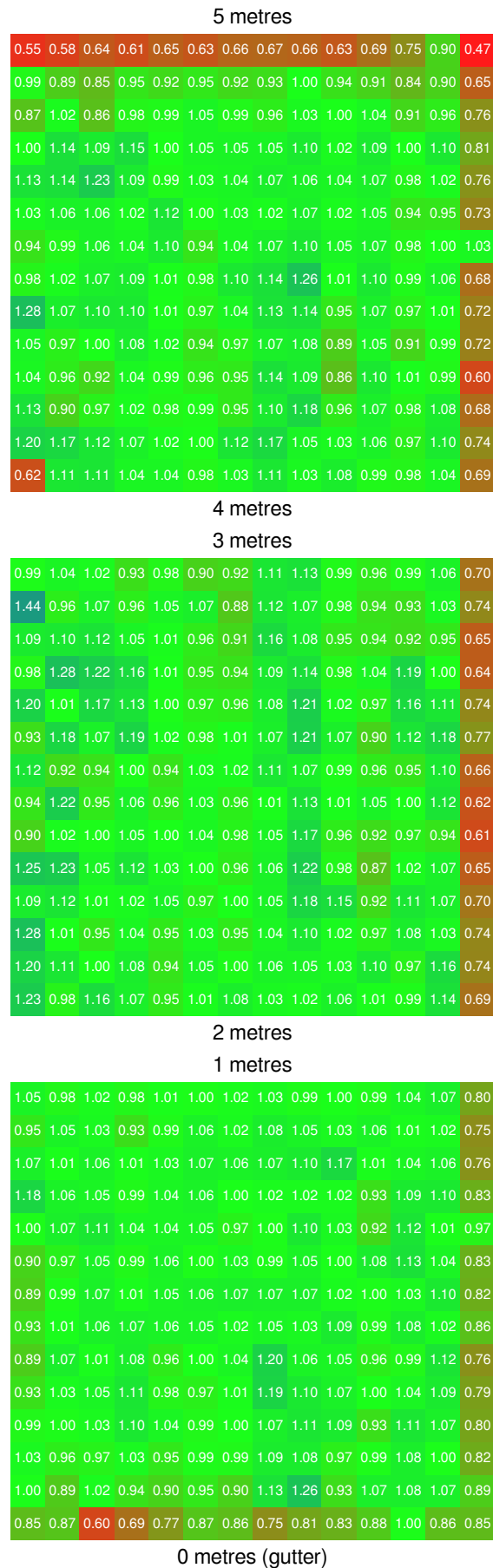| 1.05 | 0.98 | 1.02 | 0.98 | 1.01 | 1.00 | 1.02 | 1.03 | 0.99 | 1.00 | 0.99 | 1.04 | 1.07 | 0.80 |
0.95	1.05	1.03	0.93	0.99	1.06	1.02	1.08	1.05	1.03	1.06	1.01	1.02	0.75
1.07	1.01	1.06	1.01	1.03	1.07	1.06	1.07	1.10	1.17	1.01	1.04	1.06	0.76
1.18	1.06	1.05	0.99	1.04	1.06	1.00	1.02	1.02	1.02	0.93	1.09	1.10	0.83
1.00	1.07	1.11	1.04	1.04	1.05	0.97	1.00	1.10	1.03	0.92	1.12	1.01	0.97
0.90	0.97	1.05	0.99	1.06	1.00	1.03	0.99	1.05	1.00	1.08	1.13	1.04	0.83
0.89	0.99	1.07	1.01	1.05	1.06	1.07	1.07	1.07	1.02	1.00	1.03	1.10	0.82
0.93	1.01	1.06	1.07	1.06	1.05	1.02	1.05	1.03	1.09	0.99	1.08	1.02	0.86
0.89	1.07	1.01	1.08	0.96	1.00	1.04	1.20	1.06	1.05	0.96	0.99	1.12	0.76
0.93	1.03	1.05	1.11	0.98	0.97	1.01	1.19	1.10	1.07	1.00	1.04	1.09	0.79
0.99	1.00	1.03	1.10	1.04	0.99	1.00	1.07	1.11	1.09	0.93	1.11	1.07	0.80
1.03	0.96	0.97	1.03	0.95	0.99	0.99	1.09	1.08	0.97	0.99	1.08	1.00	0.82
1.00	0.89	1.02	0.94	0.90	0.95	0.90	1.13	1.26	0.93	1.07	1.08	1.07	0.89
0.85	0.87	0.60	0.69	0.77	0.87	0.86	0.75	0.81	0.83	0.88	1.00	0.86	0.85

0 metres (gutter)

Figure 4.6 – Christiansen's coefficient of uniformity test (CU) for the high-flow replacement dripper network.

10.8 grams; before the start of these three tests, the digital balance used to weigh the cups in most of the previous mesh tests had been replaced by a new digital balance with a finer resolution of 0.1 grams. Values of CU for the low-, medium- and high-flow networks are 0.457, 0.833 and 0.912 respectively.

It was noted during these calibration tests that the total quantity of water captured per grid was always very close to the expected value of 18.8 litres, derived by assuming that the circular cups cover $\pi/4$ of each square metre grid, each grid covers 1/5 of the channel bed area and 120 litres of rain falls per test. This observation confirmed that the actual flow rates of the drippers were similar to their stated flow rates.

4.4.3.5 Drainage Length

It was decided that the experimental programme would assess the characteristics of the drainage layer components at varied drainage lengths. A trapezoidal sheet, measuring approximately 6 metres in length, 1.15 metres along the top edge and 1.57 metres along the bottom edge, was produced from the same rubbery material used to waterproof the simulator channel. Small incisions were made along the length of both non-parallel sides, through which cable ties were threaded. Whenever a drainage length of 2 metres was required during the experimental programme, the trapezium was pulled lengthways into the simulator chamber, short edge first, and the cable ties secured to the dripper network frame such that the sheet entirely obscured the rearmost three-fifths of dripper rows when viewed from directly below. The gradient of the installed sheet directed any water released from the rear three-fifths of the dripper networks towards an unmonitored collecting barrel located behind the simulator chamber (Figure 4.3). Hence, only rainfall released from drippers in the front 2 metres of the simulator landed on the channel bed or component, and only runoff resulting from this rainfall was monitored. As the sheet can slide to any point within the simulator and the cable ties can be secured to any point on the frame, it is possible to simulate any drainage length from 0 to 5 metres in discrete steps corresponding to one row of drippers (one-twelfth of a metre for the medium- and high- flow networks, one-sixth of a metre for the low-flow network).

When the simulator was used at a 10° tilt angle, a collecting sheet measuring approximately 6 metres in length, 1.15 metres along the top edge and 1.9 metres along the bottom edge was used, to continue to provide a gradient towards the unmonitored barrel against the now steeper gradient of the simulator chamber. In practice, water ponded in this sheet, rather than flowing out of the back of the simulator. Ponded water was first manually removed using a 1 litre measuring cylinder and then later by a siphon improvised from a leftover length of 15 mm diameter pipe and a tap.

4.4.4 Drainage Layer Test Programme

It is proposed that the key factors influencing the runoff response of the drainage layer are: choice of drainage component(s); drainage length; and roof slope. Hence, these are the three factors that were varied in this experimental programme. A fourth factor, inflow intensity (supplied by the drippers, but not named "rainfall intensity", as the drainage layer normally receives inflow from the overlying substrate), was also varied, to test the assumption that any variation in modelling parameter values should be independent of variations in inflow intensity; this assumption is a requirement of the proposed hydrological modelling methodologies. In total, five possible combinations of drainage components were used. These were:

- Bare channel of the rainfall simulator – a rubbery grey waterproofing sheet

- ZinCo Floradrain FD 25 – an eggbox-style polyethylene module of thickness 25 mm

- ZinCo Floradrain FD 25 above ZinCo Protection Mat SSM 45, a fibrous ZinCo protection and moisture retention mat

- ZinCo Floradrain FD 40 – a scale-enlargement of the FD 25 design to a 40 mm depth

- ZinCo Floraset FS 50 – an expanded polystyrene component with large voids on the underside

Product data sheets for all of these components are available from Alumasc's website (Alumasc, 2012c). It should be noted that datasheets are there given for Floradrain FD 25-E and FD 40-E, which refer to the "export" versions of these products, sold only in 2×1 m panels. The export versions of FD 25 and FD 40 were used in this experimental programme, though all different versions of each component are regarded by ZinCo as identical in performance. All tested components are shown in Figure 4.7.

Two roof slopes were used. These were:

- $1.15°$ (2% or 1 in 50)

- $10°$ (17.6% or 1 in 5.7)

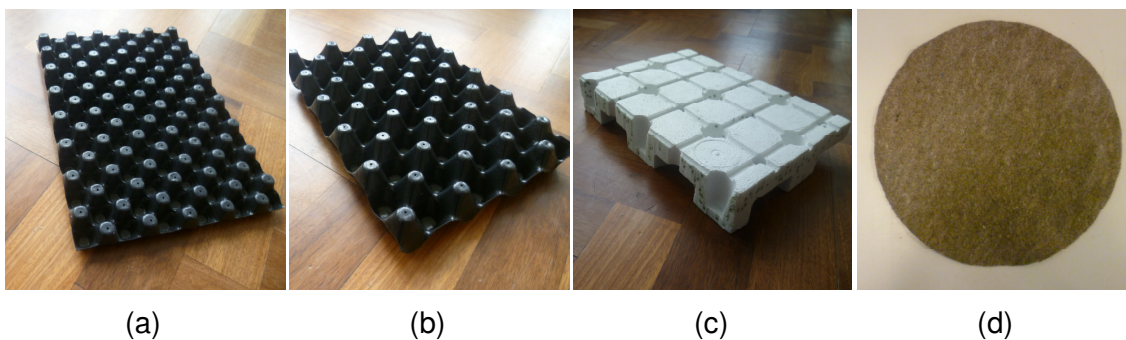<div align="center">(a)   (b)   (c)   (d)</div>

Figure 4.7 – Test drainage layer components: Floradrain FD 25 (a); Floradrain FD 40 (b); Floraset FS 50 (c); Protection mat SSM 45 (d).

Two drainage lengths were used. These were:

- 2 m

- 5 m

Five approximate inflow intensities were used. These were:

- 0.1 mm/minute – low-flow dripper network operated in programmed on/off cycles of 10 s/16 s

- 0.3 mm/minute – low-flow dripper network continuously on

- 0.6 mm/minute – medium-flow dripper network operated in programmed on/off cycles of 10 s/4 s

- 1.2 mm/minute – medium-flow dripper network continuously on

- 2.0 mm/minute – high-flow dripper network operated in programmed on/off cycles of 10 s/8 s

Though these inflow rates are high or very high in comparison to the actual rates that may be experienced by a real green roof drainage layer, the large rainfall simulator was designed, and is intended, to simulate intense storms falling on complete systems. Furthermore, simulating lower, more realistic rates of inflow would either require fewer drippers, reducing the spatial uniformity of rainfall, or on/off cycles with greater ratios of off-time to on-time, reducing temporal uniformity. Additionally, as the proposed modelling methods are independent of inflow intensity, the actual choice of values of inflow rate is perhaps less important than their range, as it should be possible to verify that the model parameter values are in fact independent of inflow rate over a large range.

As all possible combinations of the four factors above were tested, the test programme contained 100 different situations, consisting of 20 physical configurations, each tested at five inflow rates. The initial retention capacity in all components, across all tests, was zero.

4.5   Small Rainfall Simulator

4.5.1   Overview

The small rainfall simulator (Figure 4.8) is located in the Department of Civil and Structural Engineering at the University of Sheffield. It was built by members of the department in 2011, for the purpose of recording time-series runoff curves from various green roof substrate mixes. As it was purpose built for the exact type of tests performed in this experimental programme, it was not necessary to modify the simulator after initially receiving access to it. However, certain calibration checks were performed before the experimental programme commenced. A detailed description of the small rainfall simulator follows.

Figure 4.8 – Small rainfall simulator as used in substrate experimental programme.

4.5.2   Description

The small rainfall simulator consists of the following components: Water supply tank; peristaltic pump; header tank with drippers; substrate holder; collector funnel; measuring cylinder with pressure transducer; data logger; and computer. The overall design of this simulator is partly inspired by the rainfall simulators produced by Bowyer-Bower & Burt (1989) and Dunnett *et al.* (2008).

The water supply tank is simply a bucket of approximately 25 litres capacity, which is manually filled with de-ionized water to maintain a quantity sufficient for any scheduled tests. A small diameter pipe is weighted so that its end lies on the floor of the tank. This pipe runs up to the pumphead of a Watson Marlow 505 Du peristaltic pump. The peristaltic pump has a speed range of 1 to 220 RPM, which is adjustable in 0.1 RPM increments. The pumphead itself consists of an equilateral triangle with rounded edges, rotating inside a circular arc boundary. A section of flexible pipe with 6.4 mm internal diameter is trapped inside this arc. The pipe is pushed closed where the rounded points of the triangle are nearest to the boundary but is open elsewhere. Hence, as the pumphead rotates, a volume of water in the pipe is trapped and pushed through the pump. The same volume of water is always trapped between two of the triangle's points, therefore the rate at which water is moved through the pump is proportional to the pump speed in RPM.

From the peristaltic pump, the pipe continues to the header tank, which it feeds from above. The header tank is of the same diameter as the substrate holder and is approximately 16 mm deep. The drippers are connected to the underside of the header tank. The purpose of the header tank

is to ensure that each of the drippers is subject to the same pressure head; this improves the consistency of drip rate and hence the regularity of the simulated rainfall distribution. However, the depth of the tank is necessarily low so that the capillary tension within the needles is not overwhelmed by the water head in the header tank (Yio, 2011). A pipe with a tap is also attached to the underside of the header tank; this is used to empty the header tank e.g. to allow debris removal by a full flushing of the tank. The upper side of the header tank contains a threaded hole, normally plugged by a removable metal seal. This seal is only removed to allow filling of the header tank, if so required.

The drippers are BD Microlance 3 medical syringes at 23G (0.337 ± 0.019 mm internal diameter) with a nominal length of 40 mm. This needle gauge was chosen to allow the rainfall rates specified in the test programme to be achieved within a reasonable range of the pump's operating speed. The drippers, totalling 37, are arranged in a regular hexagon, measuring four drippers along each side and seven drippers across the longest axis. Within the hexagon, the drippers are arranged in a regular equilateral triangular pattern. The distance between adjacent drippers is 50 mm. Hence, the hexagon has sides of 150 mm and measures 300 mm across its longest axes. Each dripper is individually replaceable; prior to performing a day's tests, the pump is operated at 40 RPM for 30 minutes, both to top-up the water content of the substrate in the holder to field capacity and to check all drippers for blockages that may require attention. It should be noted that, although the header tank maintains a constant head above each dripper, the internal cross-sectional area of a 23G medical syringe may vary by up to 25%. Similarly, while all of the syringes used were of reasonably consistent length, some were noticeably (~5 mm) shorter or longer than the nominal length. Due to these two factors, the distribution of rainfall within the small rainfall simulator is expected to have varied throughout the experimental programme.

The substrate holder consists of a hollow vertically-standing cylinder, with internal diameter 360 mm and height 300 mm. The cylinder has horizontal flanges at the top and bottom to allow it to vertically stack above the funnel and below the header tank. The top of the cylinder is open. A ZinCo Systemfilter SF filter sheet is stretched across the base of the cylinder. This has an effective opening width of 95 μm, according to EN ISO 12956 (BSI, 2010b), allowing only very small substrate particles through, and a flow rate of 70 mm/s, according to EN ISO 11058 (BSI, 2010c), significantly greater than any rainfall rates used in this experimental programme. Below the filter sheet is a coarse steel grid, which holds the filter sheet in place, preventing it from sagging and thereby ensuring that the substrate sample maintains a flat cylindrical base. One set of parallel grid bars sits perpendicularly atop the other, thus the filter sheet is only supported by one set of parallel grid bars. The top bars are point-down triangular in cross-section, with a

maximum width of 2.5 mm and a centre-to-centre spacing of 8.5 mm. The lower, non-supporting set of parallel grid bars are point-up triangular in cross section, but their maximum width is 6 mm and centre-to-centre spacing is 12 mm.

Directly below the substrate holder assembly is a smooth polypropylene funnel, of slope angle 54° and slightly larger diameter than the substrate holder. Directly below this is the collecting cylinder. This is a uniform cylinder of 50 mm internal diameter and approximate height 810 mm. Contained within the cylinder is another smaller cylindrical pipe, internal diameter 24 mm, and a Druck PDCR 1830 pressure transducer. The top of smaller pipe push-fits onto the bottom of the funnel and the bottom of the smaller pipe is below the water level; this reduces oscillations caused by water entering the collecting cylinder. The pressure transducer monitors the pressure of the water column above it at 5-second intervals, at an effective depth resolution of 0.00506 mm of rainfall. As the smaller pipe and pressure transducer together fit very tightly inside the collecting cylinder, no means of securing the pressure transducer is required or used.

The highest rainfall intensity in the test programme requires a larger collecting cylinder to be used. Aside from the physical dimensions (approximately 87.5 mm internal diameter and 740 mm height) and the requirement for the pressure transducer and cable to be taped vertically to the inside wall of the barrel, the qualitative description of this setup is identical to that of the smaller cylinder. The effective depth resolution of the pressure transducer is 0.0172 mm of rainfall when used in the larger cylinder.

The pressure transducer is connected to a Campbell Scientific CR800 data logger, which continuously records the output of the pressure transducer on its internal solid-state memory. As the capacity of the internal memory is only 2 MB, the oldest data is continually overwritten and the newest data has a lifespan of around 17 days. To overcome this limitation, the data logger is connected to a Toshiba Satellite Pro laptop via a USB/RS-232 interface, onto which the data recorded on the solid-state memory is periodically downloaded and permanently stored. Sections of the data record corresponding to individual tests are also isolated, saved to individual files and stored on a Dropbox account.

4.5.3   Calibration

Before starting the experimental programme, it was determined that calibration checks would be required to establish the relationship between pump speed and rainfall rate, and the relationship between collected depth of water and recorded pressure for both collection cylinders.

To calibrate the pressure transducer to the small cylinder, the pressure transducer and small pipe were inserted in the small cylinder, arranged as they would be during the experimental programme. Water was added to the collection cylinder to fully immerse the transducer. At this
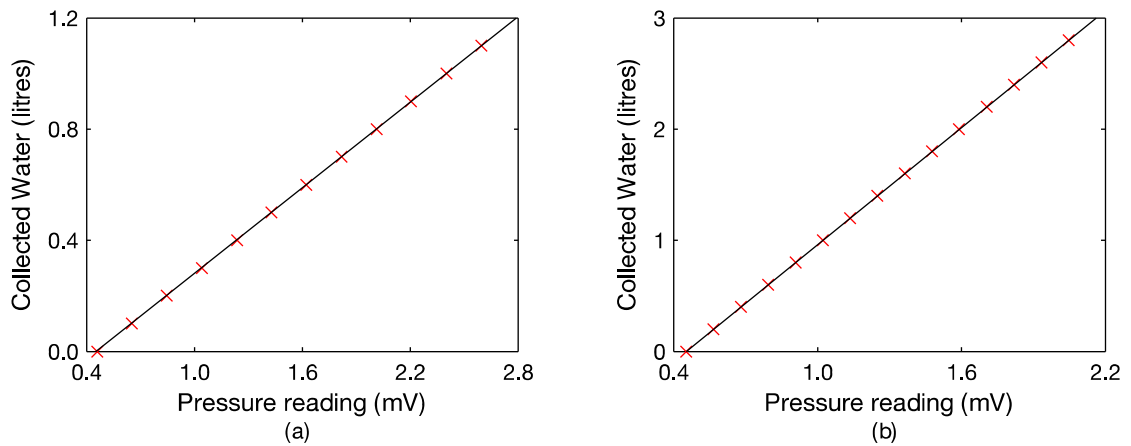
Figure 4.9 – Calibration plots for the small (a) and large (b) collection cylinders

point, the first pressure reading was recorded. Water, measured using a 100 ml Griffin-style pyrex beaker, was added to the collection cylinder in 100 ml increments and the pressure recorded after each addition. This was repeated until the cylinder reached full capacity, and the entire process repeated twice more. The differential increase in pressure between each addition was noted and three obvious outliers were discarded, leaving 30 valid data points. From these, a value of 0.1942 mV was assigned as the pressure increase resulting from the collection of 100 ml of water (Figure 4.9 (a)).

To calibrate the pressure transducer to the large cylinder, the pressure transducer was taped to the wall of the large cylinder, as it would be during the experimental programme. The small pipe was also taped to the wall, so that it would remain vertically oriented throughout the calibration procedure. Water was added to the collection cylinder to fully immerse the transducer. At this point, the first pressure reading was recorded. Water, measured using a 250 ml Griffin-style pyrex beaker, was added to the collection cylinder in 200 ml increments and the pressure recorded after each addition. This was repeated until the cylinder reached full capacity, giving 14 data points, of which none were outliers. From these, a value of 0.114 mV was assigned as the pressure increase resulting from the collection of 200 ml of water (Figure 4.9(b)).

To calibrate the pump speed to rainfall rate, the pump was operated at 11 different speeds (5, 10, 15, 20, 25, 36, 42, 49, 55, 62.5 and 70 RPM) for 900/RPM minutes, to the nearest integer number of minutes. No substrate was used and the rainfall was collected in the small cylinder. The pressure transducer recorded each rainfall event in its entirety, at a temporal resolution of 5 seconds. The pressure increase for every time step, in mV/minute, was determined by subtracting the pressure reading at every time step from the pressure reading 12 time steps previously. For each event, a section of constant pressure increase, corresponding to constant rainfall rate, was found. This was converted from mV/minute to litres/minute and then

mm/minute using the conversion factors previously found. Pump speed, in RPM, was plotted against rainfall rate, in mm/minute (Figure 4.10), and a linear relationship was found:

$$PS = 84.77I + 1.45$$ **Equation 4.5**

Where *PS* is pump speed in RPM and *I* is rainfall rate in mm/minute. It is worth noting that Equation 4.5 contains a small offset term. This may be due to an incomplete seal being formed between the circular arc boundary and rotating triangle points in the peristaltic pump, causing a relatively small quantity of water to escape back to the water supply tank during normal operation.

The calibration suggested pump speeds of 9.9, 26.9 and 52.3 RPM for rainfall rates of 0.1, 0.3 and 0.6 mm/minute. These predicted values were then checked by operating the pump at these three speeds for 30 minutes and evaluating the constant rainfall intensity as before. The results of these tests suggested that pump speeds of 9.0, 26.1 and 51.6 RPM would be more appropriate to simulate the required rates of rainfall. These values were confirmed by operating the pump at these speeds for the length of time required to fill the small cylinder, three times for each speed, and evaluating the constant rainfall intensity. These three speeds were found to be accurate and a new relationship between pump speed and rainfall rate was created:

$$PS = 85.2I + 0.5$$ **Equation 4.6**

Where *PS* and *I* have the same meaning as before.

4.5.4   Substrate Test Programme

It is proposed that the factors influencing the shape of the time-series runoff curve for the vertical model are substrate composition and substrate depth. Hence, these were the two factors
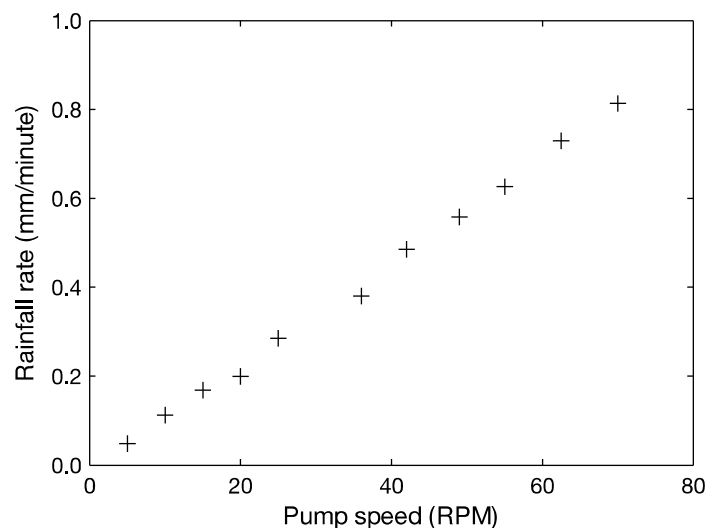

Figure 4.10 – Calibration curve of rainfall rate vs. pump speed.

that were varied in this experimental programme. A third factor, the presence of a moisture/protection mat (ZinCo Protection Mat SSM 45) below the substrate was investigated, as it was anticipated that this may provide significant resistance to vertical flow-through. The fourth factor of rainfall intensity was also varied, again to test its independence from the modelling parameter values. Two different substrate mixes were tested. These were:

- Marie Curie (a proprietary mix developed as part of the wider Green Roof Project, containing 85% Zincolit+, 10% compost and 5% coir)

- LECA mix (80% expanded clay, 10% John Innes No. 1, 10% composted bark)

- The response of the empty simulator chamber was also tested

Both substrates were tested at two depths:

- 5 cm

- 10 cm

Four rainfall intensities were used:

- 0.1 mm/minute (pump speed 9.0 RPM)

- 0.3 mm/minute (pump speed 26.1 RPM)

- 0.6 mm/minute (pump speed 51.6 RPM)

- Design storm – 8.8 mm of rainfall, distributed according to the 75% summer storm profile (NERC, 1975), discretized into 5 steps of constant intensity, each of 6 minutes duration.

The rainfall intensities used for each six-minute step of the design storm were, in order: 0.065 mm/minute, 0.16 mm/minute, 1.0 mm/minute, 0.16 mm/minute, 0.065 mm/minute (pump speeds of 6.0, 14.1, 85.5, 14.1 and 6.0 RPM calculated from Equation 4.6)

The three constant rainfall rates were chosen to allow easy combination with the drainage layer nonlinear storage routing model. The two highest rates used in the drainage layer experimental programme, 1.2 mm/minute and 2.0 mm/minute, were not included in the substrate experimental programme, to avoid damaging the pump through continuous operation at high RPMs. The design storm was chosen to evaluate the model's output when attempting to fit to a rain profile of varying intensity.

In addition, the test configuration with Marie Curie substrate only was repeated at both substrate depths and all rainfall intensities with a 360 mm diameter disc of ZinCo Protection Mat SSM 45 placed underneath the substrate. The total number of test situations is therefore 28, consisting of seven physical configurations, each tested at four rainfall intensities. Table 4.1 presents characteristics of the Marie Curie Substrate and LECA mix, along with equivalent characteristics

Table 4.1 – Representative substrate properties.

Substrate	Particles < 63 μm (%)	Particles < 4 mm (%)	Dry Density (g/cm³)	Pore Volume (%)	MWHC (%)	Permeability (mm/min)
Marie Curie	0.95	62.2	1.01	61.6	36.9	130.1
LECA mix	0.35	27.9	0.45	83.0	33.0	133.4
Heather w/ Lavender	3.60	15.8	0.95	63.8	41.2	2.41
Sedum Carpet	1.80	16.0	1.06	59.8	39.0	14.8

for two additional substrates that are considered in Chapter 7. Values for Marie Curie and LECA mix were derived from FLL tests conducted in August 2012 by Stephan Vogt, an undergraduate student at the University of Sheffield, on the same substrate batches as used in this thesis. Values for Heather with Lavender and Sedum Carpet are as reported by Poë *et al.* (2011), using material sampled from the Hadfield roofs (see Chapter 7). It should be noted that all values in Table 4.1 are representative only; greatly differing values for all substrate properties have been found between different samples of substrate, even from the same batches.

4.6 Experimental Setup for Two-Layered System Tests

After the development and parameterization of separate drainage layer and substrate models, both were combined in series to give a two-stage model for predicting the runoff response of a two-layered green roof system, consisting of a substrate layer over a drainage layer. As the roof runoff in any such system emerges from the drainage layer, the large rainfall simulator, with its side outlet, was used to conduct the programme of verification tests. Further modifications were made to the large rainfall simulator between the end of the drainage layer test programme and the beginning of the system test programme; these modifications and the motivations for implementing them are discussed in detail in Section 7.3, which also contains specifications for the substrate and drainage layer components, and full details of the test programme.

4.7 Experimental Setup for Storage Recharge Tests

Another set of tests was also conducted, aiming to quantify the rate at which the storage capacities of the drainage layer and protection mat are recharged by evaporation between storm events. Following two preliminary experiments, it was concluded that such measurements would be subject to large uncertainties that could not be practically removed or sufficiently reduced. A full report on these experiments, including experimental setup, as well as results and conclusions, can be found in Appendix A.

5 Results and Discussion – Drainage Layer

5.1 Chapter Overview

This chapter opens with an introduction to the use of the hydrological models, previously selected in Section 2.5.4.3, for the analysis and characterization of the data collected in the large rainfall simulator. An explanation of the processing required to convert the raw data record into usable runoff records is given. Basic performance characteristics of the drainage layer components are determined and presented. The modelling methods are applied independently to the runoff records and the results evaluated. Modelling parameters are evaluated for statistical similarity and value-averaged as far as possible, to allow for the potential use of generic parameter values for similar, but so far untested, configurations of drainage layer. The sensitivity of the model to changes in parameter values is tested. Finally, the models are evaluated against each other in terms of ease of use, applicability and accuracy of results.

Earlier analyses and discussion of the data presented here formed the basis of a conference paper (Vesuviano & Stovin, 2012) presented in September 2012 at the *9th International Conference on Urban Drainage Modelling* in Belgrade, Serbia, and published in revised form in the journal *Water Science and Technology* (Vesuviano & Stovin, 2013).

5.2 Selection of Hydrological Models

From all of the hydrological models considered in Sections 2.4 and 2.5, two were selected for further consideration: nonlinear storage routing and the Muskingum method. Both of these methods are robust, well-established and in common use in the field of hydrology.

The unit hydrograph method was previously studied by Villarreal & Bengtsson (2005) for modelling green roof runoff. It was then later studied by the thesis author (Vesuviano, 2011), but was shown to work with only limited and inconsistent success. It is believed that the inconsistency of this method results from the poor temporal and volumetric resolution of the inflow and runoff profiles, coupled with the specific methodology used in fitting the unit hydrograph: each successive runoff point from the first was fitted exactly, in sequence, until the ordinates of the unit hydrograph first became negative. Unit hydrograph methodology could potentially be appropriate for fitting a unit hydrograph to a perfect inflow/runoff pair, but quantization artefacts are overemphasized when data with poor resolution are used as inputs. Use of more advanced deconvolution techniques and/or higher-resolution data series may reduce issues associated with quantization and noise, but another problem remains – that of generic applicability. The specific criteria for averaging the values of potentially hundreds of ordinates across "similar" unit hydrographs, hence allowing the modelling of untested but similar roof configurations, are very widely open to interpretation.

5.3 Data Collection and Processing

The experimental programme for the drainage layer began on 2nd August 2011 and continued until 7th October 2011, at ZinCo GmbH international headquarters, then in Unterensingen, Germany. Initially, each test configuration was repeat-tested four times. When it was confirmed that the variability between repeat tests was low, the number of repeat tests for each configuration was reduced to three. 313 tests were performed in total, excluding those for which data records were rendered unusable by equipment malfunction or human error. To avoid any possible weighting effects towards any particular configuration, exactly 300 tests are considered (three for each test configuration) in the following results and discussion sections.

In order to minimize the effect of runoff from one test impacting on a subsequent test, no further tests were started until the rate of runoff from the current test had decreased to a rate at which the pressure transducer output remained stable for a minimum of five minutes. For some tests occurring later in the experimental programme, particularly those with long runoff tails, the time-pause criterion was reduced to four minutes; without this slight relaxation, it may not have been possible to complete the entire experimental programme in the available time.

The data series generated by the pressure transducer over the test period is stored in individual .dat files for each test, at a time resolution of one sample per second. Sampling was performed at this high temporal resolution in order to capture a high level of time-series runoff detail that could be lost at lower temporal resolutions. It should be noted that, if necessary, a data series can be decreased but not increased in resolution. Each sample consists of three comma-separated fields: date and time, record number (an integer which increases by one with each new data point), and pressure in mV to six decimal places, where an increase of 1.000000 mV approximately corresponds to a water level increase of 20 mm in the collection barrel.

The size of a normal pressure step in this record varies from 0.009890 to 0.009900 mV. However, the pressure transducer does not increase in a stable manner from one step to the next; every fourth step is stable, and the pressure transducer oscillates back and forth between three interstitial unstable values when increasing from one stable value to the next, with the centre of the oscillation gradually moving upwards from the lower to the higher stable value (Figure 5.1). In addition to instabilities in the data record, noise is generated by the action of water entering the barrel from above. Furthermore, the pressure transducer generates its own noise, apparent in the numeric output record as increases or decreases in the region of 1×10^{-6} to 1×10^{-4}. Before analyzing the collected data, it was considered important to mitigate the effects of these three potential sources of error on the pressure value, producing cleaner data for the evaluation of the chosen hydrological models. Separation of the transducer data record, into individual runoff records for each test, was performed simultaneously with the experimental programme. Prior to
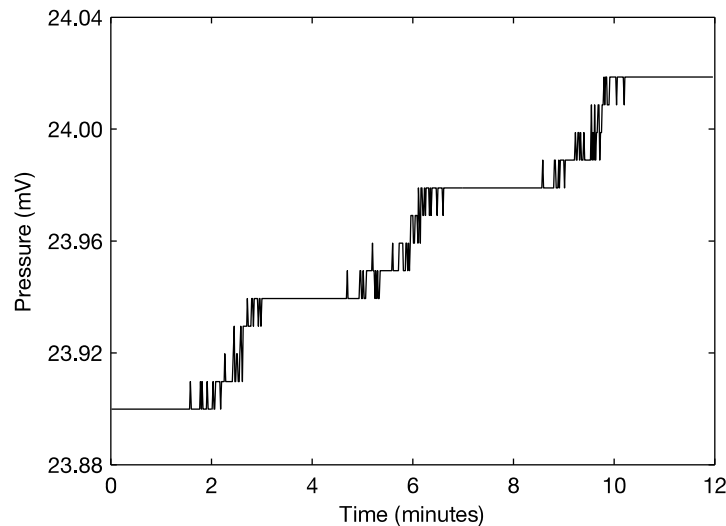
Figure 5.1 – "Stable" pressure readings (at approximately 23.90, 23.94, 23.98 and 24.02) and "unstable" pressure readings between them.

analysis of the runoff records, two processes, normalization of the pressure step size and subsequent application of a 19-sample moving average, were performed to reduce noise in the data. An example of the effects of these operations on typical runoff record is shown in Figure 5.2, where three sequential applications of the moving average are shown to greatly reduce oscillations in the runoff profile without over-blurring or over-smoothing its underlying shape; it is these three-times smoothed runoff profiles that were used in the subsequent analyses. Finally, to prevent the modelling methods from unduly prioritizing long strings of near-zero values during the optimization routine, each smoothed runoff profile was trimmed – after the average runoff rate over 60 consecutive samples had fallen below 1% of the inflow rate, all subsequent samples in that record were deleted. Ultimately, due to the approximation of a continuous process (runoff) by a stepped signal in discrete time steps, not all runoff records could be completely divested of all oscillation. This is more apparent for tests at lower inflow rates and tests with long, gradually reducing, falling runoff limbs (those using Floradrain FD 25 with SSM 45 at a 5 metre drainage length).

The rate of inflow supplied by the dripper networks was not directly monitored during this experimental programme; for each single test, an inflow profile was reconstructed from the corresponding runoff record for that test. In each case, this was approximated as a constant intensity over the exact duration of the inflow event, including, for repeated pulse inflow events, the "off" and "reset" times following the final inflow pulse. The intensity of the inflow event was matched to an estimate of the steady-state runoff rate reached during each test. This was estimated by finding the maximum rate of runoff after a further seven (for a total of ten) smoothing operations on the runoff profile. At this point all oscillations at steady-state were fully eliminated and the maximum runoff rate was determined to be equal to the steady-state runoff
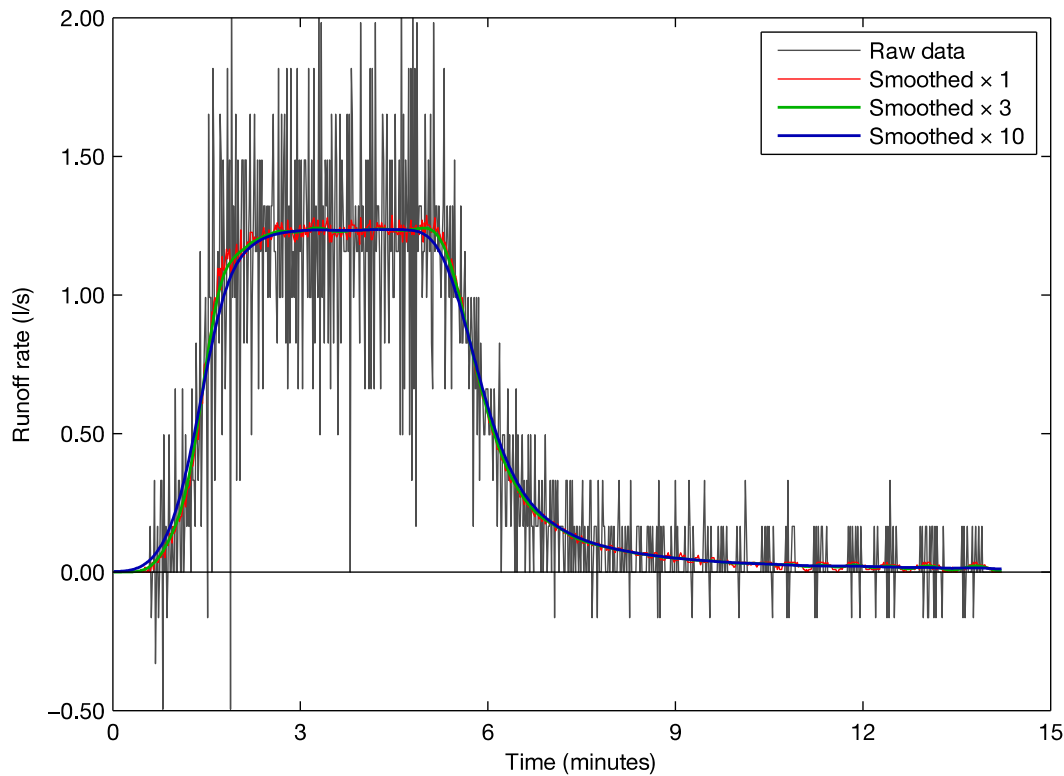
Figure 5.2 – Comparison of unsmoothed, once-smoothed three times-smoothed and ten times-smoothed time-series runoff profile for one test of Floradrain FD 25 at 1.15° roof slope, 5 metre drainage length and 1.2 mm/minute inflow intensity.

rate. It is noted that the ten-times smoothed runoff profiles are not appropriate representations for runoff modelling purposes, as the transitions between the rising limb, steady-state section and falling limb are too greatly attenuated to represent the actual occurrences of the test programme. In the tests of FD 25 with SSM 45, steady-state was not reached when a drainage length of five metres was used. For these 30 tests, the rate of inflow was estimated as the mean rate of inflow for all other tests with the same nominal inflow rate. This was, again, applied as a constant value over the exact duration of the inflow event. In three other tests, the recorded runoff profile contained a large spike, resulting from high-magnitude oscillations, that was not sufficiently reduced by ten smoothing operations. The constant inflow rates for these three tests were set as the mean derived inflow rate for the other equivalent tests using the same physical configuration and nominal inflow rate.

5.4   Overview of Drainage Layer Performance

5.4.1   Repeatability and Accuracy of Tests

The runoff response for every test situation was found to be highly repeatable, so much so that, when plotted together on the same axes, the smoothed runoff records for the three repeats of each test situation almost entirely overlap, even showing the same small oscillations during tests

Table 5.1 – Summary of test inflow rates.

Nominal Rate	Mean of Actual Rate	St. Dev. of Actual Rate	No. of Tests
0.1 mm/minute	0.108 mm/minute	0.0042 mm/minute (3.9%)	60
0.3 mm/minute	0.306 mm/minute	0.0053 mm/minute (1.7%)	60
0.6 mm/minute	0.603 mm/minute	0.0167 mm/minute (2.8%)	63
1.2 mm/minute	1.223 mm/minute	0.0172 mm/minute (1.4%)	57
2.0 mm/minute	1.909 mm/minute	0.0306 mm/minute (1.6%)	60

with non-constant inflow intensity, on a second-by-second basis. The nominal inflow rates of 0.1, 0.3, 0.6, 1.2 and 2.0 mm/minute were generally closely and consistently approximated by the dripper networks. This is summarized in Table 5.1.

As mentioned previously, steady-state was not reached when FD 25 with SSM 45 was tested at a drainage length of five metres. The values given in the "Mean of Actual Rate" column were used as appropriate for all of these tests. The values of standard deviation were calculated for a population size of six less than the number in the corresponding No. of Tests column, as the "Actual Rate" for six tests at each nominal rate was a calculated average, rather than a measured value. Due to a programming error on the dripper network controller, Floraset FS 50 at a slope of 1.15° and a drainage length of 2 metres was tested six times at the nominal inflow rate of 0.6 mm/minute and zero times at the nominal inflow rate of 1.2 mm/minute. This is the cause of 63 tests being conducted at 0.6 mm/minute and only 57 being conducted at 1.2 mm/minute.

5.4.2   Runoff Responses

For the great majority of tests, the runoff response was of one general shape: a rising limb, whose gradient decreased as the rate of runoff approached steady-state, a steady-state section, where the

Figure 5.3 – Cumulative (a) and time-series (b) runoff response comparison of all five drainage components at 1.15° roof slope and 5 m drainage length, with a nominal inflow rate of 0.6 mm/minute. t_{50} is shown by the horizontal grey line on (a).

rate of runoff was equal to the rate of inflow (or, in the case of tests with non-constant inflow, oscillated around the time-averaged rate), and a falling limb, starting soon after the end of the inflow event, whose gradient reduced with time (Figure 5.3 and Figure 5.4). For the majority of test configurations, the greatest difference between runoff profiles was the gradient of the rising and falling limbs. The only exceptions to this general response were those 30 tests conducted with FD 25 and SSM 45 at a 5 metre drainage length. The runoff records from these tests followed a more complex profile, with a stepped rising limb and, usually, no steady-state section. The falling limb was similar to other tests. The stepped profile of the rising limb, in which the rate of runoff decreases and increases twice in addition to the final decrease towards steady-state, is believed to be related to the very different properties of the two simultaneously tested components and their arrangement in the test chamber. The FD 25 is a smooth plastic, whereas the SSM 45 is a fibrous mat. The FD 25 in the test chamber consisted of three separate pieces, as only the 2×1 metre board form of the product was available for testing. As a result, although all inflow to the test system started on the upper surface of the FD 25, most (if not all) water that landed more than 2 metres from the downstream end of the rainfall simulator would transfer to the SSM 45 layer at a joining point between FD 25 panels. Therefore, approximately two-fifths of the test inflow would flow exclusively over the surface of an FD 25 panel, another two-fifths would flow over the surface of an FD 25 panel and then through two metres of SSM 45, and one-fifth would flow over the surface of an FD 25 panel and then through four metres of SSM 45. This also explains why the flattest sections of the rising limb are at around 40 and 80% of the steady-state runoff rate, and why, at a 2 metre drainage length, the addition of SSM 45 to FD 25 has very little noticeable effect (Figure 5.4).

(a)   (b)

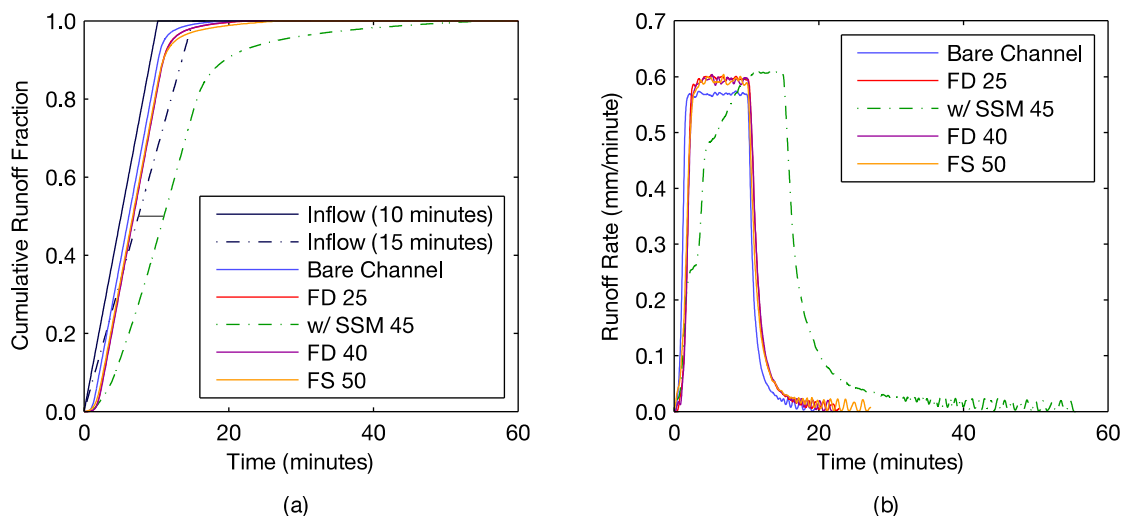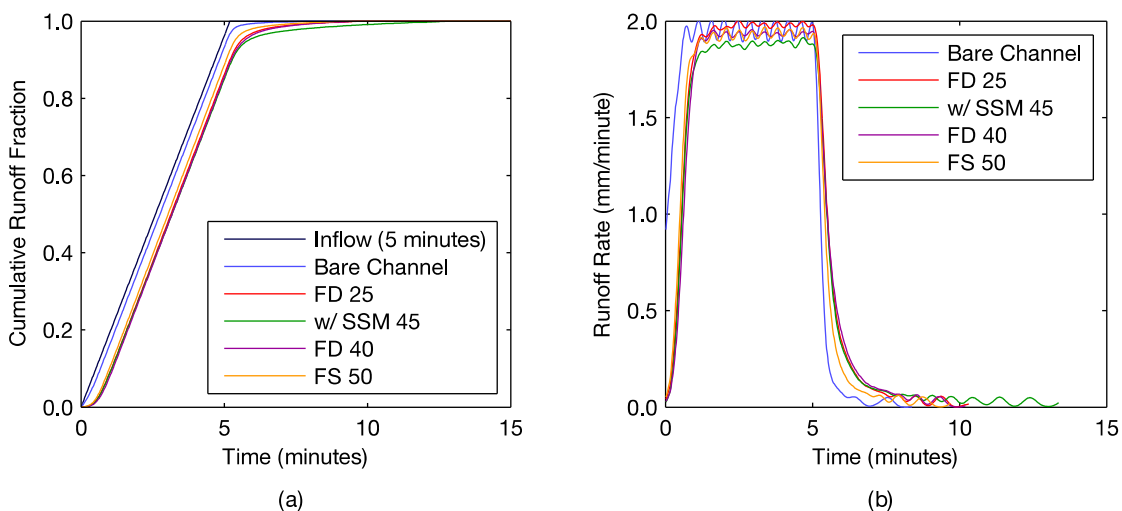**Figure 5.4 – Cumulative (a) and time-series (b) runoff response comparison of all five drainage components at 10° roof slope and 2 m drainage length, with a nominal inflow rate of 2.0 mm/minute**

Averaged across all tests, the time delay between the mid-point of cumulative inflow to the system and the mid-point of cumulative runoff from the system (t_{50}, see also the grey line on Figure 5.3 (a)) was found to be 110 seconds. This value was lowest on average for the tests involving the bare channel (54 seconds) and highest on average for the tests involving FD 25 in combination with SSM 45 (192 seconds). However, the largest variation in t_{50} was found across different inflow rates, ranging from 213 seconds for the tests with an inflow rate of 0.1 mm/minute, down to only 44 seconds for the tests with an inflow rate of 2.0 mm/minute. The effect of drainage length was lower (85 seconds for 2 m vs. 135 seconds for 5 m) as was the effect of roof slope (122 seconds at 1.15° slope, 98 seconds at 10° slope). In the extreme case of bare channel, high roof slope, short drainage length and the highest inflow rate, t_{50} times were only 8-9 seconds, whereas, in the opposite extreme case of FD 25 with SSM 45, low roof slope, long drainage length and the lowest inflow rate, t_{50} times were as high as 606-636 seconds, or approximately ten minutes. Considering that the primary aim of a drainage layer is to quickly remove excess water that has percolated through the substrate, it appears that all of the tested drainage layers are adequate for this purpose in all configurations. Figure 5.5 plots t_{50} times for all 300 tests.

A catchment's time of concentration is defined as the duration required for the entire catchment area to be contributing to runoff from the outlet. It follows that this, under a constant-intensity event, is the time taken for the rate of outflow to equal the rate of inflow. Appendix B of BS EN
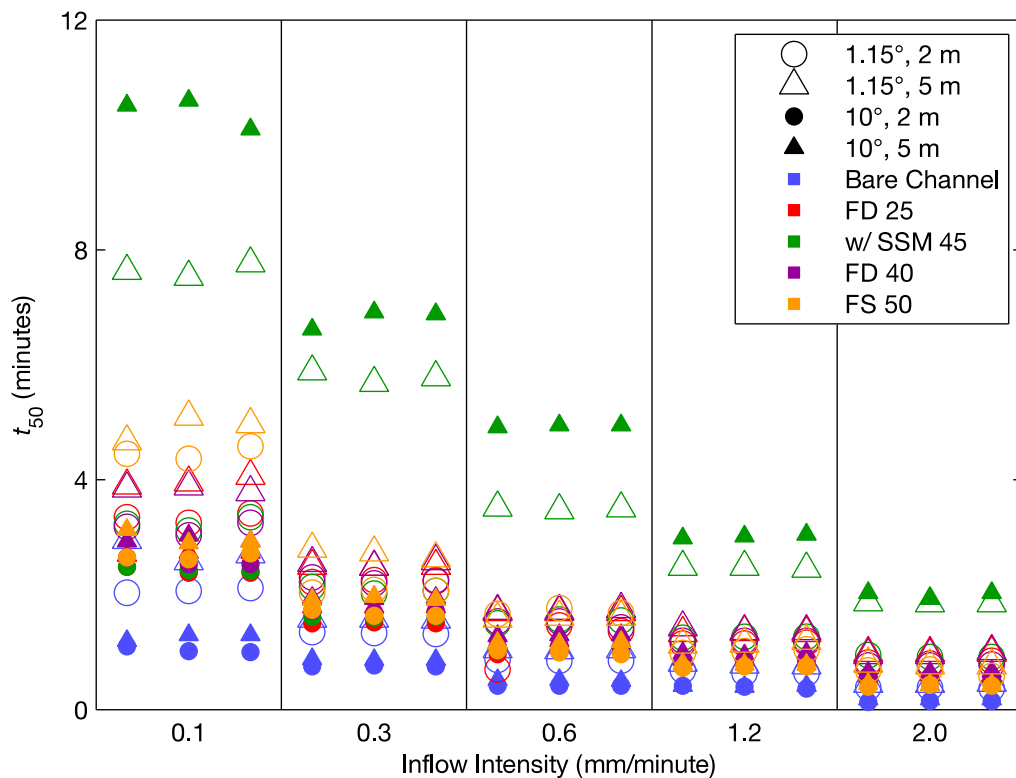

Figure 5.5 – t_{50} for all tests.

12056-3 (BSI, 2000) states that the typical time of concentration for a conventional roof is two minutes. In this experimental programme, the mean t_{CO} (defined here as the time required for the rate of runoff to exceed 95% of the inflow rate, due to the uncertainties associated with small oscillations in the smoothed runoff profiles) for all tests, excluding those using FD 25 with SSM 45 at a 5 metre drainage length, was 151 seconds. This is only 31 seconds longer than the two-minute value given in BS EN 12056-3, indicating that the drainage capability of a green roof drainage layer, without a protection mat, is broadly comparable to that of a conventional hard roof surface. Furthermore, the two-minute value given in BS EN 12056-3 is, in practice, applicable to storms whose intensity is around 2.0 mm/minute (for which drainage layer mean t_{CO} is 91 seconds) and is likely, for safety reasons, to be towards the low end of real roof behaviour. It is therefore highly plausible that green roof drainage layers are equal to conventional roof surfaces at draining roof runoff.

5.5 Nonlinear Storage Routing

5.5.1 Overview and Optimization

The general methodology for storage routing was described in detail in Section 2.4.5.3. Nonlinear storage routing is a modification, also described in that section, for which the rate of runoff is linked to the volume in storage by a non-linear relationship. In the interpretation used by Kasmin *et al.* (2010), predicted Q (rate of outflow) in a time step is equal to the current depth in temporary storage (cumulative inflow minus cumulative outflow) which has been raised to an exponent, here called b, and scaled by a multiplier, here called a (i.e. $S_t = S_{t-1} + (I_t - Q_t)\Delta t$ and $Q_t \Delta t = a S_{t-1}^{b}$). The same interpretation of nonlinear storage routing is used in the analyses following in Sections 5.5 and 5.6. It is clear from this methodology that the accuracy of a time-series runoff profile generated by nonlinear storage routing depends on the numerical values chosen for the b and a parameters. For individual runoff records taken from pressure transducer data, the best values for b and a are in all cases unknown. The aim of the following data analysis was therefore to find optimal values for b and a for each modelled runoff record i.e. those values which maximized R_t^2 (Young *et al.*, 1980) in the comparisons of corresponding modelled-monitored time-series runoff profiles. The optimization process was conducted using *lsqcurvefit*, a Matlab function which solves nonlinear data fitting problems in the least-squares sense, given an input data record, a user-specified function with variable parameters and an output data record to be fitted by the function. In the case of this optimization study, the input data is the inflow profile and smoothed runoff response, the user-specified function is the nonlinear storage routing equation with variable a and b parameters, and the output data is the time-series runoff profile.

In addition to the two parameters a and b, a *delay* parameter is included to account for any time delay between a quantity of runoff leaving the simulator chamber and that quantity being

recorded by the pressure transducer. The *delay* parameter models time delays by shifting the predicted runoff profile by an integer number of time steps, such that the value of Q_i is shifted to become the value of $Q_{i+delay}$. For each configuration, the best-fitting values for *a* and *b* were identified for all integer *delay* values from 0 to 300 seconds. The single combination of *a*, *b* and *delay* for which R_t^2 was maximized was saved for each test, along with the corresponding value of R_t^2 and total processing time to optimize that modelled runoff profile.

All optimizations were performed in Matlab 7.12.0 (R2011a) on a Toshiba Tecra A11 laptop, with an Intel Core i5-520M processor and 3 GB of DDR3-1066F RAM, running Windows 7 Professional 32-bit, Service Pack 1.

5.5.2   Applicability of Method at One-Second Resolution

Based on preliminary trials, the run of *lsqcurvefit* used starting estimates of 2.5 and 0.01 for *b* and *a* respectively. To increase optimization speed, lower and upper bounds were set on the two parameters, namely [1,6] for *b* and [10^{-5},1] for *a*. Setting a lower bound of 1 on *b* simultaneously with an upper bound of 1 on *a* also prevented the predicted value of *Q* from exceeding the value of *S* at any time step, preventing the prediction of a negative depth of stored water in the drainage layer. An upper bound of 80 seconds was applied to *delay*, again based on preliminary trials. The total time required for optimization was 9 minutes and 36 seconds, and working solutions were found for all 300 tests, with R_t^2 taking a mean value of 0.9922 and exceeding 0.99 in 244 cases. R_t^2 was below 0.9 in only three cases, all testing FD 25 with SSM 45 at a roof slope of 10°, drainage length of 5 metres and inflow rate of 0.1 mm/minute. These used an averaged inflow profile, estimated from a population with a 4% standard deviation. It is therefore not unreasonable to expect that the true value of inflow for these tests may have been as little as 96% or as great as 104% of the estimated inflow value used, either of which may have produced better-fitting predicted runoff profiles.

Figure 5.6 plots four time-series runoff profiles resulting from this optimization: the best-fitting profile, worst-fitting profile, profile with R_t^2 closest to mean and profile with R_t^2 closest to median (150th best-fitting profile). The physical configurations of these tests are written onto each plot. These are selected to show the range in the quality of results produced by the model, along with examples of a "typical" model output.

Aside from the modelled runoff profiles shown in Figure 5.6, many of the less successful curve-fitting optimizations were for tests of FD 25 with SSM 45 at a 5 metre drainage length. Though this may be partly attributed to the fact that the rectangular inflow profiles for these tests were not fitted to the monitored runoff profiles, it has also been commented upon that the monitored runoff profiles for these tests are very differently shaped from all other monitored runoff profiles.
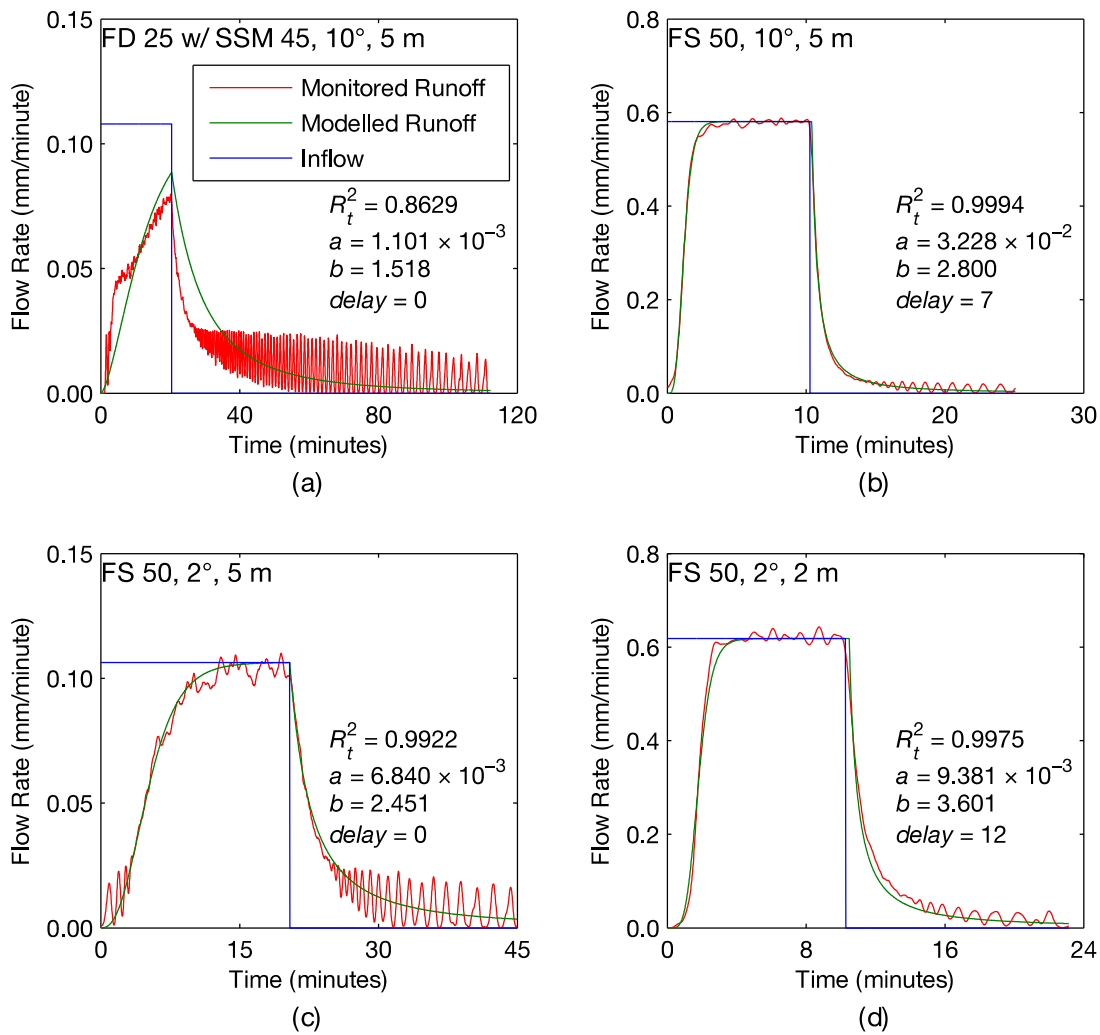
Figure 5.6 – Worst- (a), best- (b), mean- (c) and median- (d) fitting modelled runoff profiles with optimized *a*, *b* and *delay* parameters.

The curve-fitting algorithm was not very successful at identifying the steps in the monitored runoff profile, instead producing modelled runoff profiles which average the stepped shape into a smooth curve.

Optimized values of *a*, *b* and *delay* for all 300 tests are shown in Figure 5.7, Figure 5.8 and Figure 5.9. The same key should be used as for Figure 5.5; this is repeated in Figure 5.9.

5.5.3   Statistical Analysis

5.5.3.1   Procedure

For a fixed inflow profile, the modelled runoff profile may take a range of shapes. In any case, the shape taken is dependent on the values assigned to *a*, *b* and *delay* for the storage routing operation. Ultimately, it is envisaged to link the values of these parameters to measurable characteristics of the drainage layer, hence the motivation behind a test programme throughout which measurable characteristics were varied by defined amounts.
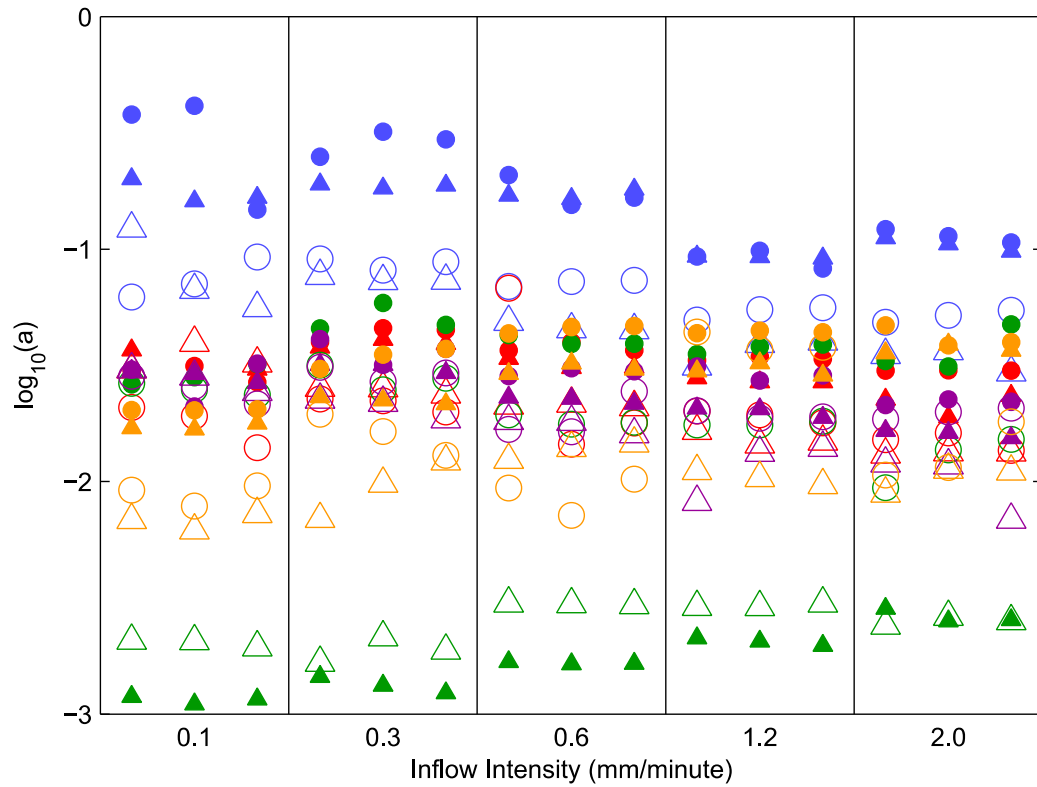
Figure 5.7 – *a*-values for all tests.
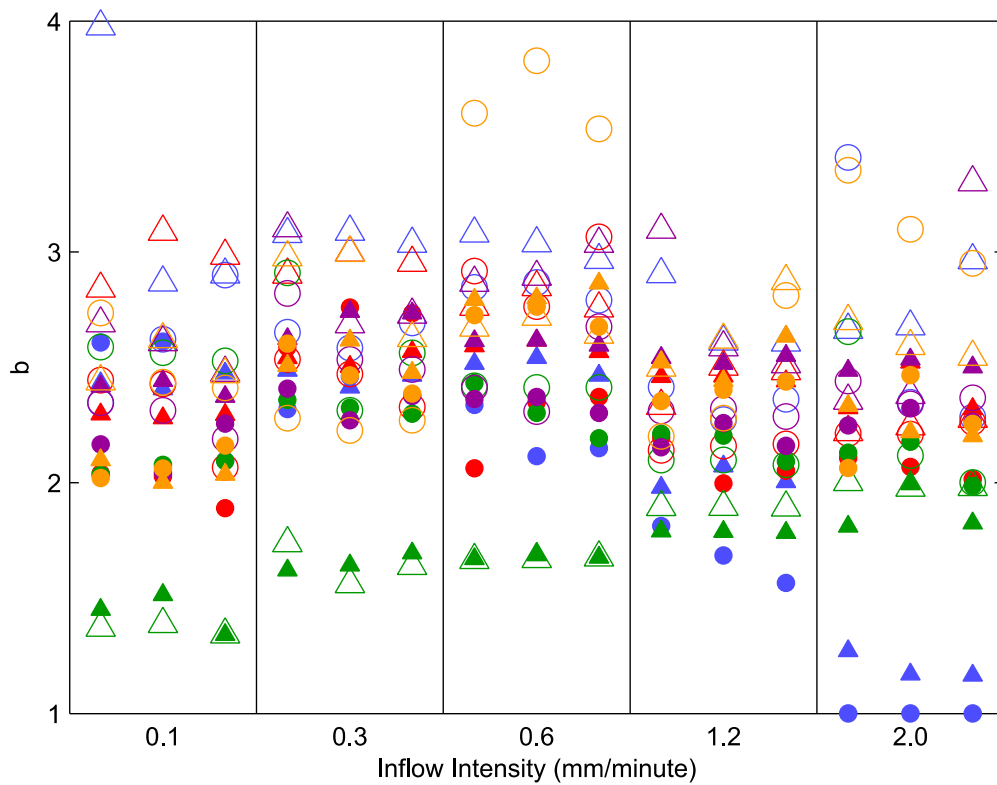
Figure 5.8 – *b*-values for all tests.
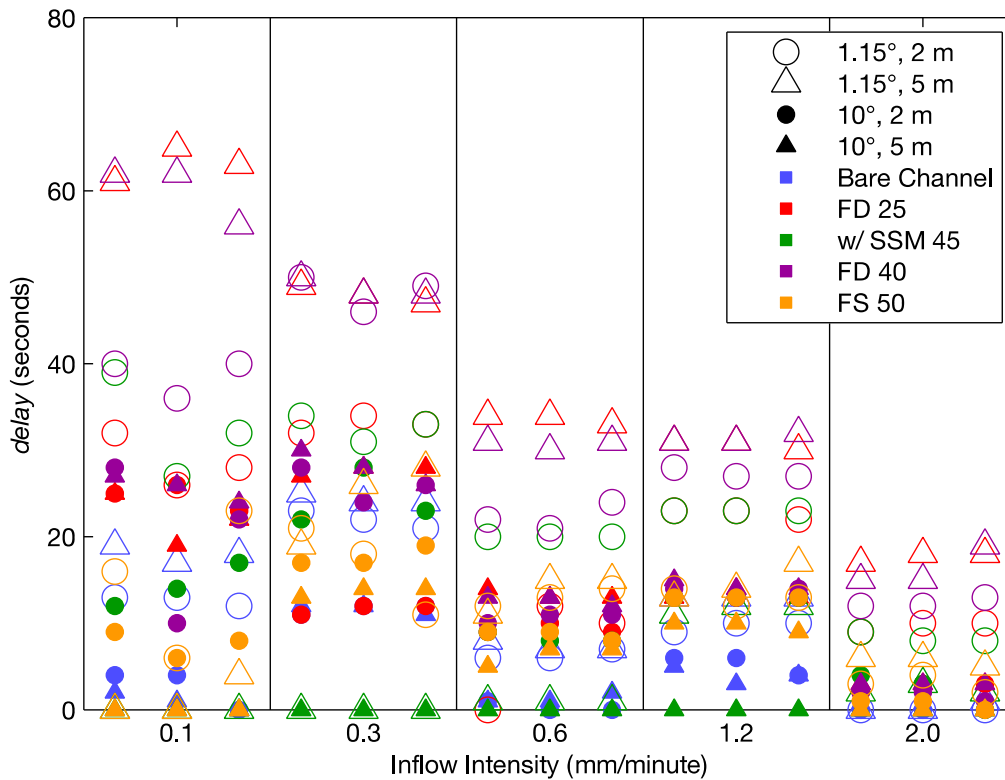
Figure 5.9 – *delay*-values for all tests.

To ascertain the importance of each configuration variable on the optimal values of the model parameters, a statistical analysis was performed on the optimized values of *a*, *b* and *delay*. The optimized values of each were grouped according to the divisions within one test variable (roof slope and drainage length each divide into two equally-sized groups of 150 members, drainage component divides into five equally sized groups of 60 members, and inflow rate divides into five similarly-sized groups of mean, median and mode 60 members). For roof slope and drainage length, both Student's unpaired two-sample *t*-test and Welch's unpaired two-sample *t*-test, a modification of Student's *t*-test for populations with unequal variances (Welch, 1947), were used to assess whether the means of both groups were different from each other at a 0.05 significance level. Levene's test for equality of variances was employed simultaneously, to determine which of Student's or Welch's statistic was most appropriate in each particular case.

For drainage component and inflow rate, either Fisher's LSD or Tamhane's T2 post-hoc test was used at the same significance level of 0.05 to simultaneously compare the means of all five groups, following one-way ANOVA and Levene's test. IBM SPSS Statistics 19 was employed for all statistical tests and analyses presented in this thesis.

5.5.3.2   Discussion of Parameter Values

Figure 5.10 plots the mean and standard errors for *a*, *b* and *delay*, for all categories within each test variable. Statistical groupings are shown by capital letters above each bar. It should be noted
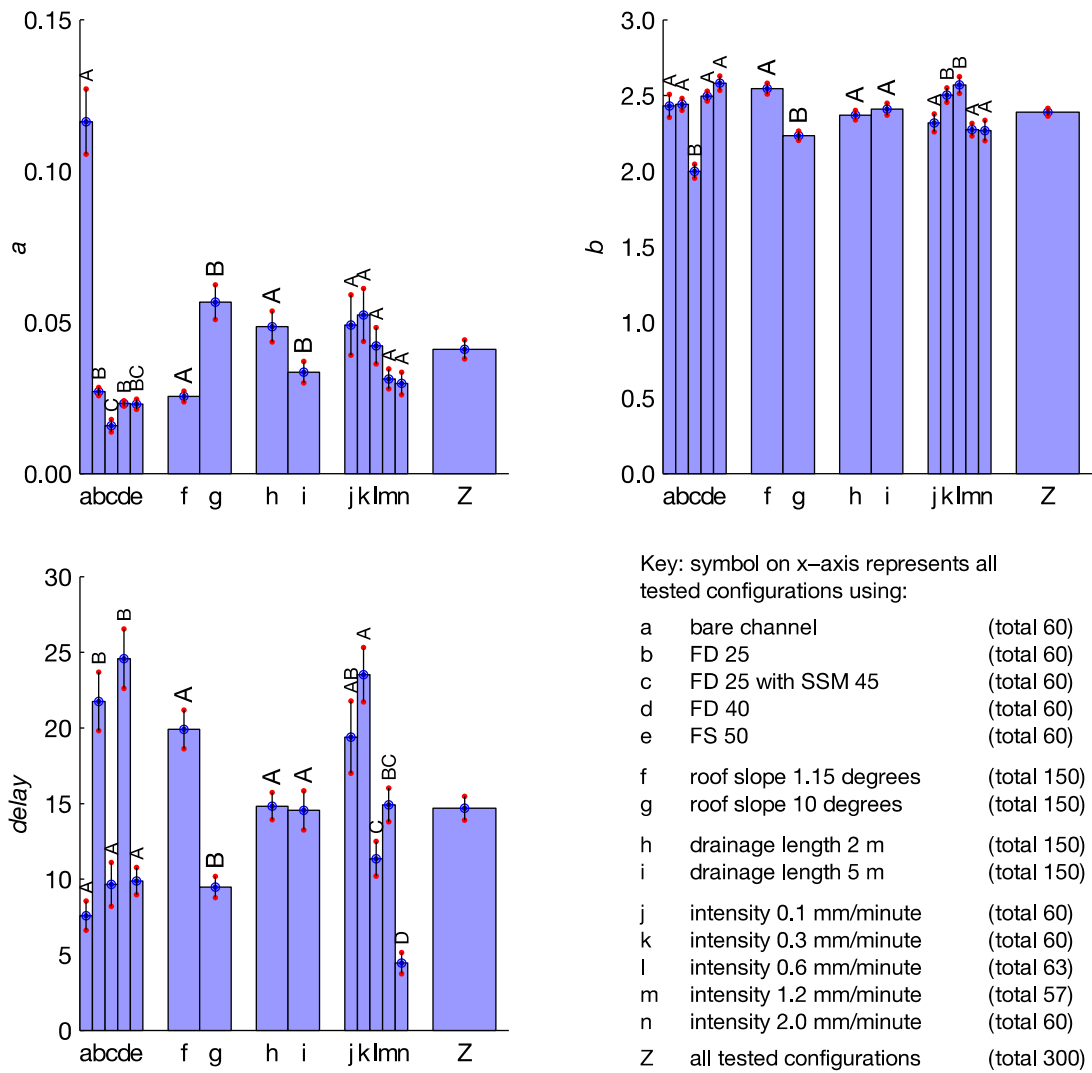
Figure 5.10 – Mean (light blue bars) and standard error (black lines terminated by red dots) of optimized values for *a*, *b* and *delay*.

that the capital letters denoting significance groups for one test variable (one group of touching columns) do not represent the same groups as the same letters above a different variable, or the same variable in a different sub-plot e.g. group A for drainage component is not the same group A as for roof slope, and group A for drainage length on the plot of *a*-values is not the same group A as for drainage length on the plot of *b*-values. For all three parameters, it is shown that standard error (Z columns in Figure 5.10) is low in comparison to the mean i.e. Student's *t*-statistic is high. This is especially apparent for *b*, where the *t*-statistic is 94, though the *t*-statistics for *a* and *delay* are also very high, at 13 and 19 respectively. The respective mean values of these parameters are 2.390, 0.0411 mm^{1-b}/s and 14.69 seconds. The high values of *t*-statistic show that the overall sensitivity of the modelling parameter values to the variable test configurations is low. The mean parameter values, with *delay* rounded to 15 seconds, could therefore be assumed as a "default" set for runoff modelling in the absence of more specific information, with regards to modelling parameter values.

The ratio of highest to lowest parameter values is smallest for b at 3.98:1. In three optimizations, b is less than 1.00005, implying that the optimization routine would ideally wish to set values of b below 1 for these optimizations. However, goodness-of-fit (R_t^2) is also above the mean value in these three cases, suggesting the possibility of the a parameter being able in some way to compensate for the action that would have been performed by the b parameter value had it not been forbidden.

The ratio of highest-to-lowest value of a is far greater than for either b or $delay$, at 375:1, though no value is near to either the upper or lower bound set on a. Despite the maximum value of a being 0.413, the mean is less than one-tenth this and the median lower still. The very highest values for a correspond almost entirely with the bare channel at a slope of 10°. This is also the configuration for which three values of b are practically 1, further suggesting the possibility of compensation between a and b.

The values of the $delay$ parameter range from 0 to 65 seconds. The most common value is 0, accounting for 50 optimizations. 13 is the second most common value, accounting for a further 26 optimizations, while the three values in the range 12-14 seconds account for a total of 54 optimizations between them. This bi-modal distribution may relate to differences between the actual and assumed inflow profiles. For events consisting of pulsed inflow, the assumed rectangular inflow event was extended to include the pause after the final pulse, meaning that runoff from the simulator would begin to drop before the event, according to the assumed inflow profile, had finished. Physically, delay was introduced to the model to account for the time required for a quantity of runoff that has left the simulator chamber to arrive in the collecting cylinder. However, for pulsed inflow events, the effect described here would counteract the monitoring delay to some extent. For monitored runoff profiles with long runoff tails, a better fit may be found by minimizing the difference between monitored and modelled runoff tails, through the use of the $delay$ parameter, while for monitored runoff profiles with shorter runoff tails, the importance of fitting using the $delay$ parameter would be diminished.

To evaluate the importance of delay in curve-fitting, one test (FD 25, 10° roof slope, 5 m drainage length, 0.6 mm/minute inflow) was selected and every value of R_t^2 reported, for $delay$ taking every integer value from 0 to 80. The optimal $delay$ value was 13 seconds, giving an R_t^2 of 0.9987. However, for values of delay from 4 to 22 inclusive, R_t^2 was greater than 99.9% of its maximum value. It is especially noteworthy that the optimized value of a is 0.0209 when $delay$ is 5 seconds, but more than double this, 0.0477, when $delay$ is 22 seconds, yet both values are considered equally good for runoff modelling. The value of b raises from 2.52 to 2.67 over the same range of $delay$ values, consistent with the low standard error in b overall.

5.5.3.3   Significance of Test Configuration

For all three parameters, the effect of roof slope is found to be significant (Figure 5.6). However, the effect of drainage length is found to be significant for *a* only. This may be a result of the physical range over which the configurations are varied; 5 metres is two-and-a-half times 2 metres, but a 10° slope is almost nine times steeper than a 1.15° slope. The statistical groupings by component are not similar between the *a*, *b* and *delay* parameters, although FD 25 and FD 40 share a statistical group in all three parameter sets. This may be a result of the two components being made of the same material and therefore having similar properties regarding interaction with water e.g. surface roughness. All values of *a* are statistically independent of inflow intensity, though the same is not true of *b*. This is an unusual result, as the storage routing method is theoretically independent of rainfall (or in this case inflow) intensity in general. The division of *b* into two statistical groups based on inflow intensity may be a consequence of the very low standard error in *b* for each group of nominal inflow intensity. The group means of A and B are close, at 2.279 and 2.534 respectively. The non-divisibility of *a* is to be expected, though it can be seen that the values of *a* are subject to higher standard error, which will have contributed towards this. The optimal values for *delay* may be expected to decrease as inflow intensity increases, depending on how the parameter is interpreted. A general decrease in *delay* with increasing inflow intensity can be observed. The fact that mean *delay* is lower for 0.1 than 0.3 mm/minute is probably due to the pulsing inflow method used to supply water, extending the assumed rectangular event beyond the end of any actual inflow. In addition, intermittent inflow is being supplied at 0.3 mm/minute, but the runoff only needs to achieve one-third of this rate for steady-state to be reached. The same principles apply to the similar observation for inflow rates of 0.6 and 1.2 mm/minute.

5.5.3.4   Parameter Value Averaging of *a*

The statistical analysis of storage routing parameters (Section 5.5.3) suggests that the values of certain parameters are independent of certain test characteristics. This may allow the grouping and averaging of parameter values with respect to that characteristic e.g. the value for *b* is independent of roof slope, so it should be possible to average the value of *b* for the entire group of tests where the only variable is roof slope, without a great loss in modelling accuracy. The purpose of parameter value averaging is to allow sensible parameter estimates to be applied to roofs with reasonable but untested characteristics, such as a 5° roof slope. Parameter value averaging therefore genericizes the model.

Fundamental to storage routing is the assumption that both of the *a* and *b* parameters are independent of inflow rate. Though Figure 5.10 only shows independence for *a*, it is plausibly suggested that multiple optimizations of near-equal value exist for each monitored runoff profile and that all three optimization parameters are interlinked. It was therefore assumed that the

number of individual *a*-parameter values could be reduced from 300 to 20 with minimal effect on the quality of the modelling, by grouping each set of fifteen optimized *a*-values (all tests using one physical configuration, regardless of inflow rate) into a single mean value. In addition, it was assumed that the *a*-values for FD 25 and FD 40 could be averaged, further reducing the number of individual *a*-values from 20 to 16. After averaging and specifying fixed *a*-values for each test, the *b*- and *delay*-values were re-optimized to the newly-specified *a*-values. The total time required for this run was 4 minutes and 45 seconds, slightly below half of the time required for the bounded optimization of *a*, *b* and *delay*. This approximate halving in processing time is presumably due to the halving in the number of parameters optimized by *lsqcurvefit*, from two to one. The mean R_t^2 correlation between monitored and modelled runoff over all tests was reduced very slightly from 0.9922 to 0.9913, while the number of tests with R_t^2 above 0.99 was also reduced slightly, from 244 to 239. The worst-fitting modelled runoff profiles were again those for the configuration of FD 25 with SSM 45 at a roof slope of 10°, a drainage length of 5 m and an inflow rate of 0.1 mm/minute. These remained the only three optimizations with R_t^2 below 0.9. It can therefore be concluded that parameter value averaging of *a* simplifies the modelling method without compromising on accuracy.

Figure 5.11 shows four plots resulting from this optimization, selected using the same criteria as for Figure 5.6. The worst-fitting modelled runoff profile is generated for the exact same test; grouping of *a*-values across all inflow rates produces a fixed value of *a* = 0.00173, about 57% higher than first optimized. Use of the specified *a*-value generates a re-optimized value for *b* of 1.622, which is higher than, but still reasonably close to, its optimized value. As a result, the peak rate of runoff is greatly overestimated and the sharpness of the rising and falling limbs is increased. The best-fitting runoff modelled runoff profile is to a different individual test conducted at the same test situation as in the original optimization (Section 5.5.2). Both the monitored and modelled runoff profiles, and the R_t^2 goodness-of-fit, are near-identical between Figure 5.6 and Figure 5.11, as are the specified averaged value of *a* and corresponding newly-optimized values of *b* and *delay*. The mean and median runoff profiles are not for the same configurations as those shown in Figure 5.6; these different configurations are included at this stage to show monitored and modelled runoff profiles for a variety of test configurations and demonstrate the model's typical performance after averaging of *a* values by significance group. It has been mentioned previously that the shapes of the monitored runoff profiles, and therefore corresponding well-fitting modelled runoff profiles, are similar for all tested component configurations excluding those using SSM 45 at a 5 metre drainage length. Figure 5.11 (c), however, does show one reasonably well-fitting modelled runoff curve to a test using SSM 45 at a 5 metre drainage length. It is important to note that equilibrium appears to have been reached during that test.
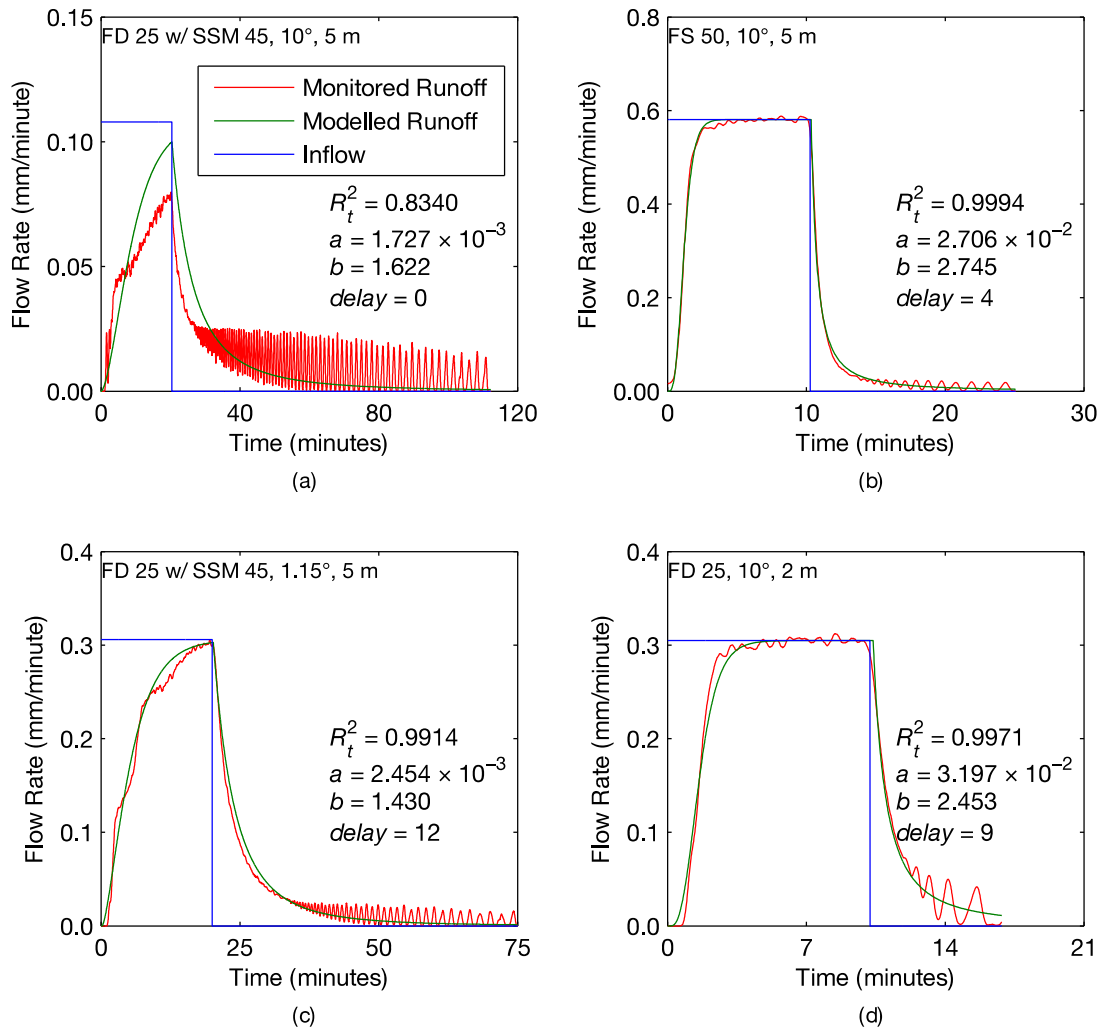
Figure 5.11 – Worst- (a), best- (b), mean- (c) and median- (d) fitting modelled runoff profiles with optimized *b* and *delay* parameters, after parameter value averaging of *a*.
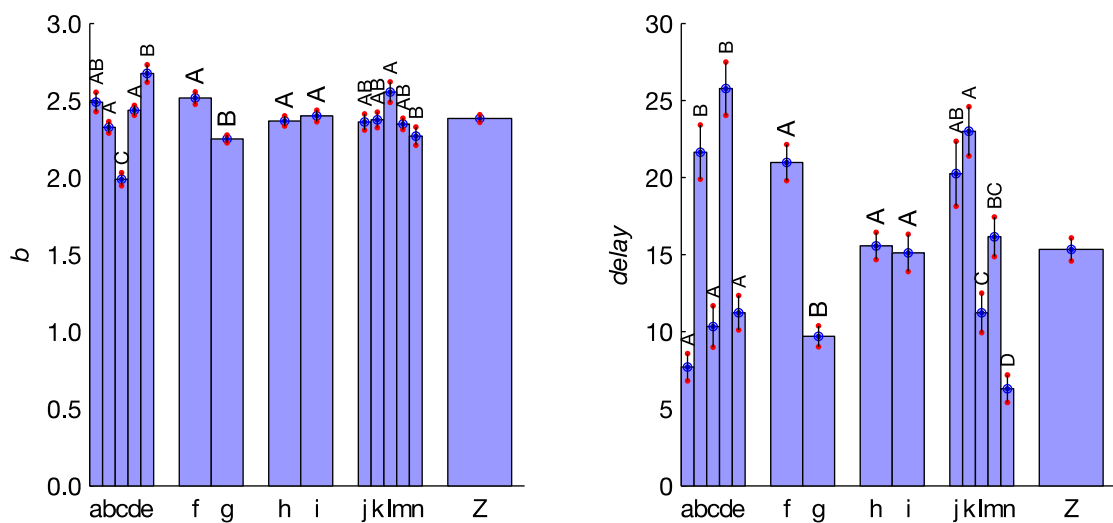

Figure 5.12 – Mean and standard error of optimized values for *b* and *delay*, after parameter value averaging of *a*.

The same statistical analyses were performed on the re-optimized b and *delay* parameter sets, the results of which are shown in Figure 5.12. To save space, the key is not reproduced; all columns are shown in the same order as in Figure 5.10. As all a-values were specified prior to re-optimization, a plot of a-values is omitted.

For b, averaging of a-values affected the statistical groupings of component and inflow rate. The range of group means for component statistical groups was slightly increased. FD 25 and FD 40 were still found to share a statistical group, though FS 50, an expanded polystyrene component, became separated into its own group. Inflow rates were still found to divide into two groups, though now, three inflow rates belonged to both groups. The group means of A and B were 2.412 and 2.338, reducing the difference between group means to less than a third of its previous value and strengthening the argument for the independence of b from inflow intensity.

For *delay*, averaging of a-values had no effect on statistical groupings and very little effect on group means and standard errors. Most notably affected were the group means for inflow rate: averaging of a reduced the range between the means of groups A and D by 2.37 seconds. However, consideration only of group means hides the effect of a-value averaging on individual parameter values; only 76 of 300 remained unchanged after parameter value averaging of a, and 20 of 60 tests using FS 50 underwent a change of 5 or more seconds in *delay* value – in consideration of group means, an increase and a decrease of the same magnitude will cancel out.

5.5.3.5 Further Parameter Value Averaging of *b*

To further test the generic applicability of the model, the same parameter value averaging methodology was applied to values of the b-parameter. One-way ANOVA on the original set of b-values suggested that the optimized b-values for FD 25, FD 40, FS 50 and the bare channel belonged to a single large statistical group, though following averaging of a-values, it became the case that only the b-values of FD 25 and FD 40 could be grouped. Drainage length was shown to have no statistical effect on the value of b, either before or after averaging of a. b-value was not shown to be entirely independent of inflow rate, though it was decided to group the values of b by inflow rate as if only a single statistical group existed. This was for two reasons: the storage routing model assumes both a and b are independent of inflow rate; and the difference between the two group means was greatly decreased following parameter value averaging of a. Therefore, it was anticipated that *delay* could compensate for the effects of averaging the values of the b parameter by significance groupings. The number of individual b parameter values was decreased from 300 to 8, with each of the 8 new values being the mean of either 30 or 60 values derived from the previous optimization. It should be noted that *lsqcurvefit* was not required for the optimization of *delay* as both a and b were specified; all values of delay, from zero to the upper limit, were tested sequentially.

The total time required for the selection of the best *delay* value for all 300 tests was 12.0 seconds, representing 1/25th of a second per test on average. Mean R_t^2 was again reduced, but remained high, at 0.9902. Slightly fewer models, 234, maintained R_t^2 above 0.99. Lowest R_t^2 was reduced to 0.8295 and a fourth model had its R_t^2 reduced below 0.9; this was for one test using the same physical configuration as the worst-fitting model, but an inflow rate of 0.3 mm/minute. It may be concluded that the model's predictive capability remains high.

Figure 5.13 plots the worst, best, mean and median modelled runoff profiles, similarly to Figure 5.6 and Figure 5.11. The worst-fitting profile remains the same, with *a* and *b* now set 57% and 30% above their optimized values (and *delay* unchanged at 0). The result of this increase in *b* (to a further 21% above its re-optimized value as plotted in Figure 5.11) is to further increase the peak value and sharpness of the modelled runoff profile, though the additional effect of the second-level parameter averaging over the first is much less. The best-fitting profile remains for the same configuration, but reverts back to the same specific test as shown in Figure 5.6. Relative to their optimized values, parameter averaging causes *a*, *b* and *delay* to reduce by 16%, 10% and 1 second respectively. A visual comparison of Figure 5.6 (a) and Figure 5.13 (a) shows little difference, although a very slight decrease in the steepness of the rising and falling limbs, due to a reduction in the modelling parameters, is apparent upon close inspection. The mean-fitting and median-fitting profiles are again different from those shown previously, but are again both included to demonstrate the model's applicability to different test configurations and present examples of the model's typical performance at this level of parameter value averaging. It may be concluded that the model's predictive capability remains fit for purpose.

The same statistical analyses as are shown in Figure 5.10 and Figure 5.12 were performed, the results of which are shown in Figure 5.14.

Averaging of *a* and *b* parameter values has little effect on the statistical groupings of the *delay* parameter values; the only change is the formation of a third component group, containing FD 25 with SSM 45 and FD 25 alone. However, large individual changes, though rare, are present and masked by the consideration of averages; six *delay* values are changed by over 20 seconds relative to the bounded optimization with no parameter value averaging. In all cases, the specified values of one or both of *a* and *b* are set below 80% or above 120% of their originally optimized values; evidently, greatly changing the values of *a* and *b* greatly changes the value of *delay* at which the modelled runoff profile is most similar to the monitored runoff profile. It is noted that, with *a* and *b* fixed, the shape of the modelled runoff profile is fixed, and the function of *delay* is to "slide" this shape along the time axis until the closest fit is found. If the shape is fixed poorly, by values of *a* or *b* which are distant from their optimal values, it is possible that the goodness-of-fit can still be increased by moving this lower-quality shape through the time dimension.
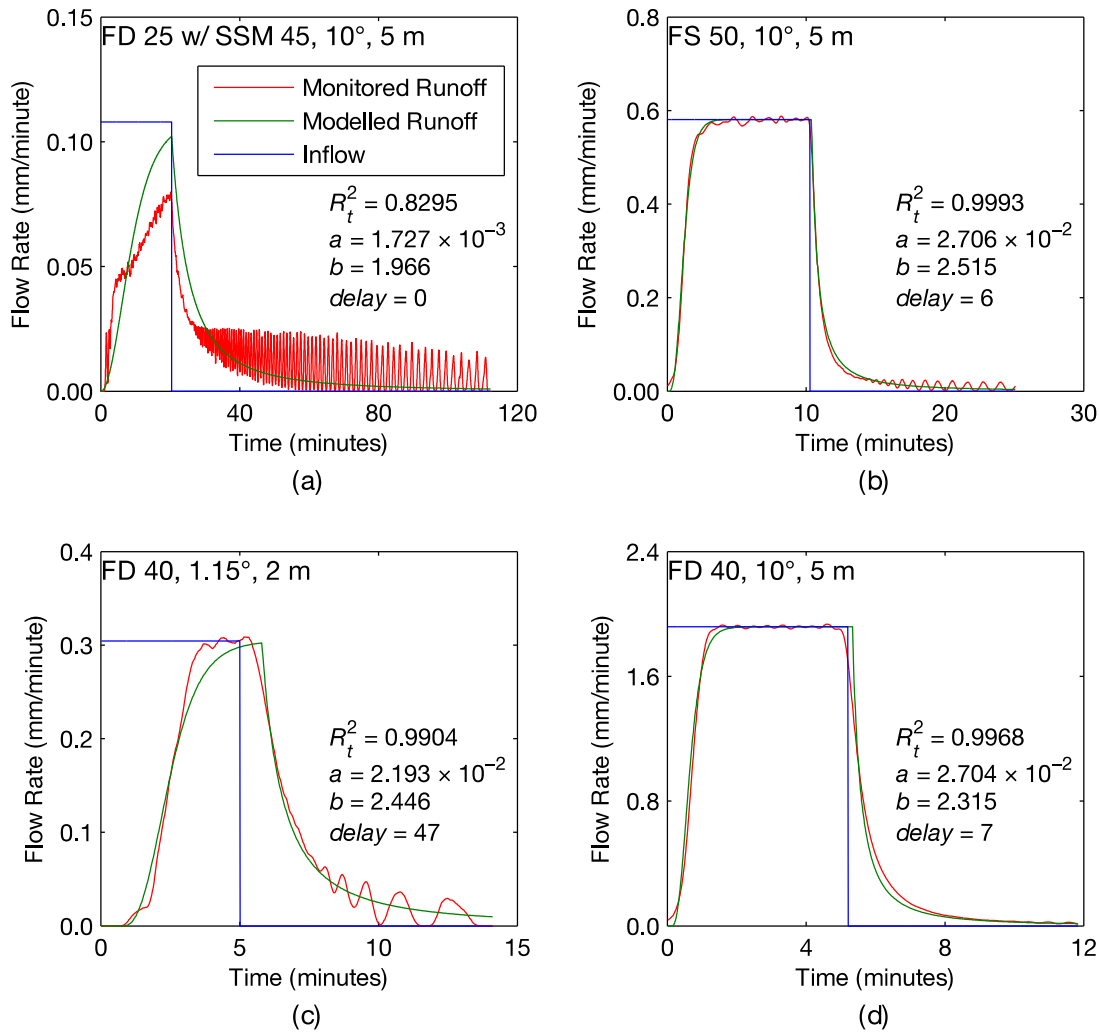
Figure 5.13 – Worst (a), best (b), mean (c) and median (d) modelled runoff profiles with optimal *delay* parameter, after parameter value averaging of *a* and *b*.
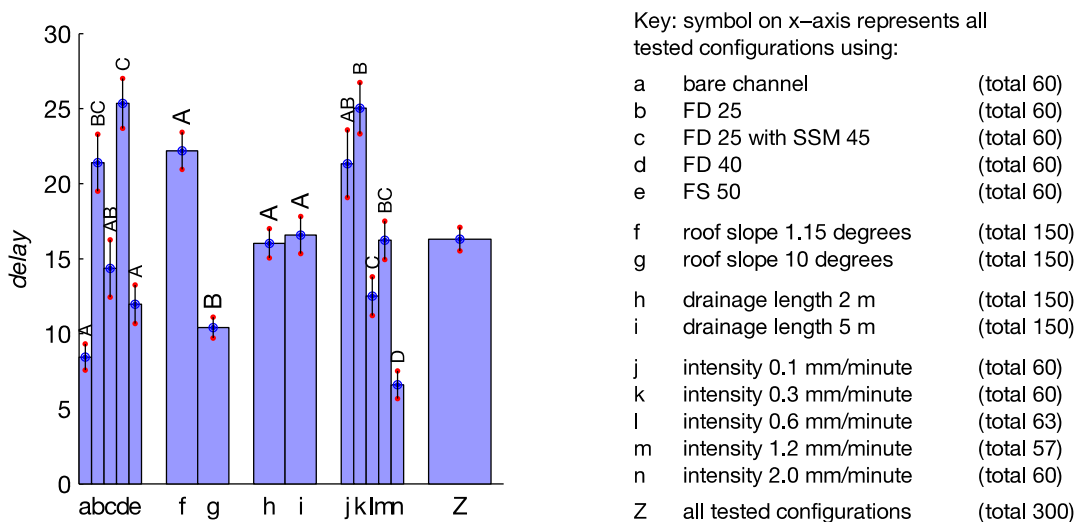

Figure 5.14 – Mean and standard error of optimized values for *delay*, after parameter value averaging of *a* and *b*.

Relative to the initial parameter value sets, only 12 out of 300 tests have averaged values of both *a* and *b* within 5% of optimized values, and only four of these maintain exactly the same value of *delay* before and after parameter value averaging. The fact that the great majority of tests do not use a highly accurate value for *a* or *b* (or both), but that the great majority of tests do have high goodness-of-fit, suggests that the model fit is relatively insensitive to the exact values of the parameters used: even one of the top ten best fitting models uses a specified *a* parameter that is more than 20% below its optimized value, and the best fitting model overall uses estimates for both *a* and *b* which are more than 10% below their optimal values. In this model, *delay* is reduced from 7 to 6 seconds after averaging of *a*- and *b*-values by statistical group, which may suggest either compensation from that parameter or extreme insensitivity of *a* and *b* in relation to modelled runoff.

5.5.3.6   Conclusions of Parameter Statistical Analysis and Averaging Study

An optimization routine, *lsqcurvefit*, was used in Matlab to optimize the scale and exponent parameters of 300 time-series runoff profiles, modelled by nonlinear storage routing, to best fit 300 monitored time-series runoff profiles. This optimization was performed multiple times, with the modelled profile shifted relative to the start of the inflow event by a different amount each time, to account for a suspected time delay in the runoff and collection monitoring system. The nonlinear storage routing method was found to be very successful, in terms of goodness of fit (mean $R_t^2 = 0.9922$) and speed (mean optimization time per test = 1.92 seconds). The method was more successful for modelling runoff profiles with non-stepped rising limbs, which constituted 270 of the 300 profiles input to the model. One-way ANOVA and unpaired *t*-tests were performed on the optimal values of all three modelling parameters to determine which, if any, of the test variables had no significant effect on the parameter values. As values of *a* were shown to be fully independent of inflow rate, it was decided to group and average the optimized values of *a*; all 15 values of *a* derived from tests at a single physical configuration were averaged to give a single mean value. AS FD 25 and FD 40 were shown to be statistically similar, they were treated as one component for this parameter averaging. The optimization routine was run again, with *a* fixed at one of a reduced set of 16 specified values. This run was also found to be very successful: mean optimization time per test was approximately halved to 0.95 seconds, while mean R_t^2 was almost unchanged, at 0.9913. Evidence for a proposed compensative effect between all three modelling parameters was strengthened, as specifying fixed values of *a* caused the statistical groups for inflow rate for *b* to overlap, and the difference between their means to greatly reduce. Based on the theoretical methodology of storage routing and the observed contraction of the mean difference between the two statistical groups, the new parameter values for *b* were grouped by inflow rate and averaged per-group. Further parameter value averaging took place for *b*, by drainage length and component. This reduced the number of different *b*

parameter values to a small set of 8. With modelling values of both *a* and *b* specified in advance, *lsqcurvefit* was not used for this run. Instead, the storage routing model was run at multiple *delay* values and the value corresponding to the best fitting modelled runoff profile saved. Mean test run time was greatly reduced to approximately 0.04 seconds while R_t^2 was only slightly further reduced to 0.9902. Parameter value averaging of *b* had little effect on the statistical groupings of *delay*, only causing a third group to be formed in the "component" variable without affecting the members of the existing two groups.

As values both *a* and *b* were able to be grouped, fixed and specified in advance with only a minimal loss in modelling accuracy, it is hypothesized that the shape of the modelled runoff profile is relatively insensitive to changes in *a* and *b* parameter values. In all statistical analyses, it was noted that consideration of parameter values by groups can obscure large changes to parameter values in a small number of individual tests.

5.5.4   Parameter Sensitivity Analysis

It is anticipated that, if this modelling method is extended more widely to other drainage layer configurations, the parameter values found here will be superseded by more generic values with lower precision. As an example, all optimized *a* and *b* parameter values for ZinCo Floradrain FD 25 and FD 40 were statistically similar and could be averaged to a single modelling value with no great loss in accuracy. Bauder DSE 20/40 and Optigrün FKD 25/40 are both untested, but physically and materially similar drainage components to Floradrain FD 25 and FD 40. If, following testing, they were found to be statistically similar, then single values of *a* and *b* should be assigned to all drainage layer configurations which vary only between the choice of component from the six listed above. Untested components, including future designs, would be modelled with presumed reasonable accuracy, by using the generic parameters for the statistical group which contains the components that are most similar to the untested component. The parameter value averaging study showed that the goodness-of-fit of the profiles generated by the nonlinear storage routing model was, in many cases, relatively insensitive to reasonable modifications to the values of *a* and *b*, as evidenced by the small reduction in mean R_t^2 following one, and then two, levels of parameter value averaging.

To test the relationship between modelled runoff profile and parameter value precision, four tests, covering a range of configurations and modelled runoff accuracies were selected for further consideration. These were: the worst-fitting test; the test with the closest-to-mean *b*-value; the test with the closest-to-mean *a*-value; and one moderately-fitting test with a long rising limb.

In terms of monitored runoff profile shape, the worst-fitting test is unique among this selection for its stepped rising limb and lack of equilibrium with inflow. The two profiles with closest-to-

mean a- and b-values are similar in shape and typical of many of the monitored runoff profiles recorded during this experimental programme. Both consist of a smooth, steep rising limb, a flat section of equilibrium and a smooth, steeper-than-exponential falling limb. The moderately-fitting test's runoff profile features an extended rising limb of 5-7 minutes duration. It is hoped that the exact contributions made by the values of a and b to the modelled runoff profile will be clear to see in a comparative plot of modelled runoff profiles using a range of a- and b-values.

For each of the four selected tests, five a and b parameter value pairs were proposed. The first pair consisted of the optimized values which maximized the R_t^2 value. For the remaining parameter value pairs, the values of a and b were separately halved or doubled, so that each pair contained exactly one parameter at its optimized value. In all cases, *delay* was fixed at its optimal value; the effects of *delay* are discussed separately. The results of routing using these parameter values are shown in Figure 5.15, while the exact R_t^2 values relating to each profile are given in Table 5.2. For the worst-fitting profile, ½b is approximately 0.76 and modelling with this value for exponent eventually gives a negative depth of water in storage, followed by complex runoff in the falling limb. As this is clearly undesirable, a ½b-value of exactly 1 is used; this is for convenience still referred to as ½b.

Considering first only the relationship between goodness-of-fit and modelling parameter values, it is clear and obvious that shifting either parameter from its optimized value reduces the accuracy of the model. However, it is not conclusive which parameter most strongly influences goodness-of-fit. For the closest-to-mean a and long rising limb profiles, doubling or halving the value of b reduces R_t^2 by more than twice as much as doubling or halving the value of a. However, for the worst-fitting and closest-to-mean b profiles, doubling or halving the value of a affects the goodness of fit more negatively than doubling or halving the value of b. It is unusual that the goodness-of-fit of the profiles with closest-to-mean b and closest-to-mean a should be affected so differently when it is considered that both have similar optimized values of a and b. Additionally, the goodness-of-fit of the profile with closest-to-mean b is almost unaffected by any doubling or halving of the value of either a or b.

Considering the shapes of the time-series runoff profiles generated, the exact influence of the a and b parameter values on profile shape can be seen clearly, especially for the test with the long

Table 5.2 – Values of *a*, *b* and R_t^2 for *a*- and *b*-value sensitivity analysis.

Configuration	a	b	R_t^2 using				
			a, b	$a, \frac{1}{2}b$	$a, 2b$	$\frac{1}{2}a, b$	$2a, b$
Worst-fitting	1.10×10^{-3}	1.518	0.8629	0.8495	0.8184	0.8037	0.7983
Mean b	5.14×10^{-2}	2.401	0.9990	0.9949	0.9956	0.9933	0.9948
Mean a	4.10×10^{-2}	2.408	0.9968	0.9539	0.9637	0.9868	0.9892
Long rising	1.91×10^{-2}	2.428	0.9780	0.8452	0.8648	0.9505	0.9561

Figure 5.15 – Selected modelled runoff profiles using optimized values of *a*, *b* and *delay*, and fixed multiples of optimized *a*- and *b*-values individually.

rising limb. The value of a appears to directly influence the gradient of the rising and falling limbs; increasing the value of a increases the gradient and decreasing the value of a decreases the gradient. Except for where the modelled runoff profile approaches equilibrium, changing the value of a effectively tilts the modelled runoff line. This can be more clearly seen in the worst-fitting test profiles, where equilibrium is not close to being reached at the end of the inflow event and the maximum modelled value of runoff rate varies significantly depending on the value of a used. Variations in the value of b appear to affect the modelled runoff profile in a different way. For the rising limb, reducing the value of b causes the rise to begin quickly and flatten off as the runoff rate increases, while increasing the value of b causes the rise to remain slow and gradually become steeper until equilibrium is near. Considering an example plot of $S = Q^2$ with equivalent plots for the exponent value doubled and halved ($S = Q$ and $S = Q^4$), as shown in Figure 5.16, the observed behaviour of the modelled runoff profile with respect to b should be physically logical.
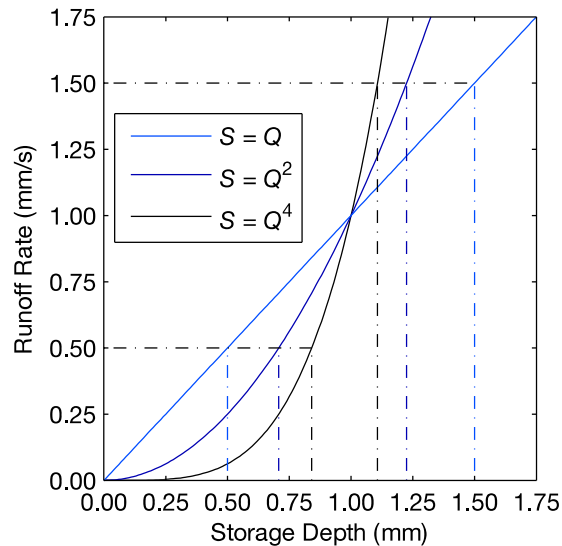
Figure 5.16 – Example storage-discharge relationships: $S = Q$, $S = Q^2$ and $S = Q^4$.

Specifically, when the depth in storage is below 1 mm at the beginning of a test, the value of Q is highest for $S = Q$. When the depth in storage rises above 1 mm, which happens further into the rising limb, if at all, the value of Q is highest for $S = Q^4$. As increasing the value of b can delay the point at which the modelled runoff profile begins to rise sharply, it can be proposed that the value of b may interact with the value of *delay*. However, this does not appear to be the case, as shifting the value of *delay* also shifts the point at which the modelled runoff profile transitions from steady-state to falling limb. Re-considering the test for which *delay* could be varied from 4 to 22 seconds with little loss of goodness-of-fit (Section 5.5.3.2), the corresponding range of b-values was from 2.52 to 2.67. It would therefore be unrealistic for any compensation between b and *delay* to exist over the range of b-values (doubling and halving) discussed in this section.

To evaluate the combined effects of the a and b parameter values, modelling for both the worst-fitting and long-rising test was repeated with a- and b-values simultaneously either halved or doubled. The results of this modelling run are shown in Figure 5.17.

The results of this analysis show that the effects of changing the values of a and b are cumulative. In the right plot, regardless of how b is set, the steepness of the profiles is ranked according to a-value. In addition, regardless of how a is set, increasing b delays the main rise in runoff. This is not consistently true of the left plot, due to the greater depths of water in storage, resulting from little runoff emerging as the inflow event progresses. Thus, lower values of b initially correspond to a faster rise in the runoff profiles, but later, to a slower rise.

So far, it has been assumed that, with a and b parameters fixed, *delay* acts only to move a modelled runoff profile of fixed shape along the time-axis to the position at which the difference

(a)   (b)

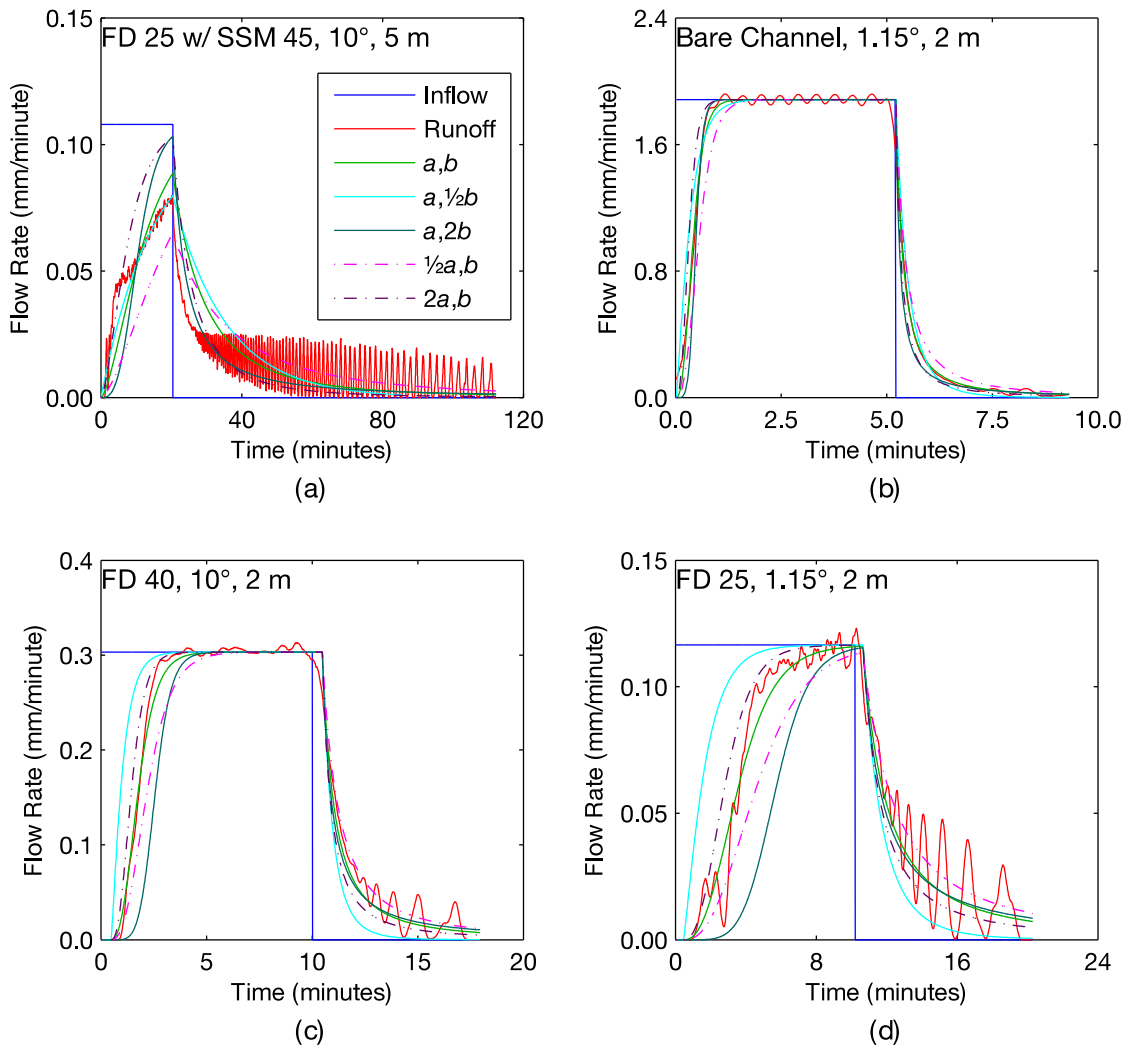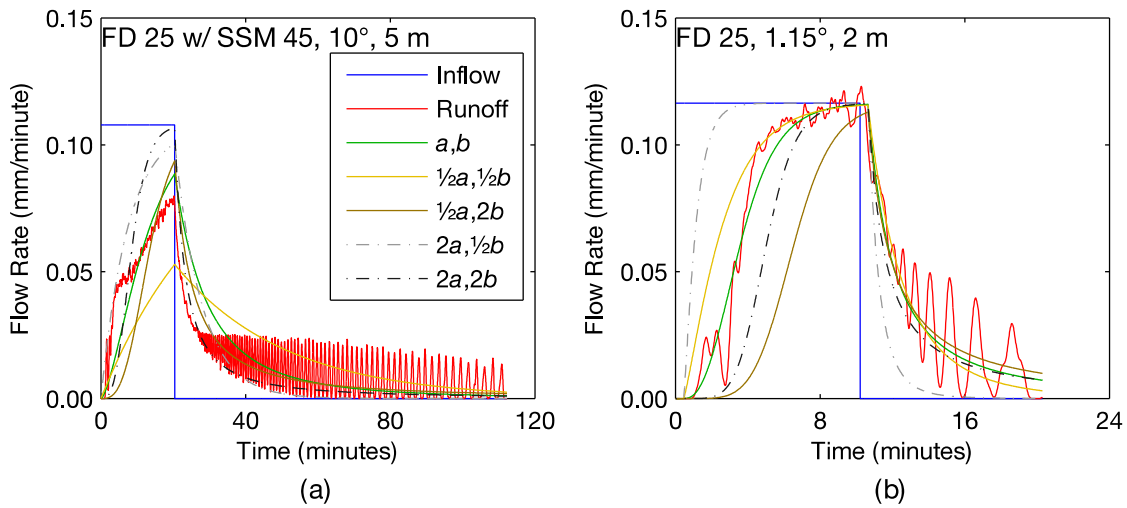**Figure 5.17 – Modelled runoff profiles using optimized values of *a*, *b* and *delay*, and fixed multiples of optimized *a*- and *b*-values simultaneously.**

between the monitored and modelled runoff profiles is minimized. To confirm that *delay* can perform no action other than translation in time, two tests were selected and their *delay* values shifted from optimal. These two tests were chosen as the worst-fitting and long-rising tests from the previous sensitivity analyses, to allow easy visual inspection. The optimized *delay*-values for these tests were 0 and 26 seconds, respectively, and both were tested with *delay* set to 0, 26, 78 and 260 seconds. This is plotted in Figure 5.18, where it is confirmed that adjusting the value of the *delay* parameter serves exclusively to translate the modelled runoff profile, the shape of which is controlled by the parameter values of *a* and *b*, along the time axis.
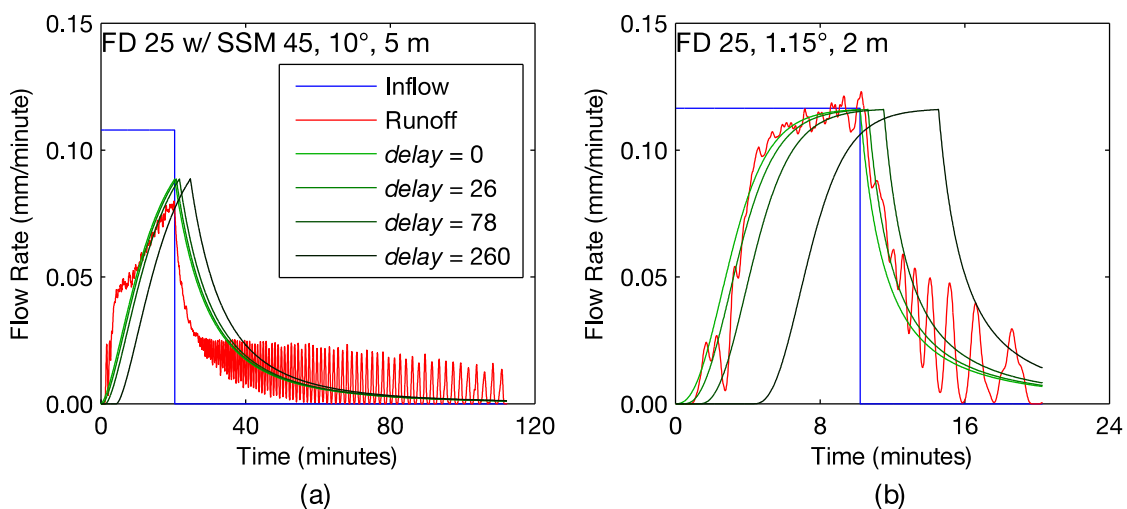

(a)   (b)

Figure 5.18 – Modelled runoff profiles using optimized values of *a* and *b*, and a variable value of *delay*.

5.5.5 Applicability of Manning's Equation to Parameter Estimates

5.5.5.1 Background

Manning's Equation is an empirical formula used to relate velocity, flow depth, flow cross-sectional area, bed slope and surface roughness in open-channel flow. As discussed in Section 2.5.4.2, She & Pang (2010) use a wide-channel approximation of this equation as the basis of a nonlinear storage routing model for a green roof drainage layer. Previously in Section 5.5, averaging of statistically-similar optimized scale and exponent nonlinear routing parameters eliminated the dependence of the model upon inflow rate, drainage length and partially upon drainage component. However, insufficient data existed to generate empirical formulæ for the estimation of parameter values from the remaining significant variables. Manning's Equation offers a storage depth-discharge formula with only one empirical parameter, the roughness coefficient n, which incorporates easily measurable properties of the drainage layer and permits them to take any value. This approach, if valid, has some advantages over the parameter reduction study, which effectively generated lookup tables that only allowed e.g. roof slope to be either 1.15° or 10°, or assumed sensible interpolation to be valid for other roof slopes between those two.

By combining and re-arranging Equation 2.2, Equation 2.13 and a nonlinear storage depth-discharge relationship with a fixed exponent of 5/3, the following equation is produced:

$$n = \frac{10 S_R^{\frac{1}{2}}}{aL}$$

Equation 5.1

where n is Manning's n, S_R is roof slope, a is the scale parameter from nonlinear storage routing and L is drainage length. A full derivation is given in Appendix C. Both Equation 5.1 and the SWMM RUNOFF routing module (James *et al.*, 2000) suggest that a runoff routing method based on Manning's Equation is independent of inflow rate, but directly dependent on roof slope and drainage length. Manning's n is a measure of surface roughness, suggesting an indirect dependence on drainage layer component. Therefore, Manning's n is ideally similar for all test configurations using the same drainage layer component and reasonably similar for all test configurations using either FD 25 or FD 40. For Manning's n to be constant for each drainage component, the optimized scale parameter, a, must be related to the square root of roof slope and inversely related to drainage length. No dependence of a on drainage length was observed in the statistical analysis (Section 5.5.3), even after the values taken by the exponent were fixed, as is the case in Manning's Equation. The use of a fixed exponent value of 5/3 for the head-discharge relationship in Manning's Equation suggests its independence from all test variables and any other potential variables that were not explicitly tested.

For all 300 tests, *lsqcurvefit* was used to optimize the scale parameter, *a*, for nonlinear storage routing based on a *Q-S* relationship with a fixed exponent value of $b = 5/3$, for all 300 tests. Manning's *n* was then derived from *a* through Equation 5.1. The range of tested *delay*-values extended from 0 to 80 seconds. The starting estimate for *a* was 0.01 and its bounds were $[10^{-4}, 1]$. The same laptop was used as in all previous optimizations.

5.5.5.2   Discussion of Parameter Values

A real optimal value of *a* (and hence Manning's *n*) was found for all 300 rainfall-runoff pairs, requiring a total process time of 5 minutes and 38 seconds. In no case was the estimated value of the scale parameter *a* (from which Manning's *n* was derived via Equation 5.1) constrained by either the upper or lower bound set on the optimization routine. Highest, lowest and mean R_t^2 were 0.9989, 0.8620 and 0.9892 respectively; modelling goodness-of-fit is broadly comparable to that for the optimized-then-averaged scale and exponent parameter sets (Section 5.5.3.5). 213 test configurations had R_t^2 above 0.99. Exactly three tests had R_t^2 values below 0.9; these were the same three as in previous optimization studies. However, the best-fitting test in the original three-parameter optimization was the 91st best-fitting in the optimization for Manning's *n*.

Optimal value for *delay* was never more than five seconds different from the value derived in the three-parameter optimization. In 269 cases the difference was not more than one second and in 152 cases, more than half, the difference was zero. Because exact delay values were so similar for each test, the distribution was consequently similar: bi-modal, with 48 instances of zero seconds, 27 instances of 13 seconds and 53 instances in the range 12-14 seconds. This indicates that despite *b* being fixed, in some cases far away from its freely-optimized value (which ranged approximately from 1 to 4), similar optimal solutions were found for *delay* in most cases and, therefore, it is probable that the solutions found here are generally as close as is possible to the freely-optimized solutions, given the set constraints.

In many cases, the optimized value for *a* differed greatly from that found in the three-parameter optimization, even for tests where the difference in *delay* was zero. However, it is worth noting that, in Section 5.5.3.2, one configuration was shown to have nineteen modelled fits of almost equal goodness, in which exponent value remained almost unchanged while *a* varied over a large range as *delay* was incremented i.e. small differences in exponent or *delay* may result in large shifts in the value of *a* to adjust the modelled profile to its new best fit.

The optimized value for Manning's *n* was derived from the optimized value for *a* through the use of Equation 5.1. The lowest, highest and mean values for this parameter were 5.72×10^{-3}, 0.778 and 0.0703 respectively. Tests of the bare channel dominate the low end of the range, while values above 0.1 almost always correspond to tests involving FS 50 or SSM 45, and the very

highest values (above 0.2) correspond only to the fifteen tests of FD 25 with SSM 45 at a 5 metre drainage length and 10° roof slope. This distribution matches well with the calculated t_{50} times, as well as the texture and physical appearance of the components. However, the actual highest values seem to be numerically incomparable to any kind of channel given in popular literature (e.g. Chow, 1959). However, at the tested flow rates, much of the water flow in tests involving SSM 45 is through the fibrous matrix, and therefore incomparable to any normal kind of channel. It is noted that a team from the United States Geological Survey and Illinois Department of Natural Resources occasionally observed flow behaviour consistent with a Manning's n value in excess of 0.8 in a drainage ditch in Illinois (Soong *et al.*, 2012). Hall & Freeman, working for the United States Army Corps of Engineers Wetlands Research Program, observed flow behaviour consistent with a Manning's n value in excess of 0.9 in a concrete-lined drainage channel planted with dense bulrush vegetation, under a low-flow rate (Hall & Freeman, 1994). This planted channel could be considered broadly comparable to a fibrous matrix of SSM 45.

The mean value of Manning's n for FD 25 is 0.0469, while for the similarly-textured FD 40 it is 0.0459. These mean values are both comparable to each other, and to the value of 0.05 used by She & Pang (2010) to model the drainage layer of an extensive green roof in Portland, Oregon. It is therefore likely that the drainage layer, which is not described in that paper or in an earlier paper concerning the same roof (Hutchinson *et al.*, 2003), is FD 25 or similar; this is a sensible choice of component for a green roof system of that design. It is unusual that a smooth HDPE component should have a Manning's n as high as 0.05, as this is even considered high for a jagged and irregularly-excavated rock cut (Chow, 1959). However, when considering the surface texture of HDPE relative to the typical millimetre-high flow depths in an egg box-style drainage layer, and also those flow depths relative to the dimensions of the raised peaks of the egg box profile, this parallel cannot be immediately dismissed as unreasonable. A slightly lower roughness coefficient might be expected for FD 40 in comparison to FD 25 as the spacing between the raised peaks is larger; this is observed.

The fixed exponent value of 5/3 is lower than the optimized value in 282 of 300 three-parameter optimizations. It is also around 30% lower than the mean exponent value of 2.39 found in those optimizations and lower than all eight averaged exponent values. It is noted that Manning's equation is empirical and designed for prismatic rectangular channels; the designation of a green roof drainage layer as a typical channel, while superficially logical, may not be entirely realistic, due to reasons given in the previous paragraph. It is furthermore noted that many other empirically-derived nonlinear head-discharge relationships use other exponent values e.g. 1.5 for rectangular weirs, 2.5 for triangular weirs, and multiple values with mean 2.04 and range > 9 for real flow recession curves observed at 100 river gauging stations (Wittenberg, 1999).

5.5.5.3 Significance of Test Configuration

The optimization of the scale parameter produced 300 different optimized values for Manning's *n*. These were analyzed statistically for dependencies on test configuration variables, ideally to be able to ultimately specify a small set of Manning's *n*-values that is applicable to a wide range of situations. As Manning's *n* is a roughness coefficient, a dependence on component was expected to be found. No dependence was expected on roof slope or drainage length; Manning's formula already contains separate terms for these parameters. Finally, in common with all storage routing models, no dependence on inflow rate was expected.

The results of the statistical analysis are presented in Figure 5.19. The *x*-axis key is unchanged from all previous similar plots and can be found in Figure 5.10 or Figure 5.14.

For *delay*, the mean values of each group (i.e. column heights) are near-identical to those for the bounded three-parameter optimization (Figure 5.10). This provides further evidence to suggest that the optimizations found here are similar to those found for the bounded three-parameter optimization. The statistical groupings are identical, showing that the standard errors are also not significantly changed.

An obvious correlation between component and Manning's *n*-value is shown in Figure 5.19. Furthermore, the values for the group means for each component increase with surface roughness or restriction, starting at the lowest value for the bare waterproofed channel, increasing to two very similar values for the two HDPE components, increasing again (though not significantly) for the expanded polystyrene component and increasing greatly and significantly for the configuration including a fibrous mat. Manning's *n* is found to be statistically similar for the two HDPE components but also for FS 50, the expanded polystyrene component. This may be due to the fact that all components were wetted to remove storage capacity prior to
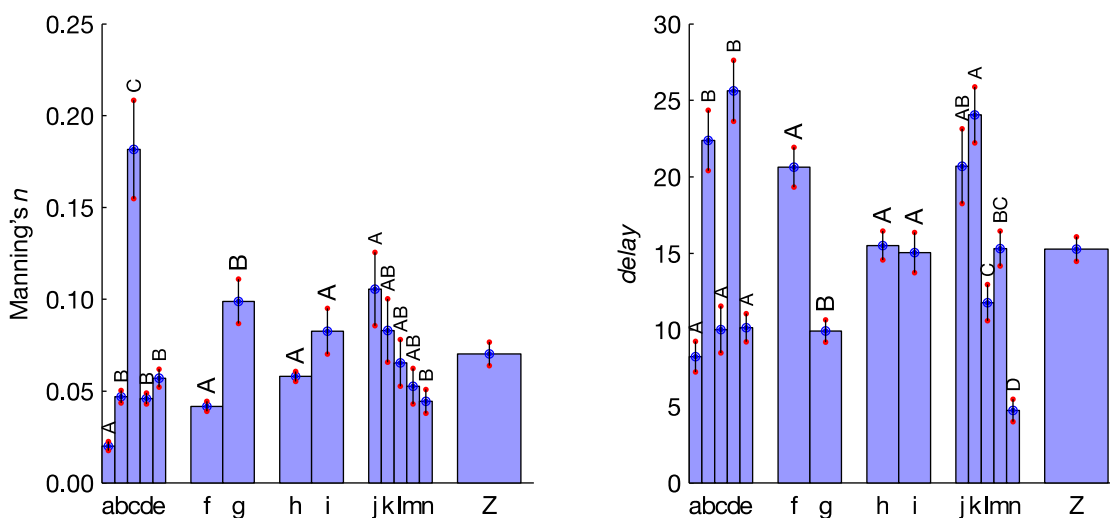

Figure 5.19 – Mean and standard error of optimized values for Manning's *n* and *delay*.

being tested. For FS 50, this would result in the expanded polystyrene surface holding as much water as possible on its surface, thereby smoothing over much of the surface roughness. The water supplied for the test would then travel over a thin film of held water, which could, at this scale, be similar in roughness to HDPE.

In agreement with Manning's equation, Manning's n is shown to be significantly independent of drainage length, though the significance value of 0.056 is only slightly above the 0.05 threshold. In disagreement with Manning's equation, roof slope is shown to be a highly significant factor in determining Manning's n. However, Manning's equation is intended for uniform flow. This requires the energy line, water surface and channel bottom to be parallel. At the steeper roof slope of 10°, it is more likely that these conditions are not met, rendering the use of Manning's equation invalid and resulting in less meaningful values of Manning's n which cannot strictly be compared to those found for the shallower roof slope of 1.15°.

It should be noted that, strictly, uniform flow refers to flow in which velocity is constant at all points. Due to the physical forms taken by the two-dimensional surfaces of the tested drainage components, velocities cannot be constant spatially; flow over FD 25 or FD 40, for example, must change direction regularly to avoid the "egg-box" obstructions. However, the uniform flow condition is often liberally interpreted to mean that the average velocity across all points is constant. Though this condition is much more likely to be met in a green roof drainage layer, it is still a simplifying assumption. Manning's n is shown to decrease smoothly with inflow rate to the drainage layer, though the range of values at any one inflow rate is such that only the highest and lowest group mean values are found to be statistically different. Though this observation was not expected, it is not unprecedented; a similar correlation between increased flow rate and decreased Manning's n was observed by Hall & Freeman (1994).

5.5.5.4   Applicability Following Adaptation to Theoretical Form

The statistical analysis of parameter values has shown that the assumptions of Manning's equation, with respect to roof slope and inflow rate, are not valid. However, it was decided to repeat the modelling with the optimized values of Manning's n averaged across all test variables, except component, for two reasons. First, if successful, a model would be created that is suitable for all roof slopes and lengths, with only one semi-arbitrary parameter. It is possible, though highly unlikely, that compensation by the *delay* parameter may have prevented Manning's n from forming groups independent of roof slope and drainage length. For this model run, Manning's n was fixed at one of four values, with each value corresponding to the mean of all values optimized in tests using one component configuration. Plots of the worst-, best-, mean- and median-fitting modelled runoff profiles (Figure 5.20), demonstrate that this parameterization method is generally suitable, excluding tests involving SSM 45, for which R_t^2 can drop below 0.7.
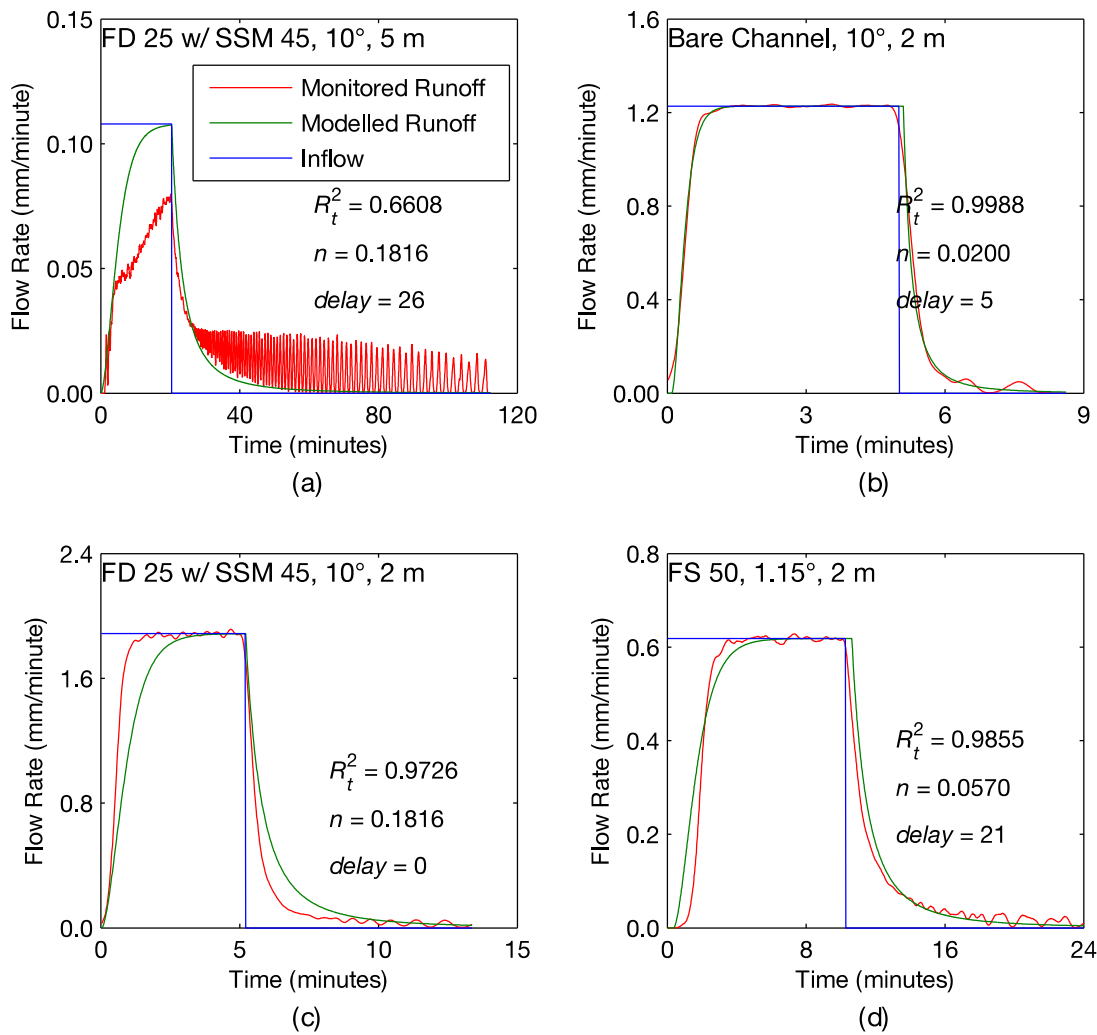
Figure 5.20 – Worst- (a), best- (b), mean- (c) and median- (d) fitting modelled runoff profiles, according to the theoretical interpretation of Manning's equation.

It is considered appropriate to further divide the Manning's roughness coefficient for tests involving SSM 45 into two groups, corresponding to whether or not a majority of the inflowing water interacts with the fibrous layer or the HDPE component above it. A repeat run, with Manning's n divided in this way (to give two greatly differing values of 0.062 and 0.301), yielded an R_t^2 value of 0.7610 for the (same) worst-fitting test. This is an improvement, but further improvement is required for this method of parameter specification to be more fully applicable.

Interestingly, if only the goodness-of-fit of the FD 25 and FD 40 tests are evaluated, the mean R_t^2 is 0.9860. As it is assumed that the drainage layer modelled by She & Pang (2010) is, or is similar to, one of these components, it is believable that their Manning's Equation-based drainage layer model could give accurate results for their specific roof.

5.6   Nonlinear Storage Routing at One-Minute Resolution

5.6.1   Motivation

The runoff data collected throughout this experimental programme was sampled at a temporal resolution of one second, allowing for the consideration of highly detailed runoff profiles. However, it is unreasonable to expect most green roof monitoring systems to produce, or indeed urban drainage software packages to use, data at temporal resolutions as high as this. To test the applicability of the storage routing method under more realistic data input conditions, the data records for each test were reduced in temporal resolution to one minute. Appropriate values for *a*, *b* and *delay* were input to the same modelling framework. The same statistical analyses and parameter value averaging studies were performed using these optimized values for a one-minute time step. The results of this study are presented here.

5.6.2   Additional Preparatory Work

Further processing was required to convert the original data records to one-minute temporal resolution. This initially consisted of downsampling the processed second-scale rainfall and runoff records analyzed in Section 5.5, by combining the total value of 60 consecutive samples into one. Each of the minute-scale records produced in this way therefore consisted of 120 or fewer samples, in comparison to the hundreds or thousands of samples in the corresponding second-scale runoff record. The inflow event in each test was reduced to a length of 5-20 samples. As a result, much of the temporal detail was obviously lost.

The dimensions of the three optimization parameters *b*, *a* and *delay*, are [-], $[L^{1-b}T^{-1}]$ and [T] respectively. It therefore follows that if the unit of time is changed from seconds to minutes then, theoretically, the derived *b* parameter values should be unaffected, while the derived *a* and *delay* parameter values should be valid after multiplication and division, respectively, by 60. However, for *delay*, many of the optimized parameter values do not remain as integer number of time steps after conversion from seconds to minutes.

The one-second scale optimization was run again, with delay permitted to take values of 0, 60 or 120 seconds only – equivalent to exactly zero, one or two sample(s) at one-minute resolution. This test run produced, as expected, three somewhat different parameter value sets. *a*- and *b*-values were maintained for 50 configurations – those for which delay value was 0 in the one-second optimization. The further the optimal *delay* value was from 0 or 60, the more scattered the new values of *a* and *b* were as a percentage of their optimized values. Interestingly, most of these optimized parameter values, for both *a* and *b*, were below their one-second optimized values, usually simultaneously. The optimized values of *b* were affected least, with one-minute optimized values being 85% to 104% of their one-second optimized values. The optimized

values of a were affected much more greatly – one-minute optimized values of a were 34% to 617% of their one-second optimized values, but in only 28 of 300 cases was the value of a greater than that of the one-second optimized value. Increases in *delay* from some value between 30 and 60, to 60, corresponded with increases in a. As an increase in a generally corresponds to an increase in the sharpness of the modelling profile (see Figure 5.15 and its related discussion), it is not surprising that a was decreased in the majority of cases (where the modelled runoff profile was forced to begin too early) but increased in a minority of cases (where the modelled runoff profile was forced to begin too late and therefore needed to catch up with the monitored runoff profile).

Despite the occasionally large deviations from their optimized values, the parameter value sets with forced *delay* values are generally appropriate for runoff modelling, with a mean R_t^2 of 0.9889 between monitored and modelled runoff profiles. However, it should be noted that, by the R_t^2 performance metric, they are equal to the Manning's Equation-derived parameter sets and inferior to the sets of averaged a- and b-values with freely-selectable *delay*.

5.6.3 Applicability of Scaled Parameter Values at One-Minute Resolution

With all values of *delay* forced to either 0 or 60, it became possible to convert all values of this parameter from seconds to an integer number of minutes, either 0 or 1. Parameter values of a, in units of mm^{1-b}/s, were multiplied by 60 to give values in units of mm^{1-b}/minute. Parameter values of b were dimensionless and therefore unchanged.

For each of the 300 test cases, the scaled parameter values of a, b and *delay* were input directly to the model and fixed in value; no further optimization took place. Monitored and modelled runoff profiles were compared, and goodness-of-fit evaluated by R_t^2.

As a fail-safe against complex runoff predictions, the modelled depth of runoff was checked against the modelled depth of water in storage at each time step. If the predicted runoff depth exceeded the storage depth, the modelled runoff depth was set equal to the storage depth and the storage was fully depleted, resulting in a predicted runoff of zero at all subsequent time-steps. In 103 out of 300 tests, use of the scaled parameter values and minute-resolution inflow record caused a growing oscillation in the routed runoff prediction, eventually triggering the fail-safe. These growing oscillations were caused by inappropriate estimates of a and b which alternated between predicting more outflow than inflow, and predicting a greatly reduced outflow, due to the loss of storage depth. Goodness-of fit for these 103 tests was generally low, with a mean R_t^2 value of 0.1944, though occasionally goodness-of fit was high; the maximum R_t^2 value for a test triggering the fail-safe was 0.9303, which is below the median, but still fit for purpose.

For the 197 more successful tests, maximum, minimum and mean R_t^2 were 0.9965, 0.5118 and 0.9490, indicating some relatively well-modelled runoff profiles along with some less well-modelled profiles. However, 120 of the 197 successfully modelled runoff profiles enter an oscillation where runoff should be steady-state. Of these, 100 decay with time, but 20 grow, suggesting that the fail-safe may be triggered over longer inflow events using the same modelling parameters. Furthermore, with the fail-safe already being triggered in over a third of all tests, it is clear that modelling parameters derived at one monitoring time step cannot practically be scaled to a different time step in this case, regardless of the strong theoretical basis behind such logic.

5.6.4 Derivation of New Parameter Values for Use at One-Minute Resolution

Concluding that temporal scaling could not be successfully applied to time-dependent parameters when changing time step, the *lsqcurvefit* routine was run again, to find the best-fitting values of *a*, *b* and *delay* through optimization. It was suspected that the total time required for optimization would be greatly reduced, due to the 60-fold reduction in the number of samples contained in each rainfall and runoff record, and the large reduction in the number of *lsqcurvefit* optimization repeats required per test; three *delay* values of 0, 1 and 2 minutes correspond to all *delay* values in the range 0 to 120 seconds. The upper bound on *a* was increased from 1 to 60. The upper bound on *b* was initially unchanged, but later increased to 20 when the original upper bound of 6 was found to constrain the optimization routine. As a result of the greatly reduced complexity of the problem, the total time required for optimization of all 300 tests was 1 minute and 17 seconds. As this is still over an eighth of the time required for the optimization of all 300 tests at a one-second resolution, it is clear that processing time does not scale linearly with either data length or number of optimizations.

Working solutions were found for all 300 tests. The mean value of R_t^2 was 0.9676 and 111 tests had R_t^2 above 0.99. No test had R_t^2 below 0.8, though the six worst-fitting tests, all for the bare channel at slope of 10° and an inflow rate of 1.2 mm/minute (at both drainage lengths), had R_t^2 values below 0.84, *b*-values near to 1 and *a*-values near to 1. Six of the thirteen further tests with R_t^2 between 0.84 and 0.9 were for exactly the same two physical configurations, but with the highest inflow rate of 2.0 mm/minute. These all had *b*-values around 6.8, despite the only difference from the six worst-fitting tests, all with $b \approx 1$, being inflow rate.

Figure 5.21 shows the worst and best-fitting modelled runoff profiles, along with one close neighbour to each of the mean- and median-fitting profiles. The actual mean and median profiles are not shown, as they are both for exactly the same physical configuration as the best-fitting profile. The configuration shown in (d) is normally a poorly-fitting test, but came slightly above
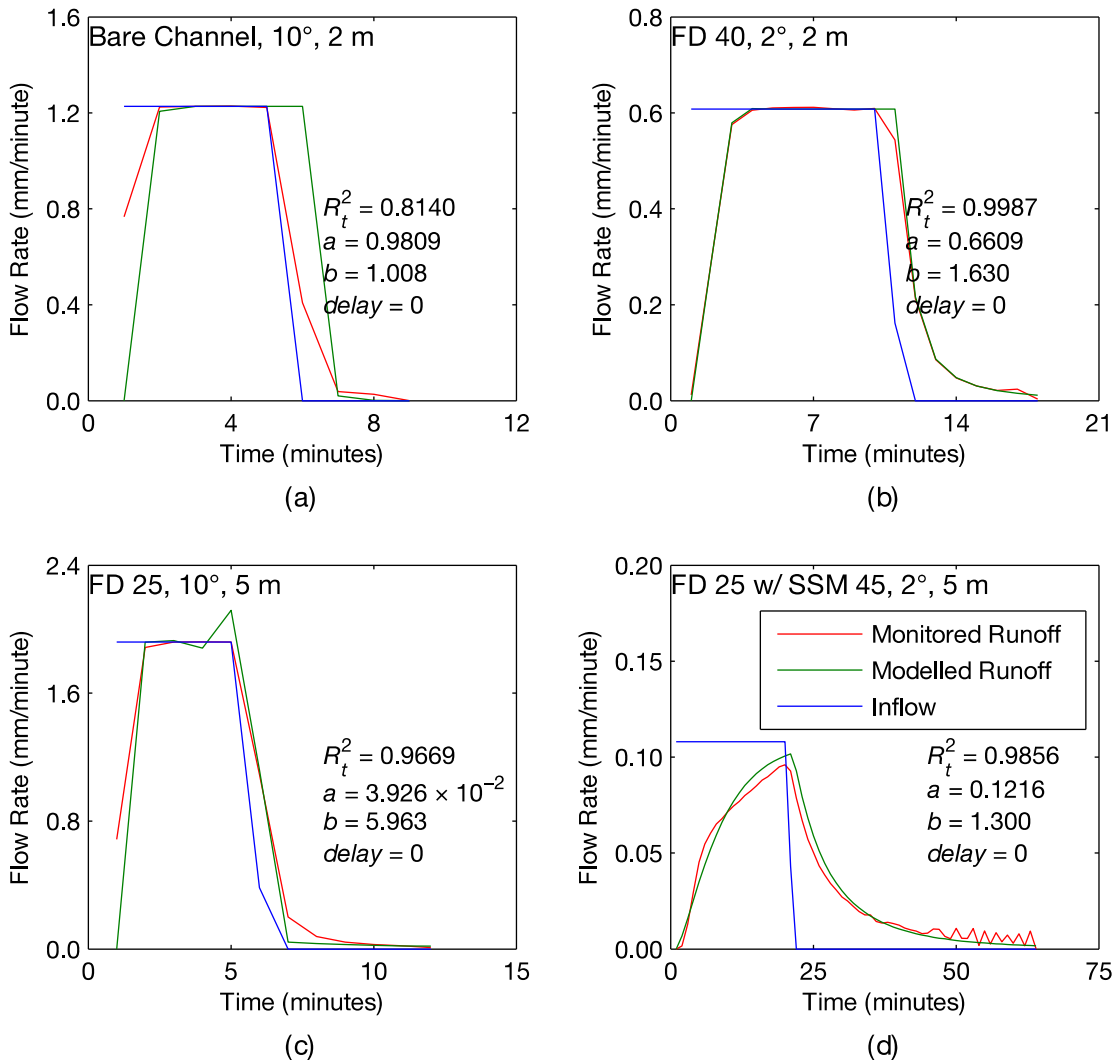
Figure 5.21 – Worst- (a), best- (b), near mean- (c) and near median- (d) fitting profiles, for optimized *a*, *b* and *delay* at one-minute resolution.

median goodness in this optimization run. Figure 5.21 shows that the inaccuracy associated with the worst-fitting profile is primarily due to the iterative nature of the routing equation, coupled with the rapid rise and fall in runoff rate at the start and end of the inflow event. The relative improvement in modelling for the configuration using FD 25 with SSM 45 is probably due to the extra smoothing of the very long runoff tail introduced by downsampling the runoff record.

For 27 tests, *b* is less than 1.01, implying a desire from *lsqcurvefit* to optimize *b* to a value below 1. To avoid complex values in the modelled runoff profile, values of *b* below 1 should not be permitted. Setting a value of 1 as the lower bound on *b* is therefore a compromise between interfering with the optimization and avoiding possible model instability.

The distribution of *b*-values contains none between 3.12 and 5.28, but a further 42 from a value of 5.29 up to a value of 9.10. Because of the large gap in the distribution of *b*-values, it was believed that two optima of near-equal value may have existed for all tests, and that in these 42

cases, the optimum with a high *b*-value was found and reported. However, repeating the optimization with an upper limit of 4 on *b* did not cause *lsqcurvefit* to find the proposed other optimal value of *b*. As *b* was greater than 3.9999 in 42 cases, it was concluded that no other optimum existed. Of the 42 tests with *b* above 4, the 36 tests with $4 < b < 8$ correspond to the smallest 36 *a*-values, though it is noted that there is no great discontinuity between the 36th and 37th smallest *a*- value (36th: $a = 0.0621$ for $b = 5.29$, 37th: $a = 0.0637$ for $b = 1.40$). The six tests with $b > 8$ correspond to the only double-digit values of *a*, which are all over 40. As *delay* is zero for all 42 tests with $b > 4$, any effect that the *delay* parameter might have had can be ignored. The unusual distribution of *a*-values when *b* is above 4 suggests that the modelling method breaks down when this occurs. To avoid oscillatory behaviour and inexplicable effects on *a*, it is suggested that an upper bound of 4 is applied to *b* when using nonlinear storage routing methods. It was observed that, at a one-second resolution, the nonlinear storage routing method stopped just short of finding an optimized *b*-value of 4, or more, in the highest cases.

The modelled runoff profiles for two tests with the same configuration but different inflow rate are similar in form, despite the great difference in *a*-value and notable difference in *b*-value (Figure 5.22). By studying the model at each time step, it is found that these *a*- and *b*-values are such that the modelled runoff rate is raised to approximately the inflow rate in one time step, which is also approximately the modelled runoff rate at that time step. The spike in modelled runoff that occurs at the end of both rainfall events is the start of a growing oscillation. Extending the input inflow event to 10 minutes caused a greater volume of runoff to be predicted than was present in the storage reservoir at one time step. It is due to the slight differences between inflow rate and monitored runoff rate at each time step during which steady-state conditions occur, that an oscillation starts in the modelled runoff profile.
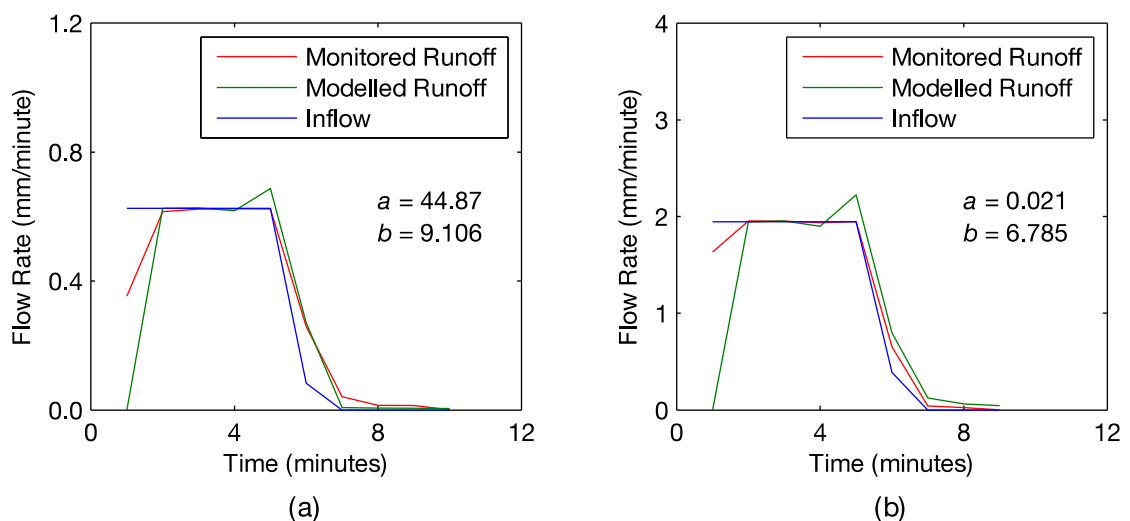
Figure 5.22 – Monitored and modelled runoff profiles for the bare channel at a roof slope of 10°, drainage length of 2 metres and inflow rate of 0.6 (a) and 2.0 (b) mm/minute.

For all tests with $b > 4$ (and no tests with $b < 4$) the modelled runoff profile shows growing oscillatory behaviour during the time over which runoff should be steady-state. This threatens the stability of the model. Decaying oscillatory behaviour, which does not threaten the stability of the model, is observed for certain tests with $b < 4$, all of which used pulsed inflow profiles. This may be a deliberate attempt by *lsqcurvefit* to maximize similarity with an oscillatory monitored runoff profile, though this is very unlikely, as the reduction in temporal resolution to the minute scale largely eliminates the oscillations seen in the one-second resolution runoff profiles.

5.6.5   Statistical Analysis

A statistical analysis was conducted, using exactly the same methodology as given in Section 5.5.3, to assess the contribution of test variables to specific parameter values. The results of this analysis are summarized in Figure 5.23. It is noted that the black vertical bars attached to each column do not always appear to be near for every member of a statistical group. These bars plot
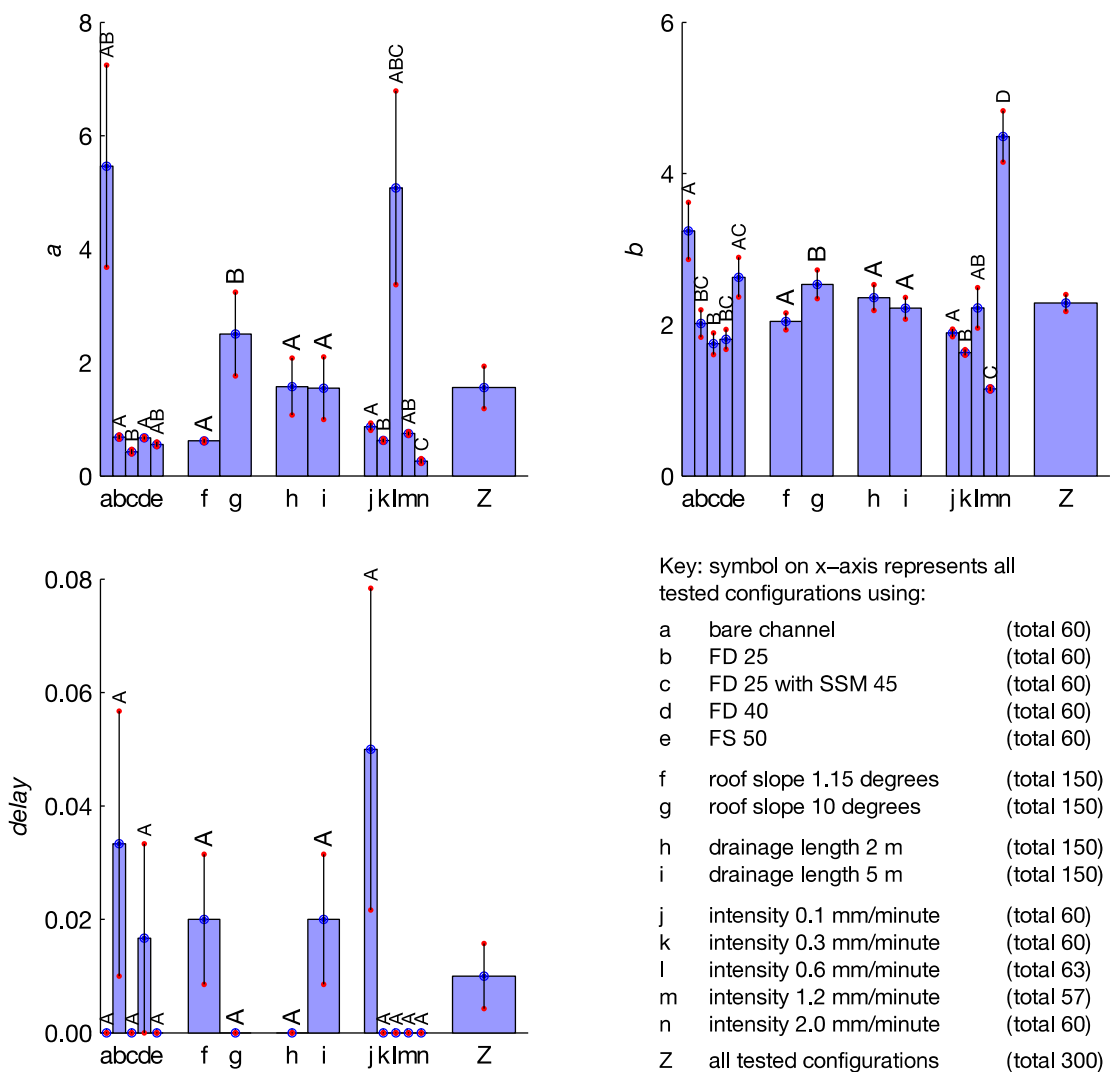
Figure 5.23 – Mean and standard error of optimized values for *a*, *b* and *delay* at one-minute temporal resolution.

the standard error of the mean, which is in some cases greatly smaller than the 95% confidence interval used to determine statistical groupings.

At a one-minute data record resolution, *delay* is independent of all test variables. This is not greatly surprising, as in 297 out of 300 cases, *delay* value is 0, and in the remaining three cases, it is 1. As a result, the mean for most configuration groupings is zero and the standard error of the mean incalculable. The test configurations for which *delay* value is not always zero, and the number of non-zero instances for each, can be inferred from Figure 5.23. Due to this full independence, a first-level parameter averaging at this temporal resolution could sensibly consist of specifying all *delay* parameter values, regardless of test configuration, to be zero.

For *a*, the general mean value trends regarding component and roof slope are similar at a one-minute and one-second resolution, although the statistical groupings for component are different, due to the increased variance of the bare channel group. The increased variance of *a* within this group relates to the presence of six values of *b* above 8, corresponding to the largest values of *a*, and a further 12 values of *b* between 4 and 8, corresponding to the lowest values of *a*. As $b > 8$ only for tests with inflow rates of 0.6 mm/minute, the mean *a* value of the 0.6 mm/minute group is far above the mean values for the other inflow rate groups. However, the variance of *a*-values in this group is large enough for the 0.6 mm/minute group to be statistically similar to all other groups of inflow rate. As $4 < b < 8$ only for, and for the majority of, tests with inflow rates of 2.0 mm/minute, mean value of *a* is significantly lower for this group than for any other inflow rate group. Drainage length is shown to be statistically insignificant in influencing *a*-value; visually, the means of both groups are near-identical.

For *b*, the general trends in mean value at a one-minute resolution do not relate well to the trends at a one-second resolution. For example, four different inflow rates each have their own exclusive significance grouping, and the mean value-ordering of the two significance groups for roof slope are reversed. The overall spread of *b* values is also greater at a one-minute resolution.

It can be seen that FD 25 and FD 40, the two most similar components, belong in exactly the same statistical groupings for *a*, *b* and *delay*. This is not a surprising result in theory but could not be automatically assumed in practice due to the limited robustness of the optimization routine at a one-minute resolution.

5.6.6   Conclusions of Methodology at One-Minute Resolution

A set of *a*, *b* and *delay* parameters, accurate at one-second resolution, were scaled by a factor of 60, for conversion into equivalent "minute" and "per-minute" values. The 300 test inflow and runoff records were downsampled, by summing the total of each set of 60 consecutive samples into a sample representing one minute. The nonlinear storage routing model was employed, with

the scaled parameter value sets and one-minute resolution inflow profiles, to generate modelled runoff profiles, which were compared to the equivalent monitored runoff profiles. In more than a third of the 300 test cases, no real modelled runoff profile was generated, as a result of growing oscillations in the modelled runoff profile causing negative predicted runoff values, which were subsequently raised to a non-integer exponent. Of the 197 real runoff profiles, 120 entered an oscillation over the period for which runoff should have been steady-state. It was concluded that the parameters predicted at one temporal resolution could not be successfully scaled to another.

New parameter sets for *a*, *b* and *delay* were optimized using *lsqcurvefit* directly with the one-minute resolution inflow profile. Real runoff profiles, with a mean R_t^2 of 0.9676, were generated for all 300 test cases. In 42 cases, the value of *b* was greater than 4, and in six of those cases, the value of *b* was greater than 8. These situations corresponded to unusual values of *a*: the 36 smallest *a*-values were paired with *b* values between 4 and 8, and the six largest *a*-values, by a large margin, were paired with *b*-values above 8. The use of *b*-values above 4 may lead to growing oscillations in the modelled runoff profile (Figure 5.22). A statistical analysis of these parameter sets revealed that *delay* could be eliminated from the model i.e. fixed at zero.

Overall, it is concluded that the use of *lsqcurvefit* on the one-minute resolution data sets may not be sufficiently robust for consistently useful estimates of the nonlinear storage routing constants. It is suggested that this may be a consequence of the very small size of the data records and rapid runoff response times; equilibrium between runoff and inflow rate is often reached within the first two or three samples, as is a reduction in runoff rate to near-zero after the end of an inflow event.

5.7   Muskingum Method

5.7.1   Overview and Optimization

The Muskingum Method is a variant of storage routing that separates the volume of water in storage into a steady-state prism and a transient wedge. The result of this modification is that the relationship between storage and discharge becomes a relationship between storage and a combination of discharge and inflow (see Section 2.4.5.4 for further information). The shape of a time-series runoff profile generated using Muskingum routing depends on the value of two parameters, travel time, *K*, and storage weighting, *x*. For all tests, the values of *K* and *x* that generate the most similar modelled runoff profile to the monitored runoff profile were unknown. The purpose of the following study was to find the values of the parameters *K* and *x* which minimize the sum-of-squares error between all data points in the monitored and modelled runoff profile for each test case. For optimal values of *K* and *x*, R_t^2 is maximized. To find these values, an optimization process was undertaken by applying the *lsqcurvefit* function in Matlab to the equations governing Muskingum routing.

A *delay* parameter, performing exactly the same function as in the nonlinear storage routing study, was also included and permitted to take any value from 0 to 100 seconds. For each test, the highest value of R_t^2 was located and it, the corresponding *delay*-value, and optimized K and x values were saved, along with the computational time required for that entire test optimization. All optimizations were performed on the same computer as used in all other studies conducted in this chapter, a Toshiba Tecra A11 laptop (Section 5.5.1).

5.7.2   Applicability of Method at One-Second Resolution

For all tests, initial values of K and x were supplied to *lsqcurvefit* as 1 and 0 respectively. Noting, from the nonlinear storage routing study, that very large reductions in process time could be achieved by bounding the values of the parameters to be optimized in *lsqcurvefit*, x was bounded over the range [0,0.5], consistent with Muskingum routing methodology. A lower bound of 0 was set on K; the travel time, K, is intended to be positive. The upper bound was set to Inf (positive infinity) as a reasonable value for it was not known. For stability it is required that $2Kx < \Delta t < 2K(1-x)$. The actual travel time of the drainage layer was not measured, though t_{50} values are, for all 300 tests, many times greater than the one-second time step used for runoff monitoring. The stability criteria are therefore met for small values of x. The total time required for all 300 optimizations was 6 minutes and 15 seconds. This compares favourably with the speed of the nonlinear storage routing optimization, requiring around 35% less processing time. However, with neither method requiring more than 2 seconds per test on average, both could be considered "fast" modelling methods. Figure 5.24 plots the worst- (a), best- (b), mean- (c) and median- (d) fitting modelled runoff profiles.

Following optimization of K, x and *delay*, the mean R_t^2 value for all 300 tests was 0.9751, while 73 tests had $R_t^2 > 0.99$. Though a mean R_t^2 value of 0.9751 seemingly indicates a high goodness-of-fit, the nonlinear storage routing model was a noticeably more successful modelling tool, even after two stages of parameter value averaging (mean $R_t^2 = 0.9902$, $R_t^2 > 0.99$ for 239 tests). In common with the nonlinear storage routing method, many of the less-successful models were to runoff profiles derived from tests which used SSM 45 at a 5 metre drainage length. This means that many of the worst-fitting Muskingum models are also the worst-fitting nonlinear storage routing models. However, for the Muskingum routing method, the three worst-fitting models (which are the same as for nonlinear storage routing) had R_t^2 values below 0.7.

5.7.3   Discussion of Parameter Values

A consideration of the actual values of the K and x parameters reveals means of 83.4 and 2.85×10^{-14} respectively, and standard errors of 4.36 and 4.16×10^{-16} respectively. The physical interpretation of K is as a travel time. For the 270 configurations which reached an obvious steady-state between inflow and outflow, the steady-state depth of stored water calculated by the
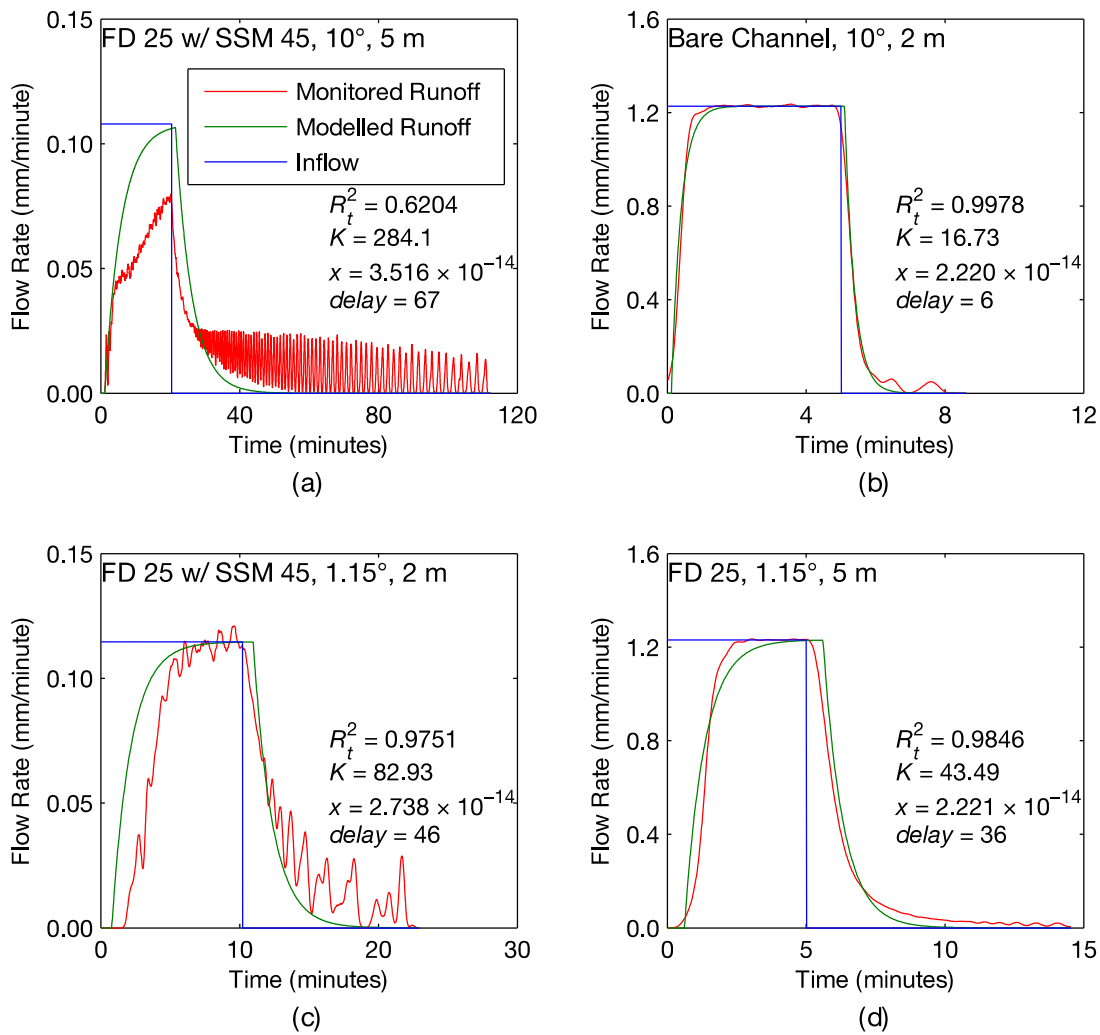
Figure 5.24 – Worst- (a), best- (b), mean- (c) and median- (d) modelled runoff profiles with optimized *K*, *x* and *delay* parameters, at one-second resolution.

Muskingum model was divided by the steady-state rate of outflow to give an estimate of the travel time. This was found to be almost identical to the value of K for each optimization (mean and standard error of $98.5 \pm 1.1\%$ of K).

All optimized values of x fall in the range $2\text{-}5 \times 10^{-14}$. This indicates that, in all 300 test cases, S is practically equal to KQ and the Muskingum model functions as a storage routing model with a linear storage depth-discharge relationship, where storage and outflow are related by the travel time of the drainage component. It is therefore not surprising that those tests for which the nonlinear storage routing model optimized a b-value near to 1 perform particularly well in the Muskingum model. Additionally, it is not surprising that the product of storage routing scale parameter a and Muskingum travel time parameter K is near to 1 for each of these three tests, as combining the Muskingum routing equation, $S = KQ$, with the linear equivalent to the storage routing equation, $Q = aS$, gives $Ka = 1$. From this, it can be inferred that the scale parameter a in

the storage routing method, tested in Section 5.5, is the inverse of the travel time for the special case of exponent b equal to 1. More generally, the scale parameter is equal to the inverse of the travel time multiplied by the volume in storage raised to one minus the exponent i.e. S^{1-b}/K. In terms of outflow rate, this is equivalent to $Ka = 1/(KQ)^{b-1}$.

Physically, the outflow from the rainfall simulator chamber can be considered a weir, with an effectively unlimited hydraulic gradient in the direction of flow. Similarly, the drainage layer can be considered a reservoir that temporarily holds inflow before it flows over the weir. As such, there is no physical reason to expect x to be greater than zero in any of these tests.

5.8   Muskingum Method at One-Minute Resolution

5.8.1   Motivation

Despite the relative failure of the Muskingum method in comparison to nonlinear storage routing at a one-second resolution, it was decided to investigate the robustness of the methodology at a larger time step. The use of a one-minute time step for inflow and runoff records was chosen to allow direct comparison with the results of the nonlinear storage routing in Section 5.6, as a trade-off between a reasonable and a realistic temporal resolution for data from other monitoring projects, and as a duration greater than the value of travel time K in the majority of optimizations at one-second resolution. The method by which the one-minute resolution data records were created for this optimization is given in Section 5.6.2.

5.8.2   Additional Preparatory Work

Of the two parameters inherent to all applications of the Muskingum method, K has units of time and x is dimensionless. Therefore, if the unit of time is changed from minutes to seconds, all values of K must be divided by 60 and all values of x should remain unchanged. *delay* also has units of time, but is differs from K in that it is required to take an integer value. Therefore, from the original optimization, only values of K and x that were found with *delay* values of 0 or 60 can be directly transferred to a Muskingum model that uses a one-minute time step.

With the same motivation as the re-optimization of nonlinear storage routing parameters in Section 5.6.2, the Muskingum optimization was repeated with *delay* permitted to take values of 0, 60 or 120 seconds – 0, 1 or 2 minutes – only. The values contained in the K and *delay* parameter sets were then divided and multiplied, respectively, by 60, to convert the time unit from seconds to minutes. As expected, K and x values were maintained for the 22 optimizations for which *delay* was originally, and remained, zero. The value of *delay* was not 60 seconds for any of the original 300 optimizations. Also as expected, R_t^2 was reduced for all of the other 278 tests, as a consequence of the optimization routine no longer being permitted to find the most

optimal value of *delay* to the same high resolution. The greatest reductions in goodness-of-fit generally occurred when the new value of *delay* was most different from the originally optimized value.

The parameter values for *K* were generally increased when the new value of *delay* was below that originally optimized and were generally decreased when the new value of *delay* was above that originally optimized. The newly-optimized *K* values ranged from half to approximately double their originally-optimized values. However, the actual change in the sum of *K* and *delay* was less than five seconds in all except 26 tests. This implies a level of interaction between these two parameters. It should be noted that the estimated travel times, which were found in Section 5.7.3 to be very similar to the value of *K* by itself, were calculated from the Muskingum routing equation, which offsets the inflow record by the value of *delay*, and so already incorporated an offset equal to *delay* into the storage depth. The full travel time of the test system and monitoring delay is therefore equal to $K + delay$.

The parameter value set for *x* contains 24 significantly larger values, ranging from 2×10^{-11} to 0.083. For this largest *x* value, the storage routing relationship is $S = K(0.917Q + 0.083I)$ implying that storage has some dependency on inflow. It is unusual that the 24 larger values of *x* are distributed over eleven physical configurations, rather than representing three repeats each of eight physical configurations. However, the nine largest *x* values do represent three repeats of three physical configurations, and the largest of the remaining fifteen values is 0.0122, which is arguably close enough to zero (or 5×10^{-14}) that the behaviour of the Muskingum model is similar to a linear storage routing model. The three test situations for which the value of *x* is largest all have 1.15° roof slope, 2 metre drainage length and 1.2 mm/minute inflow rate. The component configuration varies and is either: FD 25, the similar FD 40, or FD 25 with SSM 45, which functions primarily as FD 25 when the shorter drainage length is tested. As the design of the tests is unchanged, it is unclear how the greater-than-insignificant *x*-values are found; they may be an unexpected consequence of optimization, in the general sense that a two-parameter model may produce more accurate results than a physically-valid one-parameter model, simply because it contains an extra parameter for calibration.

5.8.3 Applicability of Scaled Parameter Values at One-Minute Resolution

The parameter values found above were scaled in time from seconds to minutes and input directly to the Muskingum routing model, along with the minute-scale inflow and monitored runoff profiles created in Section 5.6.2, to test the applicability of the best-fitting parameter values after a reduction in temporal resolution of the inflow and monitored runoff profiles.

For all 300 tests, a real modelled runoff profile was produced. The governing equations for Muskingum routing contain only linear terms; oscillating output series therefore cannot be generated from block rainfall-type input series. Oscillations were observed in 35 modelled runoff profiles, corresponding exactly to the 35 tests for which optimized K was below 0.5 minutes, and hence Δt was greater than $2K(1 - x)$. The magnitude of these oscillations is smaller when the value of K is closer to 0.5 and all of these oscillations decay with time. However, the same mechanism which causes the rising limb of the modelled runoff profile to initially overshoot also causes the falling limb to initially overshoot, giving a negative runoff value immediately after the end of the inflow event. The worst-, best- and mean-fitting profiles are presented in Figure 5.25, along with one for which the value of x is high (0.0733).

The mean R_t^2 of all 300 tests is 0.9657 and 57 tests have R_t^2 above 0.99. The downsampling of the data records from seconds to minutes slightly improved the fit of the worst three profiles, adding 0.017-0.033 to the R_t^2 of each. This is probably due to the smoothing of the long runoff tails resulting from the downsampling – comparing Figure 5.25 (a) with e.g. Figure 5.13(a) shows the extent of the smoothing.

Overall, the scaling of parameters from a one-second to a one-minute resolution is less problematic for the Muskingum model than for the nonlinear storage routing model, as runoff predictions could be made for all tests and the mean goodness-of-fit for the modelled runoff profiles is slightly higher. However, the existence and use of non-zero x-values are a potential cause for concern and should be treated with caution.

5.8.4 Derivation of New Optimized Parameter Values

The one-minute resolution data sets were input to the optimization routine in order to compare the optimized parameters at a one-minute resolution with the scaled parameters optimized at a one-second resolution. Initial values for K and x were 1 minute and 0, respectively. The respective bounds were unchanged at [0, Inf] and [0, 0.5].

Real solutions were found for all 300 tests. The mean R_t^2 was 0.9761 and R_t^2 was above 0.99 for 112 tests. This is comparable to the performance of nonlinear storage routing at this resolution.

Highly unusually, the worst-fitting runoff profiles are now those for the bare channel at a 10° slope, 2 m drainage length and 2.0 mm/minute inflow – exactly those for which the nonlinear storage routing found an optimal exponent value of 1, and therefore those which should be modelled well by a linear model such as the Muskingum model. For all three repeats, the inflow weighting coefficient x was optimized to below 10^{-13}, reducing the model to linear storage routing, but travel time K was optimized to approximately 0.4 minutes – almost three times the value found by the Muskingum optimization at a one-second resolution, where the three runoff
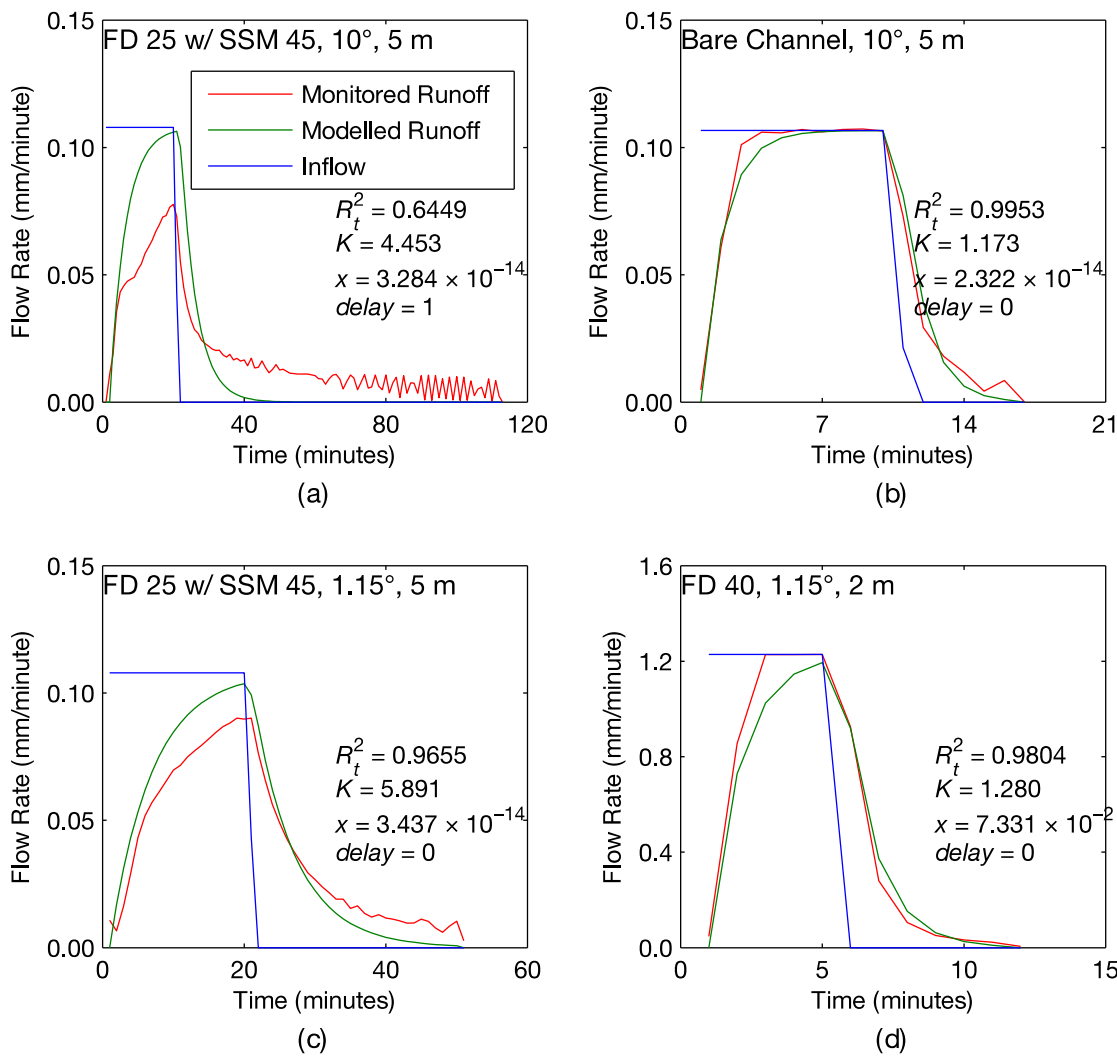
Figure 5.25 – Worst- (a), best- (b), mean- (c) and high *x*-value (d) fitting modelled runoff profiles with optimized *K*, *x* and *delay* parameters, at one-minute resolution.

profiles from these tests were fitted extremely well. It should be noted that the optimal travel time, whether 8 seconds or 0.4 minutes, is below half of the time step, therefore it is impossible to avoid oscillations in the modelled runoff profile for these tests, despite them being ideal candidates for a linear routing method. In total, oscillations were observed in 33 modelled runoff profiles, again corresponding exactly to those tests for which optimized *K* was below 0.5 minutes.

The optimized value of *x* was above 0.01 in 107 cases, above 0.1 in 33 of those and 0.19 at its maximum, giving a storage routing equation of $S = K(0.81Q + 0.19I)$ in the most extreme case. This would not be unexpected for many rivers and is another unusual result, as it has already been established that, physically, *x* should be zero for all of these tests. It is suggested that the slightly better performance of the Muskingum model, in comparison to the nonlinear storage routing model at a one-minute resolution, may be due to this extra model-fitting, but physically meaningless, parameter.

5.9 Conclusions of Drainage Layer Model Selection Study

Runoff profiles were recorded, by high resolution monitoring equipment, for 300 tests on green roof drainage layer configurations, representing three repeats each of 100 different situations of component, roof slope, drainage length and water inflow rate. The amount of lag, measured by cumulative median-to-median delay (t_{50}), introduced by a drainage layer test configuration ranged from 8 to 636 seconds, indicating that, in all tests, the drainage layer adequately performed its primary duty of quickly removing excess water.

A nonlinear storage routing model was proposed, employing continuity of volume and a direct relationship, of the form $Q = aS^b$, between the rate of discharge and the mean depth of water stored in the drainage layer. A *delay* parameter was also included, which time-shifted the entire modelled runoff profile by an integer number of time steps, to account for any delays in the monitoring system. An optimization routine, *lsqcurvefit*, was employed in Matlab to find, separately for each test, the values of the constants *a*, *b* and *delay* that would minimize the difference between the monitored runoff profile and the runoff profile produced by the model. The mean goodness-of-fit (R_t^2) for modelled runoff profiles in relation to observed runoff profiles was very high, at 0.9922. Approximately 1.9 seconds was required per optimization.

Statistical analyses were performed in SPSS 19 in order to identify which of the test variables e.g. roof slope, had no statistical effect on the optimized values for *a*, *b* and *delay*. After it was established that the value of *a* was independent of inflow rate and partly independent of component configuration, the value of *a* was averaged across all situations for which these were the only variables. The optimization routine was repeated, to find new optimal values of *b* and *delay* with all *a*-values specified. Averaging similar values of *a* reduced modelling accuracy only slightly (mean $R_t^2 = 0.9913$) and approximately halved the optimization time required.

According to similar principles, the value of *b* was averaged across all inflow rates, drainage lengths and partly across components. *delay* was then varied for optimal fit between the monitored runoff profile and the now fixed-shape modelled runoff profile for each test. It was found that, by fixing the values of *a* according to inflow rate and component material, and the values of *b* according to inflow rate, drainage length and component material, goodness-of-fit remained high (mean $Rt^2 = 0.9902$). This showed that the model was potentially insensitive to the exact values of *a* and *b*.

A parameter sensitivity analysis was performed, to assess exactly the purpose of each of the three modelling parameters, and how far the values of each could be perturbed without affecting the quality of the modelling. If was found that, in certain cases, doubling or halving the value of either *a* or *b* had an almost negligible effect of the quality of the modelled runoff profile,

implying that the values derived here may provide reasonable estimates to the performance of a much wider range of drainage layer components. In addition, *a* was found to positively correlate to the steepness of the rising and falling limbs of the modelled runoff profile, while *b* was found to negatively correlate to the "bulge" of the rising limb. *delay* was found simply to translate the profile, the shape of which is defined by the values of *a* and *b*, along the time axis.

An approach based around Manning's Equation was then taken to nonlinear storage routing. Manning's roughness coefficient was found to range from 0.00572 to 0.778, which is not considered unbelievable when the depth of flow is considered relative to the form roughness of the tested drainage layer components and configurations. The roughness values found for FD 25 and FD 40, which were around 0.05, correlate well with those used in a previous Manning's Equation-based modelling exercise for a green roof drainage layer (She & Pang, 2010). Overall however, Manning's equation was not considered to be a more practically useful approach to nonlinear storage routing than the semi-empirical parameter optimization and value averaging approach.

The applicability of the nonlinear storage routing method was tested at a one-minute resolution more typical of conventional monitoring systems. The optimized parameters derived at a one-second resolution were scaled to a one-minute resolution and input directly to the nonlinear storage routing model, using downsampled versions of the existing 300 inflow and monitored runoff profiles. In more than one third of test cases, use of the given parameters resulted in a growing oscillation, causing the model to stop its runoff predictions prior to reaching the end of the input rainfall profile. *lsqcurvefit* was again employed, to derive optimized parameters for fitting to the downsampled monitored runoff profiles. The optimization routine was successful for all 300 tests, with a mean R_t^2 of 0.9676. However, in 42 cases, all with optimized $b > 4$, a growing oscillation was produced in the modelled runoff profile, with the potential to prematurely terminate the model during longer inflow events of the same intensity.

As a possible alternative to nonlinear storage routing, the applicability of the Muskingum routing method was also tested, first at a one-second data resolution. *lsqcurvefit* was again employed to find the values of the Muskingum coefficients *K* and *x*, and the monitoring *delay*, which minimized the difference between the predicted and monitored runoff profiles. Following optimization, the mean R_t^2 of all 300 test profiles was 0.9751, indicating a poor fit in comparison to nonlinear storage routing, but a good fit overall. In all cases, *x* was near zero, causing the Muskingum method to function as a linear storage routing model. In theory, *x* is expected to be zero if a weir exists between the two points at which inflow and outflow are measured. Because all terms in the Muskingum model are linear, real runoff profiles always exist, and continue to exist when the parameters are scaled to any other time step. However, for values of *K* below 30

seconds, instabilities will form when a time-step of one minute is used, assuming x is zero. If higher time steps are used for modelling (e.g. to match the resolution of monitored data) instabilities will form if the travel time is less than half of the time step. This could potentially result in many more drainage layer configurations being affected by modelling instability. As the value of x increases, the minimum value of K required to avoid instability also increases. It should be noted however that, as the outlet from the drainage layer is effectively a weir, no physical basis appears to exist for non-zero values of x.

Following optimization of the Muskingum parameters on the same rainfall/runoff data set downsampled to a one-minute resolution, 300 successful modelled runoff profiles were produced with a mean R_t^2 of 0.9761. Values of x up to 0.19 were observed in certain tests. Despite technically giving the best possible fit in that test, non-negligible values of x are considered nonsensical. Instabilities were observed in 33 tests, where the optimized value of K was below 0.5 minutes. This will cause an issue in general, as the travel times for smooth components over short distances should be less than 0.5 minutes.

Purely by measures of R_t^2, it may be concluded that both methods are equally good at modelling runoff recorded at a one-minute resolution. However, some of the results given by the Muskingum method are difficult to explain relative to the physical configuration of the tests, and the short travel times of drainage layer components are a potential an unavoidable source of modelling instability. Nonlinear storage routing produces results of similar quality and is potentially a more robust runoff modelling method. However, care should be taken when transferring parameter values from one time-step to another, as it may not be possible or appropriate to simply scale them conventionally. Values of b greater than 4 should be treated with caution, as they appear to always lead to growing oscillations.

Table 5.3 presents a small set of scale and exponent parameter values for nonlinear storage routing at one-second resolution which are applicable to all drainage layer configurations tested here and potentially to similar untested configurations. The corresponding values of *delay*, given these values for a and b, are generally in the range 10-20 seconds and can therefore be ignored for most modelling purposes. For most extensive green roofs, it is expected that the parameter values for HDPE or Fibrous will be most appropriate.

Table 5.3 – Suggested scale and exponent parameter values for nonlinear storage routing at one-second resolution.

Roof Slope	Drainage Length	Component							
		Waterproofing		HDPE		Polystyrene		Fibrous	
		a	b	a	b	a	b	a	b
1.15°	2 m	0.067	2.84	0.022	2.45	0.017	2.84	0.020	2.01
	5 m	0.054		0.020		0.010		0.002	
10°	2 m	0.198	2.14	0.032	2.32	0.037	2.52	0.039	1.97
	5 m	0.147		0.027		0.027		0.002	

In order to use the parameter values given in Table 5.3 with inflow data presented at e.g. one-minute resolution, it is currently suggested that the inflow records be "upsampled" to one-second resolution by distributing the inflow quantity found in each one-minute sample into 60 consecutive one-second samples. After modelling the runoff response according to the parameter values given in Table 5.3, the time-series runoff record may be "downsampled" to its original resolution by summing the total predicted runoff depth in each set of 60 consecutive samples.

Although drainage length was not found to significantly affect the runoff response of the drainage layer in this experimental programme, it is important to note that the spacing between drainage outlets in large green roof projects may be many times greater than the largest distance of 5 metres (equivalent to 10 m outlet spacing) tested here. According to the specifications given by the FLL (2008), rainfall simulators with a drainage length of 10 metres (equivalent to 20 m outlet spacing) are acceptable for FLL-defined coefficient of discharge tests, suggesting that a number of these larger simulators may exist. Using larger rainfall simulators at controlled variable drainage lengths will allow for a more comprehensive study of the effects of drainage length over a larger range and may lead to a situation in which extrapolation of runoff performance to greater outlet spacing is made possible. Research of this kind is, however, beyond the scope and equipment budget of the Green Roof Systems project.

Overall, it is concluded that, for the two-stage model that will be tested in Chapter 7, nonlinear storage routing is the most suitable method by which to model water flow through the drainage layer.

6 Results and Discussion – Substrate

6.1 Chapter Overview

This chapter opens with an introduction to the use of the hydrological models, previously selected in Section 2.6.3.6, for the analysis and characterization of the data collected in the small rainfall simulator. An explanation of the processing required to convert the raw data record into usable runoff records is given. Basic performance characteristics of the tested substrate configurations are found and presented. The modelling methods are applied independently to the runoff records and the results evaluated. The parameters of the nonlinear storage routing model are evaluated for similarities and genericized as far as possible, to allow the potential use of this model on similar, but so far untested, substrate configurations. An optimum level of parameter genericization is identified, where the accuracy of runoff modelling is not greatly affected by the grouping and averaging of input parameter values. The Hydrus-1D model is tested for its ability to accurately model the recorded runoff curves with specified substrate properties. finally, the models are evaluated against each other, in terms of ease of use, applicability and accuracy of results.

As much of the analysis in this chapter is similar to the analyses in Chapter 5, extended discussions and explanations are not repeated, if the results and reasoning are already reported in Chapter 5.

It was previously noted in Section 1.4 that some of the data analyses presented here differ to those found in a related conference paper (Yio *et al.*, 2012) and its resulting journal paper (Yio *et al.*, 2013) to which the thesis author had input. In that paper, cumulative median-to-median delay (t_{50}) was evaluated between the response of the empty simulator and the tested substrate sample. Here, t_{50} is evaluated between the input rainfall and recorded runoff. However, t_{50} is also evaluated for the empty test apparatus, to allow comparison with the related conference and journal publications. In both publications and in this chapter, the assumed rainfall profile is used directly as input data for hydrological modelling. Here, this decision is justified as the substrate model is intended to be the first stage of a two-stage green roof model. Hence, modelling a filter sheet below the substrate (and above the drainage layer) is physically consistent with the system assembly of the majority of extensive green roofs. The routing effects of water, from just below the filter sheet to the collection cylinder i.e. through the funnel and downpipe, are inseparable from the modelling of the filter sheet without a complete dismantling and rebuilding of the rainfall simulator. As the filter sheet is a thin (0.6 mm depth) geotextile with high permeability (70 mm/s according to EN ISO 11058; BSI, 2010), and the funnel and downpipe are both steeply-angled smooth plastic components that, in this experimental programme, were wetted typically one to four hours prior to each test, it was assumed that neither the filter sheet nor the

funnel and downpipe introduced significant routing effects. However, the actual t_{50} times recorded for the empty simulator chamber did indicate routing in the order of tens of seconds.

6.2   Selection of Hydrological Models

From those hydrological models considered in Sections 2.4 and 2.6, two were selected for further consideration: nonlinear storage routing and the Richards' Equation, implemented through Hydrus-1D. Both models have been previously shown to be robust and suitable for green roof hydrological modelling (Kasmin *et al.*, 2010; Palla *et al.*, 2012). However, the two models differ significantly in their approach. Nonlinear storage routing considers the substrate sample as a generic reservoir and employs only continuity of volume and a storage-discharge relationship to determine the rate of outflow; it can therefore be applied to any situation in which inflow is routed through a storage volume. In contrast, the Richards' Equation directly models the movement of water through a porous medium and employs various data about the medium in order to make its calculations. It is therefore highly dependent on the reservoir being a soil, substrate or similar. Aside from the two methods selected here, all other substrate-specific methods were rejected due to the difficulty in defining values for the necessary input variables in the governing equations. Darcy's Law was further rejected for its requirement of saturation at all times. The unit hydrograph method was rejected for the difficulties in genericization that would be inherent with highly-parameterized outputs, and the Muskingum method was rejected due to the existence of an effectively infinite hydraulic gradient at the base of the rainfall simulator chamber.

6.3   Data Collection and Processing

The experimental programme for the substrate was conducted in parts over 2012 and early 2013, simultaneously with the analysis of the data collected from the drainage layer tests and writing up research outputs. Each test configuration was repeat-tested three times, for a total of 84 tests to be considered in the following sections of Chapter 6. In order to minimize the effects of a runoff tail from the end of one test overlapping into the beginning of the subsequent test, a period of 30 minutes over which no runoff could be observed was a prerequisite to starting the subsequent test. This condition was maintained throughout the entire experimental programme.

The data generated by the pressure transducer is output every five seconds as a voltage to three decimal places, where an increase of 1.000 mV corresponds to a water level increase of approximately 400 mm in the small collection cylinder. In contrast to the monitoring setup of the large rainfall simulator, the pressure step size of the pressure transducer is invariant at 0.001 mV and no step value appears to be any more or less "stable" (see Section 5.3) than any other step value. Potentially due to the lower precision at which the pressure data is stored, the pressure

transducer does not itself generate any noise that is visible in the data record. The experimental setup of the small rainfall simulator is less vulnerable to the wave-based noise present in the data collection from the large rainfall simulator, due to the much smaller quantities of water involved and the mounting of the pressure transducer outside of the pipe through which runoff enters the collection barrel. As a result of the above, the only processing applied to each runoff record was a smoothing operation of a 19-sample moving average applied to the differential of each test's pressure record, repeated twice for a total of three smoothing operations.

The rate of inflow to the simulator was not directly monitored during this experimental programme. Though the use of a peristaltic pump implies that rates of inflow should be exactly related to pump speed, this is an idealization. It would not be unreasonable to expect some dilation of the pipe, for example, to occur over months of regular use. In common with the assembly of inflow records for the drainage layer, the inflow rate for each test was assumed equal to the steady-state runoff rate after the differential runoff record had undergone ten smoothing operations. Steady-state was definitively reached in 81 of 84 tests, and no tests used "pulsed" inflow. For the design storms of variable intensity, the steady-state runoff rate was found for the peak of the storm, and this was used for minutes 12-18. Minutes 6-12 and 18-24 used the peak rate multiplied by 0.1628, and minutes 0-6 and 24-30 used the peak rate multiplied by 0.0678, following the profile of a 75% summer storm discretized into five steps (NERC, 1975). For three tests, all applying the design storm profile to 10 cm of LECA, it was questionable whether steady-state had been reached at the peak. As a result, the rainfall profile for this event was averaged from the 18 comparable profiles that clearly did reach steady-state.

6.4   Overview of Substrate Performance

6.4.1   Repeatability and Accuracy of Tests

The runoff response for every test configuration was found to be highly repeatable, with only very minor differences between repeat tests. The nominal inflow rates of constant 0.1, 0.3, 0.6 and peak 1 mm/minute were, overall, slightly under-supplied by the pump, but delivered with very high consistency. This is summarized in Table 6.1. In terms of consistency, the use of the peristaltic pump compares favourably with the dripper networks used in the large rainfall simulator. It is noted that the mean and standard deviation for the design storm were calculated based on 18 profiles, rather than 21, as three profiles (for 10 cm of LECA) were based on the average of the other 18.

6.4.2   Runoff Responses

For all constant-intensity tests, the runoff response is of a consistent general shape: a rising limb, smoothly transitioning to a steady-state section, followed by a falling limb after the rainfall event

Table 6.1 – Summary of test inflow rates.

Nominal Rate	Mean of Actual Rate	St. Dev. Of Actual Rate	No. of Tests
0.1 mm/minute	0.0962 mm/minute	0.00323 mm/minute (3.4%)	21
0.3 mm/minute	0.2884 mm/minute	0.00326 mm/minute (1.1%)	21
0.6 mm/minute	0.5659 mm/minute	0.00583 mm/minute (1.0%)	21
Design Storm (peak 1 mm/minute)	0.9730 mm/minute	0.02222 mm/minute (2.3%)	18

ends, smoothly approaching zero. A runoff response of this shape was also commonly observed for drainage layers. For some tests, a delay between the start of rainfall and the start of runoff is clearly visible, particularly when rainfall intensity is low and substrate is deep; the tests using 10 cm LECA mix under a constant 0.1 mm/minute intensity event show a delay of around 10 minutes. In all cases the delay is believed to be a function of the time required for water to percolate through the pores of the medium. For the variable-intensity design storms, the runoff response tends to follow a similar shape for each of the six-minute steps and for the period following the end of the storm: the runoff profile for the first three six-minute steps consists of a rising limb, which decreases in slope as an equilibrium with the rainfall nears, while the runoff profile for the next two six-minute steps and the post-storm period consists of an initially steeply falling limb, which levels off as it comes closer to reaching equilibrium with the rainfall rate (which is obviously zero after the end of the storm). Whether the rainfall is constant- or variable-intensity, the maximum steepness of the runoff profile i.e. the maximum rate of change in the rate of runoff, is dependent on the resistance offered by the substrate; more resistance corresponds to slower rates of change, visible as shallower rising and falling limbs.

For one test, of 5 cm Marie Curie Substrate over an SSM 45 protection mat, with a rainfall rate of 0.6 mm/minute, the remainder of the runoff record immediately after the end of the storm event has been lost. For the discussion immediately below, an approximation of the full runoff record up to 120 minutes was made using the nonlinear storage routing model which, for this configuration has an R_t^2 of 0.99993 over the 30 initial minutes of the monitored runoff record.

The time delay between the mid-point of cumulative inflow to the system and the mid-point of cumulative outflow from the system (t_{50}), averaged across all tests, was found to be 244 seconds (271 seconds excluding the 12 tests with no substrate). The t_{50} for all 84 tests is plotted in Figure 6.1, where quick visual comparisons can be made on the effect of substrate configuration, rainfall rate, substrate depth and repeat testing.

While the mean t_{50} of the substrate is clearly larger than that of the drainage layer, the difference between them is not great; 271 is around 2.5 times 110. The delay increases non-linearly with substrate depth; its mean value is 83 seconds for the 12 tests with no substrate, 159 seconds for the 36 tests with 5 cm substrate depth and 381 seconds for the 36 tests with 10 cm substrate
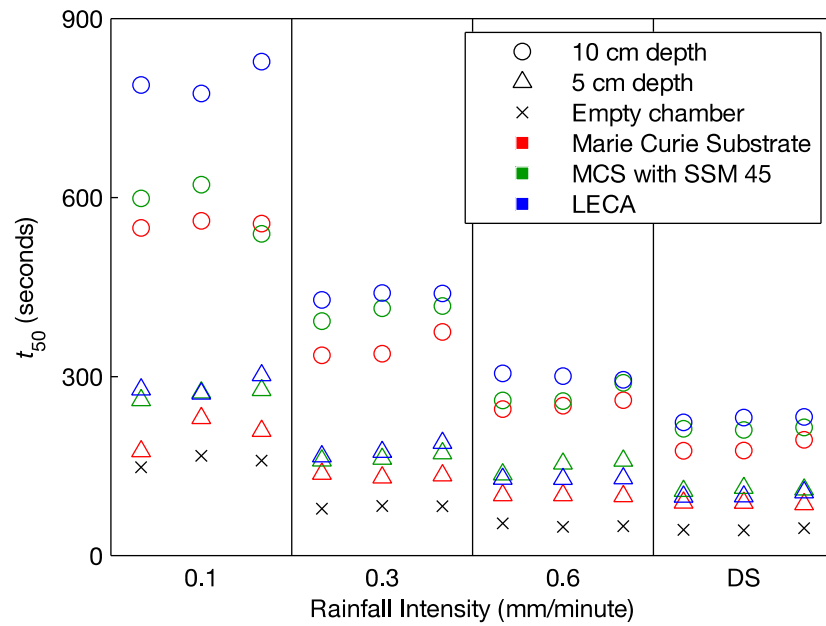
Figure 6.1 – t_{50} times for all tests.

depth. The mean delay decreases non-linearly with rainfall rate, falling from 408 seconds at 0.1 mm/minute, to 250 seconds at 0.3 mm/minute, and to 179 seconds at 0.6 mm/minute. The mean delay for the design storms is the lowest: 138 seconds. This is plausible, as the peak rainfall rate for the design storm is 1.0 mm/minute, and almost 70% of the storm's depth (including the 50th percentile) falls during the central peak step. The mean time delay introduced by the LECA mix (307 seconds) is greater than that introduced by either the Marie Curie Substrate with the SSM 45 mat (271 seconds) or the Marie Curie Substrate alone (233 seconds). This is due to the high (20%) organic content of the LECA mixture, which exceeds that of the Marie Curie Substrate (15%). The use of a moisture-holding mat below a substrate sample does not greatly restrict the movement of water. This is shown in Figure 6.2, where the time-series runoff profiles for tests of Marie Curie Substrate with and without the moisture retention mat underneath are similar. This observed lack of effect is because the flow path through the mat is around 5 mm. In the drainage layer tests, the effect of SSM 45 was noticeable as the flow path could have been up to 1000 times the length: 5 metres.

The time of concentration is not discussed for the substrate, as it was concluded from the drainage layer study that it did not give any additional useful information over the t_{50} statistic.

6.5   Nonlinear Storage Routing at Five-Second Resolution

6.5.1   Overview and Optimization

The general methodology for storage routing is described in detail in Section 2.4.5.3, as is the adaptation of that methodology to nonlinear form. The governing equations used to model the
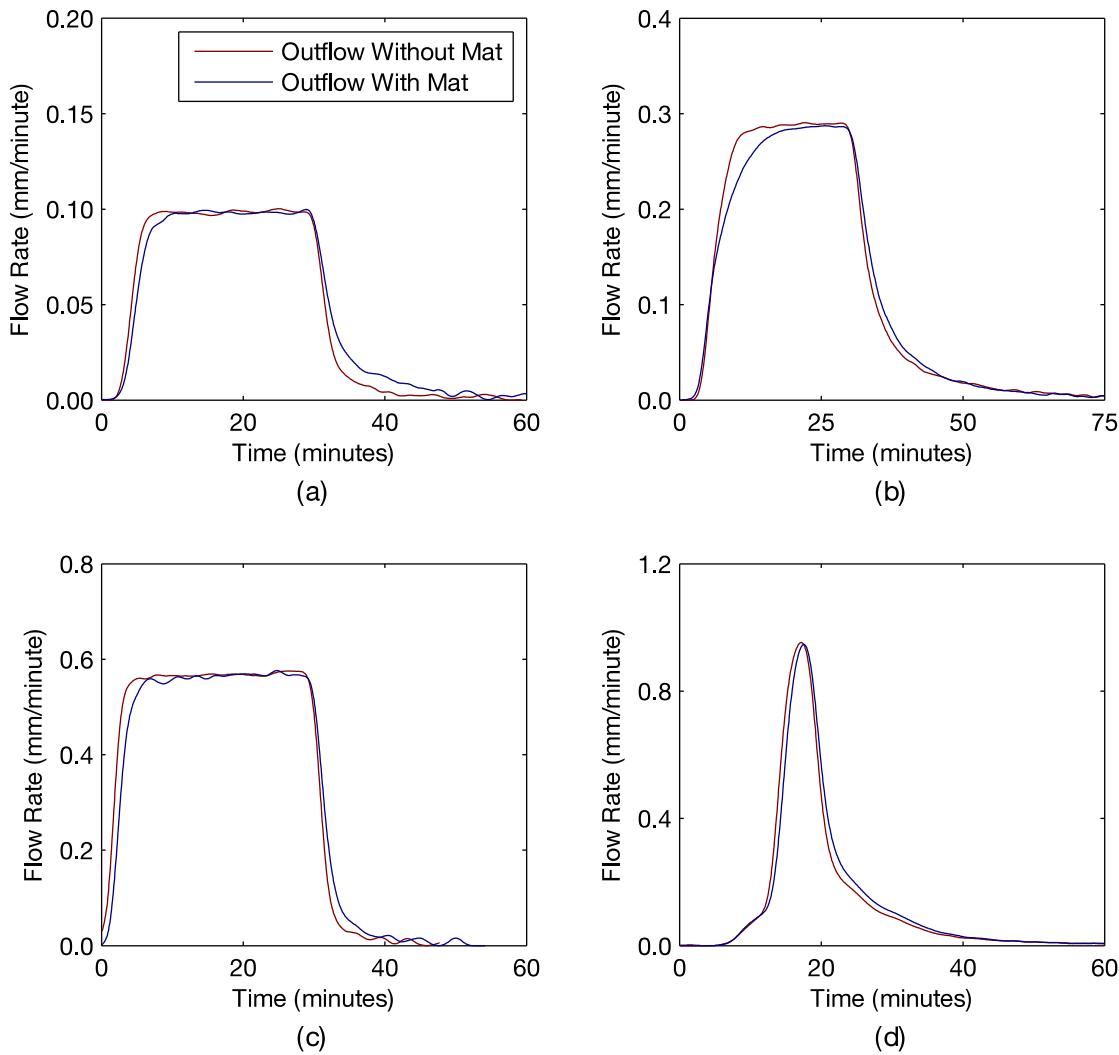
Figure 6.2 – Comparison of runoff responses for Marie Curie Substrate with and without an underlying SSM 45 moisture retention mat. Plots (a) and (c) use 5 cm substrate, plots (b) and (d) use 10 cm substrate.

runoff response of the substrate are identical to those used for the drainage layer. The use of *lsqcurvefit*, to optimize scalar *a* and exponent *b* was unchanged, as was the use of a *delay* parameter and its range (300 seconds, here 60 samples). The same code, software and hardware were used to run the optimization routine. Section 5.5.1 can be consulted for further information, if required.

Due to the increase in time step from 1 to 5 seconds, the interpretation of the three modelling parameters is slightly changed. *b* remains dimensionless. However, *a* now takes the dimension $mm^{1-b}/5$ seconds. It is shown in Chapter 5 that values of *a*, with one unit of time, cannot necessarily be scaled to a different unit of time. *delay*, which must always take a non-negative integer number of samples, can now only be a multiple of five seconds for each test. t_{50}, discussed previously, took more precise values by linear interpolation.

6.5.2   Applicability of Method at Five-Second Resolution

The first optimization run of *lsqcurvefit* used starting estimates of 0.01 and 2.5 for *a* and *b* respectively. Bounding values were specified from the start: [0.0001, Inf] for *a* and [1, Inf] for *b*. *delay* was permitted to take any multiple-of-five value from 0 to 300 seconds. The total time required for this first run was 1 minute and 54 seconds and working solutions were found in all 84 cases. The mean R_t^2 across all monitored-modelled runoff pairs was 0.9972 and the minimum was 0.9876 (these figures are 0.9975 and 0.9895 when only the 72 tests including substrate are considered). Clearly, while nonlinear storage routing can be considered a successful method by which to model the runoff response of the drainage layer, the R_t^2 values found are notably higher when the same methodology is applied to model the substrate. The three tests (all design storms over 10 cm of LECA) for which the rainfall profile was averaged from other tests have, understandably, some of the lowest correlations between modelled and monitored runoff, though it should be noted that, in the context of the extremely high goodness-of-fit observed here, this relates to R_t^2 values around 0.995. The single closest fit between monitored and modelled runoff ($R_t^2 = 0.99993$) relates to the test for which the falling limb is lost; here, the modelled runoff profile is optimized to fit the rising limb and steady-state section only. However, even excluding this test, the mean R_t^2 across all remaining tests remains at 0.9972, while the new highest R_t^2 is 0.9994.

As the difference in goodness-of-fit between the best-, worst-, mean- and median-fitting tests is minimal, Figure 6.3 plots instead four sets of rainfall, monitored runoff and modelled runoff profiles representing a wide range of test configurations. As previously, the test configurations resulting in the plots shown are written onto each plot.

The optimized values of *a*, *b* and *delay* for all 84 tests are plotted in Figures 6.4, 6.5 and 6.6.

6.5.3   Statistical Analysis

6.5.3.1   Procedure

As commented upon in the extended discussions on nonlinear storage routing in Chapter 5, the shape of the runoff profile generated by the model is dependent on the values assigned to the parameters *a* and *b*, while the positioning of this shape along the time axis is dependent on the value assigned to the *delay* parameter. An assessment of the statistical significance of the optimized modelling parameters is beneficial in this study, as a judgement of the applicability and effects of parameter genericization. The test variables in the substrate experimental programme were the rainfall rate, dividing into four groups (design storm and constant 0.1, 0.3, 0.6 mm/minute) with 18 tests each, the substrate configuration, dividing into three groups (Marie Curie, Marie Curie above SSM 45, LECA) with 24 members each, and the substrate depth,
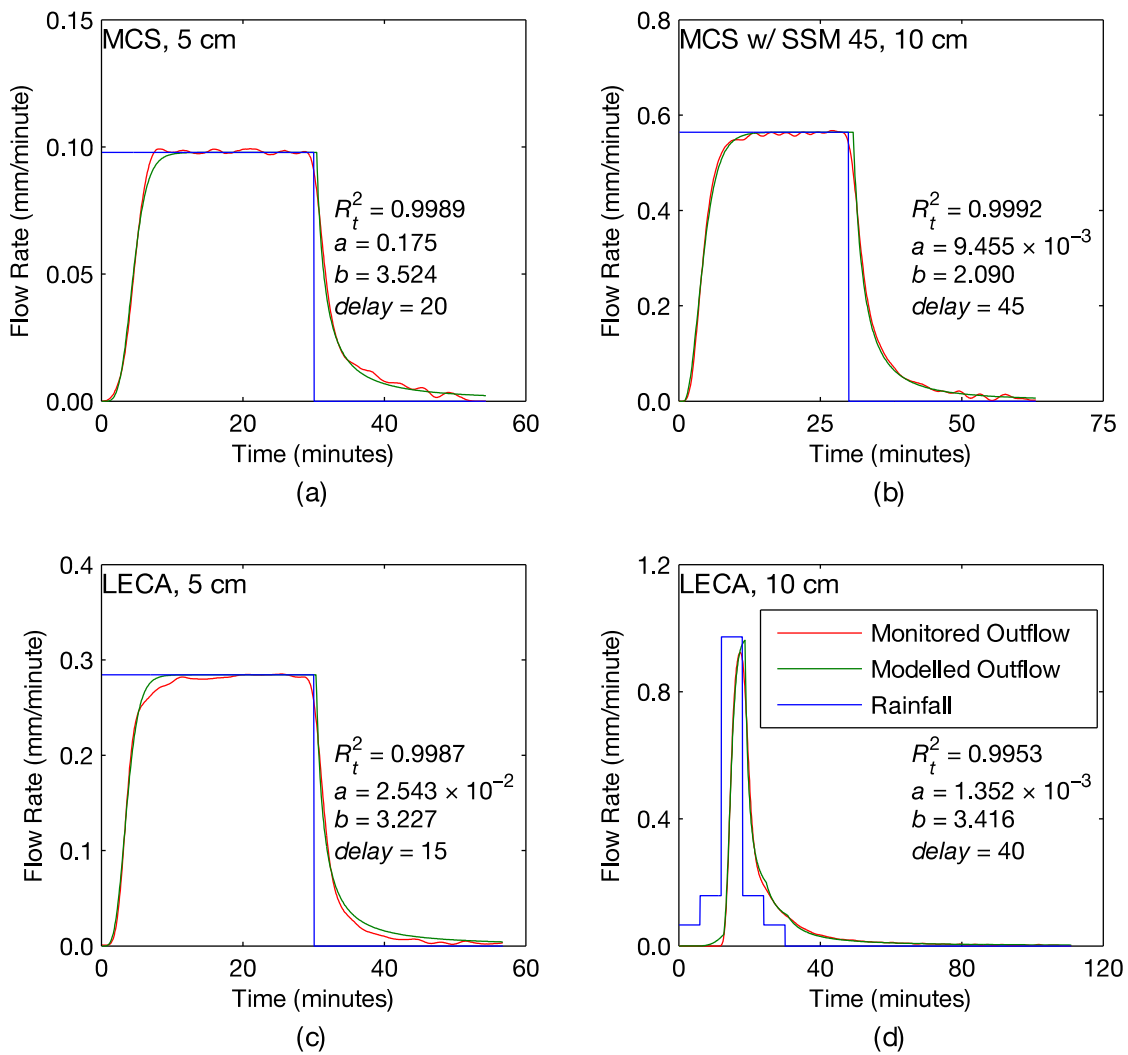
Figure 6.3 – Representative rainfall, monitored runoff and modelled runoff profiles with optimized *a*, *b* and *delay* values.
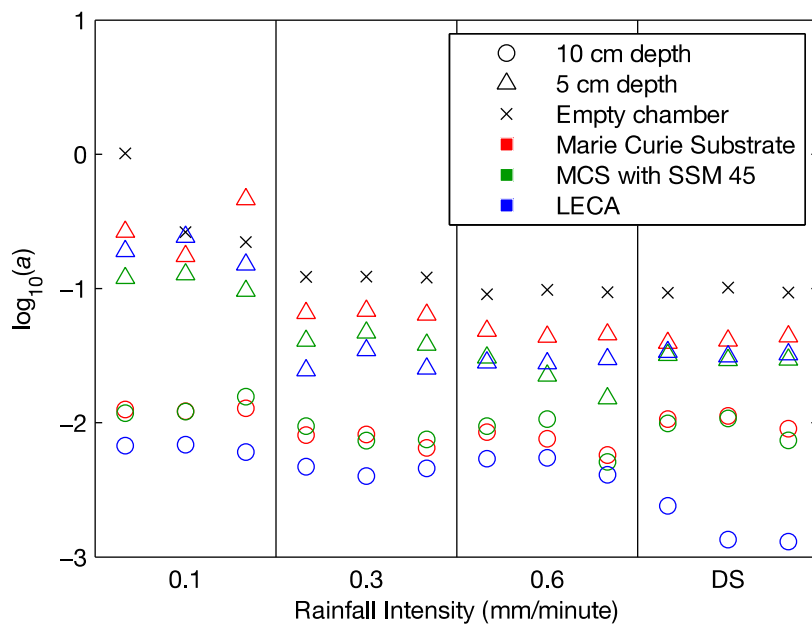
Figure 6.4 – *a*-values for all tests.
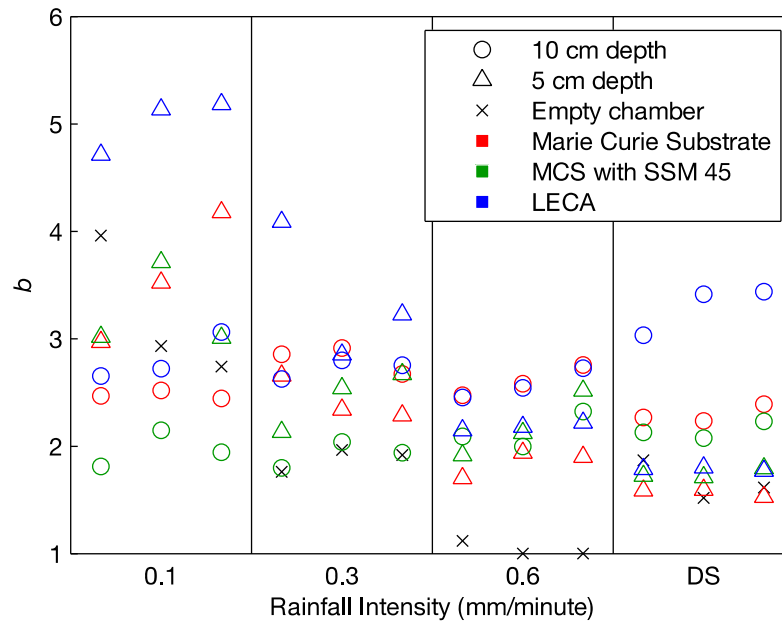
Figure 6.5 – *b*-**values for all tests.**
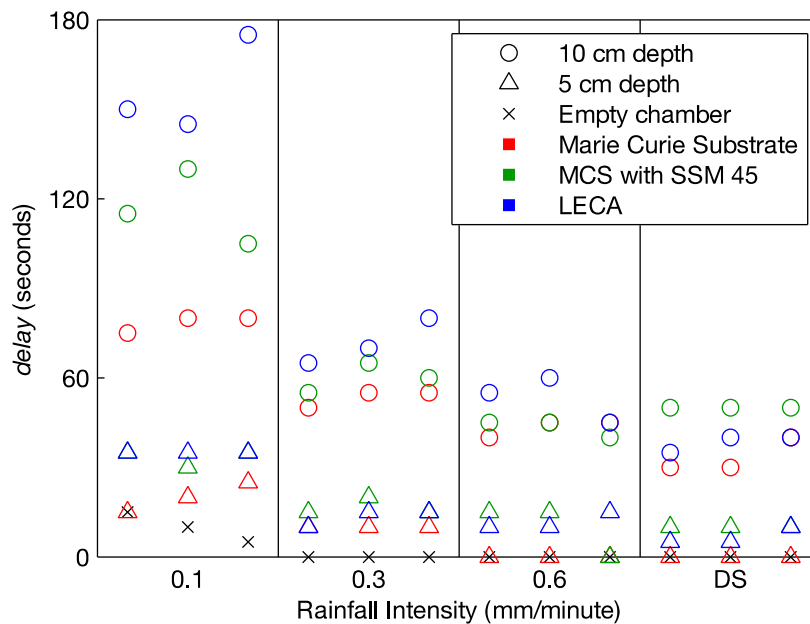
Figure 6.6 – *delay*-**values for all tests.**

dividing into two groups of 36 members each (5 cm and 10 cm). The group of 12 tests using no substrate was not considered to be a test of substrate for this statistical analysis. Student's and Welch's unpaired two-sample *t*-test were used to assess whether the means of the two groups of substrate depth were different at a significance level of 0.05. One-way ANOVA was used for statistical significance analyses of substrate type and rainfall rate. Following Levene's test, either Fisher's LSD or Tamhane's T2 post-hoc test, as appropriate, was used at a significance level of 0.05 to simultaneously compare the means of all groups within a test variable.
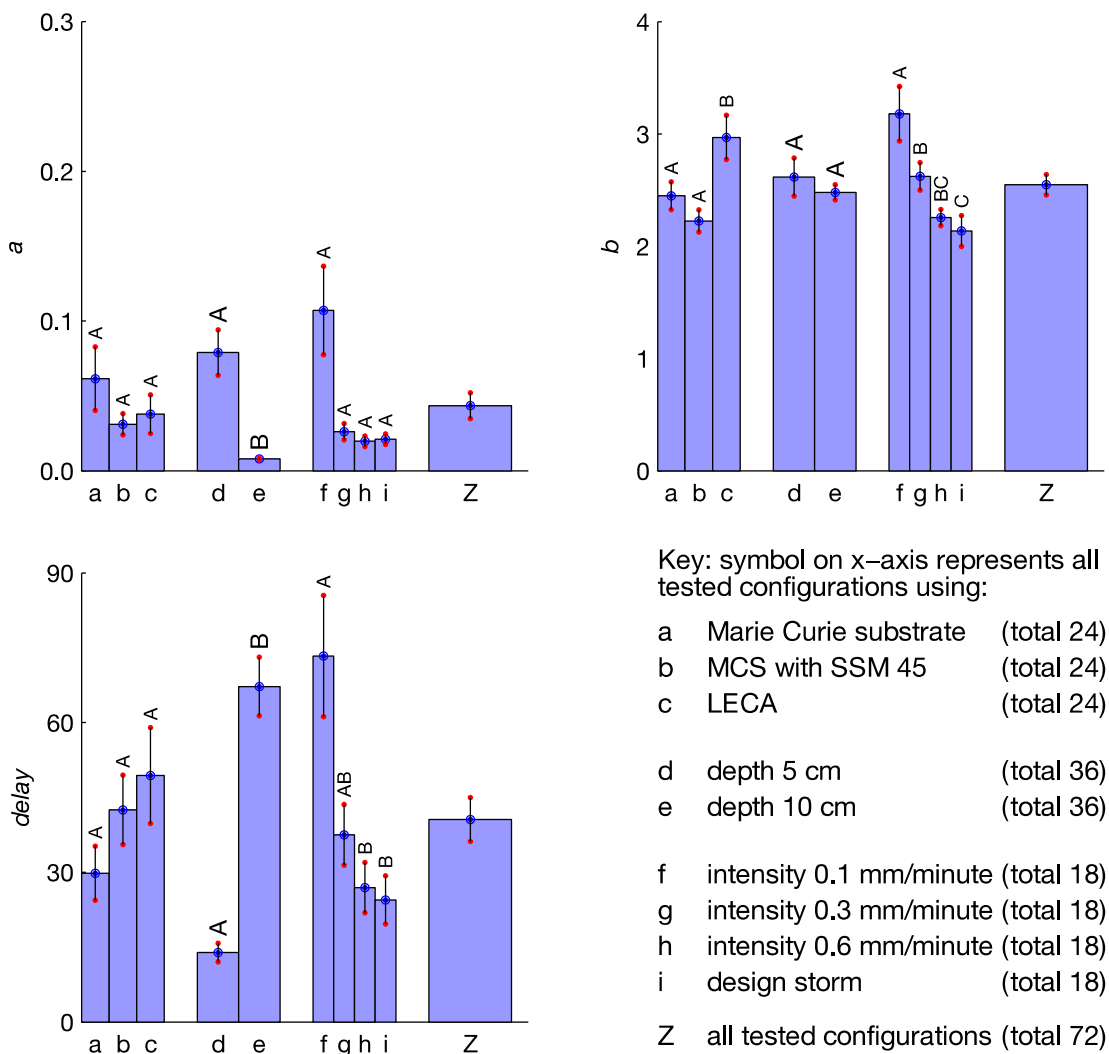
Figure 6.7 – Mean (light blue bars) and standard error (black lines terminated by red dots) of optimized values for *a*, *b* and *delay*.

6.5.3.2   Discussion of Parameter Values

Figure 6.7 presents the mean and standard errors for *a*, *b* and *delay*, for all divisions within each test variable. Statistical groupings are shown by capital letters above each bar. It should be noted that these groupings exist independently for each combination of variable and modelling parameter i.e. the significance groups A, B, etc. cannot be transferred from one group of touching columns to another.

As the monitored runoff profiles for repeat tests show even less deviation from each other than was observed for repeat tests of the drainage layer, it is unsurprising that the modelled runoff profiles for repeat tests often optimize with similar values of *a*, *b* and *delay*. For all three parameters, the standard error is relatively low in comparison to the mean, though not as low as for the drainage layer. Mean parameter values are 2.548 for *b*, 0.0435 mm^{1-b}/5s for *a* and 40.56 seconds for *delay*. Ratios of mean value to standard error are 28.1, 5.0 and 9.2 for *b*, *a* and *delay*

respectively, in all cases around 30-50% of the ratios found for the drainage layer parameter values. The mean values of both *a* and *b* across all substrate tests are similar to those found for *a* and *b* across all drainage layer tests, though the time unit of *a* is not the same.

The range of parameter values is smallest for *b*: from 1.53 to 5.19. In five cases, *b* takes a value above 4; this was shown to cause decaying oscillations in a study of the drainage layer (Chapter 5). However, no such oscillations are discernible in any of the five modelled runoff profiles which take a value of *b* above 4. The optimized values of *a* for $b > 4$ are not distinguishably lower than the optimized values of *a* for $b < 4$. The lowest optimized value of *b* is 1.53 and therefore not near to the lower boundary on optimization. The optimization routine therefore did not wish to set a value of *b* below 1 at any time. Values of *b* below 1 are still considered to be potentially unstable and so were in any case prevented during optimization.

The ratio of highest to lowest *a*-value is very large, at 255:1 though, as in the drainage layer study, a few large values skew the entire distribution: the maximum value is around 10.5 times the mean value, and the median value is approximately 35% of the mean value. Further discussion on this will take place in Section 6.5.5.3, but the exceptionally high values of *a* do not appear to correlate with any single specific test characteristic.

The value of *delay* ranges from 0 to 175 seconds. The most common value is 10 seconds, occurring in 10 optimizations. In contrast to the drainage layer study, it is plausible that the value of *delay* relates physically to the test configuration, in addition to its physical relation to the monitoring delay. If it is assumed that the water reservoir is built upwards through large pores, starting from the bottom of the substrate sample, then a time delay exists between water falling onto the surface of the substrate and that water entering the reservoir. *delay* could therefore realistically be related to both substrate composition and depth.

6.5.3.3   Significance of Test Configuration

Almost none of the test variables are shown to affect the optimized value of *a*, which is statistically independent of both substrate composition and rainfall rate. Independence of *a* from rainfall rate is expected and desirable, as it is a theoretical assumption of the method. However, a suggested independence of *a* from substrate type is unusual in its implications. The only significance groupings for *a* relate to substrate depth: the value of *a* is reduced almost ten-fold when the depth of substrate is doubled from 5 to 10 cm. A nonlinear dependence of *a* on substrate depth is a physical possibility, as the value of *a* is shown in Section 5.7.3 to be nonlinearly inversely related to the "travel time" of a reach. However, the full expression relating *a* to travel time also involves the nonlinear storage-discharge exponent *b* and steady-state runoff rate. It is also noted that, while the value of *a* is statistically independent from rainfall rate, the

group mean for the lowest rainfall rate is approximately 4-5 times the group mean for any other rainfall rate. Inspection of Figure 6.3 suggests that, at a rainfall rate of 0.1 mm/minute, the value of *a* is noticeably higher for the subset of 12 optimizations using a 5 cm substrate depth than for the subset using a 10 cm substrate depth. This indicates that the influence of rainfall rate cannot be considered significant by itself.

The optimized value of *b* is shown to have a significant dependence on every test variable except for substrate depth. An observed dependence on rainfall rate is in direct contradiction to storage routing theory but, as happened in the drainage layer study, this may be shown to reduce following parameter value averaging of *a*. Additionally, group averaging this parameter, regardless, may be shown to not interfere with the quality of the model. The value of *b* is found to depend on the choice of substrate material. However, the presence or absence of the SSM 45 moisture mat layer below a sample of Marie Curie substrate is not shown to significantly alter the value of *b*. As the value of *a* is already shown to be independent of all tested substrate configurations, it can be concluded that the presence or absence of the SSM 45 moisture/protection mat below the substrate does not significantly affect the storage-discharge relationship for the substrate layer, at least for Marie Curie substrate (which is of a typical composition for extensive green roofs). SSM 45 may have been found to have no significant effect on the storage-discharge relationship here due to the greatly-reduced flow length involved in comparison to the drainage layer experimental programme: while the length of flow through the moisture mat, parallel to the drainage layer, was up to 5 metres horizontally, the length of flow through the moisture mat, perpendicular to its plane, is only 5 mm.

The value of *delay* is expected to be related to the test configuration, as water falling onto the surface of the substrate is not thought to immediately enter the storage reservoir. Figure 6.7 shows a strong increase in the mean delay time as the substrate depth is increased from 5 cm to 10 cm. In common with the observations made by Yio *et al.* (2012), the increase in *delay* is not linear with the doubling of depth. Though it is not considered in the statistical analysis, the mean *delay* found for the simulator chamber without substrate is 2.5 seconds; this could realistically relate to the time required for a water droplet to travel into the collection barrel, starting from the air gap immediately below the chamber. The mean *delay* for each substrate ranges from 30-50 seconds, though each of the values plotted by columns a-c contains enough variance that no substrate may be considered statistically different from any other. However, *delay* is clearly not a direct measure of permeability, as dividing substrate depth by *delay* gives undefined values for 10 tests and no value below 2000 mm/hour. *delay* decreases with peak storm intensity. In a theoretical system, this would be unexpected as runoff should start immediately as the volume of stored water rises above zero. Permeability should be unrelated to rainfall rate, as, all other

factors being equal, the first water should enter storage after the same time delay, regardless of the rainfall rate. However, in practice, it may be that a quantity of water is required to build up before the reservoir activates. The time taken to reach that quantity would depend on rainfall rate. However, for this to be relevant, the mean *delay*-value should be highest for the design storm, as its initial rainfall rate is below even 0.1 mm/minute.

6.5.3.4 Parameter Value Averaging of *a*

The statistical analysis showed some independence from test configuration for all modelling parameters, potentially allowing value averaging to simplify and genericize the model. The greatest level of independence from configuration was shown for the mean value of *a*, which statistically only depends on substrate depth, being apparently independent of both rainfall rate and substrate type. It was therefore assumed that the number of individual *a*-parameter values could be reduced from 72 to two with minimal loss of modelling accuracy, by grouping and averaging of the 72 different values according to substrate depth. After specifying fixed *a*-values for each test (7.900×10^{-2} at 5 cm, 7.874×10^{-3} at 10 cm) the *b*- and *delay*-values were re-optimized to the newly- specified *a*-values. The mean R_t^2 correlation between monitored and modelled runoff was reduced, but remained very high at 0.9953 (for 72 tests), while the lowest R_t^2 correlation was reduced to 0.9846. Both of these values are still very high and indicate the continued suitability of the simplified modelling method.

Figure 6.8 plots the same four events as shown in Figure 6.3 using the parameter sets found after averaging of *a*-values. The modelled runoff curves shown in Figure 6.8 (a) and (c) are both generated using the same *a*-value of 7.900×10^{-2}. The modelled runoff curves shown in Figure 6.8 (b) and (d) are both generated using the same *a*-value of 7.87×10^{-3}. In addition, for (b) and (d), the values of the *b* and *delay* parameters are similar (2.220 vs. 2.275, 40 seconds vs. 50 seconds), yet both tests differ in substrate type and rainfall profile. However, R_t^2 values are very high for both of these modelled runoff curves. Hence, the general applicability of nonlinear storage routing in practice, where modelling parameter values may need to be estimated or transferred from existing studies, is shown. It is noted that the *a*-value used in Figure 6.3 (b) to generate the modelled runoff curve was more than six times the value of the *a*-parameter used in Figure 6.3 (d). As both could be brought to the same value without greatly compromising the accuracy of the results (as in Figures 6.8 (b) and (d)), the predicted runoff response is shown to be insensitive to the exactness of the parameterization of *a*.

The same statistical analyses were performed on the re-optimized *b* and *delay* parameter sets, the results of which are shown in Figure 6.9. To save space, the key is not reproduced; all columns are shown in the same order as in Figure 6.7. As all *a*-values were specified, a plot of *a*-values is omitted.

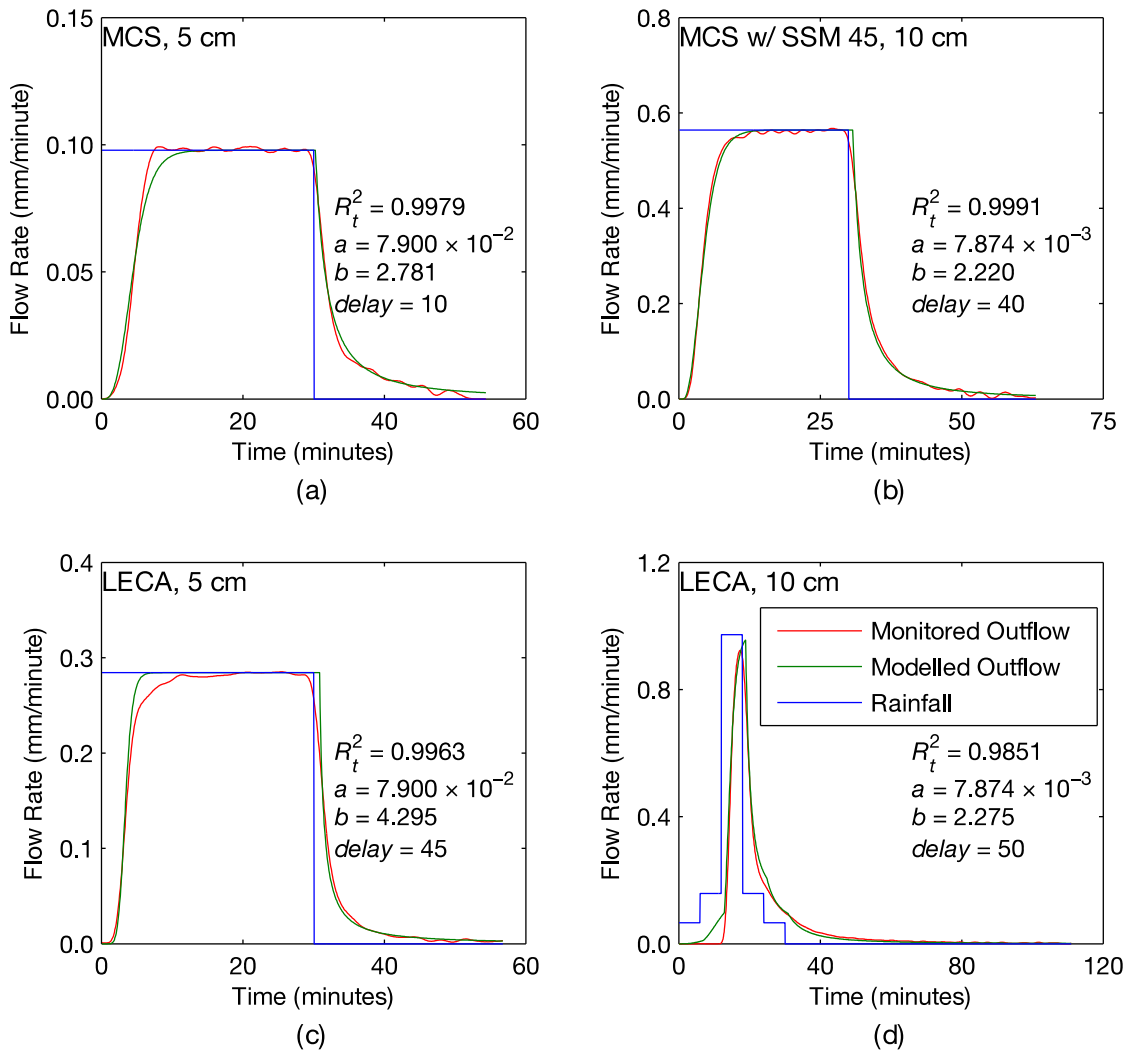**Figure 6.8 – Representative rainfall, monitored runoff and modelled runoff profiles after parameter value averaging of *a*.**
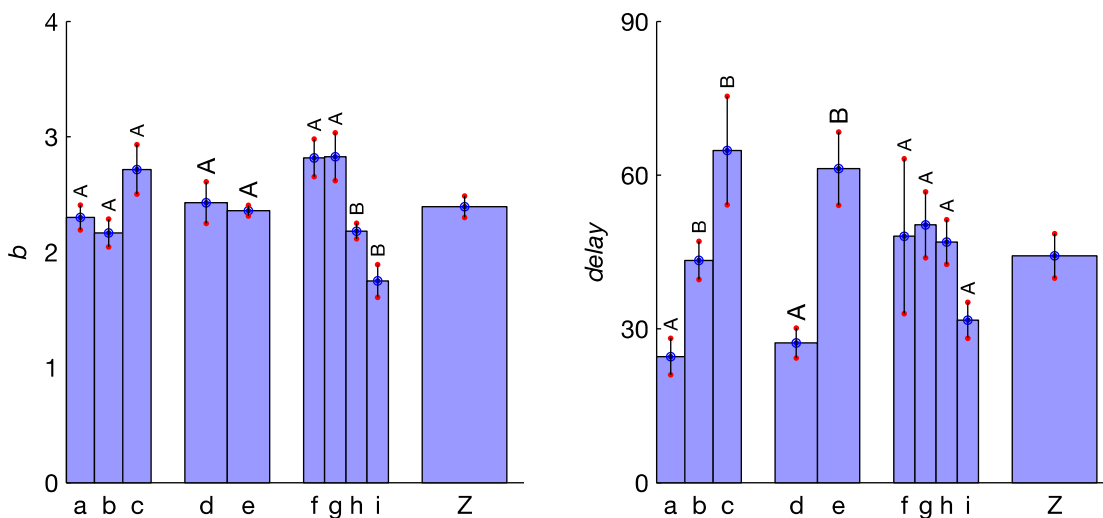

Figure 6.9 – Mean and standard error of optimized values for *b* and *delay*, after parameter value averaging of *a*.

In the case of *b*, grouping the values of *a* has had the effect of reducing the number of significance groupings by component (columns a-c) from two to one. Though the mean *b*-value for tests using LECA is still higher than for any use of Marie Curie, it is no longer significantly so. This now implies that no substrate (of those tested) has any significant effect on the storage-discharge relationship found at the effective weir that would be found between the filter sheet at the bottom of the substrate, and the drainage layer in a standard green roof. Grouping of the values of *a*, has not caused the newly-optimized values of *b* to fall into a single group with respect to test rainfall intensity. However, grouping and averaging of *a* has reduced the absolute difference in value between columns f and i, and reduced the number of significance groupings from three to two. It is not necessarily unexpected that fixing the value of *a* has not caused *b* to compensate, as the compensation effects between *a*, *b* and *delay* are limited, complex and variable in their scale.

For *delay*, grouping and averaging of *a*-values has not affected the significance groupings with respect to substrate depth. The number of significance groupings for substrate type has increased from one to two, as has the spread between each of the columns a-c. This may more strongly suggest that *delay* is affected by substrate composition, and is related to the time taken for water to percolate through the substrate from the surface to the storage reservoir. In addition to this observation, columns d and e show *delay* to relate more linearly to substrate depth than previously. For a well-mixed and homogeneous substrate sample, permeability would be expected to be constant throughout its depth and therefore, ignoring all other variables, *delay* would be expected to scale linearly with substrate depth. However, it is unusual that Marie Curie substrate coupled with a layer of SSM 45 should share a group with LECA, but not share a group with Marie Curie substrate alone, if the effects of SSM 45 are proposed to be insignificant (Section 6.5.3.3). *delay* is also now found to not depend significantly on rainfall rate. It was proposed in Section 6.5.3.3 that, if storage routing began immediately after the first water entered the reservoir, *delay* should be independent of rainfall rate; that is now observed here.

6.5.3.5   Further Parameter Averaging of *delay*

In order to further test the applicability of the model in generic situations, averaging by group was applied to the values of the *delay* parameter (Table 6.2). The reason that group averaging of *delay* was chosen over group averaging of *b* is that, following the grouping of *a*-values, the new observed values of *delay* appeared to most strongly correspond to theoretical methodology and sensible physical explanations. It was suggested by the statistical analysis in Section 6.5.3.4 that the new optimized values of *delay* were independent of rainfall rate, but dependent on substrate composition and depth. The 72 values of *delay* were therefore grouped into six: one for each tested combination of substrate type and substrate depth. It is noted that the statistical analysis suggested no significant difference between the mean value of *delay* for LECA and Marie Curie

Table 6.2 – Group-averaged parameter values for *a* and *delay*.

Configuration	*a*	*delay* (s)
MCS, 5 cm	7.900×10^{-2}	10
MCS, 10 cm	7.874×10^{-3}	35
MCS + SSM 45, 5 cm	7.900×10^{-2}	40
MCS + SSM 45, 10 cm	7.874×10^{-3}	50
LECA, 5 cm	7.900×10^{-2}	30
LECA, 10 cm	7.874×10^{-3}	100

Substrate over an SSM 45 mat. However, these were left as separate groups, as the mean *delay*-value for Marie Curie Substrate over SSM 45 was closer to the mean *delay*-value for Marie Curie Substrate alone than it was to the mean *delay*-value for LECA. All six group *delay*-values were rounded to the nearest multiple of five seconds, for an integer number of offset samples. All *a*-values were fixed as in Section 6.5.3.4.

The total time required for optimization of all 72 *b*-values, after fixing all *a*- and *delay*-values, was 1.1 seconds. Mean R_t^2 was 0.9933, while for 58 tests R_t^2 was above 0.99. It is only after grouping and averaging the values of a second parameter that some less well-fitting modelled runoff curves are produced; the lowest R_t^2 is 0.9632 for a test of 10 cm LECA under a design storm rainfall profile. R_t^2 is below 0.98 in only three other tests; the other two tests of 10 cm of LECA under the variable design storm profile and one test of 10 cm of LECA under a constant 0.1 mm/minute storm event.

Figure 6.10 plots the new model predictions for the same four profiles shown previously. For (a) no change is shown as the equivalent modelled runoff profile in Figure 6.8 was generated using, by coincidence, the mean value of *delay* for that physical configuration. Averaging of the values of the *delay* parameter therefore did not affect the *delay*-value in this specific test.

For the design storm shown in Figure 6.10 (d), value averaging of the *delay* parameter caused the modelled runoff profile to be shifted by 50 seconds rightwards along the time axis. As a result, the initial steepness of the modelled falling limb after the rainfall peak was required to be increased, to catch up with the monitored runoff profile which had already fallen significantly by the time that the time-shifted rainfall peak had passed in the model. To achieve this, the value of the *b* parameter was increased greatly, from 2.275 to 3.165. The parameter sensitivity analysis of the drainage layer (Section 5.5.4) showed that increasing the value of *b* increases the steepness of the modelled runoff curve when the volume of water in storage is greater than 1 mm; this appears to be its function here.

For the constant-intensity storm in Figures 6.10 (b), group averaging the values of the *delay* parameter results in another highly insignificant loss in modelling accuracy. The initial grouping
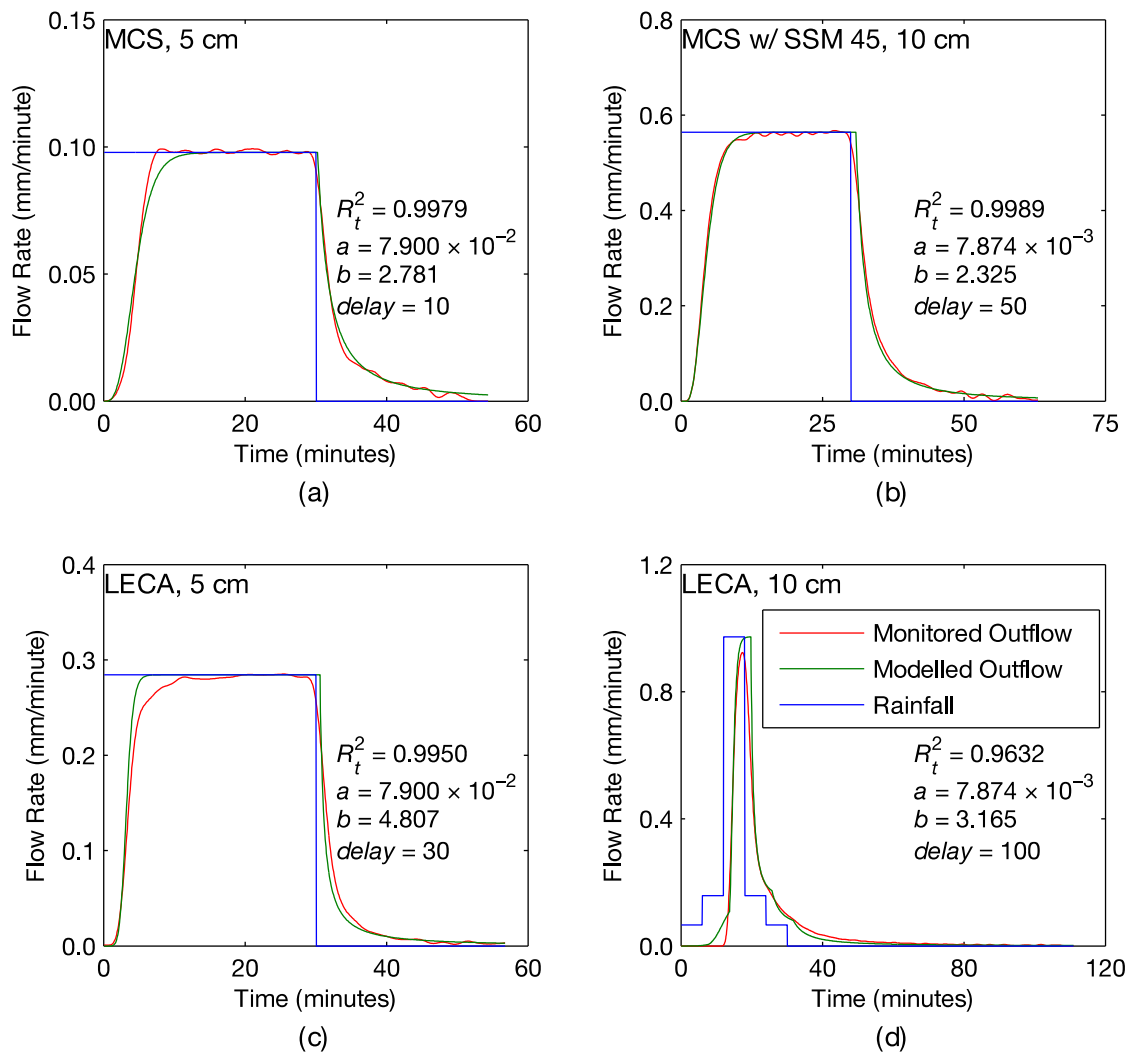
Figure 6.10 – Representative rainfall, monitored runoff and modelled runoff profiles after parameter value averaging of *a* and *delay*.

of *a*-values resulted in the value of *delay* re-optimizing itself to five seconds (one time-step) below its freely-optimized value, while the group averaging of *delay*-values results in *delay* being set to one sample above its freely-optimized value, in both cases, one sample away from its original value. Similarly, the averaged value of *a* used here is 83.3% of its freely-optimized value. Overall, group averaging of parameter values did not greatly affect the quality of the modelled runoff curve generated for this test because the freely-optimized values are, coincidentally, not very different from the averaged parameter values. The potential effects of group averaging are more clear in Figure 6.10 (c), where the values of *a* and *b* are increased by approximately 200% and 50% above their freely-optimized values, respectively. As expected, this results in an increased steepness in the rising limb of the modelled runoff profile. However, the reduction in modelling accuracy is far from significant – R_t^2 remains very high, at 0.9950.

Figure 6.11 shows the results of the statistical analysis performed on the values of *b*, the only parameter whose values were not specified prior to modelling. Again, the value of *b* is shown to
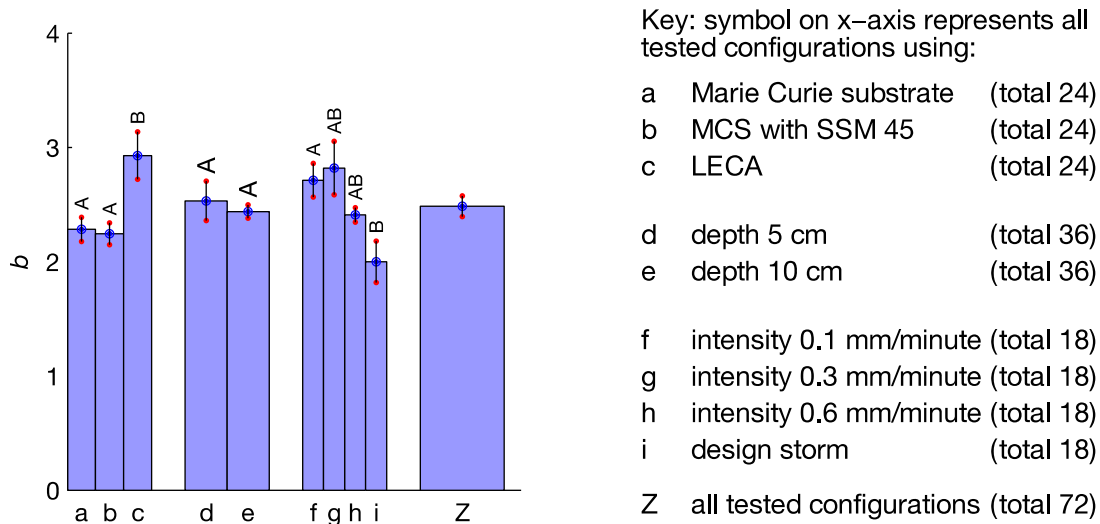
Figure 6.11 – Mean and standard error of optimized values for *b*, after parameter value averaging of *a* and *delay*.

be independent of the substrate depth, and again, this is an expected result, as the substrate depth does not affect the properties of the effective weir at the base of the simulator. The mean *b*-values for different substrates again divide into two significance groupings. Now, however, both configurations of Marie Curie Substrate (with and without the SSM 45 mat) form a single group separately of the LECA mix. Against storage routing theory, the mean *b*-value is found to be statistically different at different rainfall rates, and therefore different runoff rates, although the two significance groups now overlap considerably. Relative to the first statistical analysis, the behaviour of the *b* parameter is closer to theoretical expectations, but still does not exactly follow storage routing theory.

6.5.4 Parameter Sensitivity Analysis

It was shown in Section 6.5.3 that the runoff curves produced by the nonlinear storage routing model are of a very good fit, even after the number of free modelling parameters is reduced from three to one. The implication of this is that the actual parameter values used in the model do not necessarily need to be near to their optimized values for the modelled profile to be of use to drainage engineers. Consequently, it is suggested that generic parameter values could be suitable for a wide range of substrate types. As in Section 5.5.4, a parameter sensitivity analysis was conducted, in which modelled runoff profiles were produced and studied for four selected tests, setting the values of *a* and *b* individually and simultaneously to half and double their optimized values, while leaving *delay* unaltered. The selected tests were: the second worst-fitting test, using 10 cm LECA under a constant 0.1 mm/minute; the test with closest-to-mean *b*-value, using 10 cm Marie Curie Substrate under a constant 0.1 mm/minute; the test with closest-to-mean *a*-value, using 5 cm of Marie Curie Substrate under a constant 0.3 mm/minute; and a design storm

Figure 6.12 – Selected modelled runoff profiles using optimized values of *a*, *b* and *delay*, and fixed multiples of either optimized *a*-value or optimized *b*-value.

test, using 5 cm of Marie Curie substrate with an underlying SSM 45 mat, under a design storm. The results showing a scaling of the value of only one of the *a* and *b* parameter values are shown in Figure 6.12 and the goodness-of-fit of the modelled runoff profiles is reported in Table 6.3. For the design storm profile, ½*b* is approximately 0.86 and using this modelling value causes complex runoff to first appear at 525 samples (43 minutes and 45 seconds). The length of the full record is 727 samples (60 minutes and 35 seconds). To avoid complex runoff, a value of ½*b* = 1 is used for the design storm and the R_t^2 reported in Table 6.3 corresponds to this.

Table 6.3 – Values of *a*, *b* and R_t^2 for *a*- and *b*-value sensitivity analysis.

Configuration	*a*	*b*	R_t^2 using				
			a, *b*	*a*, ½*b*	*a*, 2*b*	½*a*, *b*	2*a*, *b*
Poor-fitting	6.07×10^{-3}	3.063	0.9895	0.9629	0.9676	0.9628	0.9663
Mean *n*	1.26×10^{-2}	2.466	0.9940	0.9762	0.9758	0.9525	0.9858
Mean *k*	6.56×10^{-2}	2.658	0.9988	0.9880	0.9956	0.9954	0.9928
Design storm	3.20×10^{-2}	1.725	0.9960	0.9494	0.9550	0.9721	0.9808

The effects of scaling one parameter can be seen to be identical to the effects observed in the previous parameter sensitivity analysis of the drainage layer (Section 5.5.4), namely that increasing the value of *a* increases the gradient of the rising limb except for where it nears equilibrium, and increasing the value of *b* initially decreases the gradient of the rising limb, then increases it when the volume of water in the storage reservoir begins to exceed 1 mm. For the substrate, the volume of water in the storage reservoir exceeds 1 mm for a greater proportion of each test's duration and so the gradient of the rising limb flattens more significantly on its way to steady-state when the value of *b* is decreased. As the volume in storage rises most slowly for the 0.3 mm/minute test, the light blue curve (representing *b* at half its optimized value) remains ahead of the dark blue curve (representing *b* at double its optimized value) almost until steady-state runoff is reached. For the falling limb, similar trends are observed as the values of *a* and *b* are varied: increasing the value of *a* increases steepness until equilibrium is neared and increasing the value of *b* results in a steeper curve until the volume in storage falls below 1 mm. A sharp knee resulting from this effect can be seen in both top plots for *b* set at double its optimized value.

The results of a simultaneous scaling in the value of both parameters are shown in Figure 6.13. Though not as visually obvious, the overall results are as observed in Section 5.5.4 – scaling both parameters simultaneously results in both effects occurring simultaneously. The effect of changing the value of the *delay* parameter is to translate the modelled runoff curve in time; no further analysis of this effect is required.

6.6   Nonlinear Storage Routing at One-Minute Resolution

6.6.1   Motivation
As was the case in Section 5.6, the motivation for testing the nonlinear storage routing method at one-minute resolution was to assess its applicability and accuracy at a lower time resolution that is more realistically comparable to other monitoring systems and software packages.

6.6.2   Additional Preparatory Work
To convert the data records to a one-minute temporal resolution, each group of 12 consecutive rainfall or runoff values in each processed rainfall and runoff record was summed and combined into one.

To be scaled to a one-minute resolution, the values of *a* found in Section 6.5 must be multiplied by 12, while the corresponding values of *delay* must be divided by 12. However, as *delay* must always take an integer value, no set of parameter values optimized in Section 6.5 is fully suitable for conversion to one-minute resolution.
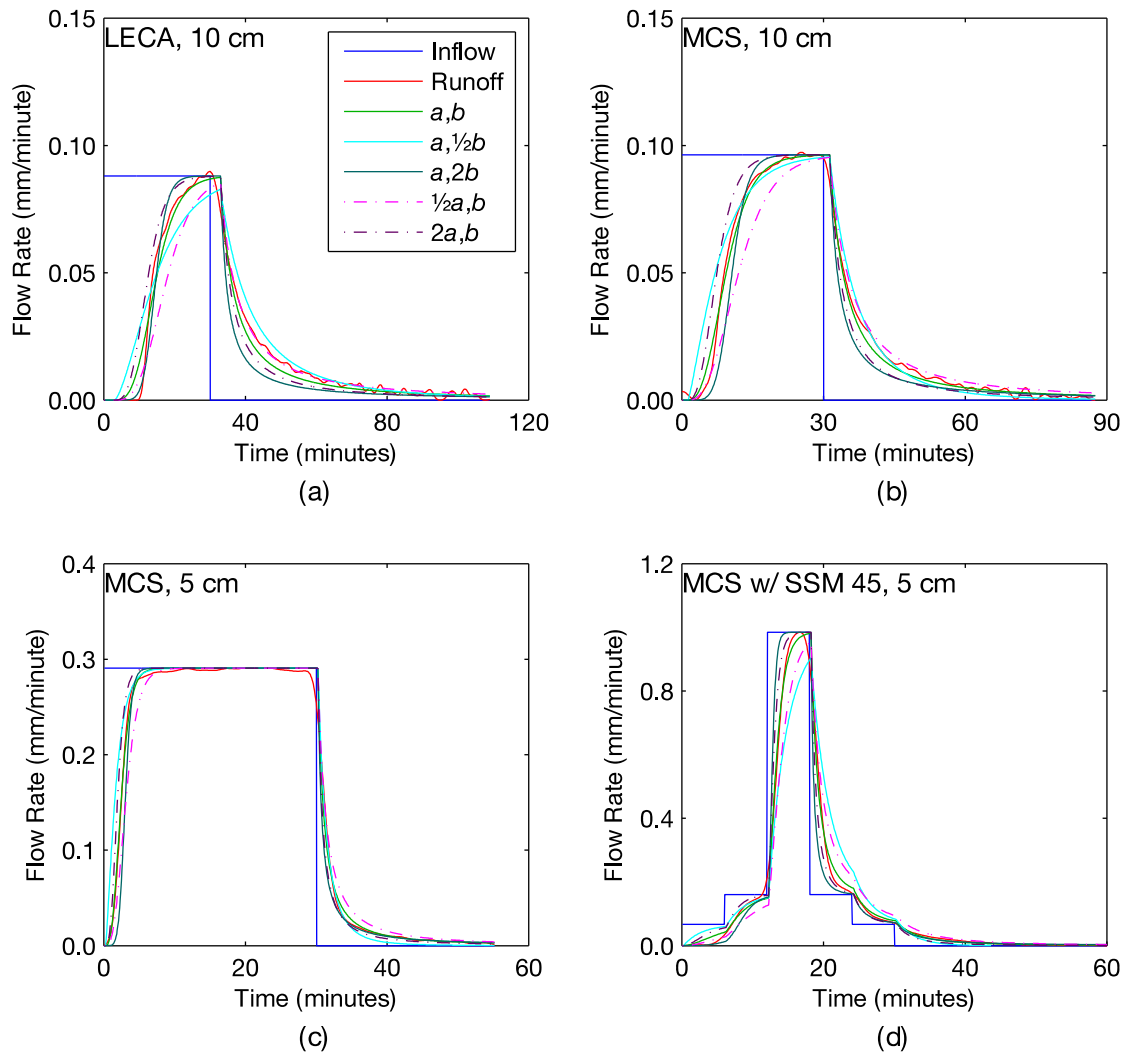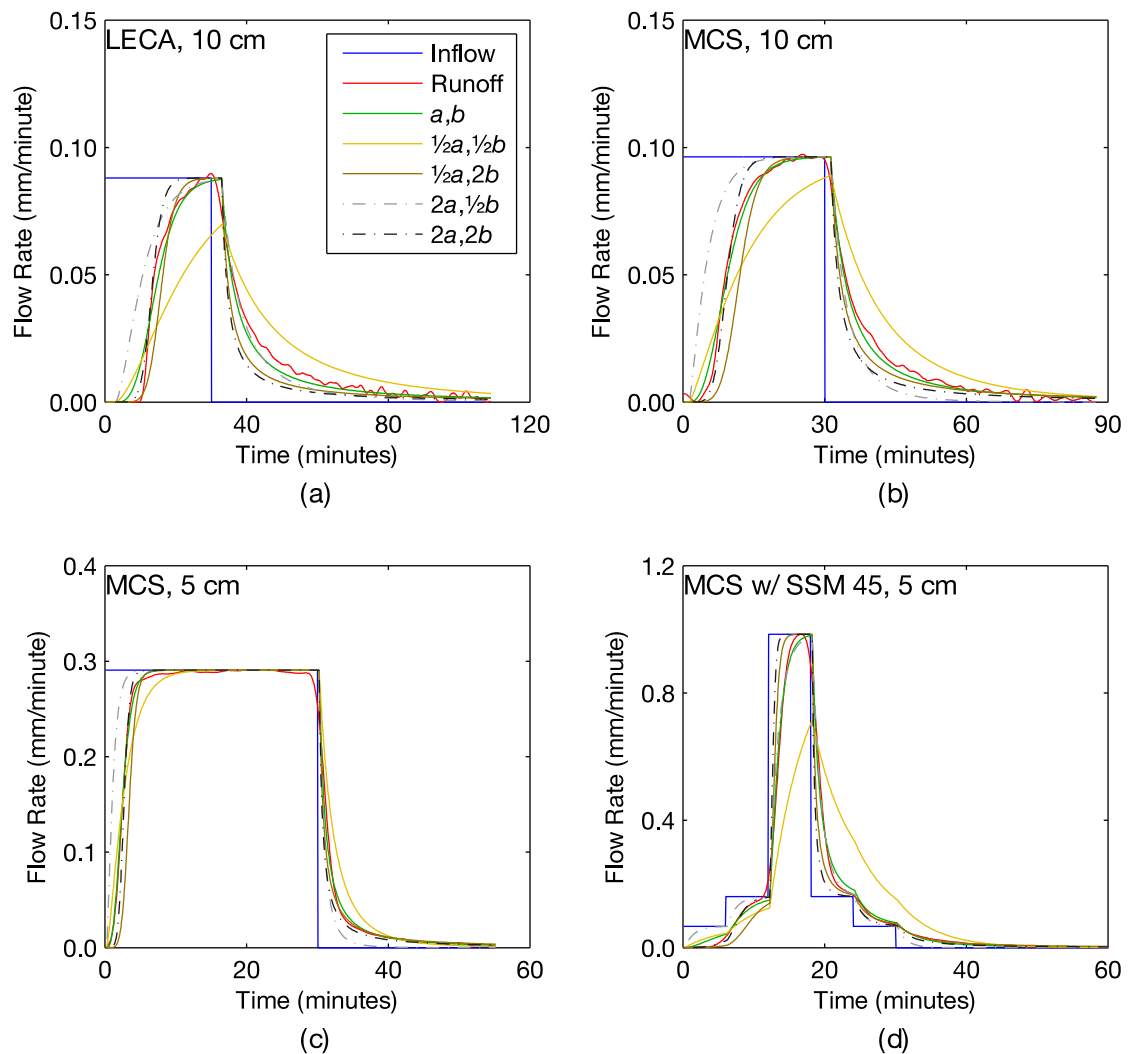
Figure 6.13 – Selected modelled runoff profiles using optimized values of *a, b* and *delay*, and fixed multiples of optimized *a*- and *b*-values simultaneously.

An optimization of the five-second resolution data set was run again, this time with *delay* permitted to take values of 0, 60, 120, 180, 240 or 300 seconds only. *a* and *b* were freely optimizable within the original bounds and the original starting values were used for both. Reducing the number of possible values available for the *delay* parameter did not have significant consequences on the accuracy of the modelling – Mean R_t^2 was almost unaffected at 0.9967, while minimum R_t^2 was exactly the same, at 0.9876. For all 84 optimizations, the optimal one-minute resolution value of *delay* was the closest possible to that found at a five-second resolution. In four test cases, the original *delay*-value was exactly midway between two possible minute values. Two of these were rounded up and two were rounded down.

6.6.3   Applicability of Scaled Parameters at One-Minute Resolution

The parameters found in the optimization run in Section 6.6.2 were multiplied or divided by 12 as appropriate, to scale the time unit of each parameter to minutes. These values were input

directly to the storage routing model with their corresponding rainfall profiles. Monitored and modelled outflow profiles were compared, and goodness-of-fit evaluated by R_t^2.

For all 84 tests, the mean R_t^2 is 0.9748, rising to 0.9806 when only the 72 tests which actually included substrate are considered. The lowest R_t^2 for tests including substrate is 0.8992, higher than the lowest R_t^2 observed for the drainage layer at a one-second resolution. The modelling results for the four representative tests (also depicted in Figure 6.3, Figure 6.8 and Figure 6.10), are shown in Figure 6.14.

In three out of 84 tests (all empty chamber, 0.6 mm/minute intensity), the model predicted more runoff for the time-step immediately after the end of the storm than was available in storage. This was prevented by controls on the storage depth, which allowed as much runoff as physically possible in that time-step and then treated the storage as fully depleted. Oscillations, all decaying, were also present in six other modelled runoff profiles, though the model did not attempt to

Figure 6.14 – Representative rainfall, monitored runoff and modelled runoff profiles using optimized *a*, *b* and *delay* parameters, scaled from a five-second to one-minute resolution.
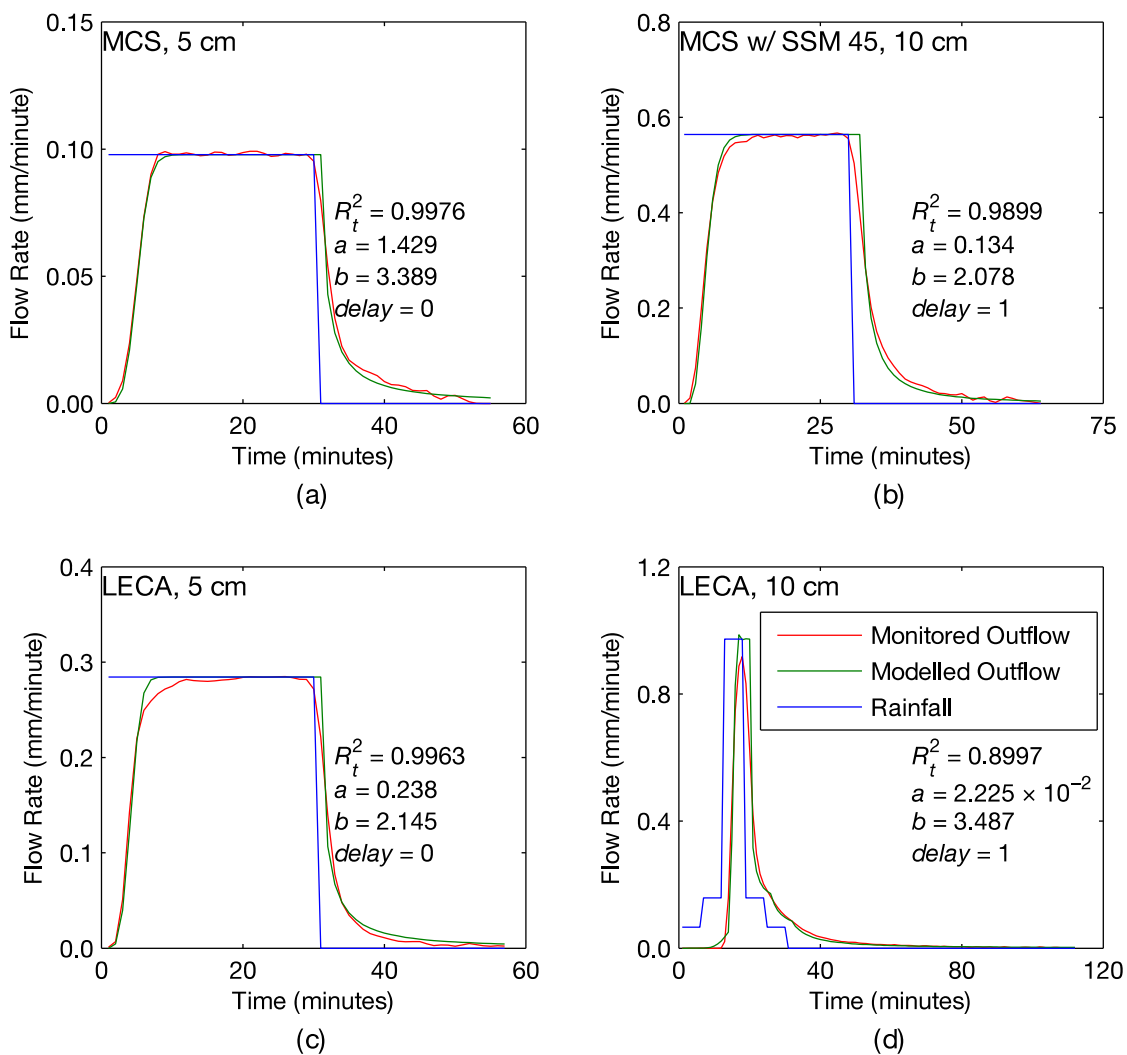
produce more runoff than was available in storage in any of these cases. All nine oscillating profiles were for the empty chamber, specifically for the three test configurations with the highest overall rainfall rates. It has already been shown for the drainage layer that the most unstable models are to those tests with the shortest travel times, and the same appears to be true here. However, the formation of instabilities in modelling the response of the empty chamber is not considered to be a weakness of the substrate modelling method. It is noted that instabilities never formed when modelling the runoff profiles of tests that actually included substrate. Furthermore, as the mean goodness-of-fit for substrate tests remained high, the parameters derived for modelling at a 5-second time step can be considered scalable up to a 60-second time step.

6.7   Hydrus-1D (Richards' Equation)

6.7.1   Overview

Hydrus-1D (Šimůnek *et al.*, 1998) is a public domain and open source Windows software package, published by PC-Progress, for modelling water flow, heat and solute transport in variably-saturated media. The 1D in its name refers to its discretization of the media in one spatial dimension. For the applications considered in this chapter, only water flow is required to be modelled. To do this, Hydrus-1D numerically solves the Richards' equation for saturated-unsaturated water flow to produce its modelled runoff profiles. The latest update as of May 2013 is version 4.16, which was released in February 2013; this version was used throughout this thesis.

A similar package, Hydrus-2D/3D, also published by PC-Progress, can discretize variably-saturated media in two or three spatial dimensions; this is distributed under commercial licensing agreements. The commercial HYDRUS package was not used in this thesis, as the potential gains to be made in modelling water flow were not considered to justify the costs of licensing.

For the prediction of time-series runoff profiles, Hydrus-1D requires information about the porous medium, which is given through six parameter values. Three: Residual water content (θ_R), saturated water content (θ_S) and saturated hydraulic conductivity (K_S), can be measured, while the other three: α, n and pore connectivity (l), are empirical. Suggested values for all three empirical parameters are given by Hydrus-1D for a selection of soil types or, if these are not appropriate, a neural network prediction tool (ROSETTA Lite) is included, which estimates five of the six parameters (all except pore connectivity) from either the input of a textural class or the input of a percentage sand, silt and/or clay with the option to additionally specify bulk density, water content at 33 kPa and water content at 1500 kPa. For both the Marie Curie Substrate and the LECA mix, all parameters were first estimated from percentage sand and bulk density by ROSETTA Lite, then θ_R and K_S were adjusted to values determined by laboratory testing in

Table 6.4 – Modelling parameters used in Hydrus-1D.

Substrate	θ_R	θ_S	α	n	K_S	l	θ_{field}
Marie Curie Substrate	0.0324	0.575	0.0450	2.9961	0.053	0.5	0.3692
LECA	0.1643	0.368	0.1033	1.6633	0.049	0.5	0.3295

Sheffield. θ_S was adjusted until the command "Set Initial Conditions Equal To field Capacity" in the soil profile editor gave the field capacity determined in the same laboratory testing. Table 6.4 shows the values used for both substrates. No attempt was made to model the behaviour of the SSM 45 mat as it had already been shown to affect runoff minimally and is not a soil-type material.

In addition to the information given and/or solved for above, the depth of the medium, the number of materials, time discretization, the choice of hydraulic model, boundary conditions, precipitation, evaporation and the initial water content profile are also required to be input. For each test, the depth of medium was set to either 5 or 10 cm and the number of materials was set to 1; the SSM 45 mat is not considered as a separate material. Though Hydrus-1D is able to vary its modelling time step to trade speed against accuracy, constant time steps of 5-second duration were specified, to allow direct comparison with the nonlinear storage routing method, and to allow the generation of an R_t^2 statistic relating monitored and modelled runoff. A single-porosity van Genuchten-Mualem model was specified, as used by Hilten *et al.* (2008) and Palla *et al.* (2012). The upper and lower boundary conditions were set to "atmospheric with surface layer" and "seepage face", respectively. Precipitation profiles were set individually for each test; in all cases they were the same profiles as used in the nonlinear storage routing tests. Evaporation was set to zero and the initial water content of the substrate sample was set uniformly to the field capacity found by testing in Sheffield to FLL standard. This was 0.3692 for Marie Curie Substrate and 0.3295 for LECA. The tests of the empty chamber were not modelled in Hydrus-1D, as the depth of medium for these tests was effectively zero.

6.7.2   Applicability of Method

The time required for the generation of each runoff profile was around 0.5 seconds. Each test was set up manually; batch processing is not possible. Hydrus-1D saves its previous state after every test and on exit so, in many cases, manually setting up a test simply required the rainfall profile, final time step and/or substrate depth to be changed. A re-specification of the substrate parameters was required whenever the substrate type was changed. The lack of batch processing is not a limitation of the Richards' equation itself, but rather of Hydrus-1D, and a different solver may allow automated batch processing. While none of the manual inputting is particularly difficult or time consuming, a lot of interaction and time with the Hydrus-1D software was required, in comparison to the nonlinear storage routing code, to generate the same results. It is,
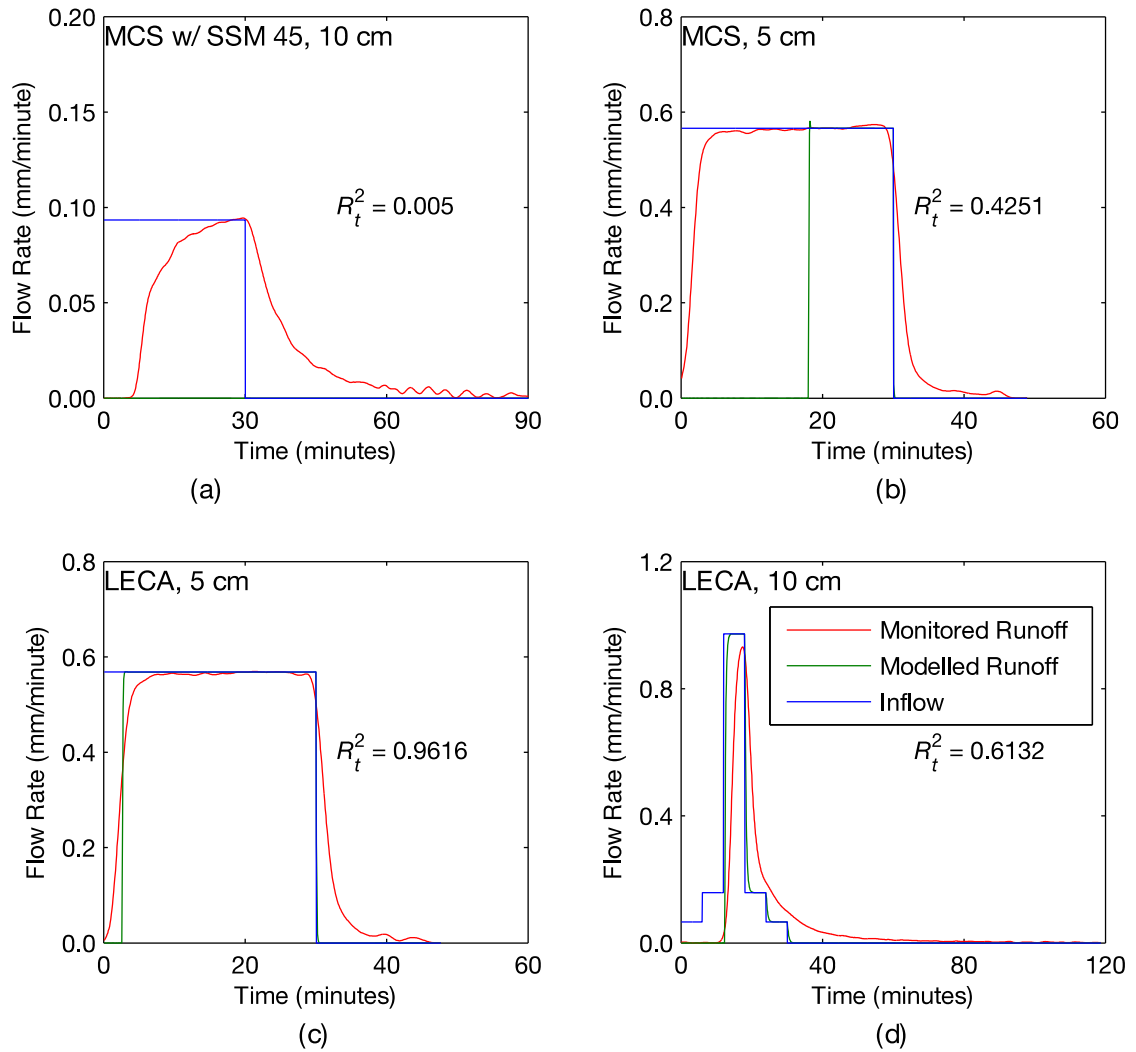
Figure 6.15 – Representative rainfall, monitored runoff and modelled runoff profiles produced by Hydrus-1D at a five-second resolution.

however, appreciated that few practical applications will entail batch processing on the large scale necessary for the analysis of this experimental programme.

Four modelled runoff profiles are shown in Figure 6.15, demonstrating a typical (zero-runoff) model for Marie Curie Substrate (a), one test with Marie Curie Substrate for which some runoff was predicted (b), the best-fitting test (c) and a modelled runoff profile showing some routing effects (d).

In 42 of the 48 tests using Marie Curie Substrate, Hydrus-1D produced a modelled runoff profile that showed near-zero water flux through the bottom of the substrate for the entire test duration. The only exceptions were for the six tests of 0.6 mm/minute constant intensity rainfall over a 5 mm substrate depth, which showed an initial section of near-zero runoff, followed by an immediate increase to the steady-state runoff rate after approximately 20 minutes, followed by an immediate drop to a near-zero runoff rate immediately following the end of the rainfall event

(Figure 6.15 (b)). Subtracting the modelled runoff depth from total rainfall depth for these tests gives a mean of 10.21 mm water stored per test, with almost zero standard deviation. A stored volume of 10.21 mm is equivalent to 0.204 mm water/mm substrate. This is very near to the difference between the substrate's field capacity, 0.3692, and its saturated water content, 0.575. The implication of this is that Hydrus-1D models the Marie Curie Substrate, which was initially set to field capacity, as a reservoir able to store water up to its saturation level, but discharging any further water according to the relationship $I = Q$. This model seems extremely unrealistic. Nevertheless, it is notable that Hilten *et al.* (2008) produced modelled green roof runoff profiles of the same form using Hydrus-1D: no runoff before saturation, followed by an (almost) exact overlap between rainfall and modelled runoff. This also explains why no runoff was modelled when 0.6 mm/minute storms were applied over 10 cm of Marie Curie substrate – the now-doubled storage capacity was of a larger depth than the test rainfall event.

For the 12 tests using 5 cm of LECA mix, modelled runoff was first produced when the volume of water in storage reached a value in the range 1.466-1.481 mm. This is slightly lower than the 1.925 mm storage depth that would be expected given the difference between field capacity, 0.3295, and saturated water content, 0.368 in 50 mm of substrate. The existence of a delay between the start of rainfall and the start of modelled runoff is not necessarily inappropriate, and is in fact visible in the monitored runoff records for these tests, particularly at lower rainfall intensities. This is assumed to be due to the time required for water to percolate through the medium. The three highest R_t^2 values achieved by Hydrus-1D are around 0.961, all for the three tests of 5 cm LECA under a 0.6 mm/minute constant intensity event. Even though the modelled runoff profiles are visually too steep in all cases (Figure 6.15 (c)), the R_t^2 is high due to the modelled rising limb being well positioned, as the 1.47-1.48 mm of water stored before runoff is produced, is near in value to the difference between cumulative rainfall and monitored runoff at steady-state. R_t^2 values for other tests using 5 cm of LECA reduce as the difference between cumulative runoff and cumulative rainfall at steady-state moves away from ~1.47 mm.

For the 12 tests using 10 cm of LECA mix, modelled runoff was first produced at 1.551-1.561 mm, far below the 3.85 mm difference between field and saturation water contents. In addition, the modelled runoff curves showed some routing, with modelled runoff at approximately 50% of the steady-state rate four samples after the end of the rainfall event, and approximately 10% of the steady-state rate eleven samples after the end of the rainfall event. Routing is also shown in the rising limb, which rises from half to full steady-state value over 12-20 samples. However, even though the substrate is shown to offer some attenuation, the modelled runoff profile is not attenuated enough to accurately represent the actual behaviour of the LECA mix. R_t^2 values for these tests are typically lower than for their equivalents at 5 cm substrate

depth, due to the increased difference in the attenuation between the monitored and modelled rising and falling limbs.

6.7.3   Inverse Solution

In addition to predicting the movement of water resulting from given boundary conditions and properties of the medium, Hydrus-1D can solve the inverse problem – predicting properties of the medium from given boundary conditions and known fluxes. In this experimental programme the rainfall and runoff records are known for each test. Other, easily quantifiable properties of the medium (e.g. saturated hydraulic conductivity) can be fixed, if they are known. This reduces the number of soil parameters that Hydrus-1D must optimize. If approximate values are known, upper and lower bounds can also be specified, to avoid unrealistic predictions that also happen to coincidentally produce accurate results.

In application to this experimental programme, the runoff predictions, to which Hydrus-1D attempts to fit its modelled runoff profile, must be manually inputted for each test. Pasting data into Hydrus-1D from an external source fills as many fields as are currently specified, without automatically increasing the number of fields to accept all of the pasted data. As a compromise between the level of information made available to Hydrus-1D and the time required to manually add large numbers of fields, preliminary studies into the inverse problem used 16-30 data points per test, sampling the cumulative runoff at three-minute intervals up to 45 minutes, then at five-minute intervals from that point to the end of the record. Precipitation profiles were set individually for each test; in all cases they were the same profiles as used in the nonlinear storage routing tests.

These preliminary studies were not considered to be very successful. In most cases, residual water content would tend towards its upper bound and saturated water content would tend towards its lower bound, regardless of where these were set. The range between θ_R and θ_S could be reduced far below the range observed between θ_R and θ_{Field} in laboratory testing if the boundaries were set to allow this. In addition, the optimized value of n was rarely considerably different from its starting value, again regardless of the tested starting values. This suggests that either the runoff profile is very insensitive to the value of n or the starting estimate is required to be near to its real value. An alternate optimization method, such as *lsqcurvefit* could potentially be employed, as this function can produce optimized values that differ greatly from their starting estimates. However, use of *lsqcurvefit* would require the entire Hydrus-1D water modelling code to be rewritten in Matlab script, tested for modelling robustness and then integrated with the *lsqcurvefit* solver. While potentially allowing a more accurate model, still grounded in a physical basis, the required work to achieve this is beyond the scope of this thesis.

6.8   Further Study of the SSM 45 Moisture Retention Mat

The substrate experimental programme was devised partly to investigate the potential for runoff to be detained further by the addition of a non-substrate material, in this case a ZinCo SSM 45 protection and moisture retention mat placed below the substrate. It has so far been shown that including this extra component has little effect on the time-series runoff profile. At the beginning of all tests, the mat is retaining the maximum amount of water possible under gravity. It is therefore entirely possible that, in this state, the mat would not impede the flow of water significantly. However, the mat may contribute to green roof performance through retention, rather than detention. According to the FLL standard determination of field capacity for a substrate, six samples of SSM 45 mat were immersed fully for at least 24 hours and drained for two hours on a flat rack. All were found to have field capacities in the range 0.7-0.8, far higher than possible with any substrate. This behaviour superficially suggests that a thick layer (e.g. 25 mm) of this material could be used to provide all of the water retention benefits of an extensive green roof at a lower mass. However, the very high field capacity is unlikely to scale linearly with material depth and runoff from larger storms will not be greatly attenuated. Furthermore, a number of other benefits that would be given by a green roof, such as carbon dioxide sequestration, urban greening and provision of habitat, are not possible.

6.9   Conclusions of Substrate Model Selection Study

Runoff profiles were recorded, at high temporal and depth resolution, for 84 tests on green roof substrate configurations, representing three repeats each of 28 combinations of rainfall profile, substrate depth and substrate type/configuration, including control tests with no substrate. The amount of lag introduced by a substrate layer, measured by centroid-to-centroid delay, ranged from 86 to 828 seconds, with a mean of 271 seconds, indicating that approximately 2.5 times as much lag is introduced by the substrate in comparison to the drainage layer.

The monitored runoff profiles were proposed to be modelled by a nonlinear storage routing model, as used on the drainage layer (Sections 5.5 and 5.6). The same governing equations were optimized by *lqscurvefit* to find the values of *a*, *b* and *delay* minimizing the sum-of-squares error for each modelled runoff profile in relation to that monitored. The mean R_t^2 across all tests was very high, at 0.9975, and approximately 1.4 seconds was required per optimization.

Statistical analyses were performed in SPSS 19 in order to identify which of the test variables had no statistical influence on the optimized values for *a*, *b* and *delay*. After the parameter value of *a* was established to be statistically independent of all tested variables except for substrate depth, the mean values of *a* were averaged at each tested substrate depth to give two averaged values for *a*. The optimization routine was repeated with the value of *a* fixed at whichever

averaged value was appropriate to the depth of the substrate being tested. Mean R_t^2 was reduced, though with no great loss of modelling accuracy, to 0.9953, while optimization time was approximately halved. Grouping and specifying of *a*-values removed the dependence of newly-optimized *b*-values on substrate type and depth, and caused *delay*-value to become independent of rainfall rate.

Further parameter value averaging was performed on the values of *delay*, and the optimization routine was run again, with specified values for *a* and *delay*. Goodness-of-fit was slightly reduced further but remained very high (mean $R_t^2 = 0.9933$, minimum $R_t^2 = 0.9632$). In contravention of storage routing theory, the newly-optimized parameter values of *b* were not entirely independent of rainfall rate. It is possible that the formation of drops at the base of the rainfall simulator chamber, rather than the free-flow of water that would be expected at a typical weir, was the cause of this contravention.

A parameter sensitivity analysis was performed, in which the values of the *a* and *b* parameters were halved and doubled, and the effects on the modelled runoff profiles observed, for four chosen representative tests. The conclusions found were similar to those found when the same analysis was performed on the drainage layer (Section 5.5.5). However, due to the generally larger quantities of water in the substrate storage reservoir relative to the drainage layer, increasing the value of *b* tended to correspond to increasing the steepness of the rising limb earlier into the test.

The storage routing method was shown to be successful at five-second resolution. Following this, the optimized parameter values derived at that resolution were scaled to a one-minute resolution more common in typical monitoring systems, by division or multiplication by 12 as and where appropriate. These parameter values were input directly to the model along with downsampled versions of the existing 84 rainfall and monitored runoff profiles. Modelled runoff profiles were produced in all cases, with mean $R_t^2 = 0.9806$ and minimum $R_t^2 = 0.8992$, when only tests including substrate are considered. In contrast to the drainage layer study, scaling parameter values optimized for the substrate does not greatly affect the applicability of the nonlinear storage routing model.

Hydrus-1D, a software package that solves the Richards' equation for variably-saturated media in one dimension, and therefore is based more explicitly around physical processes than the nonlinear storage routing approach used here, was assessed for its comparative performance in the modelling of water flow through substrate. Residual water content, saturated water content and saturated hydraulic conductivity were found for both substrates through laboratory testing, while α (inverse of air-entry value) and *n* (pore-size distribution index) parameter values were

predicted by ROSETTA Lite 1.1, through neural network analysis of a very large data set of mainly American and some European soils. For 42 of the 48 tests using Marie Curie Substrate, Hydrus-1D predicted zero runoff. It was found that in all of the runoff predictions made for Marie Curie Substrate all rainfall was retained until saturation was reached, and all remaining rainfall was discharged as runoff according to rainfall rate = runoff rate. Though this was clearly not observed in the recorded runoff profiles, the highly unrealistic results found here were very similar to those published by Hilten *et al.* (2008). For the LECA mix, slightly more realistic runoff profiles, with noticeable rising and falling limbs at 10 cm substrate depth, were produced, and runoff began before the substrate reached saturation. However, the monitored level of attenuation introduced by the LECA mix was not well-simulated in Hydrus-1D. The reasons for the relative failure of a completely process-based model are probably due to unrealistic parameterization – the observed θ_R, θ_S and K_S values were combined with predicted α and n parameter values belonging to a soil with completely different values for θ_R, θ_S and K_S. Marie Curie Substrate and LECA mix are not at all typical of soils and it is certainly possible that the predicted values of α and n apply to some material completely unlike either. Preliminary attempts at predicting the substrate property parameters from known rainfall and runoff profiles were not successful. It is proposed that a different optimization routine may produce more realistic runoff curves and parameter values, but the work required to implement such a routine is beyond the scope of this thesis.

It was shown that the inclusion of a layer of SSM 45 moisture retention mat under the substrate had negligible effect on the monitored runoff profile in response to any storm. However, the field capacity of SSM 45 was found to be very high, in the range 0.7-0.8 even with a free-draining base. Though this suggests that the inclusion of extra SSM 45 layers may be beneficial for retention, the high field capacity is unlikely to scale to greater material depths and very limited detention will be provided when the storage depth is exceeded.

Table 6.5 presents a small set of scale, exponent and *delay* parameter values for nonlinear storage routing at five-second resolution, which is applicable to all substrate configurations tested here and potentially to similar untested configurations. The values given for the exponent parameter, *b*, are averaged across inflow rates for each of the significance groupings found after grouping

Table 6.1 – Suggested scale and exponent parameter values for nonlinear storage routing at five-second resolution.

Substrate Depth	Substrate Type					
	Marie Curie			LECA mix		
	a	*b*	*delay*	*a*	*b*	*delay*
5 cm	0.0790	2.23	25	0.0790	3.13	30
10 cm	0.0079	2.29	45	0.0079	2.73	100

and averaging of *a* and *delay* parameter values. Though it is not strictly statistically valid to do this, the model was shown in Section 6.5.4 to be insensitive to specific parameter values. Therefore grouping and averaging of values of *b* across inflow rates is not expected to greatly affect modelling accuracy. It is shown in Section 6.6 that the parameter values derived for a five-second resolution data series can be scaled for applicability at one-minute resolution by dividing or multiplying by 12, as appropriate. It is later suggested in Chapter 7 that parameter values for the Marie Curie substrate give acceptable results when used as estimates for modelling other brick-based substrates.

Overall, it is concluded that, for the two-stage model that will be tested in Chapter 7, nonlinear storage routing is the most suitable of the two methods tested by which to model water flow through the substrate.

A Two-Stage Runoff Detention Model for a Green Roof

7 Application of Drainage Layer and Substrate Models to Green Roof Systems

7.1 Chapter Overview

This chapter considers the suitability of combining the substrate model, selected in Chapter 6, in series with the drainage layer model, selected in Chapter 5, to predict the runoff response of two-layered green roof systems, consisting of unplanted substrate over a drainage layer. The runoff response of a control system, based on previously-studied configurations of substrate and drainage layer was tested under laboratory conditions. The rainfall profiles applied during these tests were input to the combined two-stage substrate and drainage layer model to give predictions for runoff profiles, which were compared to the monitored profile shapes. The two-stage model was then applied to predict the runoff response of three monitored green roof test systems, using untested substrate and drainage layer configurations, in response to real storms. The predicted runoff profiles were evaluated for their accuracy in comparison to the observed runoff profiles.

The laboratory-based experimental validation of this model, discussed in Section 7.3, forms the basis of a conference presentation given in March 2013 at the *Marie-Curie IAPP 'Green Roof Systems' Project, The Green Roof Research Conference* in Sheffield, UK (Vesuviano, 2013). It also forms the basis of a conference paper (Vesuviano *et al.*, 2013) presented in June 2013 at the *8th International Conference Novatech* in Lyon, France, and selected by the scientific committee of *Novatech* as suitable for publication in the journal *Water Science and Technology* (Vesuviano *et al.*, in press). An extension of the Hadfield-based experimental validation and model adaptation (Section 7.4) forms the basis of a journal article, submitted to *Hydrological Processes* in November 2013.

7.2 Two-Stage Substrate and Drainage Layer Model

It was concluded at the end of Chapter 5 that nonlinear storage routing was the most suitable method of those tested for modelling the runoff response of the drainage layer resulting from an inflow event. Nonlinear storage routing was also concluded, at the end of Chapter 6, to be the most suitable method, of those tested, for modelling the runoff response of the substrate resulting from a rainfall event. As the interface between these two green roof components only allows the flow of water in one direction (down), it is proposed that combining the substrate model in series
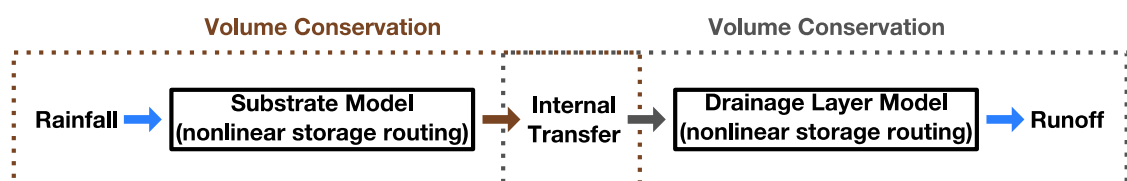

Figure 7.1 – Representation of two-stage model.

with the drainage layer model accurately represents the internal processes of a green roof. By combining the two models in series, the outflow from the substrate model becomes the inflow to the drainage layer model (Figure 7.1).

As when modelling either component separately, the accuracy of the modelled runoff profile is dependent upon the values of *a*, *b* and *delay* used in both stages of the model. In order to test the generic applicability of the modelling stages, the parameter values used in Chapter 7 are not optimized to the tested systems, but are instead the values found for the system components when tested in isolation.

7.3   Laboratory Validation

7.3.1   Experimental Setup

The two-stage storage routing model was initially tested and validated under laboratory conditions for three reasons: to remove or greatly limit the impact of environmental variations; to allow constant and design storm profiles to be applied and consistently repeated; and to match the system configuration to previously tested substrate and drainage layer components, hence to known values of *a*, *b* and *delay*. The test system, as used in this validation programme, consisted of 10 cm of Marie Curie substrate, uncompacted, over a Systemfilter SF filter sheet, over a Floradrain FD 25 drainage layer over an SSM 45 protection mat. This system was built into the large rainfall simulator (described in detail in Chapter 4). The full, five-metre length of the simulator was used at a channel slope of 1.15°.

Five rainfall profiles, all of duration 60 minutes, were tested three times each. These were: 0.3 mm/minute constant intensity; 0.6 mm/minute constant intensity; 1.2 mm/minute constant intensity; 1-in-10 year 75% summer storm for Sheffield, UK of total depth 21.94 mm; and 1-in-100 year 75% summer storm for Sheffield, UK, of total depth 44.81 mm. The total depths of the two variable-intensity storm profiles were calculated by methods given in the Flood Estimation Handbook (NERC, 1999) and their profiles discretized into 15 steps of four minutes each (Table 7.1) according to the Flood Studies Report (NERC, 1975). The valve timings necessary for the dripper networks to produce the discretized profiles were calculated using the "calc_rain" script (see Section 7.3.2). Exactly 16 hours of extended detention time was allowed after each rainfall

Table 7.1 – Discretization of design storm profiles.

Step Number	8	7,9	6,10	5,11	4,12	3,13	2,14	1,15	Total Depth
Fraction of total depth	$^{23}/_{100}$	$^{31}/_{200}$	$^{1}/_{15}$	$^{31}/_{600}$	$^{11}/_{300}$	$^{2}/_{75}$	$^{1}/_{40}$	$^{7}/_{300}$	1
1-in-10 year intensity (mm/minute)	1.262	0.850	0.366	0.283	0.201	0.146	0.137	0.128	21.94 mm
1-in-100 year intensity (mm/minute)	2.577	1.736	0.747	0.579	0.411	0.299	0.280	0.261	44.81 mm

event, before the next was started. This was considered sufficient to capture all runoff resulting from one test, without allowing significant evaporation to take place. The order of tests was randomized to minimize any possible systematic effects imparted from one test to the next. Prior to the first test, a constant 1.2 mm/minute rainfall was applied for 60 minutes and the system subsequently allowed to drain for 16 hours. This ensured that the system would be at field capacity at the beginning of the first test. The entire test programme was conducted over the period 15-26th September 2012 under the observation of Fred Sonnenwald, a PhD student seconded to ZinCo from the University of Sheffield. The thesis author was not present for the tests, though he was responsible for defining the test programme.

7.3.2 Additional Modifications to the Large Rainfall Simulator

Further modifications were made to the rainfall simulator throughout spring and summer 2012, after the experimental programme described in Chapter 5 was completed. These were primarily directed towards improving the runoff collection system and the dripper network control system. The thesis author was not significantly involved in the design, installation and testing of these modifications.

To allow tests with greater rainfall and runoff depth to be performed, the 50-litre runoff collection barrel, as used in the drainage layer experimental programme, was replaced by a garden water barrel of 205 litres capacity. Within this barrel was fitted a Gardena Comfort 5000/5 (Art. 1734) pump attached to a Gardena Suction Filter with Backflow Preventer (Art. 1728). Activating this pump during a test allows an effectively infinite depth of runoff to be monitored. In order to minimize surface waves in the barrel, the downspout leading from the gutter into the barrel was fitted with a pipe, terminating below the permanent low water level, similarly to the small rainfall simulator. The pressure transducer was housed inside a third pipe, opening below the permanent low water level, in order to further minimize the effect of pressure fluctuations associated with surface waves directly above it. A calibration curve between pressure and volume (reproduced in Figure 7.2) was produced by the seconded PhD student.

To both simplify and improve the functionality of the rainfall control system, a Campbell Scientific SDM-CD16AC AC/DC Relay Controller was connected to the existing Campbell Scientific CR1000 data logger. This controller allows the data logger to open and close the electromagnetic valves gating each dripper network. The advantages of this system over the Netafim MiraclePlus AC6 controller installed in 2011 are that one, two or three valves, each with different timed opening and closing patterns, can be operated simultaneously, and that the "reset" time associated with the Netafim controller is eliminated. The Netafim controller was removed from the simulator control system. The relay also allows the data logger to activate the pump in the collection barrel when a trigger level is sensed by the pressure transducer, and to record flow
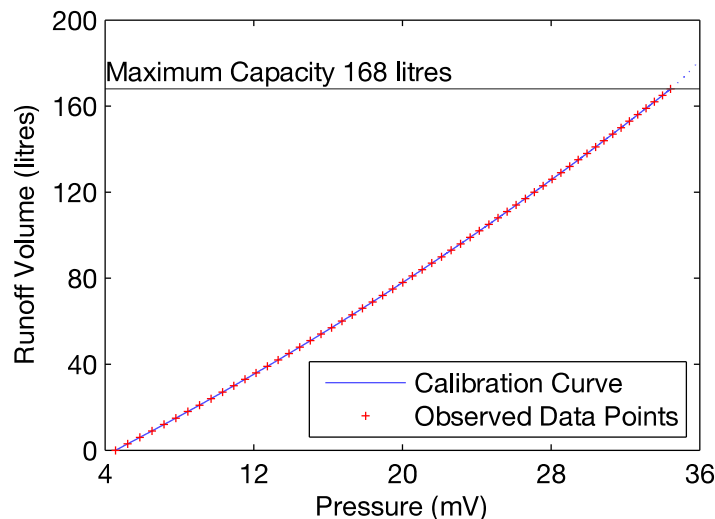
Figure 7.2 – Runoff volume vs. recorded pressure for new collecting barrel for large rainfall simulator.

data from the Badger Meter located before the electromagnetic gate valves. Previously, this data was recorded by a separate Ahlborn Almemo data logger; this has also been removed from the control system.

To make use of the functions of the CR1000 data logger, new code was written to control the three dripper networks separately, activate the pump, record pressure from the pressure transducer, record flow rate from the flow meter and chain together multiple tests with extended detention periods between them. A new script, "calc_rain", was written, to transform a desired rainfall profile into an equivalent time-series of valve operations. The script algorithm allocates as much of the event time as possible to valves being turned on, to produce the smoothest rainfall profile possible.

To minimize evaporative losses, a plastic screen was fitted above the drippers at the top of the simulator chamber. This had previously been left open, including during the period when the drainage layer experimental programme was undertaken.

7.3.3 Additional Testing of Substrates and Drainage Layers

It is stated in Section 7.3.1 that an uncompacted substrate was installed in the large rainfall simulator for use in the laboratory validation tests. Use of an uncompacted substrate was considered unavoidable, as no consistent methodology could be employed for uniform substrate compaction over a large surface area. In order to generate more suitable parameters for the substrate stage of the two-stage storage routing model, further tests were performed in the small rainfall simulator on a 10 cm deep sample of uncompacted Marie Curie substrate. In addition to three repeats of each of the four different rainfall profiles used throughout Chapter 6, a higher

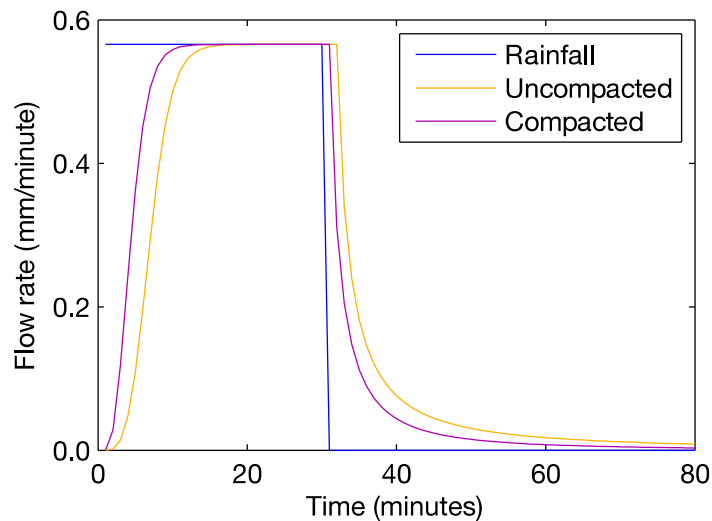**Figure 7.3 – Modelled runoff response of 10 cm compacted and 10 cm uncompacted Marie Curie substrate to a constant-intensity rainfall event.**

constant intensity, 1.2 mm/minute, was also applied, to determine whether the modelling parameters were consistent at double the previous highest tested rainfall intensity. After optimizing the modelled runoff curves, the parameter values of *a*, *b* and *delay* were averaged by group, across all tests, to give modelling values of $a_G = 9.49 \times 10^{-3}$ mm$^{1-b_G}$/minute, $b_G = 3.10$ and $delay_G = 1$ minute, where subscript *G* refers to growing medium (substrate). The value of a_G is similar to that of the compacted substrate, though the value of b_G is noticeably higher.

Figure 7.3 presents the modelled runoff profiles of a compacted and an uncompacted sample of Marie Curie Substrate in response to nominally identical rain events. Both samples were taken from the same batch and both 10 cm deep before compaction. Unexpectedly, the compacted substrate introduced the least attenuation. This may be due to the more fixed structure of the compacted substrate – the particles are locked in place and water flows around them, whereas in the uncompacted substrate, the particles are able to move to some extent and the flow of water through the substrate transports some of the smaller particles downwards, blocking flow paths on the way. Another explanation may simply be that the compacted substrate is, after compaction, not as deep as the uncompacted substrate.

The original proposal for the two-layered system specified a drainage layer consisting solely of Floradrain FD 25. However, due to concerns from ZinCo about possible permanent damage to the rainfall simulator, a layer of SSM 45 protection mat was included by request. Though a combination of FD 25 and SSM 45 had previously been tested and modelled in this configuration, the derived modelling parameters were not considered to be robust with certainty, as a steady-state runoff rate was not reached for any of these tests. Prior to the installation of the filter sheet and substrate layer, constant-intensity events of intensity 0.1, 0.3, 0.6, 1.2 and

2.0 mm/minute, and duration 60 minutes, were applied to the FD 25 and SSM 45 combination. This ensured a long period of steady-state runoff in each test. Optimizing the modelled runoff curves and averaging the parameter values by significance group gave fixed a_D-, b_D- and $delay_D$-values of 0.202, 1.49 and 0 minutes respectively, where subscript D refers to the drainage layer. These values are not greatly different from those predicted for the original non-equilibrating tests of FD 25 and SSM 45 considered at a one-minute resolution ($a_D = 0.176$, $b_D = 1.52$ and $delay_D = 0$ respectively).

7.3.4 Repeatability and Accuracy of Tests

The experimental system exhibited excellent mass balance and reproducibility. A total of 2827.1 litres of rainfall was recorded by the flow meter and a total of 2819.7 litres of runoff was recorded by the pressure transducer, giving an overall difference of 0.26%. In terms of depth and time, this is an average discrepancy of 0.14 mm/day, seemingly consistent with expected evaporation rates indoors (Appendix A). Averaged over the 15 tests, this rate of evaporation implies an available retention capacity of 0.1 mm at the beginning of each test. Even under the 1-in-10 year design storm, which begins at the lowest intensity of this experimental programme, the 0.1 mm potential storage capacity should be filled within the first 45 seconds of the test.

Individually for each test, recovered runoff volume ranged from 98.0 to 101.0% of rainfall volume. The quantity of rainfall supplied in repeat tests varied by no more than 0.3 litres (0.06 mm) within each constant-intensity storm profile. A variation of up to 1 litre (0.2 mm) was found in the quantity of rainfall supplied for nominally identical design storms. However, for each of the five storm profiles, the mean quantity of water supplied was not more than 0.46% different from the quantity of water supplied in any individual test.

Some variation in monitored rainfall and runoff volumes may have resulted from expansion and contraction of water, due to changes in density as a result of fluctuations in temperature. The effect of this is clearly low, as evidenced by the high repeatability of tests.

The t_{50} times for these 15 tests ranged from around 4½ to 19 minutes, with a mean value of 10 minutes and 8 seconds (Figure 7.4). Higher t_{50} times corresponded to lower rainfall intensities; the lowest t_{50} times were for the 1-in-100 year storm. t_{50} times for the 1-in-10 year storms were slightly above, but comparable to, t_{50} times for the 1.2 mm/minute constant intensity storms; the peak intensity of the 1-in-10 year storms is 1.26 mm/minute. For the constant-intensity storms, t_{50} times for the full system can be reasonably predicted by adding the t_{50} times found for the uncompacted substrate and extended drainage layer tests performed in Section 7.3.3 under the same rainfall/inflow intensities. Red lines on Figure 7.4 show the range of predictions; these do not greatly or consistently deviate from the observed t_{50} times.
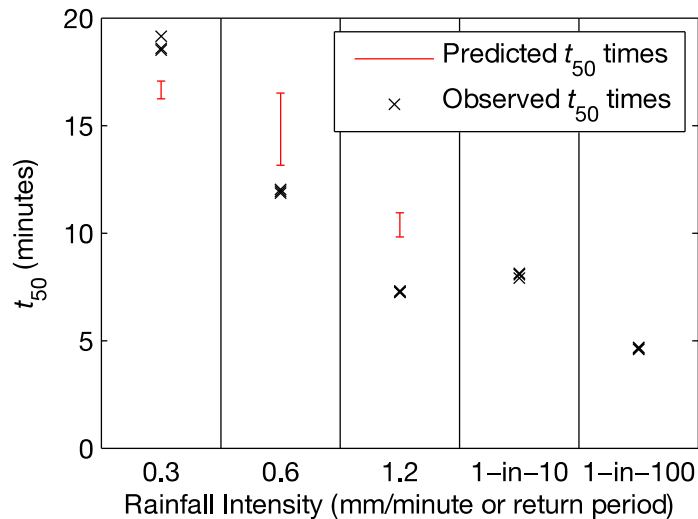
Figure 7.4 – Recorded and predicted t_{50}-values for green roof laboratory test system.

7.3.5   Applicability of Parameterized Two-Stage Model

The recorded rainfall profiles were input individually to the two-stage model for each test. Each stage was, as described earlier, based on nonlinear storage routing at a one-minute time step. The stages were arranged in series and parameterized as shown in Figure 7.5. The mean R_t^2 between monitored and modelled time-series runoff profiles is 0.9721 across all 15 tests. For only the nine constant-intensity rainfall tests, the mean R_t^2 is higher than this, at 0.9872, while for the six design storm tests, the mean R_t^2 is lower, at 0.9495. The model is therefore shown to predict the observed runoff profile well for both constant- and variable-intensity input rainfall profiles. All
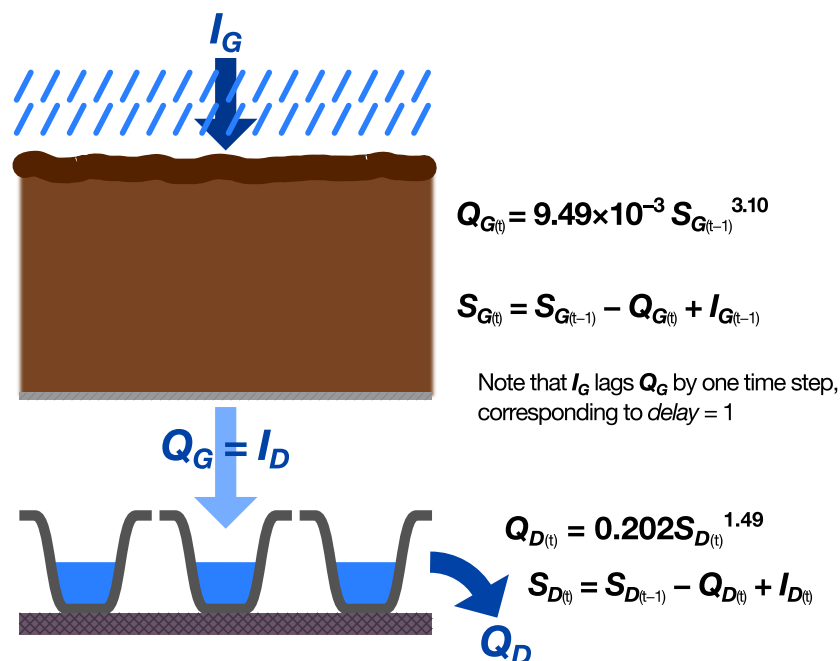
Figure 7.5 – Parameterized two-stage nonlinear storage routing model for green roof laboratory test system.

15 generated time-series runoff profiles are arranged in a 5 × 3 grid in Figure 7.6, where each row shows all three repeats of one tested rainfall profile. Corresponding cumulative runoff profiles are shown in the same place in Figure 7.7. The small spikes in recorded runoff rate, shown in Figure 7.6 (g) to (i) at approximately 35 minutes, occur due to interpolation that necessarily must occur whenever the runoff collection barrel is emptied.

Figure 7.6 shows very close agreement between monitored and runoff modelled profiles for all 15 tests, as well as the high similarity of time-series for repeat tests. In all cases, the rising limb is very closely matched, while the rate of runoff over the falling limb is slightly over-predicted until the runoff rate becomes low. This is not considered to be a serious issue, as a slight over-prediction in runoff rate offers a conservative estimate that can account for some possible unforeseen circumstances. Furthermore, the most important property of this model from a drainage design perspective is its ability to accurately predict the properties of peaks in the runoff rate. Considering the three repeat tests of the 1-in-10 year design storm (Figure 7.6 (j) to (l)), the timing of the observed runoff peak is very well-modelled, occurring just two minutes later than observed in all cases. The observed rate is very well-modelled; the model predicts peak runoff rates just 0.1-0.4% higher than observed. For the 1-in-100 year storm (Figure 7.6 (m) to (o)), the modelled peak is slightly more accurately timed, occurring just one minute after the observed runoff peak in two cases and two minutes after in the remaining case. However, the peak rate of runoff is less accurately predicted, exceeding the observed rate by 8.6-10.6%. This may be due to the shape of the rainfall peak that was produced during these tests. Ideally, each of the four-minute steps comprising either design storm should be of constant rainfall intensity. However, due to limitations of the simulator and control system, the peak of the 1-in-100 year storm was not smoothly recreated, instead consisting of four alternating minutes at approximate rainfall intensities of 2.3 and 2.75 mm/minute. Inputting an oscillating rainfall profile to the storage routing model leads to the possibility of the output taking the form of a damped oscillation, which may over-predict the peak, to an extent which is linked to the level of damping given by the modelling parameters. The use of larger time steps is likely to increase the apparent accuracy of the predictions made by the model, by averaging over local peaks and troughs in the input rainfall profile, and smoothing over small-scale time-dependencies in the monitored runoff curve. This will, however, be at the expense of resolution, as the input rainfall profile becomes blurred. Overall, the 8-11% over-prediction in peak runoff rate is, from a drainage design perspective, certainly preferable to an 8-11% under-prediction.

Though the model is clearly useful, Figure 7.7 shows that, in the period over which runoff falls at the end of a storm, the cumulative modelled runoff depth always exceeds the cumulative monitored runoff depth. Proportionally, this is most significant at lower rainfall rates. This means
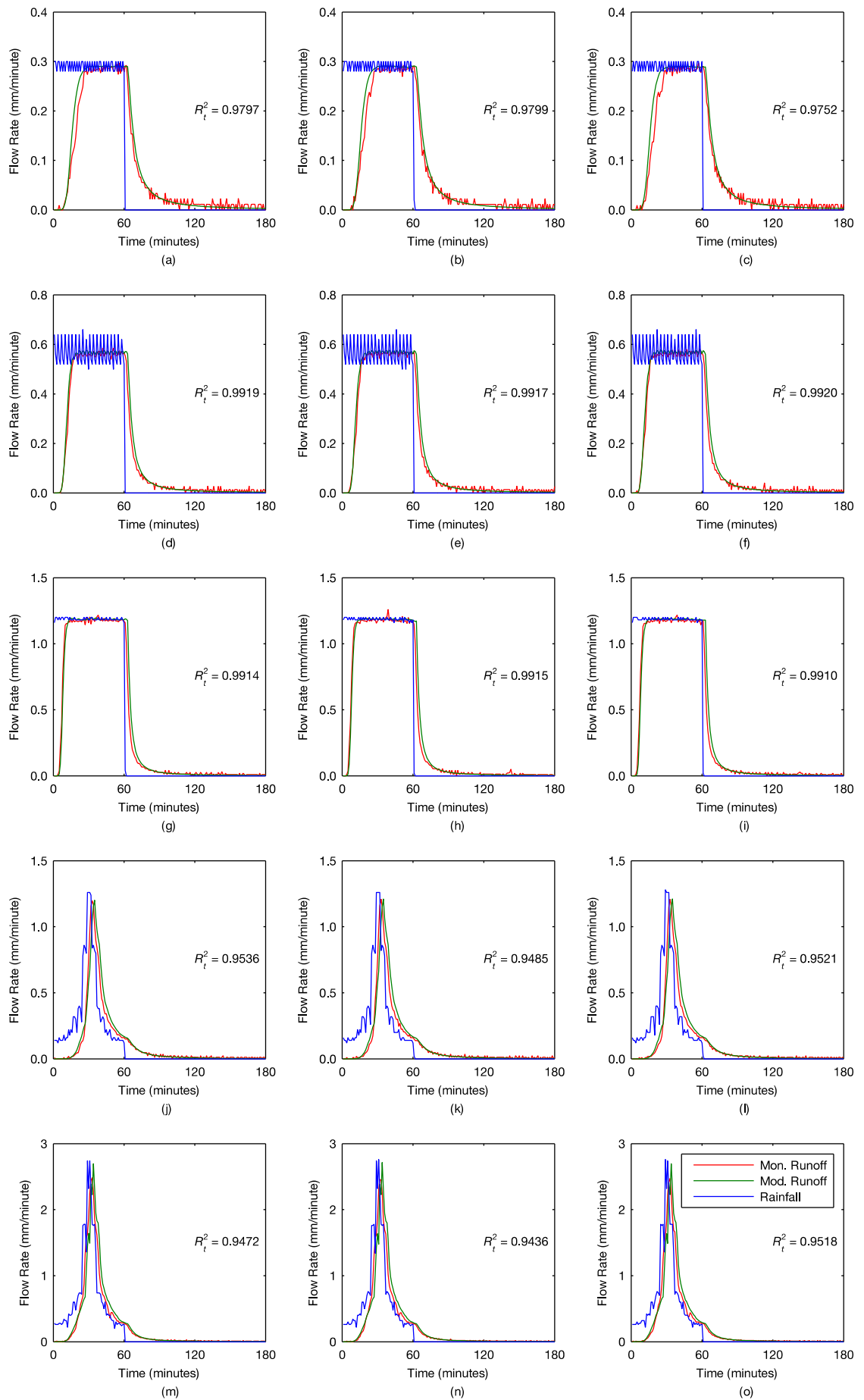
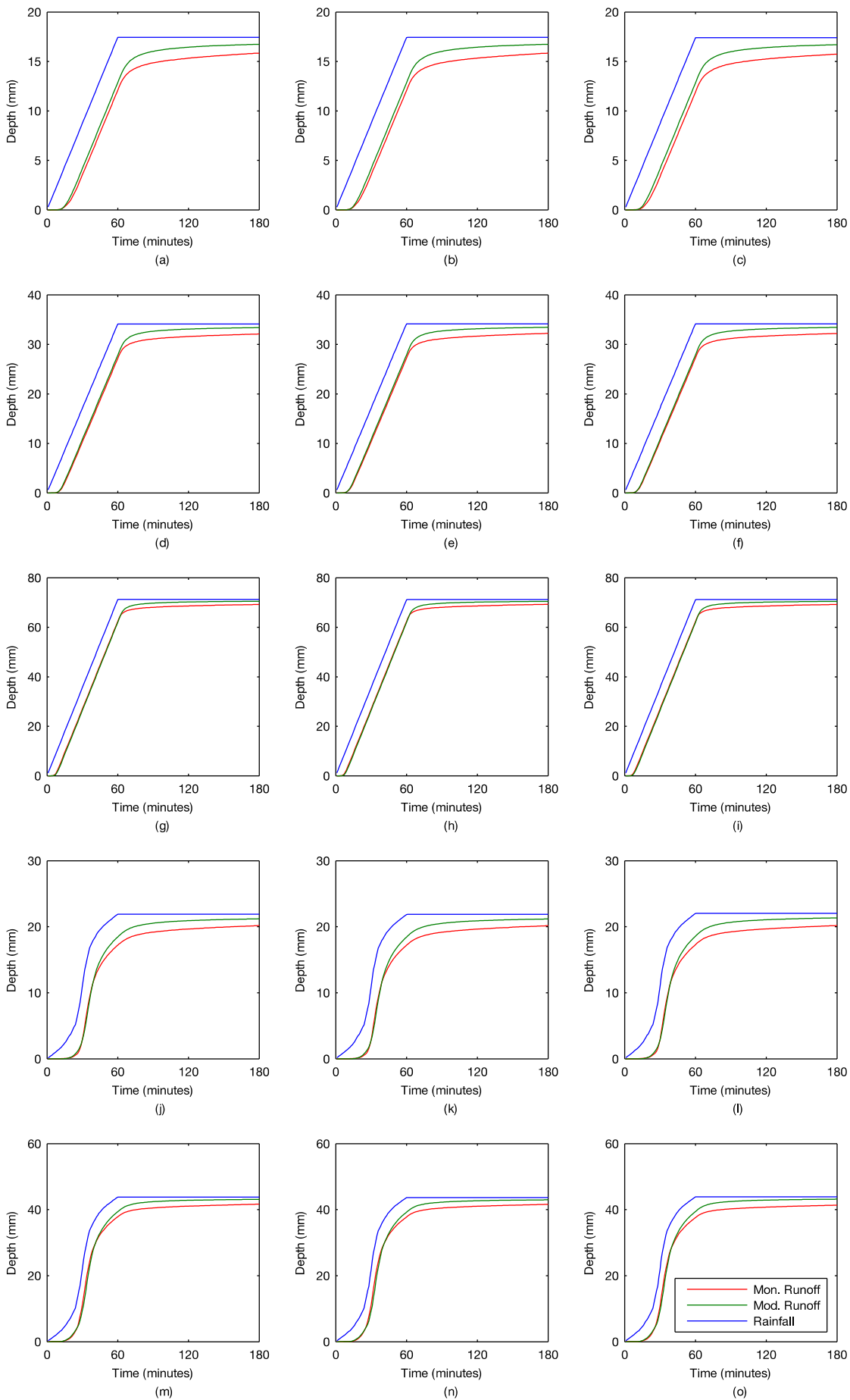**Figure 7.6 – Time-series runoff profiles for laboratory model validation tests.**

Figure 7.7 – Cumulative runoff profiles for laboratory model validation tests.

that the predicted falling limb initially falls less steeply than the recorded falling limb, but takes less time to reduce to zero. This may be indicative of a lower than optimal a-value or lower than optimal b-value in either sub-model. However, both the modelled and monitored runoff rates are arguably insignificant just two hours after the end of a storm event, even though the cumulative differences between rainfall, monitored runoff and modelled runoff at that time may not be. As the nonlinear storage routing model inherently conserves water, the modelled runoff depth will always eventually equal the rainfall depth.

It can be concluded from the study shown above that the nonlinear storage routing method is successful in its ability to model unplanted green roof systems. Two nonlinear storage reservoirs, employed in series, are shown to accurately model the runoff response of the system. The parameter values found, for the substrate and drainage layer tested in isolation, can be transferred without modification to a two-stage model of a two-layered system. Potential differences in substrate composition between different batches of the same nominal mix are shown to be unimportant with regards to the predicted runoff profile.

7.4 Experimental Validation – Hadfield Test Beds

The Hadfield test beds are a comparative study, consisting of ten separate 3×1 m green roof systems arranged side-by-side on a roof level above the fourth floor of the Sir Robert Hadfield Building, on the junction of Portobello Street and Newcastle Street in Sheffield city centre, UK (53.381633,-1.47725). All nine possible combinations of three different planting configurations (*Sedum* species, meadow flower mixture and none) and three different substrate compositions (ZinCo Heather with Lavender, ZinCo Sedum Carpet and an 80/10/10 mix of Light Expanded Clay Aggregate/John Innes No. 1/composted bark) are included in this study, and runoff is monitored to allow the significance of plant and substrate choices to be assessed separately. A tenth bed mirrors the design of the Mappin test bed almost exactly (see Section 3.2), but lacks gravel infill in its drainage layer. All ten test beds are drained by a layer of ZinCo Floradrain FD 25. It is noted that the 80/10/10 LECA mix was previously tested and parameterized in the substrate experimental programme, albeit at 5 and 10 cm depths only. The other two substrate mixes are untested; this validation will assess the applicability of using parameter values derived for the Marie Curie substrate to model them. In common with both untested substrates, Marie Curie substrate consists primarily of crushed brick and pumice.

For green roofs in general, the main function of vegetation is normally assumed to be transpiration during dry periods, which provides the majority of storage recharge in the substrate. Vegetation is assumed to have a limited effect on runoff retention during large or intense storm events, as vegetation can only store rainwater permanently on its few horizontal surfaces. Detention by the vegetation is also assumed to be limited, as water should quickly run off any

non-horizontal vegetation. Detention on horizontal surfaces can, at a maximum, only be equal to the depth that can be stored on these surfaces, divided by the rainfall rate and scaled by the fraction of the test bed area that is covered by horizontal plant surfaces.

Rainfall at the Hadfield test site is measured by three Environmental Measures ARG-100 tipping bucket rain gauges, each with 0.2 mm resolution. The depth of a rainfall event may be under-estimated if water remains in the tipping bucket at event end or over-estimated if the tipping bucket is partly full at the event start. The maximum error is in either case is ±0.2 mm. Three rain gauges, positioned between Test Bed 1 and Test Bed 2, Test Bed 5 and Test Bed 6, and Test Bed 9 and Test Bed 10, are used at this site to determine the possible microclimatic effects resulting from the shading and airflow influence of nearby buildings: the Sir Robert Hadfield Building extends upward for a further nine floors on the north side of the test site, approximately 15 metres away from the line of test beds. Runoff from each of the ten Hadfield test beds is monitored by a Druck PTX 1730 presssure transducer, similar to the Druck PDCR 1830 pressure transducers used in the Mappin test bed, large rainfall simulator and small rainfall simulator, but outputting a pressure-dependent 4-20 mA current, rather than 50 mV voltage range and manufactured from 316 stainless steel, rather than titanium.

Due to the large number of individual devices and the lack of personnel time to implement regular maintenance, the Hadfield comparative data set contains long periods over which the runoff from one or more test beds is improperly recorded. The choice of validation events is therefore limited to those events with accurate runoff records for all three unplanted test beds. Six events were chosen for validation of the runoff detention model (Table 7.2).

Retention of rainfall varies greatly throughout the validation events, ranging from zero (All test beds, 24th November 2012) to approximately 70% of the storm depth (Heather with Lavender, 26th August 2011). Across all storms, the lowest observed level of cumulative retention occurs in the LECA mix (9.7%), followed by Sedum Carpet (21.1%) and Heather with Lavender substrates (25.4%). Retention is therefore ranked according to the maximum water holding

Table 7.2 – Runoff detention model validation events.

Event	Rainfall Depth	Runoff Depth		
		Heather w/ Lavender	Sedum Carpet	LECA mix
1. 13th June 2010	19.4 mm	8.90 mm	10.91 mm	15.47 mm
2. 6th September 2010	32.6 mm	17.57 mm	19.79 mm	27.29 mm
3. 1st October 2010	18.6 mm	11.68 mm	13.45 mm	17.83 mm
4. 3rd October 2010	21.2 mm	19.61 mm	19.26 mm	20.97 mm
5. 26th August 2011	10.8 mm	3.40 mm	3.72 mm	6.69 mm
6. 24th November 2012	36.4 mm	37.07 mm	37.82 mm	36.68 mm
7. 25th November 2012	8.8 mm	8.58 mm	8.79 mm	8.34 mm
8. 26th November 2012	17.2 mm	16.30 mm	16.52 mm	15.70 mm

capacity reported by Poë *et al.* (2011). While the cumulative retention for all three tests beds is very low in comparison to that reported in Chapter 3 for a similar test bed, it is important to note that, as the purpose of this exercise is to validate a runoff model, the eight storms selected for model validation were chosen precisely because of the large quantities of runoff that resulted from them.

Seven of the eight validation events resulted in some retention in all test beds. Therefore, all rainfall, except for an amount equal to the runoff depth (the net rainfall), was assumed to be either retained in the system or lost to evaporation (Equation 7.1):

$$\sum I = \sum Q + \sum R + \sum E$$

Equation 7.1

where *I*, *Q*, *R* and *E* are rainfall, runoff retention and evaporation depths in mm, respectively.

Evaporation was assumed to occur during any dry periods within a storm, at a rate of 2 mm/day in June and August, 1 mm/day in September and 0.5 mm/day in October. For the three events occurring in quick succession in November 2012, evaporation was not modelled within events as the depths of retention were negligible. Indeed, it is noted that for all three test beds, the monitored runoff depth resulting from the event of 24th November 2012 exceeds the monitored rainfall depth. This is likely to result from microclimatic effects at the test site e.g. possible shading of the rain gauge causing an under-estimation of rainfall depth. For this event, only the first 36.4 mm of runoff is modelled.

Evaporation, where modelled, was assumed to recharge the storage capacity of the test bed, meaning that any rain falling after a (sub six-hour) dry period within a storm was always modelled to be partially retained. This requires another equation (Equation 7.3) in addition to the standard continuity of volume equation in finite difference form (Equation 7.2):

For $I_t > 0$ $\qquad\qquad S_t = S_{t-1} + (I_t - Q_t)\Delta t$ **Equation 7.2**

For $I_t = 0$ $\qquad\qquad S_t = S_{t-1} + e$ **Equation 7.3**

Where *e* is an estimate of the evaporation occurring in one time step and *S* here is the available depth of permanent retention storage in the roof.

Excluding one event, the total depth of runoff plus assumed evaporation within a storm was always less than the total depth of rainfall i.e. $\sum R$ was positive. The remaining depth of excess rainfall was assumed to be retained. After evaporation was modelled for each storm, this depth was removed from the start of the rainfall profile, resulting in a net rainfall profile with a rainfall depth equal to the depth of runoff.

The use of this green roof detention model currently requires the depth of runoff resulting from a storm to be known in advance. Hence, the runoff response to hypothetical or future events cannot yet be predicted. However, it is planned that an evapotranspiration model may be coupled with a permanent storage (retention) reservoir and placed ahead of the two-stage nonlinear storage routing model, in order to calculate the volume of storage available in a green roof at the beginning of any storm. Coupling of an evapotranspiration model with a long-term record of rainfall is beyond the scope of this thesis, which considers runoff detention only.

Data collection and analysis relating to the Hadfield test beds has been the subject of previous research at the University of Sheffield (Poë *et al.*, 2011). The eight validation events studied here were taken from a long-term data record maintained, until October 2013, by Dr Christian Berretta.

7.4.1 Selection of Modelling Parameter Values

For any substrate material, appropriate values of a_G, b_G and $delay_G$ must be determined. All ten test beds use 8 cm of substrate. It was assumed, in the absence of further data to suggest a more suitable method, that linear interpolation could be applied between any parameter values derived for a 5 cm substrate depth and any derived for a 10 cm substrate depth. It was also assumed that all parameter values are independent of rainfall rate and therefore that any optimized parameter values found in the substrate experimental programme could be averaged over all rainfall rates. Due to weathering, the substrates in use on the Hadfield test beds were assumed to behave as if compacted and parameterized accordingly; standardized FLL substrate tests specify compaction, which is intended to simulate weathering.

The LECA mix used in the Hadfield study is nominally identical to that tested in the substrate experimental programme. For a substrate depth of 8 cm, linear interpolation and scaling from Table 6.5 suggest a_G-, b_G- and $delay_G$-values of 0.436, 2.89 and 1 minute, respectively.

The Marie Curie substrate, with a 0.95% proportion of fines, contains fewer fine particles than either the Sedum Carpet substrate (1.8% fines) or the Heather with Lavender substrate (3.6% fines – both Poë *et al.*, 2011). At a dry bulk density of ~1.02 g/cm^3, it is similar in density to Heather with Lavender substrate (~1.00 g/cm^3) but less dense than Sedum Carpet substrate (~1.12 g/cm^3). In order to determine the generic applicability of reasonable parameters in the absence of better information, a_G-, b_G- and $delay_G$ values of 0.436, 2.27 and 1 minute, respectively, were used for both Sedum Carpet and Heather with Lavender substrates at 8 cm depth. These were again derived by linear interpolation of the parameter values shown for Marie Curie substrate at 5 and 10 cm substrate depths in Table 6.5, followed by scaling to appropriate units for use at a one-minute resolution.

Similarly, the hydrological properties of the drainage layer and moisture mat combination must be represented by appropriate values of a_D, b_D and $delay_D$. The drainage length of the test beds is 3 metres, between the two tested drainage lengths of 2 and 5 metres. The slope is also between the two tested slopes of 1.15° and 10°. However, at 1.5°, its slope is tens of times closer to one of the tested roof slopes than the other, so parameter values valid for a 1.15° slope were assumed equally valid for a 1.5° slope.

The drainage layer in all Hadfield test beds is ZinCo Floradrain FD 25, the runoff response of which was studied in Chapter 5. A significance study was not performed for the parameter values derived at a one-minute resolution, and study of Figure 5.23 does not suggest that any test variable except drainage length and, partially, inflow rate, has a significant effect on runoff response. However, setting $delay_D$ to zero, group averaging values of a_D by inflow rate, re-optimizing for b_D and interpolating for a 3 metre drainage length, again assuming independence from inflow rate, gives proposed a_D- and b_D-values of 0.652 and 1.72, respectively.

7.4.2   Applicability of Parameterized Two-Stage Model

Applying the two-stage nonlinear storage routing model to the Hadfield test beds gives generally well-fitted predictions for all validation events and test beds. The overall shape of the monitored runoff profile is reasonably well-modelled in both time-series (Figures 7.8 and 7.9) and cumulative (Figures 7.10 and 7.11) forms, where each set of three figures arranges storm events chronologically into rows and individual test beds into columns.

Of the three test beds, the one using LECA mix as its substrate is the best modelled. As well as matching the general shape of the runoff response, the model in many cases produces good predictions for peaks in the runoff profile. For this test bed, mean R_t^2 at a one-minute data resolution is 0.7852, while maximum R_t^2 is 0.9461 – approaching the lower end of the modelling accuracy that could be expected in controlled environments. It is not surprising that the test bed using LECA mix is the most accurately modelled, as this is the only substrate to have been previously tested and parameterized.

Both Sedum Carpet and Heather with Lavender substrates were parameterized as appropriate for the compositionally similar Marie Curie substrate. The modelled runoff responses for the two test beds using these substrates are clearly adequate, as evidenced by visual observation of Figures 7.8 and 7.9. Mean R_t^2 values for these beds are reasonable: 0.6757 for Sedum Carpet and 0.6705 for Heather with Lavender. As both of the substrates in use on these test beds are parameterized as would be valid for the separate Marie Curie substrate, it is possible that the Marie Curie substrate parameter set may provide an acceptable preliminary estimate for modelling the runoff response of untested substrates. For all three test beds, some of the apparent
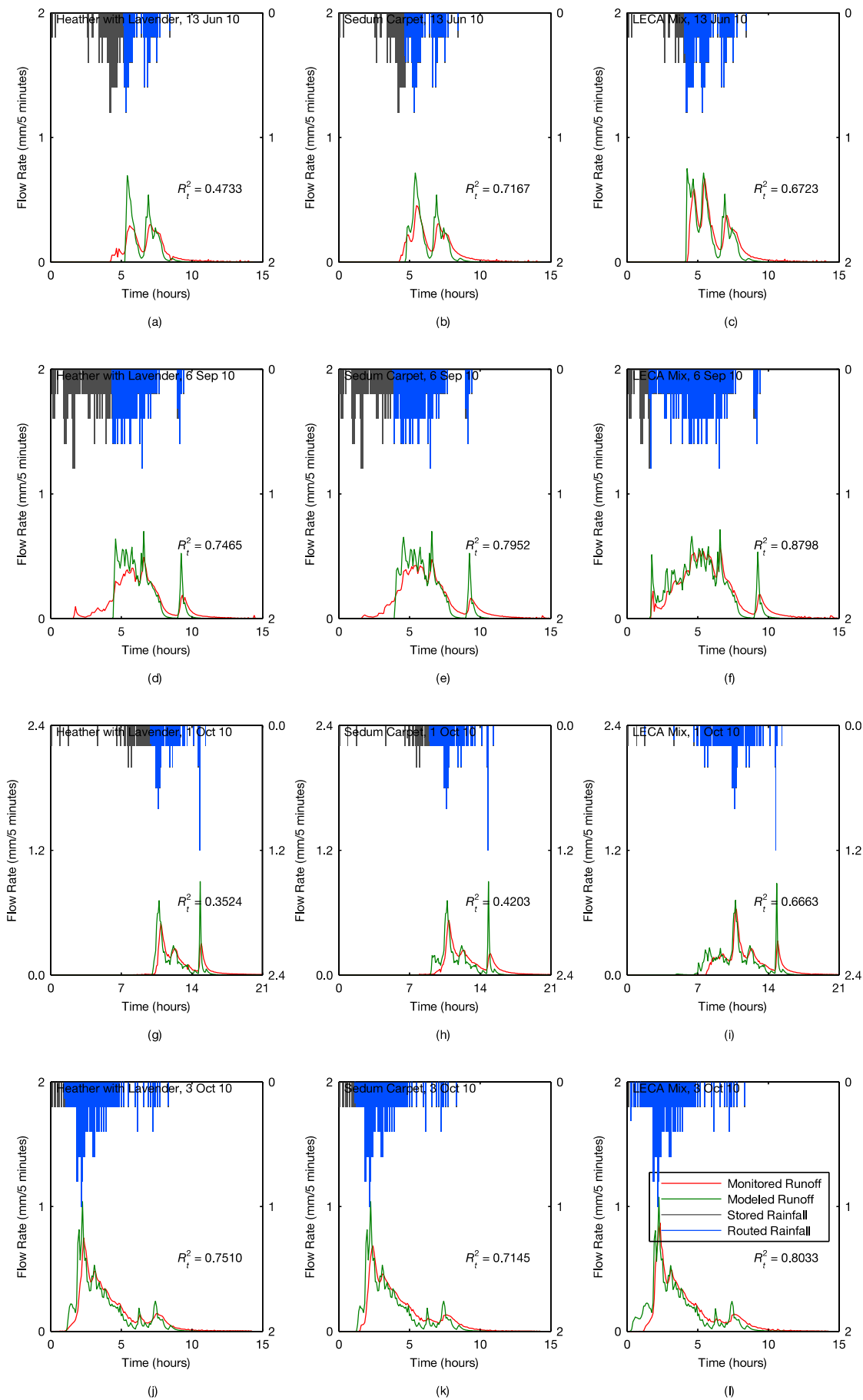
Figure 7.8 – Time-series runoff profiles for Hadfield model validation tests, storms 1-4
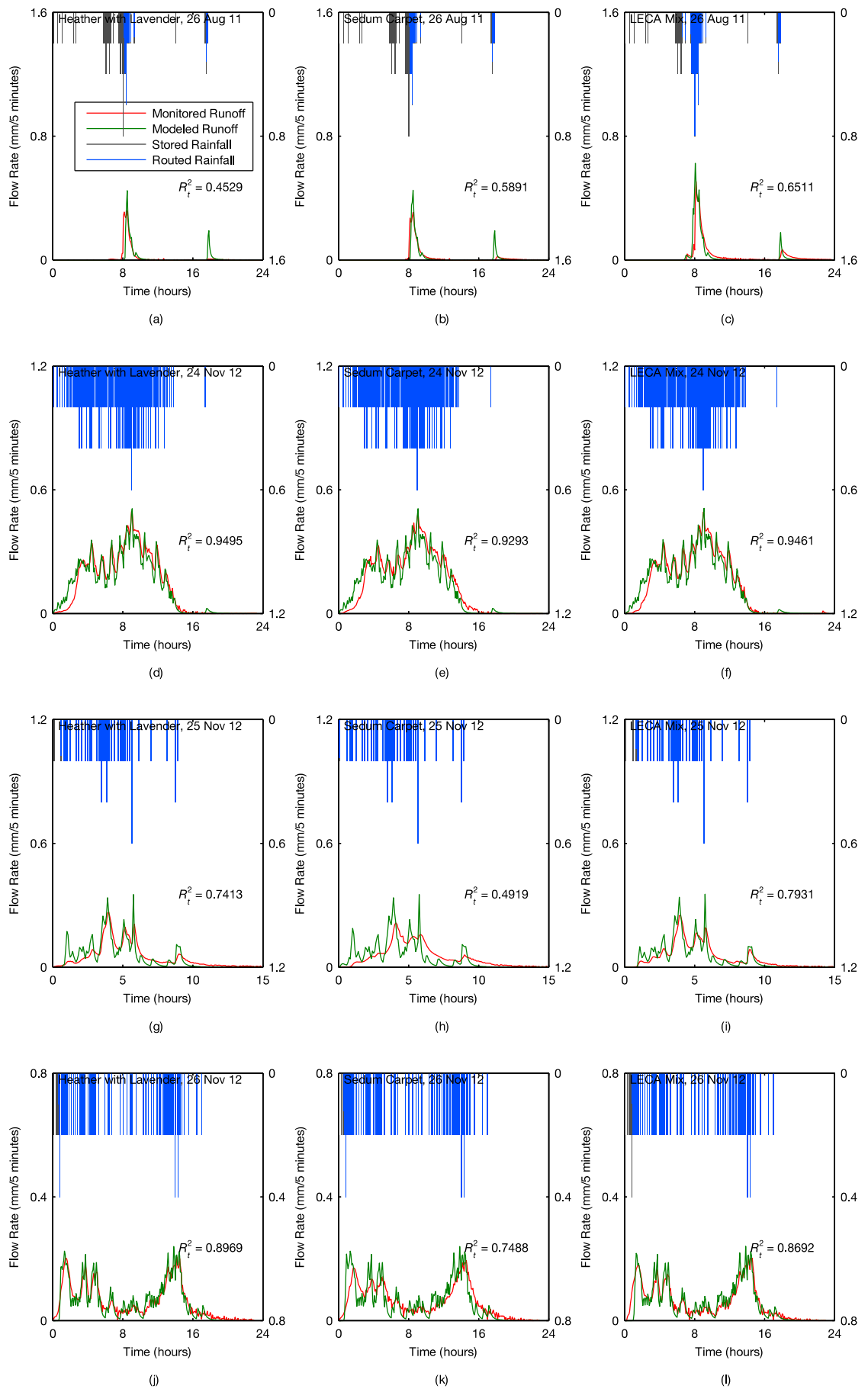
Figure 7.9 – Time-series runoff profiles for Hadfield model validation tests, storms 5-8
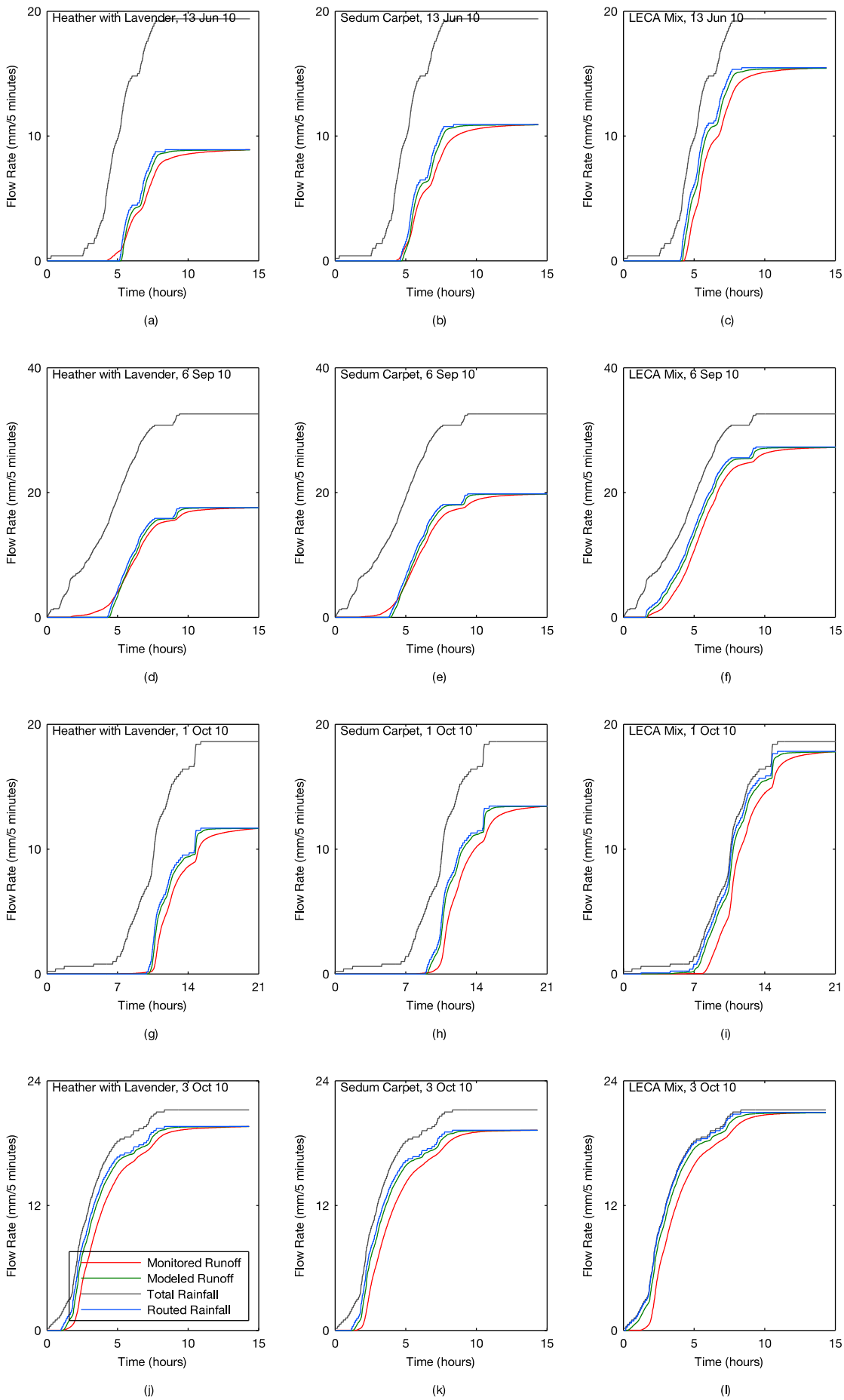
Figure 7.10 – Cumulative runoff profiles for Hadfield model validation tests, storms 1-4
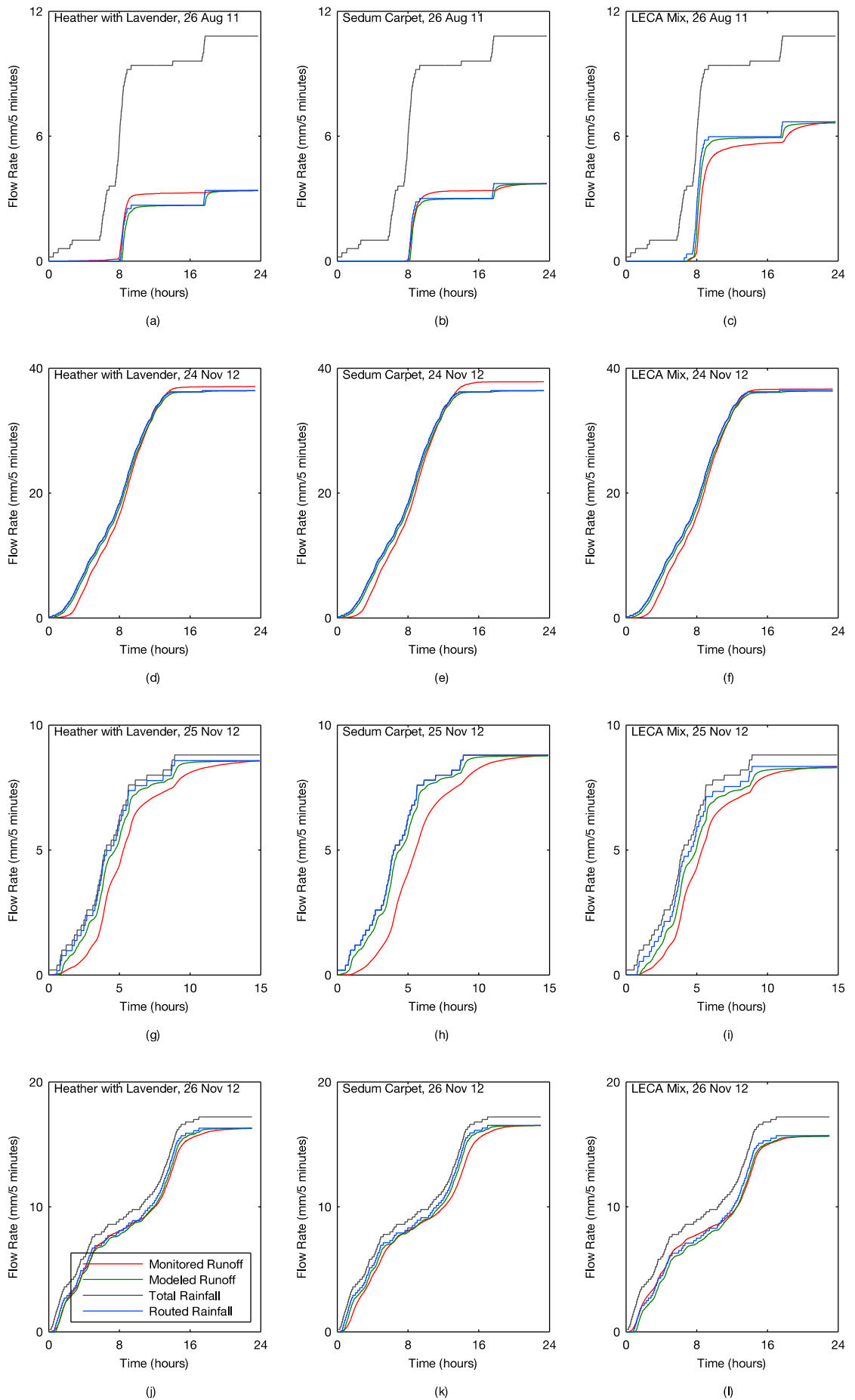
Figure 7.11 – Cumulative runoff profiles for Hadfield model validation tests, storms 5-8

inaccuracy, according to the R_t^2 statistic, could be attributed to long periods within events over which no rain falls – if any runoff occurs (e.g. due to very extended detention of small quantities of runoff) or is otherwise measured to occur (e.g. due to thermal expansion of water in the collecting barrel) during these periods, the square of the difference between recorded and modelled runoff will be large relative to the very small monitored values of runoff, and this will negatively affect the R_t^2 statistic.

Overall, the monitored runoff profiles are for all three beds are relatively similar in their response to each individual storm. At or above field capacity, the only unfilled pore spaces are macropores and so flow through the substrate is primarily driven by gravity (O'Geen, 2012). This suggests that the most important differences between substrates for detention modelling relate to macropore structure and spacing, which may vary between different batches of the same substrate. This also explains why it is the later sections of the monitored runoff profiles that are most similar between the three test beds.

For all three substrates, it is observed that some modelled runoff peaks are noticeably higher than were monitored e.g. Figure 7.8 (d-f). This is the result of a general under-prediction of attenuation, which can also be observed in the relative steepness of the modelled time-series falling runoff limbs in comparison to the monitored time-series falling runoff limbs. The observed under-attenuation is greater for the two test beds not using the previously-parameterized LECA mix substrate; while the Marie Curie substrate parameters are successful in identifying the right overall shape of the monitored runoff profile, the percentage fines in Sedum Carpet is almost double that of Marie Curie substrate (0.95%) and the percentage fines in Heather with Lavender is double that of Sedum Carpet. Hence, the under-attenuation observed in the models of Sedum Carpet and Heather with Lavender may be consistent with the use of modelling parameters suited to a coarser substrate, which may have compounded the issue of modelled under-attenuation. The substrates in use on all three test beds were installed in 2006 and it is proposed that changes to the substrate may have taken place since then. A possible cause of the greater observed attenuation in all three test beds is a partial blocking of the pores of the filter sheet with fine particles that have washed down through the substrate since 2006 and accumulated there. The effects of a partially blocked filter sheet were not considered in the laboratory testing conducted in Chapter 6. Weed growth, resulting from an inconsistent maintenance regime, may have further increased attenuation.

Another factor contributing to the observed under-attenuation of the model may be that, as suggested by Yio *et al.* (2012), linear interpolation is not appropriate to derive intermediate parameter values. It is noted that a very large difference exists between mean a_G-values at 5 and 10 cm substrate depth. Figure 7.12 plots the six hours of the time-series runoff response shown in
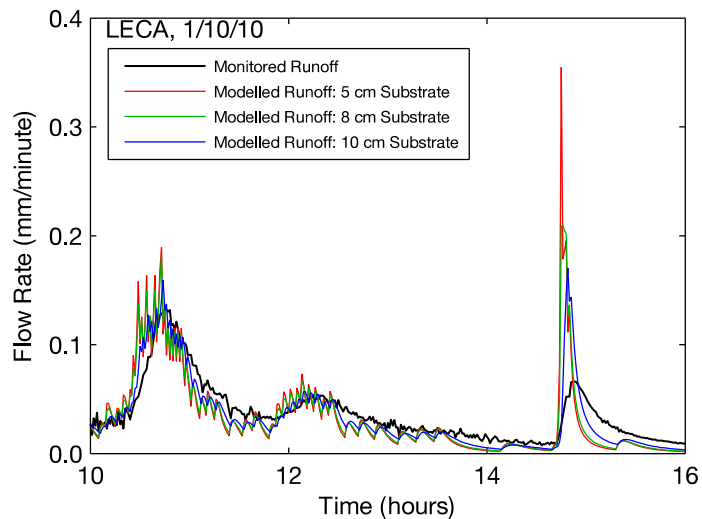
Figure 7.12 – Comparison of modelled runoff profiles assuming different substrate depths.

Figure 7.8 (i) over which the majority of runoff is released, alongside the predicted runoff response when the model is parameterized for 5 and 10 cm substrate depths; the correct parameter values for a substrate depth of 8 cm must exist within this range. The general shape of the modelled runoff profile is similar and accurate for all three parameter sets. However, parameterizing the model according to different substrate depths strongly affects the sharpness and height of modelled runoff peaks. Changing the interpolation method for parameters may improve the modelled runoff profiles. However, as only two substrate depths were tested in the substrate and drainage layer experimental programme, it is difficult at this stage to propose and justify any interpolation method over any other. It is noted that, as the modelled runoff peak for a substrate depth of 10 cm is above the observed peak in runoff intensity (at both the 11th and 15th hours into the storm), the choice of interpolation method can only be a contributory factor to the model's observed under-attenuation, and not its main cause.

In many cumulative rainfall and runoff curves (Figures 7.10 and 7.11), runoff depth can be seen to exceed net rainfall depth, especially near the beginning of an event. This implies that it is too simplistic to assume that runoff does not occur until field capacity is reached. It is hypothesized that runoff can begin before the substrate reaches field capacity if the substrate does not behave as a single reservoir. Higher values of the pore connectivity factor, *l*, imply more connection and therefore interaction, including water flow, between pores. LECA contains the least fines of the three tested substrates on average, its pore connectivity is likely to be the highest and hence it is the substrate most likely to behave as a single reservoir. This is supported by the cumulative runoff plots, which generally show monitored runoff to exceed net rainfall least for the test bed using LECA. For substrates with less connection between pores, multiple reservoirs may exist in parallel, and runoff will start after one reservoir is filled.
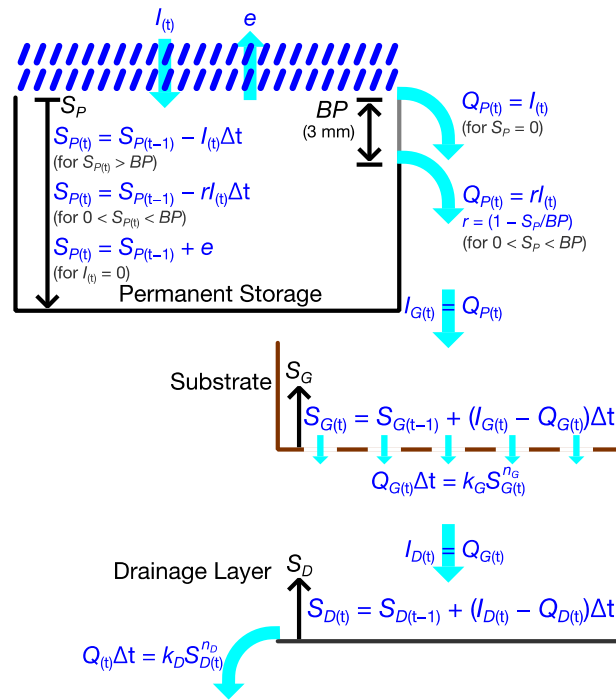
Figure 7.13 – Modified green roof model, including nonlinear substrate reservoir, nonlinear drainage layer reservoir, permanent storage with split runoff/retention and evaporation during dry periods.

The initial permanent retention reservoir was modified to allow gradual initiation of runoff at a substrate water content near to, but below, field capacity (Figure 7.13). Qualitatively, when the available permanent storage capacity (S_P) fell below a defined breakpoint value (BP, here 3 mm), a fraction (r) of any rainfall entering the permanent storage was routed through to the substrate model; the remainder was retained in the permanent storage reservoir as before. r was modelled to increase linearly from zero to one as S_P fell from 3 mm to 0 mm i.e. $r = 1 - S_P/BP$. Figure 7.14 shows the improved runoff predictions that are given by this modification of the permanent retention reservoir, for validation storms 1, 2, 3 and 5. In all cases, the overall shape of the storm is more closely matched, as is the prediction for peak runoff rate. However, this improvement in modelling is dependent on two extra modelling parameters: the substrate reservoir storage depth below which near-field capacity is reached (BP in Figure 7.13) and the proportion of rainfall that becomes runoff when the substrate is near field capacity. The increased complexity of this model may or may not be justified by its potential to more accurately predict peak runoff rates, depending on the specific modelling requirements of any particular project.

The original and improved predictions for runoff are identical when $S_P = 0$. This is intentional, as the purpose of the modification is to more accurately model the initialization of runoff in situations where a fraction of rain is routed through the substrate and a fraction is retained in the limited storage capacity that has not yet been filled. When no storage capacity remains empty, all runoff is detained, a situation which the original model was able to handle adequately.
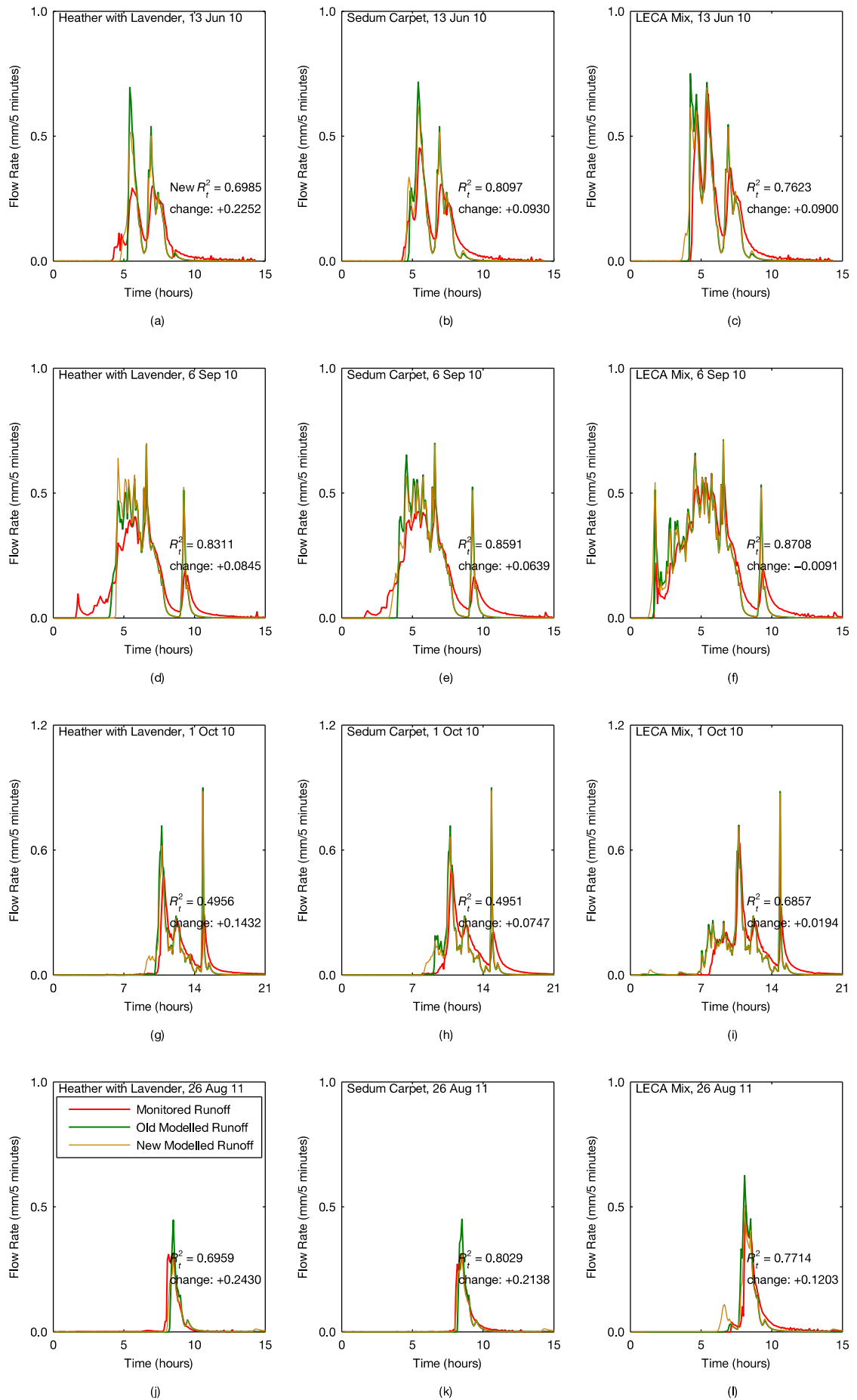
Figure 7.14 – Time-series runoff profiles for adapted model, storms 1, 2, 3 & 5.
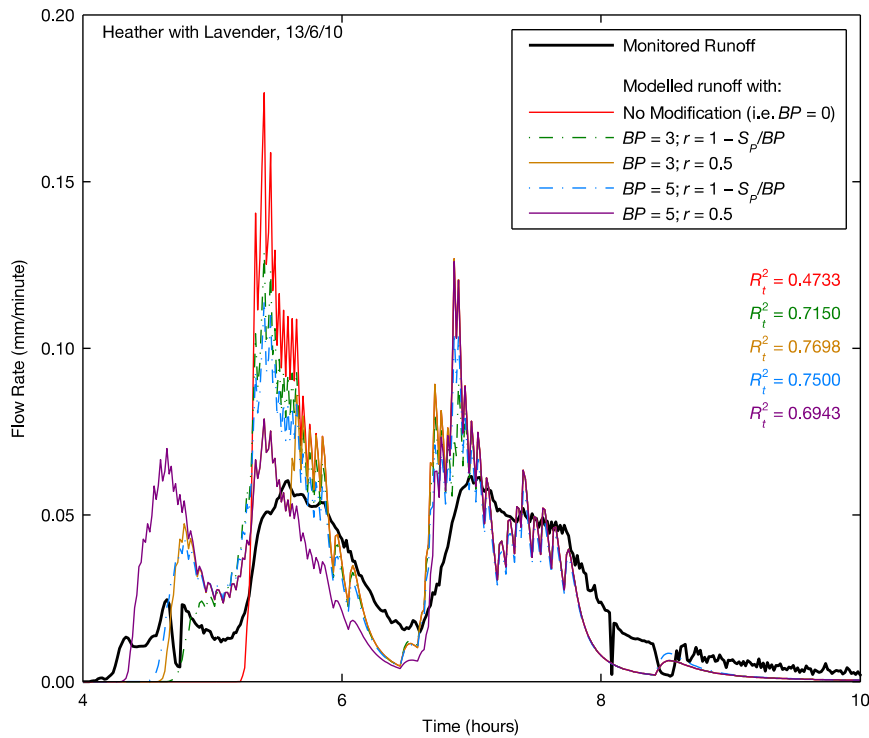
Figure 7.15 – Comparison of modelled runoff responses for different values and definitions of *BP* and *r*

The value of 3 mm assigned to *BP* is speculative, as is the use of the equation $1 - S_P/BP$ to model *r*. Improvements to the predicted runoff profile are found for a range of values for *BP* and a range of definitions for *r* (Figure 7.15). It is therefore shown that the modification made to the permanent retention reservoir is appropriate, but that its parameterization is currently uncertain. It is noted in Section 4.5.2 that all substrates used during the experimental programme were pre-wetted prior to testing, bringing them from an initial water content up to field capacity for detention testing. The runoff responses of the substrates were not recorded during these pre-wetting events as the quantities of water used far exceeded the capacity of either collection cylinder and only detention was intended to be modelled at that time. However, had the runoff responses of the substrates been monitored as their water content rose from an initial level, through near-field capacity and up to field-capacity, then some data would exist to allow less speculative estimations of *BP* and *r*.

7.5 Conclusions

The two nonlinear storage routing models, proposed separately for the drainage layer in Chapter 5 and for the substrate in Chapter 6, were combined in series to give a two-stage model for an unplanted green roof system. This was verified, under laboratory conditions, using a test system built into the large rainfall simulator. The test system consisted of an unplanted and uncompacted 10 cm layer of Marie Curie substrate, separated by a ZinCo Systemfilter SF filter sheet from a

ZinCo Floradrain FD 25 drainage layer, above a ZinCo SSM 45 protection mat. The system was pre-wetted by 72 mm of rainfall applied over 60 minutes, and drained for 16 hours. Five 60-minute rainfall profiles were applied to the test system three times each, in random order, with a 16-hour dry period between each test. The system was assumed to be at field capacity before each test, including the first. Rainfall and runoff were measured at one-minute intervals. Overall, mass balance and repeatability were excellent.

The two-stage runoff model was parameterized as appropriate for the laboratory test system and input with the 15 rainfall profiles. The modelled runoff profiles represented the monitored profiles well (mean $R_t^2 = 0.9721$), especially considering the potential differences in composition, consistency and behaviour between two samples of Marie Curie substrate taken from different batches. For the 1-in-100 year events, the peak intensity was over-predicted by approximately 10%. While this is within the range of acceptability, improvements to the dripper control system will generate smoother rainfall profiles and may reduce the peak over-prediction.

The two-stage runoff model was then parameterized as best as possible for three unplanted test beds located on the roof of the Sir Robert Hadfield Building in Sheffield, differing only in substrate composition. The parameter values for the drainage layer were interpolated for a drainage length of 3 metres, from values appropriate for drainage lengths of 2 and 5 metres. Only one of the three substrates in use on these test beds (LECA) had been previously parameterized; parameter values for this were interpolated for a substrate depth of 8 cm, from values appropriate for substrate depths of 5 and 10 cm. The other two test bed substrates were parameterized according to a material (Marie Curie Substrate) with the same crushed brick base, interpolated for an 8 cm substrate depth.

For all three test systems, the overall shape of all modelled time-series runoff profiles was fit for purpose. The fact that the Marie Curie parameter set was suitable, within reason, for the test beds using Heather with Lavender and Sedum Carpet substrates suggests that the Marie Curie parameter set may be appropriate for estimating the performance of any similar, untested substrates. The applicability of the parameter set determined in Chapter 6, to the sample of Marie Curie substrate tested in the laboratory validation, suggests that the parameter values are insensitive to potential differences in composition and soil matrix. As measured by R_t^2, the accuracy of the two-stage model as applied to the Hadfield LECA test bed approached the accuracy of the model as tested under laboratory conditions.

For each storm individually, the monitored runoff profiles were found to be generally similar for all three test beds. This was especially apparent at times when the available retention capacity was predicted to be zero. Under these circumstances, rainfall is routed exclusively through

macropores, so the movement of water through the substrates is gravity-driven. It is therefore expected that the spacing and arrangement of macropores in the soil matrix is the primary factor in determining the runoff response. It is noted that these factors are related to the settling of particles, and so may vary within batches of the same substrate as well as between substrates of different compositions.

Overall, the ability of the model to identify fine detail, such as the height of runoff peaks, was limited by an under-prediction of attenuation. It is believed that long-term changes to the substrate, or partial blocking of the filter sheet below the substrate, may not have been fully represented by the a_G- and b_G-values that were used.

Cumulative runoff was shown to exceed cumulative net rainfall at times during events, especially those with more notable depths of retention. This led to the hypothesis that runoff could occur while the substrate was approaching field capacity. The model was adapted to allow the substrates to produce limited runoff before field capacity was reached. Predictions of peak runoff rate were shown to be improved following this modification. However, the requirement for two extra parameter values to be known may or may not justify this adaptation. For larger single storms, the substrate reaches field capacity after a smaller fraction of the total rainfall depth has fallen; the model will function identically over a larger portion of the event, with or without the adaptation. However, for long-term time-series runoff modelling using real rainfall records as inputs, few events will be large. Long-term records will be characterized by many events with low depth and intermittent sub six-hour dry periods, which will make evaporation possible within an event. Therefore, the substrate water capacity may remain between the breakpoint and field capacity over the majority of the duration of many events. If so, the modification will be engaged for a large fraction of long-term runoff modelling and its use may be justified if it is considerd important to accurately predict peak runoff rates in response to routine events.

For long-term rainfall/runoff records, the available retention capacity at the beginning of each storm contained within the record must be predicted. The two-stage detention model proposed here, either with or without the near-field capacity adaptation, must be coupled with an evaporation or evapotranspiration model to be made suitable for use with long-term records.

8   Summary, Discussion and Further Work

8.1   Chapter Overview

This chapter presents a summary of the work conducted and discussed in each of the four previous research chapters (Chapters 3, 5, 6 and 7) and the main conclusions that can be drawn. This is followed by a wider discussion on the applicability of these conclusions to urban drainage and modelling. Finally, suggestions are presented for further work related to, but outside the scope of, this thesis.

8.2   Summary

8.2.1   Parametric Modelling of Green Roof Runoff Performance (Chapter 3)

Chapter 3 focused on the analysis of an existing, near-continuous, 29-month rainfall and runoff record, collected from a small green roof test bed and adjacent rain gauge, located in Sheffield, UK. Of the 432 fully-monitored storms, 232 were small (< 2 mm) and would not be expected to produce significant depths of runoff even from conventional roofs. These events were considered to be of limited interest to urban drainage engineers. 21 events were selected for their significance to urban drainage engineers, either because of a high return period or (possibly intermittent) high rainfall intensity. Key storm parameters (Table 3.3) and key weather/climatic parameters (Table 3.4) were identified for all 21 significant storms. Key performance parameters (Table 3.5) were identified for all 21 corresponding runoff responses. Statistical (single linear and multiple stepwise linear) regressions were performed to attempt to link key performance parameters to key storm and weather/climatic parameters, either singly or combined. All data sets were used both as collected and after transformations (e.g. power-law scaling), which were performed to increase normality.

Cumulative retention, per-storm retention and peak flow reduction were observed to be low in comparison to most other similar studies. This may be attributed to the local maritime temperate climate and a total rainfall depth over the study period that was 9.4% above the 30-year climatic average. However, these performance metrics were high in their own right: cumulative retention was 49.3%; mean retention was 69.6% (60.4% for the 200 storms over or equal to 2 mm); and mean peak flow reduction was 87.6% (78.9% for the 200 storms over or equal to 2 mm). High figures such as these indicate the continued validity of using even thin extensive green roofs for managing urban stormwater quantities, under disadvantageous conditions.

Of the 21 significant storms, all but four were of return period < 2 years and none were of return period > 20 years. This data set cannot therefore be considered complete for the purposes of

model validation as it does not contain any extreme (1-in-30 or 1-in-100 year) events. Mean per-event retention, at 42.7%, and peak flow reduction, at 59.2%, were notable for the set of 21 storms. These figures suggest that the urban water management utility of this extensive green roof remains high under relatively rare events (of return period 1-2 years) dispersed throughout a reasonably long (29-month) rainfall record. The retention performance of intensive or extensive green roofs with thicker substrate layers is expected to be higher still.

Attempts at relating single, untransformed key storm parameters to the single, untransformed key performance parameters that they could logically be assumed to influence (e.g. peak rainfall rate to peak runoff rate) through simple linear, exponential, logarithmic or power-law regressions, were not successful (Figure 3.5). This is because the key storm parameters do not take into account the initial conditions of the test bed, which may, for example, either allow full, partial or zero retention of a 20 mm storm event.

Stepwise multiple linear regressions were employed to identify possible complex relationships between storm/climatic parameters and key performance parameters, in an automated fashion that did not risk overlooking any less obvious relationships. A handful of moderately successful equations were generated for four of the eight key performance measures (Table 3.8), though none could be found for t_{50} that was statistically more robust than a constant value. As the stepwise linear regression failed to find any high-quality correlations between performance and possible influencing factors, it is likely that the existence of a few moderately-successesful modelling equations is a coincidental outcome of the sheer number of combinations that were made of somewhat similarly-distributed data sets.

Overall, it can be concluded that the entire range of models, produced by either simple or multiple stepwise linear regression, is not even suitable for predicting the response of the test bed from which the data was collected. By definition, these models are not transferrable between different climates or system designs. This regression-based modelling approach should be rejected in favour of continuous physically-based modelling, which derives runoff response as a function of rainfall profile through hydrological processes, and which reduces the effects of climate and system design to specifiable model inputs.

8.2.2   Experimental Data Collection and Modelling of the Drainage Layer (Chapter 5)

A large (5 × 1 metre) rainfall simulator was modified to improve the spatial and temporal consistency of generated rainfall. Specifically, the original rainfall distribution network, consisting of 48 spraying nozzles, was replaced by three separate networks of pressure-compensating drippers arranged in square grid patterns at densities of 36 and 144/m². Each

network was gated by an electromagnetic valve and each valve was operated independently by a relay controller. This allowed rainfall profiles other than constant flow to be produced consistently. A mesh grid was installed 35 cm above the channel bed of the rainfall simulator, to randomize drop size and position. The original flow meter-based runoff monitoring system was replaced by a cylindrical collection barrel and pressure transducer setup, which improved time resolution from fifteen seconds to one second, and depth resolution from 0.1 mm to approximately 0.0028 mm.

Five configurations of drainage layer component (bare channel; ZinCo Floradrain FD 25; ZinCo Floradrain FD 25 with underlying ZinCo SSM 45 protection mat; ZinCo Floradrain FD 40 and ZinCo Floraset FS 50), were tested three times each under all combinations of two possible roof slopes (1.15° and 10°), two possible drainage lengths (2 metres and 5 metres) and five possible constant rainfall rates (0.1, 0.3, 0.6, 1.2 and 2.0 mm/minute), for a total of 300 tests. Low levels of lag were observed in all tests; cumulative median-to-median delay (t_{50}) times ranged from 8 to 636 seconds. The mean t_{50} was under 2 minutes. Low t_{50} times indicate that all tested configurations of drainage layer serve their primary purpose of rapidly transporting excess water that cannot be stored towards the roof outlet.

An optimization routine (*lsqcurvefit* in Matlab) was employed to fit a runoff profile, modelled by nonlinear storage routing, to each of the 300 monitored runoff profiles. The optimization was performed by separately adjusting the two variable parameters, *a* and *b*, in the storage-discharge relationship (Equation 8.1), to minimize least-squares error at every value of *delay*, the time offset in the conservation equation (Equation 8.2), from zero to an upper limit of 80 seconds.

$$Q_{t+1} = aS_t{}^b$$ **Equation 8.1**

$$S_t = S_{t-1} + (I_{t-delay} - Q_t)\Delta t$$ **Equation 8.2**

For each test, the combination of *a*, *b* and *delay* that gave the highest Young's R_t^2 correlation between monitored and modelled runoff was taken as the optimal parameterization for modelling that test. At one-second data resolution, the mean R_t^2 correlation between a monitored runoff profile and a corresponding modelled runoff profile based on nonlinear storage routing was 0.992. This value is considered to be very high, hence demonstrating the effectiveness of nonlinear storage routing as a modelling method for a range of green roof drainage layer configurations.

Optimized parameter values were grouped by test variable (e.g. 150 parameter sets with 2 m drainage length and 150 parameter sets with 5 m drainage length). Unpaired-sample *t*-tests were used to compare group means of *a*, *b* and *delay* for variables dividing into two groups (roof slope and drainage length). One-way ANOVA was used to compare group means of *a*, *b* and *delay* for

samples dividing into five groups (component configuration and inflow rate). All values of a parameter were grouped together and averaged if a test variable (e.g. rainfall rate, drainage component) was shown to have no statistically significant effect on parameter value. Testing suggested that the values taken by the scale parameter, a, of the weir equation, $Q = aS^b$, were fully independent of water inflow rate and partly independent of component configuration (Figure 5.10). Each test was therefore assigned to one of 16 groups, representing all possible combinations of both roof slopes, both drainage lengths and the four different combinations of component materials.

The value of a was averaged within each group, and the optimization was repeated for all 300 tests with each value of a fixed to the mean value of its appropriate group. With all a-values specified in advance from a set of 16, the mean R_t^2 across all tests was very marginally reduced to 0.991. This reduction is not considered to meaningfully affect the very high quality of the modelling.

Further unpaired-sample t-tests and one-way ANOVA were performed on the new optimized parameter sets for b and $delay$. These tests suggested that the values of the exponent parameter, b, were fully independent of drainage length, and partly independent of drainage component and inflow rate (Figure 5.12). In agreement with the theory underpinning all storage routing methods, the values of b were assumed to be fully independent of inflow rate. Each test was assigned to one of eight groups, representing the eight combinations of two roof slopes and four combinations of component materials.

The value of b was averaged within each group and modelling was performed for all 300 tests, with each value of a fixed as previously and each value of b fixed to the mean value of its appropriate group. Modelling with fixed a- and b-values was performed using all values of $delay$ from 0-80 seconds, and the $delay$ value which gave the best fit was saved. Mean R_t^2 with all values of both a and b specified in advance was very marginally reduced again to 0.990. This indicates that runoff predictions of a very high quality can still be produced even when the model is given approximated parameter estimates. The parameter values found here may therefore have some utility for untested drainage layer configurations.

The storage-discharge relationship (Equation 8.1) was adapted to follow Manning's equation by setting exponent b to 5/3 and expressing scalar a as a function of Manning's roughness coefficient, n. The full derivation is given in Appendix C. The optimization routine was run again, to find optimal values of a and $delay$, with $b = 5/3$. The optimized value of a was then converted, via Equation 5.1, to give an optimized value for n. This ranged from 0.00572 to 0.778, neither of which is considered unbelievable with regards to form roughness and flow

depth. Mean roughness value across both HDPE components (Floradrain FD 25 and Floradrain FD 40) was around 0.047, correlating well with the value of 0.05 used by She & Pang (2010). This suggests similarities between the runoff behaviour observed by them and the runoff behaviour observed in this experimental programme. However, incorporating Manning's equation was not considered to increase the usefulness of nonlinear storage routing overall.

A new optimization was performed for all 300 tests, with a and b optimized freely by *lsqcurvefit*, but *delay* only permitted to take values corresponding to full minutes i.e. 0, 60, or 120 seconds. The newly-optimized values of a were scaled for use at one-minute resolution by multiplying by 60, while the corresponding values of *delay* were divided by 60. B is dimensionless, so was not scaled. The inflow and runoff records at one-second resolution were then scaled to one-minute resolution by summing the contents of each set of 60 consecutive samples into one.

Routing was performed, feeding the values of a, b and *delay* scaled for use at one-minute resolution directly into the nonlinear storage routing model. These parameter values were not found to scale well to one-minute resolution. Growing oscillations were observed in 123 modelling cases, correlating somewhat to some combination of high a-values and high ratios of inflow rate to equilibrium depth in storage. In 103 tests the model run was terminated before the end of the inflow event, as the predicted value for Q exceeded the available depth of stored water in S at that time.

A re-optimization of a, b and *delay* was performed using the one-minute resolution data sets as inputs. The a-values found in this optimization were much lower than those calculated by multiplying the a-values optimized at one-second resolution by 60. None of the one-minute optimized values for a, b and *delay* terminated the model and the mean R_t^2 across all tests was 0.968. However, for all 42 cases in which the optimized value of b was above 4, growing oscillations were observed, which may have terminated the model run in the event of a longer inflow duration. For model stability, the value of b should be limited to the range [1,4].

The same optimization routine was used to fit a modelled runoff profile to each monitored runoff profile by separately adjusting the variable parameters in the governing equations for Muskingum routing. At one-second data resolution, the mean R_t^2 for a modelled runoff profile was 0.975. In practice, the weighting coefficient was optimized to near-zero in all 300 cases and the model was therefore reduced to linear storage routing. Physically, as the outlet from the drainage layer to a gutter or downpipe is effectively a weir, x should always be zero.

Overall, it was concluded that nonlinear storage routing was a more physically valid and less problematic method than the Muskingum method for modelling the drainage layer in the two-stage runoff detention model.

Table 8.1 – Suggested scale and exponent parameter values for nonlinear storage routing at one-second resolution.

Roof Slope	Drainage Length	Waterproofing		HDPE		Polystyrene		Fibrous	
		a	*b*	*a*	*b*	*a*	*b*	*a*	*b*
1.15°	2 m	0.067	2.84	0.022	2.45	0.017	2.84	0.020	2.01
	5 m	0.054		0.020		0.010		0.002	
10°	2 m	0.198	2.14	0.032	2.32	0.037	2.52	0.039	1.97
	5 m	0.147		0.027		0.027		0.002	

A small set of modelling parameter values was produced (Table 5.3), which is proposed to be suitable for modelling the runoff response of the drainage layer when an inflow profile at one-second resolution is used as input data. This is reproduced here as Table 8.1.

8.2.3 Experimental Data Collection and Modelling of the Substrate (Chapter 6)

A small rainfall simulator (0.36 m diameter), with rainfall supplied by a peristaltic pump, and runoff monitored at five-second temporal resolution and 0.005-0.017 mm depth resolution by a pressure transducer, was used to test six configurations of green roof substrate under three constant-intensity simulated rainfall events and one variable-intensity event, three times each.

Across all tests of substrate, the mean t_{50} time was 271 seconds, approximately 2.5 times that of the drainage layer. Equilibrium was reached between rainfall and runoff rate in all but three tests. This shows that the effects of attenuation in a substrate can be low provided that it is at field capacity and subjected to sustained, intense rainfalls of 6-36 mm/hour. The fact that attenuation is often observed in green roofs which are already at field capacity (e.g. see Chapter 3) may be due to the relative rarity of sustained events with rainfall intensity above 6 mm/hour in many climates, including that of the UK.

The same optimization routine as used in the drainage layer study (*lsqcurvefit*) was used to fit a runoff profile, modelled by nonlinear storage routing, to each monitored runoff profile. The methodology, governing equations and starting estimates used here were identical to those used for modelling the runoff response of the drainage layer by nonlinear storage routing. At five-second data resolution, the mean R_t^2 between monitored runoff and modelled runoff with optimized *a*, *b* and *delay*-values was 0.997. This is considered to be very high and clearly demonstrates the applicability of this modelling method for this purpose.

Optimized parameter values were grouped by test variable (e.g. 18 members in each of four rainfall profile groups, 36 members in each of two substrate depth groups). Unpaired-sample (i.e. Student's or Welch's) *t*-tests and one-way ANOVA were used, as appropriate, to determine which

groups were statistically similar and which were statistically different, through comparison of group means and variances at a significance level of $p = 0.05$. These tests suggested that the values taken by the a parameter were statistically independent of all test variables except substrate depth (Figure 6.7). Each of the 72 tests was assigned to one of two groups, membership determined solely by substrate depth.

The mean value of a was taken for each group and the optimization repeated, with the value of a fixed in advance to its appropriate group mean value. Mean R_t^2 was very marginally reduced to 0.995; accuracy was unaffected by this simplification of the modelling method.

Further unpaired-sample t-tests and one-way ANOVA, as appropriate, were again performed to determine which test variables did not have significant influence over the parameter values of b and $delay$. These tests suggested that the value of $delay$ was independent of rainfall rate, while the value of b was independent of all test variables except rainfall rate (Figure 6.9). It was decided the next stage of model simplification should be to group-average values of $delay$, rather than b, as the suggested dependence of b on rainfall rate was contrary to storage routing theory. Each test was assigned to one of six groups, membership determined by both substrate configuration and substrate depth.

The mean value of $delay$ was taken for each of the six groups and the optimization repeated to find the optimal values of b with both a- and $delay$-values fixed in advance. Mean R_t^2 was again very marginally reduced to 0.993. The continued accuracy of the model, even when "average" parameter values are specified, indicates a reasonable insensitivity to the "exactness" of the modelling parameter values.

The parameter values were scaled to a lower time resolution of one minute, to assess the validity of runoff profiles predicted from data records at a lower, but more typical, resolution. The parameters derived at a five-second resolution were found to scale well to one-minute resolution, and no growing oscillations were observed. This is in contrast to the drainage layer study and may relate to the smaller range over which the scaling was performed – 12× for the substrate parameters, 60× for the drainage layer parameters. Mean R_t^2 was 0.975 when the scaled parameters were used.

Following this, the tested substrates were paramaterized as necessary for use in Hydrus-1D, a numerical solver for the Richards' equation. Parameter values were either found through laboratory testing or, in the case of empirical parameters, predicted by ROSETTA Lite 1.1. Time-series runoff predictions were made with Hydrus-1D at a 5-second resolution and these were evaluated against the equivalent predictions made by the nonlinear storage routing model.

Table 8.2 – Suggested scale and exponent parameter values for nonlinear storage routing at five-second resolution.

Substrate Depth	Substrate Type					
	Marie Curie			LECA mix		
	a	*b*	*delay*	*a*	*b*	*delay*
5 cm	0.0790	2.23	25	0.0790	3.13	30
10 cm	0.0079	2.32	30	0.0079	2.73	100

Predictions for time-series runoff given by Hydrus-1D were highly unrealistic, but were consistent with those published by Hilten *et al.* (2008), so not unprecedented. The poor performance of Hydrus-1D may be due to the values given to the empirical parameters, which were predicted by a neural network from a database of non-engineered soils, using atypical input data e.g. 99.65% sand and the minimum permitted bulk density of 0.5 g/cm^3 (Table 6.4)

A small set of modelling parameters was produced (Table 6.5), suitable for modelling the runoff response of the substrate at five-second resolution. These are reproduced in Table 8.2. Multiplying the *a*-values by 12 and dividing the *delay*-values by 12 gives suitable parameter sets for modelling runoff at one-minute resolution. It was later suggested that the parameter values given for Marie Curie substrate may be more generally applicable to other substrates using the same mineral components, as the movement of water through a substrate at field capacity is gravity-driven and therefore primarily dependent on the arrangement of the macropore matrix.

8.2.4 Validation of the Two-Stage System Model (Chapter 7)

The nonlinear storage routing models for the substrate and drainage layer were arranged in series to produce a two-stage model with overall conservation between rainfall depth, runoff depth, temporary storage depth in the substrate and temporary storage depth in the drainage layer, at each time step. This model was experimentally verified against a laboratory test system, which used previously-tested components kept at field capacity. The storage-discharge and conservation relationships for each layer were parameterized according to previous testing and modelling of equivalent substrates and drainage layers in isolation.

The observed t_{50} times for the laboratory test bed were between 4½ and 19 minutes. These are similar to the t_{50} times that would be predicted by adding the t_{50} times observed for 10 cm of Marie Curie Substrate in isolation and 5 metres of FD 25 with SSM 45 in isolation, under the same rainfall profiles (Figure 7.4).

The two-stage model was found to very successfully predict runoff in the laboratory validation; mean R_t^2 was 0.972 across all 15 tests. This shows that the potential differences in composition and mixing between two batches of the same nominal substrate are not greatly important from a nonlinear storage routing perspective.

For the design storms, timing of peak runoff was accurate to one or two minutes. Intensity of peak runoff was accurate to within 0.5% for the 1-in-10 year storm and 11% for the 1-in-100 year storm. The over-prediction in intensity may have resulted from an over-supply of rainfall in two of the four time steps comprising the peak i.e. the peak was produced as an oscillating profile due to the limitations of the simulator.

The model was then used to predict the runoff profiles of three roof-based test beds in response to eight monitored rainfall events. These beds used untested component configurations (e.g. a 3 metre drainage length); the required parameter values for individual substrate and drainage layers were estimated by linear interpolation between appropriate values predicted for the individual substrate and drainage layers in isolation. Two of the test beds used untested substrates which used the same base material as the Marie Curie substrate. These were both parameterized using values suitable for Marie Curie substrate. Notable retention was observed in all test beds for four storms. Hence, they did not always begin at field capacity. As the nonlinear storage routing model always eventually results in equality between rainfall and runoff depths, the rainfall profiles that were input to the model were adjusted to give "net" rainfall profiles. This process involved removing a quantity of rainfall that was assumed to be retained and removing a quantity of rainfall that was assumed to be evaporated during the dry periods contained within the event.

The model was found to adequately predict the general runoff profile shape resulting from all rainfall events and test beds. Maximum R_t^2 was 0.949, approaching the observed accuracy for model validation under laboratory conditions. Two of the three substrates had not been previously tested and were parameterized as appropriate for Marie Curie substrate, a mix of overall similar composition using the same base materials. Mean R_t^2 for all tests using these substrates was 0.673. This is considered sufficiently high to suggest that some known differences in substrate composition may not greatly affect parameterization for nonlinear storage routing. As mentioned previously, this may be due to the fact that flow through substrates at and above field capacity is through the matrix of macropores, which is likely to relate primarily to the size distribution of the larger non-organic particles.

Under-attenuation was predicted for all three test beds. This caused many runoff peaks to be over-predicted in size. As these beds were 4-5 years old at the time of the validation events, extra attenuation may have been caused by a partially blocked filter sheet or by long-term changes in the substrate, neither of which were considered in the substrate experimental programme.

The nonlinear storage routing model was adapted to allow limited runoff at near-field capacity (Section 7.4.3), by routing a fraction of rainfall through the substrate as runoff whenever the

permanent retention capacity fell below a threshold level. This modification improved peak runoff predictions, particularly for the two test beds using brick- and pumice-based substrates. The improvement in peak runoff prediction was less for the test bed using LECA mix substrate, possibly because its higher organic content resulted in a less well-connected matrix of fewer macropores. This adaptation requires two extra user inputs: the permanent storage "breakpoint", below which not all rainfall is retained, and the relationship between retention and routing when not all rainfall is retained. The increase in the required number of user inputs can be justified if peak runoff rates are required to be known accurately for long-term rainfall records. However, for larger storms, the region of substrate water contents within which runoff can be initiated (i.e. between the breakpoint and zero) is reduced relative to total storm depth. In these cases, the adaptation is unlikely to significantly alter the peak flow rate prediction and its use is therefore more difficult to justify.

Peak flow rate prediction is shown to be improved by a range of specifications for the two extra user inputs (Figure 7.15). However, it is not yet clear which are most physically valid for the modelled substrates. It was noted in Chapter 6 that the response of the substrates during pre-wetting was not monitored. Though it would not have been practical to do so in that experimental programme, monitoring the runoff response of the substrates as they were brought up to field capacity would have provided information to allow more substantiated estimates for the parameterization of the adapted model.

8.3   Discussion

The overall aim of this project was stated in Section 1.2 as: "to improve the understanding of how green roofs function in a rainfall event and to propose a model for that behaviour".

Advances in understanding how green roofs function in a rainfall event have been made through the analysis of the longest green roof data record published, which provides the basic hydrological performance metrics of a green roof test bed's response to over 400 storms, which are themselves characterized. Though this data is not directly transferrable to other climates and system designs, this limitation is somewhat mitigated by the common, generic system design and the per-rainfall-event performance metrics being available. Parametric analysis of runoff responses resulting from the storms that would most likely be of interest to urban drainage engineers was not successful in proposing a simple "black box" model for green roof behaviour. Instead, it clearly demonstrated this type of approach is neither valid nor useful, and proposed the development of a continuous simulation (hydrological modelling) approach. A detailed experimental programme was undertaken to quantify and parameterize the detention effects associated with green roof substrate and drainage layer components.

The three chapters following the experimental setup improved on this understanding, by recording and modelling climate-independent runoff profiles for individual green roof components. These can be combined to represent a range of system designs. Independence from climate was achieved by defining and controlling initial conditions in the tested components. Of all models tested for the substrate and drainage layer, nonlinear storage routing was shown to be appropriate for both, and the accuracy of the modelled runoff was shown to be insensitive to the exactness of the modelling parameter values. It is therefore concluded that nonlinear storage routing has generic applicability to a variety of configurations of substrate and drainage layer. All storage routing methods are, however, dependent on initial conditions in the sense that they can only model temporary storage, requiring the modelled component to be initially at field capacity.

Assembling the two separate layer models in series gave generally acceptable to good predictions for runoff, for both laboratory and roof-sited test beds. The level of parameter interpolation and assumption made for modelling the roof-sited test beds further demonstrates the insensitivity of the modelling parameters to deviations in configuration from those for which the parameters are technically valid. It is therefore shown that the proposed model is generic. For the roof-sited test beds, the model was adapted to allow inequality between rainfall and runoff depth by calculating in advance the depth of retained water and modifying the rainfall profile input to the two-stage substrate and drainage layer model accordingly.

It is stated here that the nonlinear storage routing model requires both the substrate and drainage layers of the green roof to be modelled to start at field capacity. This is a limitation if long-term modelling over multiple rainfall events is required as, due to evapotranspiration between events, the roof is very unlikely to be at field capacity at the start of any event. However, for urban drainage modellers predicting the worst-case runoff response of a new development, the constraint that all rainfall must become runoff is not a limitation, as this is the worst possible case. It is also noted that the detention model was always intended to be combined with a retention model, a form of which is tested in Sections 7.4.2 and 7.4.3.

Under the high and reasonably high rainfall intensities considered in the individual component test programme, the time delay between the median of rainfall depth entering a component and the same depth leaving that component was small, ranging from a few seconds to no higher than 15 minutes. It was found that, under a constant rainfall intensity of 6 mm/hour, a cumulative median-to-median time delay (t_{50}) of up to 25 minutes could be introduced by a combination of 10 cm LECA mix substrate, a HDPE drainage layer of drainage length 5 metres and an underlying fibrous protection mat. An event of 6 mm in one hour is equivalent to a 1-in-1 year storm for Sheffield (NERC, 1999). Time delays for more common events could be assumed to be even longer. However, for the 1-in-30 year and 1-in-100 year intensity events that would be of

more interest (approximately 30-45 mm in an hour for Sheffield), the cumulative median-to-median delay times for the same substrate/drainage layer/protection mat combination are around 5-10 minutes and may therefore be of limited interest in an urban drainage modelling context. The observed delay times for the drainage layer may be increased for larger roofs with longer flow paths to gutters and outlets, but as the main purpose of a drainage layer is to quickly remove excess water that cannot be stored, no properly-designed drainage layer configuration should delay runoff greatly. The delay introduced by the substrate layer does not scale with roof area, as all water flow is approximately perpendicular to the roof plan for flat and near-flat roofs.

A broader implication of the low observed t_{50} times is that typical extensive green roofs at field capacity do not greatly delay runoff under high return period events, nor were they shown in Chapter 7 to greatly reduce peak runoff rate under those events. Though this behaviour was only confirmed at field capacity, the initial portion of a large storm may bring a roof up to field capacity from an arbitrary initial state. If significant attenuation is required under large storms, a number of solutions may be possible, each with advantages and drawbacks. Increasing the substrate depth will increase the detention effects of the roof and increase total retention capacity. This will reduce the typical expected runoff depth resulting from a storm, but will add significant extra weight and will not guarantee that the potential extra capacity will be available prior to any specific storm. Peak runoff intensity could be limited by outlet flow controls, such as reducing the number of downpipes or their diameters, but international regulations set minimum values for both. Storing or detaining extra water in the drainage layer or in an extra component, with outflow controls on that component, may side-step these regulations but will result in a pool of standing water on the roof following large storm events, which will require extra support from the building. Eliminating the green roof entirely, in favour of a very deep retention/detention component, could allow significant detention of storms hundreds of millimetres deep, but would result in even deeper and heavier pools of standing water on the roof and would not effectively provide any of the secondary benefits of a green roof. A treatment train, placing another SUDS component such as a pond, rain garden or geocellular storage, after a group of neighbouring green roofs, would move this pooled water to the ground, but at the cost of on-going maintenance and possible excavation.

8.4   Further Work

The individual substrate and drainage layer models were found to perform well in the tested configurations. The following suggestions are made for further work, with the aim of potentially adding further generic applicability to the models.

Linear interpolation was used to find parameter values for untested configurations. Data presented by Yio *et al.* (2012) suggest this may be inappropriate for interpolating values over

substrate depth. However, insufficient data exist to propose a more accurate interpolation method. This is considered important, as the same data also suggest that substrate depth may be the largest determining factor on runoff response. Further testing of intermediate and other sensible configuration variants e.g. 7.5 and 12.5 cm depth for substrate, 3° and 5° roof slope for drainage layer, is suggested, to provide more data points on which to base an interpolation method for untested roof configurations. The first tests of intermediate configurations should be performed for those variables that have the most significant effect on parameter values i.e. substrate depth (for the substrate) and roof slope (for the drainage layer). An opportunity may also be taken to test e.g. a 20 cm substrate depth, extending the model's applicability to intensive green roofs, which have greater potential to detain runoff. Full implementation of this suggestion is likely to require hundreds of hours over a period of months. However, the model is currently limited in range between the upper and lower tested bounds on a configuration variable. If one or both bounds are moved by additional testing, then the range of configurations that can be modelled is extended. Additional data points may also allow extrapolation beyond the bounds of tested configurations, extending the model's range indefinitely.

The substrate model is at a lower stage of development than the drainage layer model, due to the limited information that can be derived from 24 test configurations in comparison to 100. Though it is suspected that the detention performance of a substrate depends overwhelmingly on its mineral component, tests of additional substrate mixes with variable organic contents and materials are proposed in order to confirm this hypothesis, including at typical, and so far entirely untested, intensive depths. If this hypothesis is shown to be false, then further consideration may need to be given to link modelling parameters to easily-measurable substrate mix properties, such as bulk density and particle size distribution then, if this is not possible, to less easily-measurable properties, such as saturated water content, residual water content and saturated hydraulic conductivity. Implementation of this suggestion would require undertaking a considerably larger test programme than has so far been conducted with the substrate, but has the potential to make the model applicable to all mineral-based substrates. Further automation of the substrate test chamber and monitoring equipment, to the standard employed for the large rainfall simulator, has the potential to greatly reduce the required level of human interaction to obtain this much larger quantity of test data and potentially permit continuous 24-hour running. Increased automation of the substrate test chamber and monitoring equipment is therefore considered necessary for any future extended substrate monitoring programme.

No long-term effects or changes were studied in this experimental programme, due to the impossibility of doing so in the time given to the work contained in this thesis. An example of a potentially significant long-term effect would be the gradual clogging of the filter sheet, as

substrate particles slightly larger than its effective opening size wash through and settle on its upper surface. If this happens, the detention effects of the filter sheet may increase to a noticeable level, as an increasing number of pathways through it are effectively blocked. A second long-term effect for potential further study is the change in the substrate matrix due to root growth. It is not known whether root growth would increase detention effects, by advancing into and blocking pathways in the substrate's air matrix, or reduce detention effects, by providing preferential pathways for water movement alongside the roots. Studies of the Hadfield roofs (Section 7.4) suggested that the modelled attenuation, predicted from relatively new substrates and filter sheets, was too low. A study, periodically subjecting one roof to a fixed design storm under controlled initial conditions, could provide empirical evidence to evaluate the significance of long-term changes. Though this study would potentially require years to conduct and is non-repeatable, the amount of work involved is low enough that several studies could be performed in parallel, increasing the degree of empirical evidence for long-term changes.

The effects of a vegetation layer were not considered in this thesis. It was hypothesized that the effects of vegetation on rainwater detention would be minimal under the intense rainfall and inflow rates used throughout this thesis and associated with the long-return-period design storms that are of interest to drainage engineers. However, for the many small storms that would be expected to occur throughout a long time-series record, the effects of vegetation on detention could be large. Nevertheless, since these smaller storms are of low interest in drainage design, it is proposed that the exact runoff profiles predicted in response to these storms will be of little importance and largely ignored by the end users. Preliminary tests, to determine the significance of the role played by the vegetation layer during large storm events may be justifiable, though if the effect of vegetation on runoff is shown to be low, no further tests should be conducted.

The two-stage model was found consistently applicable to the system tested at field capacity under laboratory conditions, and acceptable when tested against climate-exposed roof-level test beds. Two suggestions are made for further work, with the aim of further improving the model, specifically with regards to its applicability to long-term modelling and its predictions for peak flow rate.

The two-stage model, whether applied to the laboratory test system or the Hadfield test beds, required the depth of runoff corresponding to a rainfall event to be known in advance. This is not an issue for modelling the runoff occurring due to single, worst case scenario events, as all rainfall can be assumed to become runoff in these cases. However, the model's predictive capability for long time-series is currently limited by the lack of a robust model for evapotranspiration. Previous studies (e.g. Kasmin, 2010; She & Pang, 2010) identified the requirement to model evapotranspiration during dry periods, in order to determine the available

retention capacity at the start of a storm. Further testing and improvement of the model's handling of evapotranspiration should be considered a significant priority for future research, as an accurate evapotranspiration stage would extend the model's scope to one of both retention and detention. The amount of work required to implement this recommendation is hard to define. One approach would require monitoring of wind speed, temperature and solar radiation at the site, followed by regression of collected data to predict evapotranspiration rate as a function of these factors. Another approach would simply require optimization of a constant evapotranspiration rate in order to most closely match predicted and recorded runoff depths over both long time periods and over individual storms within those periods. However, this constant rate may not be as broadly applicable to roofs in other climates, and neither method will necessarily be suitable for predicting evapotranspiration rates when other plant species are used.

It was noticed in the analysis of the Hadfield test beds that runoff could occur before field capacity was predicted to be reached, and that this could be physically explained. The model adaptation presented in Section 7.4.3 is shown to improve peak runoff predictions for four storms (Figure7.14), but its parameterization is also shown to be highly uncertain (Figure 7.15). It is suggested that further research may be required to understand and model the runoff response of substrates at conditions approaching field capacity, but only if importance is attached to accurately predicting runoff profiles resulting from routine events in a long-term data record. It is suggested that the precision to which the response to routine events needs to be known is not high. It is also noted that, as the total storm depth increases, the roof is likely to be at field capacity for an increasing fraction of the total storm. Hence, this modification is unlikely to be of much use when considering large design storms, except possibly for roofs with very deep substrate layers. However, since the substrate stage of the model is not yet suitable for substrate layers deeper than 10 cm, this issue will not be of any concern until or unless laboratory tests on deeper substrate layers are performed.

9   Conclusions

Overview

This chapter summarizes the main conclusions, discussion and further work recommendations presented in Chapter 8, into a more succinct format. It is strongly recommended that the relevant section of Chapter 8 is consulted if further detail is required on the contents of any summarized item presented in this chapter.

Long-Term Monitoring and Parametric Modelling of Green Roof Test Bed Performance

1.   Small (3 m^2) extensive test bed monitored 27½ months of period January 2007-May 2009. Using 6-hour antecedent dry weather period, rainfall and runoff records exist for 432 storms, 200 of which are ≥ 2 mm in depth.

2.   Cumulative retention of 49.3% over monitoring period (933.8 of 1892.2 mm). Relatively low figure in comparison to similar studies, probably due to Sheffield's maritime temperate climate, the comparatively low substrate depth (80 mm) and above-average rainfall during monitoring period (9.4% greater than expected, according to 1981-2010 average).

3.   Mean per-event retention of 69.6% (all 432 storms in monitoring period) or 60.4% (only storms ≥ 2 mm). Relatively low in comparison to similar studies (e.g. Voyde *et al.*, 2010) but considerable in its own right. For both groups of storms, minimum and maximum per-event retention were ~0% and ~100%.

4.   Maximum per-event retention depth of 20 mm – or 25% of substrate depth. This correlates well with expected range between permanent wilting point and field capacity.

5.   Mean per-event peak flow reduction of 87.6% (all 432 storms in monitoring period) or 78.9% (only storms ≥ 2 mm). Relatively low in comparison to similar studies but high in its own right.

6.   "Significant" storms defined as those with: return period > 1 year; or return period of most intense 1, 6 or 12 hours > 1 year. Majority of significant events (12 of 21) occurred in summer (June, July or August), only three each occurred in autumn, winter and spring.

7.   Mean per-event retention and peak flow reduction of 42.7% and 59.2% respectively for significant storms. Minimum and maximum per-event retention were ~0% and ~100%.

8.   All significant storms were characterized by: event duration; total rainfall depth; antecedent dry weather period; mean intensity; and peak intensity over five minutes.

9.   Corresponding runoff responses were characterized by: total runoff depth; total retention depth; percentage retention; delay to start of runoff; peak runoff intensity over five minutes; percentage peak reduction; rainfall-runoff peak-to-peak delay; and cumulative rainfall-runoff median-to-median delay.

10.   No strong, physically-meaningful relationships were found to exist between the characteristics of the 21 significant storms and the corresponding runoff metrics.

11.   For each storm, antecedent weather was characterized by: rain depth in previous 24 hours; rain depth in previous 7 days; rain depth in previous 14 days; mean temperature over previous 24 hours; and mean monthly temperature over 1981-2010.

12.   Stepwise multiple linear regressions, using normalized data sets for storm and weather characteristics, were moderately successful for predicting total runoff, percentage retention, peak runoff intensity and peak runoff attenuation, using all possible pools of independent storm characteristics and antecedent weather characteristics.

13.   Overall, parametric modelling is not sufficiently accurate or generically-applicable for prediction of performance, for either the modelled roof or any other roof.

14.   Physically-based modelling approaches are proposed as the only suitable modelling methods.

Physically-Based Modelling of the Drainage Layer

1.   Experimental runoff monitoring of drainage layers was performed in a test chamber under laboratory conditions. Four test variables were defined: drainage component (five configurations); roof slope (two configurations); drainage length (two configurations); and inflow rate (five configurations). All combinations were tested systematically three times for a total of 300 tests.

2.   Typical drainage layer routing/attenuation effects are comparable to conventional roof surfaces: inflow-runoff cumulative median-to-median delay times ranged from 8 seconds to approximately 10 minutes, with a mean of around 110 seconds.

3.   A nonlinear storage routing model was modified with a delay parameter, allowing the monitored runoff record to be offset relative to the rainfall record. This was intended to account for monitoring delays in the experimental setup.

4.   For each test, the modified nonlinear storage routing method was applied and the two parameters of the storage-discharge relationship were optimized for each monitored-modelled runoff pair on a case-by-case basis. Mean R_t^2 of model fit was 0.992.

5. All optimized parameter values were grouped systematically by one configuration variable and group means were evaluated, to determine if that variable was a significant determiner of parameter value.

6. The scale parameter of the storage-discharge relationship was found to be independent of inflow rate, while the exponent parameter was found to depend on component type and roof slope. Means were taken for each statistically similar group.

7. A small set of generalized nonlinear storage routing parameter values (16 scale parameter values, 8 exponent parameter values) was found to be almost as applicable as the original, much larger set of optimized parameter values (mean Rt2 = 0.989).

8. Adapting nonlinear storage routing to follow Manning's Equation reduces the number of model variables by one, but, as the original model is not overly complex and gives more accurate predictions, this adaptation is not considered valuable.

9. The storage-discharge parameter values that are valid at one-second data resolution are not valid for use with data at one-minute resolution (after scaling by 60, where necessary, to maintain consistency of units).

10. For modelling purposes, it is currently recommended to artificially upscale all input data to one-second resolution, and downscale predicted runoff to the original resolution.

11. A Muskingum routing model was also tested. This was not considered to be a suitable (or physically-accurate) method by which to model the time-series runoff from a green roof drainage layer, at either one-second or one-minute time resolution.

Physically-Based Modelling of the Substrate

1. Experimental runoff monitoring of substrate samples was performed in a test chamber under laboratory conditions. Three test variables were defined: substrate configuration (three configurations); substrate depth (two configurations); and inflow rate (four configurations). All combinations were tested systematically three times for a total of 72 tests.

2. Cumulative rainfall-outflow median-to-median time delays ranged from approximately 2 to 13 minutes. Longer times were observed for lower peak rainfall rates, deeper substrates and for the substrate with the highest fine particle content.

3. The addition of a layer of ZinCo SSM 45 (a fibrous protection mat normally used underneath the drainage layer to protect the roof) below the substrate did not noticeably affect runoff response.

4. The nonlinear storage routing method developed for modelling the drainage layer was applied to model the substrate at five-second resolution.

5. The modified nonlinear storage routing method was applied and the two parameters of the storage-discharge relationship were optimized for each monitored-modelled runoff pair on a case-by-case basis. Mean R_t^2 of model fit was 0.997.

6. All optimized parameter values were grouped systematically by one configuration variable and group means were evaluated, to determine if that variable was a significant determiner of parameter value.

7. The scale parameter of the storage-discharge relationship was found to depend only on substrate depth, while the *delay* parameter was found to be independent of rainfall profile. Means were taken for each statistically similar group.

8. A small set of generalized nonlinear storage routing parameter values (2 scale parameter values, 6 delay parameter values) is almost as applicable as the original, much larger set of optimized parameter values (mean $R_t^2 = 0.993$ over 72 tests).

9. The storage-discharge parameter values that are valid at five-second data resolution are valid for use with data at one-minute resolution, after scaling by 12, where necessary to maintain consistency of units (Mean $R_t^2 = 0.975$ over 72 tests).

10. A commercial programme, Hydrus-1D, was also tested, and found to give highly unrealistic runoff results, presumably due to the difficulties of describing the substrate in that programme.

Validation of Combined Substrate/Drainage Layer Model

1. A combined model was created, consisting of two nonlinear reservoirs in series.

2. The combined model was parameterized to predict the runoff resulting from controlled wetting of a two-layered (substrate and drainage layer) system, using previously-tested configurations under laboratory conditions. Predictions were of very high quality (Mean $R_t^2 = 0.971$ over 15 tests).

3. The model parameterization, generated under mostly time-invariant wetting conditions, was found equally applicable to modelling runoff response during time-varying wetting events.

4. A permanent retention stage was added to the model, to allow for inequalities between rainfall and runoff. It was then applied "in the field" to three test beds located in Sheffield,

UK, built to configurations that had not been previously tested, and input with time-series rainfall records that corresponded to eight real storms monitored at that site.

5. The quality of predications, using parameter values estimated by linear interpolation between tested configurations, were reasonable (mean $R_t^2 = 0.710$ over 24 tests) and approached those of the laboratory tests in the best case (maximum $R_t^2 = 0.950$).

6. The model tended to under-predict attenuation for the field validation programme. This may be due to changes in the test beds resulting from age e.g. blocking of the filter sheet. Under-prediction is considered preferable to over-prediction of attenuation.

7. Two modifications were made to the permanent retention stage: one to allow some runoff before complete filling and one to allow evaporation during dry periods.

8. The improved model was re-applied to the 12 data records with retention above 0.2 mm. Runoff predictions were improved in almost all cases (mean increase in $R_t^2 = 0.1135$), though the greatest improvements were for events containing long dry periods.

Discussion

The overall aim of this project was "to improve the understanding of how green roofs function in a rainfall event and to propose a model for that behaviour". This has been met by

1. The publication and statistical analysis of the largest rainfall-runoff record ever published, containing 432 individual storms over 29 months.

2. Monitoring of the runoff responses of green roof components in isolation under controlled environmental conditions and rainfall/inflow profiles.

3. Evaluation, selection and testing of different modelling methods to predict time-series runoff from time-series rainfall profiles.

4. A small set of parameter values, to be used with green roof configurations matching those tested, or to be interpolated to model green roof configurations existing between the lower and upper limits of the tested configurations.

5. Validation of the developed one-layer substrate and drainage layer models in series, first under laboratory conditions using previously-tested configurations, then under field conditions with components in untested configurations.

6. Extension of the two-layer green roof system model to incorporate evapotranspiration, permanent retention and runoff initiation before field capacity is reached.

Further Work

1. Parameterization of untested components is currently interpolated linearly. It is proposed that further controlled laboratory testing of individual green roof components will offer more data to: improve the interpolation method; extend the upper and lower boundaries on the interpolation (e.g. allowing intensive substrate depths to be modelled); and potentially offer methods for predicting parameter values outside of the tested boundaries. It is recommended that substrate testing is prioritized, as this component is responsible for the majority of runoff detention.

2. Changes to the substrate are certain to happen in green roof installations over long time periods. It would be beneficial for the model to take account of these. However, years would be required to conduct this study. Though the study would not be repeatable, the evidence gained may be sufficient to improve the runoff detention model.

3. The effects of a vegetation layer were not considered in this thesis. They are, however, assumed to provide little detention in the event of large storms. It may be beneficial to conduct a small test programme to confirm this, to be stopped upon confirmation.

4. The two-stage model is currently assumed to be non-applicable to long time series, due to the low level of sophistication of the evapotranspiration model. Further instrumentation of test sites, to monitor wind speed, solar radiation and temperature will provide the data to calculate evapotranspiration as a time-varying function. If this is not possible, then a range of existing evapotranspiration models should be applied to long time series collected from multiple sites, and the results evaluated.

5. The modification allowing runoff under near-field capacity conditions is shown to improve runoff predictions, though its parameterization is uncertain. It is not recommended to improve this modification, as its effects on time-series runoff response are not substantial under the large events that are of interest to urban drainage engineers.

References

Abad M, Fornes F, Carrión C, Noguera V, Noguera P, Maquieira Á and Puchades R (2005). Physical properties of various coconut coir dusts compared to peat. *HortScience* 40 (7), 2138-2144.

Alumasc (2010). *ZinCo Green Roof Systems*. Alumasc Exterior Building Products Ltd, St. Helens, UK.

Alumasc (2012a). Product Data Sheet. Substrate "Roof Garden" (Online). Alumasc Exterior Building Products Ltd, St. Helens, UK. Available from: http://www.alumascwaterproofing.co.uk/media/68081/pd-zinco-substrate-roofgarden.pdf (accessed 17th July 2012).

Alumasc (2012b). Product Information. Floradrain® FD 25-E (Online). Alumasc Exterior Building Products Ltd, St. Helens, UK. Available from: http://www.alumascwaterproofing.co.uk/media/67985/pd-zinco-drainagelayer-floradrainfd25e.pdf (accessed 7th August 2012).

Alumasc (2012c). Alumasc Waterproofing | Product Datasheets (Online). Alumasc Exterior Building Products Ltd, St. Helens, UK. Available from: http://www.alumascwaterproofing.co.uk/downloads/product-datasheets (accessed 19th July 2012).

American Society of Civil Engineers (1996). *Hydrology Handbook, 2nd Edition*. ASCE, New York, NY.

Anderson B (2006). *Conventions for U-value calculations*, BR 443 – 2006 edition. BRE Press, Bracknell, UK.

Ashley R M, Tait S J, Styan E, Cashman A, Luck B, Blanksby J, Saul A and Sandlands L (2007). Sewer system design moving into the 21st century – a UK perspective. *Water Science and Technology* 55 (4), 273-281.

Banting D, Doshi H, Li J, Missios P, Au A, Currie B A and Verrati M (2009). Report on the Environmental Benefits and Costs of Green Roof Technology for the City of Toronto. Ryerson University, Toronto, Canada.

BBC (2009). BBC – Panorama – Mapping sewer overflow pipes (Online). British Broadcasting Corporation, London, UK. Available from: http://news.bbc.co.uk/panorama/hi/front_page/newsid_8242000/8242444.stm (accessed 17th July 2012).

Beck D A, Johnson G R and Spolek G A (2012). Amending greenroof soil with biochar to affect runoff water quantity and quality. *Environmental Pollution* 159 2111-2118.

Bengtsson L, Grahn L and Olsson J (2005). Hydrological function of a thin extensive green roof in southern Sweden. *Nordic Hydrology* 36 (3), 259-268.

Berndtsson J C, Bengtsson L and Jinno K (2009). Runoff water quality from intensive and extensive vegetated roofs. *Ecological Engineering* 35 (3), 369-380.

Bowyer-Bower T A S and Burt T P (1989). Rainfall simulators for investigation soil response to rainfall. *Soil Technology* 2 (1), 1-16.

Brenneisen S (2004). From Biodiversity Strategies to Agricultural Productivity. In: *Proceedings of the 2nd North American Green Roof Conference: Greening Rooftops for Sustainable Communities*, Portland, OR, 2-4th June 2004, pp. 391-403. The Cardinal Group, Toronto, Canada.

Brenneisen S (2006). Space for urban wildlife: Designing green roofs as habitats in Switzerland. *Urban Habitats* 4 27-36.

BSI (2000). *Gravity drainage systems inside buildings*, BS EN 12056-3:2000. British Standards Institution, London, UK.

BSI (2010a). *Geotextiles and geotextile related products – Determination of water flow capacity in their plane*, BS EN ISO 12958:2010. British Standards Institution, London, UK.

BSI (2010b). *Geotextiles and geotextile-related products – Determination of the characteristic opening size*, BS EN ISO 12956:2010. British Standards Institution, London, UK.

BSI (2010c). *Geotextiles and geotextile-related products – Determination of water permeability characteristics normal to the plane, without load*, BS EN ISO 11058:2010. British Standards Institution, London, UK.

Burian S J and Edwards F G (2002). Historical Perspectives of Urban Drainage. In: *Global Solutions for Urban Drainage* (ed. E W Strecker and W C Huber), Portland, OR, 8-13th September 2002. American Society of Civil Engineers, Reston, VA.

Butler D and Davies J W (2004). *Urban Drainage (2nd edition)*. Spon Press, London, UK.

Cabeza L F (2012). Green roofs as passive system for energy savings when using rubber crumbs as drainage layer (poster). *International Conference on Solar Heating and Cooling for Buildings and Industry*, San Francisco, CA, 9-11th July 2012.

Carpenter D D and Kaluvakolanu P (2011). Effect of Roof Surface Type on Storm-Water Runoff from Full-Scale Roofs in a Temperate Climate. *Journal of Irrigation and Drainage Engineering* 137 (3), 161-169.

Carsel R F and Parrish R S (1988). Developing joint probability distributions of soil water retention characteristics. *Water Resources Research* 24 (5), 755-769.

CEH (1999). *Flood Estimation Handbook*. Centre for Ecology and Hydrology, Wallingford, UK.

Childe V G, Bryce T H and Watson D M S (1931). *Skara Brae: A Pictish Village in Orkney*. Kegan Paul, Trench, Trubner & Co, London, UK.

Chow V T (1959). *Open-Channel Hydraulics*. McGraw-Hill Book Company, New York, NY.

Christiansen J E (1942). Irrigation by Sprinkling. California Agricultural Experiment Station Bulletin 670. University of California, College of Agriculture. Berkeley, CA. 124 pp.

CIRIA (2012a). Glossary (Online). The Construction Industry Research and Information Association, London, UK. Available from: http://www.susdrain.org/resources/glossary.html (accessed 24th January 2013).

CIRIA (2012b). SuDS components overview (Online). The Construction Industry Research and Information Association, London, UK. Available from: http://www.susdrain.org/delivering-suds/using-suds/suds-components/suds-components.html (accessed 24th January 2013).

CIRIA (2012c). SuDS management train (Online). The Construction Industry Research and Information Association, London, UK. Available from: http://www.susdrain.org/delivering-suds/using-suds/suds-principles/management-train.html (accessed 24th January 2013).

City of Copenhagen (2010). Pressrelease: Green roof ambitions in Copenhagen. Technical and Environmental Administration, Copenhagen, Denmark.

City of Portland (2005). City of Portland Green Building Policy (Online). City of Portland, Portland, OR. Available from: http://www.portlandonline.com/shared/cfm/image.cfm?id=112682 (accessed 23rd July 2012).

City of Portland (2010). *Title 33, Planning and Zoning. Chapter 33.510, Central City Plan District*. Portland, OR.

City of Portland Environmental Services (2011). Working for clean rivers. Portland's ecoroof program (Online). City of Portland, Portland, OR. Available from: http://www.portlandonline.com/bes/index.cfm?c=50816&a=261074 (accessed 23rd July 2012).

City of Toronto (2006). *Section 108, Construction of green roofs or alternative roof surfaces, City of Toronto Act. S.O. 2006, chapter 11, Schedule A, section 108*. Toronto, Canada.

City of Toronto (2009). Green Roofs in Toronto (Online). Toronto, Canada. Available from: http://www.toronto.ca/greenroofs/pdf/greenroof_bylaw_brochure.pdf (accessed 8th August 2012).

City of Toronto (2011). *BY-LAW No. 1381-2011, To amend City of Toronto Municipal Code Chapter 492, Green Roofs, by providing a cool roof alternative to the Green Roof requirements for industrial buildings*. Toronto, Canada.

Clarke M A and Walsh R P D (2007). A portable rainfall simulator for field assessment of splash and slopewash in remote locations. *Earth Surface Processes and Landforms* 32, 2052-2069.

Conrads U (1970). *Programs and manifestoes on 20th-century architecture*. Translated from German by M Bullock. Lund Humphries, London, UK.

Currie B A and Bass B (2008). Estimates of air pollution mitigation with green plants and green roofs using the UFORE model. *Urban Ecosystems* 11 (4), 409-422.

Dane J H and Topp G C (2002) *Methods of Soil Analysis, Part 4 – Physical Methods*. Soil Science Society of America, Madison, WI.

Darcy H (1856). *Les Fontaines Publiques de la Ville de Dijon*. Dalmont, Paris, France.

DEFRA (2010). UK Framework Indicators (Online). Department for Environment, Food and Rural Affairs, London, UK. Available from: http://archive.defra.gov.uk/sustainable/government/progress/national/framework.htm (accessed 8th August 2012).

DIN (2008). *Entwässerungsanlagen für Gebäude und Grundstücke - Teil 100: Bestimmungen in Verbindung mit DIN EN 752 und DIN EN 12056*, DIN-1986:2008-05. Deutsches Institut für Normung, Berlin, Germany.

Dunnett N and Kingsbury N (2004). *Planting Green Roofs and Living Walls*. Timber Press, Portland, OR.

Dunnett N, Nagase A, Booth R and Grime P (2008). Influence of vegetation composition on runoff in two simulated green roof experiments. *Urban Ecosystems* 11, 385-398.

European Commission (2000). Directive 2000/60/EC of the European Parliament and of the Council, of 23rd October 2000, establishing a framework for Community action in the field of water policy. In: *22nd December 2000), pp. 1-72. Official Journal of The European Communities L 327*, Brussels, Belgium.

Europomice (2011a). Volcanic Lapillus (Online). Europomice Srl, Grosseto, Italy. Available from: http://www.europomice.com/wp-content/uploads/2011/03/www.europomice.com/Volcanic-Lapillus-Technical-Data-Sheet-Feb-2012-ENG.pdf (accessed 29th November 2012).

Europomice (2011b). Vulcaflor (Online). Europomice Srl, Grosseto, Italy. Available from: http://www.europomice.com/wp-content/uploads/2011/03/www.europomice.com/Vulcaflor-Technical-Data-Sheet-Feb-2012-ENG1.pdf (accessed 29th November 2012).

FBB (2004). Auswertung der Umfrage Dachbegrünung an Stadtverwaltungen von Städten über 10.000 Einwohner. Fachvereinigung Bauwerksbegrünung e.V., Saarbrücken, Germany.

Fernandez-Canero R and Gonzalez-Redondo P (2010). Green roofs as a habitat for birds: A review. *Journal of Animal and Veterinary Advances* 9 (15), 2041-2052.

Fioretti R, Palla A, Lanza L G and Principi P (2010). Green roof energy and water related performance in the Mediterranean climate. *Building and Environment* 45 (8), 1890-1904.

FLL (2008). *Guidelines for the Planning, Execution and Upkeep of Green-roof sites*. Forschungsgesellschaft Landschaftsentwicklung Landschaftsbau e.V., Bonn, Germany.

Fonteno W C (1993). Problems and considerations in determining physical properties of horticultural substrates. In: *International Symposium on Horticultural Substrates other than Soil in situ* (ed. M Tattini), pp. 197-203. Acta Horticulturae, Florence, Italy.

Flood and Water Management Act. United Kingdom Public General Acts (2010). Flood and Water Management Act, 2010 c. 29.

Gayman M (1996). A glimpse into London's early sewers. In: *Cleaner*, COLE Publishing Inc., Three Lakes, WI.

Gelegenis J J and Serrano S E (2000). Analysis of Muskingum equation based flood routing schemes. *Journal of Hydrologic Engineering* 5 (1), 102-105.

Getter K L, Rowe D B and Andresen J A (2007). Quantifying the effect of slope on extensive green roof stormwater retention. *Ecological Engineering* 31 (4), 225-231.

Getter K L, Rowe D B, Robertson G P, Cregg B M and Andresen J A (2009). Carbon Sequestration Potential of Extensive Green Roofs. *Environmental Science & Technology* 43 (19), 7564-7570.

Greater London Authority (2011). *Policy 5.11. Green roofs and development site environs, The London Plan.* London, UK.

Greater Manchester Biodiversity Project (2008). Make Room for Black Redstarts. A species action plan for Greater Manchester. Greater Manchester Ecology Unit, Manchester, UK.

Green Roofs for Healthy Cities (2011). Toronto's Green Roof Bylaw Generates 1.2M Sq. Feet of New Green Space (Online). Green Roofs for Healthy Cities, Toronto, Canada. Available from: http://www.greenroofs.org/index.php/mediaresource/grhc-news-releases/3596-tor-gen-12milsqft-green (accessed 8th August 2012).

Gregoire B G and Clausen J C (2011). Effect of a modular extensive green roof on stormwater runoff and water quality. *Ecological Engineering* 37 (6), 963-969.

Gregory M A, Cunningham B A, Schmidt M F and Mack B W (1999). Estimating soil storage capacity for stormwater modeling applications. *6th Biennial Stormwater Research and Watershed Management Conference*, Tampa, FL, 14-17th September 1999.

Hall B R and Freeman G E (1994). *WRP Technical Note SD-CP-2.2 May 1994: Effects of vegetation on hydraulic roughness and sedimentation in wetlands*. US Army Corps of Engineers Wetlands Research Program, Vicksburg, MS.

Healy R W (2010). *Estimating Groundwater Recharge*. Cambridge University Press, Cambridge, UK.

Heber Green W and Ampt G A (1911). Studies on soil physics. *Journal of Agricultural Science* 4, 1-24.

Hilten R N, Lawrence T M and Tollner E W (2008). Modeling stormwater runoff from green roofs with HYDRUS-1D. *Journal of Hydrology* 358 (3–4), 288-293.

Hong T, Kim J and Koo C (2012). LCC and $LCCO_2$ analysis of green roofs in elementary schools with energy saving measures. *Energy and Buildings* 45, 229-239.

Hopkins J N N (2004). Reflections of Expansion: The Cloaca Maxima and Urban Image in Tarquin Rome (Masters Thesis). University of Texas, Department of Art and Art History. Austin, TX.

Hubbert M K (1957). Darcy's Law and the field equations of the flow of underground fluids. *International Association of Scientific Hydrology. Bulletin* 2 (1), 23-59.

Hutchinson D, Abrams P, Retzlaff R and Liptan T (2003). Stormwater Monitoring Two Eco-roofs in Portland, Oregon, USA. In: *Proceedings of the 1st North American Green Roof Conference: Greening Rooftops for Sustainable Communities*, Chicago, IL, 29-30th May 2003, pp. 372-389. The Cardinal Group, Toronto, Canada.

Ichihara K and Cohen J P (2011). New York City property values: What is the impact of green roofs on rental pricing? *Letters in Spatial and Resource Sciences* 4 (1), 21-30.

IGRA (2010). Green Roof News 01/10 (Online). International Green Roof Association, Nürtingen, Germany. Available from: http://www.igra-world.com/links_and_downloads/images_dynamic/IGRA_Green_Roof _News_1_2010.pdf (accessed 17th July 2012).

James W, Huber W C, Dickinson R E and James R C (2000). *Water Systems Models: Hydrology: Users Guide to SWMM4 Runoff and Supporting Modules*. Computational Hydraulics International, Guelph, Canada.

JHU Gazette (2004). Fallingwater Tour. In: *John Hopkins University Gazette*, 33 (34). John Hopkins University, Baltimore, MD.

Johnston C, McCreary K and Nelms C (2004). Vancouver Public Library green roof monitoring project. In: *Proceedings of the 2nd North American Green Roof Conference: Greening Rooftops for Sustainable Communities*, Portland, OR 2-4th June 2004, pp. 391-403. The Cardinal Group, Toronto, Canada.

Johnston J and Newton J (1993). *Building Green - A guide to using plants on roofs, walls and pavements*. London Ecology Unit, London, UK.

Kamin B (2010). Heads up on green roofs: How Chicago is doing. *Chicago Tribune*. Tony W. Hunter, Chicago, IL.

Kasmin H (2010). Hydrological Performance of Green Roofs (PhD Thesis). Univeristy of Sheffield, Department of Civil and Structural Engineering. Sheffield, UK. 216 pp.

Kasmin H, Stovin V R and Hathway E A (2010). Towards a generic rainfall-runoff model for green roofs. *Water Science and Technology* 62 (4), 898-905.

Kaźmierczak A and Carter J (2010). Adaptation to climate change using green and blue infrastructure. A database of case studies (Online). Interreg IVC green and blue space adaptation for urban areas and eco towns (GRaBS) project, University of Manchester, School of Environment and Development, Manchester, UK. Available from: http://grabs-eu.org/casestudies.php (accessed 17th July 2012).

Kirby R S and Laurson P G (1932). *The Early Years of Civil Engineering*. Yale University Press, New Haven, CT.

Kjeldsen T R (2005). *Flood Estimation Handbook No. 1 - The revitalised FSR/FEH rainfall-runoff method*. Centre for Ecology and Hydrology, Wallingford, UK.

Köhler M (2006). Long-term vegetation research on two extensive green roofs in Berlin. *Urban Habitats* 4, 3-26.

Köhler M, Schmidt M, Grimme F W, Laar M, de Assunção Paiva V L and Tavares S (2002). Green roofs in temperate climates and in the hot-humid tropics – far beyond the aesthetics. *Environmental Management and Health* 13 (4), 382-391.

Kosareo L and Ries R (2007). Comparative environmental life cycle assessment of green roofs. *Building and Environment* 42 (7), 2606-2613.

Kosugi K (1996) Lognormal Distribution model for unsaturated soil hydraulic properties. *Water Resources Research* 32(9), 2697-2703

Kumar R and Kaushik S C (2005). Performance evaluation of green roof and shading for thermal protection of buildings. *Building and Environment* 40 (11), 1505-1511.

Laberge K M (2003). Urban oasis: Chicago's City Hall green roof. In: *Proceedings of the 1st North American Green Roof Conference: Greening Rooftops for Sustainable Communities*, Chicago, IL, 29-30th May 2003, pp. 194-203. The Cardinal Group, Toronto, Canada.

Lagström J (2004). Do Extensive Green Roofs Reduce Noise? (examination project). University of Malmö, Eco-cycle Programme. Malmö, Sweden. 36 pp.

Lawlor G, Currie B A, Doshi H and Wieditz I (2006). *Green Roofs. A Resource Manual for Municipal Policy Makers*. Canada Mortgage and Housing Corporation, Ottawa, Canada.

Li J-F, Wai O W H, Li Y S, Zhan J-M, Ho Y A, Li J and Lam E (2010). Effect of green roof on ambient CO_2 concentration. *Building and Environment* 45 (12), 2644-2651.

Liu K and Minor J (2005). Performance evaluation of an extensive green roof. In: *Proceedings of the 3rd North American Green Roof Conference: Greening Rooftops for Sustainable Communities*, Washington, DC, 4-6th May 2005, pp. 1-11. The Cardinal Group, Toronto, Canada.

LivingRoofs (2010). Green Roof Audit of London | Latest (Online). Available from: http://livingroofs.org/20100309100/latest/resauditlondon.html (accessed 10th August 2012).

Lyrintzis A and Angelakis A N (2006). Is the "Labyrinth" a Water Catchment Technology? A Preliminary Approach. In: *IWA Specialty Conference: 1st International Symposium on Water and Wastewater Technologies in Ancient Civilizations* (ed. A N Angelakis and D Koutsoyannis), Iraklio, Greece, 28-30th October 2006, pp. 163-174.

MacIvor J S and Lundholm J (2011). Insect species composition and diversity on intensive green roofs and adjacent level-ground habitats. *Urban Ecosystems* 14 (2), 225-241.

Maurer E (2006). Green Roofs in Linz (presentation). *Green Roof Conference*, Sheffield, 20-21st June 2006.

McCarthy G T (1938). The unit hydrograph and flood routing. In: *Proceedings of the Conference of the North Atlantic Division* (ed. United States Army Corps of Engineers), New London, CT, 24th June 1938. Army Engineer District, Providence, RI.

Mentens J, Raes D and Hermy M (2006). Green roofs as a tool for solving the rainwater runoff problem in the urbanized 21st century? *Landscape and Urban Planning* 77 (3), 217-226.

Met Office (2008). Met Office: Climate averages 1971-2000 (Online). Met Office, Exeter, UK. Available from: http://www.metoffice.gov.uk/climate/uk/averages/19712000/sites/sheffield.html (accessed 7th August 2012).

Miller C (2002). Green Roof Benefits (Online). Roofscapes, Inc., Philadelphia, PA. Available from: http://www.roofmeadow.com/wp-content/uploads/Green_Roof_Benefits.pdf (accessed 25th July 2012).

Miller C (2003a). How to assess retention/drainage sheets. (Online). Roofscapes, Inc., Philadelphia, PA. Available from: http://www.roofmeadow.com/wp-content/uploads/How_to_Assess_Retention_Drainage_Sheets.pdf (accessed 17th July 2012).

Miller C (2003b). Moisture management in green roofs. In: *Proceedings of the 1st North American Green Roof Conference: Greening Rooftops for Sustainable Communities*, Chicago, IL, 29-30 May 2003, pp. 177-182. The Cardinal Group, Toronto, Canada.

Molineux C J, Fentiman C H and Gange A C (2009). Characterising alternative recycled waste materials for use as green roof growing media in the U.K. *Ecological Engineering* 35 (10), 1507-1513.

Moran A, Hunt B and Jennings G (2004). A North Carolina field study to evaluate greenroof runoff quantity, runoff quality, and plant growth. In: *Proceedings of the 2nd North American Green Roof Conference: Greening Rooftops for Sustainable Communities*, Portland, OR, 2-4th June 2004, pp. 446-459. The Cardinal Group, Toronto, Canada.

NERC (1975). Flood Studies Report. Natural Environment Research Council, London, UK.

NERC (1999). Flood Estimation Handbook (CD). Natural Environment Research Council, London, UK.

Netafim (Undated). PCJ Dripper (Online). Netafim Ltd., Tel Aviv, Israel. Available from: http://www.netafim.com/Data/Uploads/120316%20PCJ%20dripper%20product%20sheet.pdf (accessed 19th July 2012).

Ngan G (2004). Green roof policies: tools for encouraging sustainable design. Landscape Architecture Canada Foundation, Bowmanville, Canada.

O'Geen A T (2012). Soil water dynamics. *Nature Education Knowledge* 3 (6), 12.

Palla A (2009). Unsaturated flow in engineered media for hydrologic restoration (PhD thesis). University of Genoa, Department of Civil, Environmental and Architectural Engineering. Genoa, Italy. 156 pp.

Palla A, Gnecco I and Lanza L G (2012). Compared performance of a conceptual and a mechanistic hydrologic models of a green roof. *Hydrological Processes* 26 (1), 73-84.

Palomo Del Barrio E (1998). Analysis of the green roofs cooling potential in buildings. *Energy and Buildings* 27 (2), 179-193.

Peck S W, Callaghan C, Kuhn M E and Bass B (1999). Greenbacks from Green Roofs: Forging a New Industry in Canada. Canada Mortgage and Housing Corporation, Toronto, Canada.

Poë S, Stovin V and Dunsiger Z (2011). The impact of green roof configuration on hydrological performance. *12th International Conference on Urban Drainage*, Porto Alegre, Brazil, 11-16th September 2011.

Porsche U and Köhler M (2003). Life cycle costs of green roofs: A comparison of Germany, USA, and Brazil. In: *Proceedings of the World Climate and Energy Event*, Rio de Janeiro, Brazil, 1-5th December 2003, pp. 461-467.

Richards L A (1931). Capillary conduction of liquids through porous mediums. *Physics* 1 (5), 318-333.

Ristvey A G, Solano L, Wharton K, Cohan S M and Lea-Cox J D (2010). Effects of crumb rubber amendments on the porosity, water holding capacity and bulk density of three green roof substrates. In: *Low Impact Development 2010: Redefiining Water in the City* (ed. S Struck, K Lichten), pp 889-896. ASCE Press, Reston, VA.

Rivers N, Dunnett N, Sorrill J, Missen K, Nicolle D and Landscape Architecture students at The University of Sheffield (2010). Habitat Action Plan – Green Roofs. Sheffield Local Biodiversity Action Partnership in conjunction with The Green Roof Centre, Sheffield, UK.

Roehr D and Laurenz J (2008). Green living envelopes for food and energy production in cities. In: *The Sustainable City V: Proceedings of the 5th International Conference on Urban Regeneration and Sustainability* (ed. A

Gospodini, C A Brebbia, E Tiezzi), Skiathos, Greece, 24-26th September 2008, pp. 663-671. WIT Press, Southampton, UK.

Rowe D B (2011). Green roofs as a means of pollution abatement. *Environmental Pollution* 159 (8–9), 2100-2110.

Sailor D J (2008). A green roof model for building energy simulation programs. *Energy and Buildings* 40 (8), 1466-1478.

Schaap M G, Leij F J and van Genuchten M Th (2001). Rosetta: a computer program for estimating soil hydraulic parameters with heirarchical pedotransfer functions. *Journal of Hydrology* 251 (3-4), 163-176.

She N and Pang J (2010). Physically based green roof model. *Journal of Hydrologic Engineering* 15 (6), 458-464.

Sheffield City Council (2009). Sheffield Development Framework – Core Indicators. Sheffield City Council, Sheffield, UK.

Sheffield City Council (2010). Sheffield Development Framework Supplementary Planning Document – Designing for Environmental Sustainability (draft) (Online). Sheffield City Council Development Services, Sheffield, UK. Available from: https://www.sheffield.gov.uk/dms/scc/management/corporate-communications /documents/planning/Designing-for-Environmental-Sustainability--Word--236-kb-.doc (accessed 10th August 2012).

Sherman L K (1932). Streamflow from rainfall by unit hydrograph method. *Engineering News Records* 108, 501-505.

Šimůnek J, Šejna M, Saito H, Sakai M and van Genuchten M Th (2008). The Hydrus-1D Software Package for Simulating the Movement of Water, Heat, and Multiple Solutes in Variably Saturated Media, Version 4.0, HYDRUS Software Series 3. University of California Riverside, Department of Environmental Sciences. Riverside, CA. 315 pp.

Šimůnek J, Šejna M and van Genuchten M Th (1998). *The HYDRUS-1D software package for simulating the one-dimensional movement of water, heat, and multiple solutes in variably-saturated media. Version 1.0.* IGWMC - TPS - 70, International Ground Water Modeling Center, Colorado School of Mines, Golden, CO.

Snyder F F (1938). Synthetic unit-graphs. *Transactions of the American Geophysical Union* 19 (1), 447-454.

Soong D T, Prater C D, Halfar T D and Wobig L A (2012). Estimating Manning's Roughness Coefficients for Natural and Man-Made Streams in Illinois. United States Geological Survey, Reston, VA and Illinois Department of Natural Resources, Springfield, IL,

Spolek G (2008). Performance monitoring of three ecoroofs in Portland, Oregon. *Urban Ecosystems* 11 (4), 349-359.

SSI (2005). Water Environment (Controlled Activities) (Scotland) Regulations 2005, SSI 2005/348.

Stovin V, Vesuviano G and Kasmin H (2012). The hydrological performance of a green roof test bed under UK climatic conditions. *Journal of Hydrology* 414-415, 148-161.

Strelkoff T (1980). *Comparative analysis of flood routing methods.* US Army Corps of Engineers, Hydrologic Engineering Center, Davis, CA.

Takebayashi H and Moriyama M (2007). Surface heat budget on green roof and high reflection roof for mitigation of urban heat island. *Building and Environment* 42 (8), 2971-2979.

Tan P Y and Sia A (2005). A pilot green roof research project in Singapore. In: *Proceedings of the 3rd North American Green Roof Conference: Greening Rooftops for Sustainable Communities*, Washington, DC, 4-6th May 2005, pp. 399-415. The Cardinal Group, Toronto, Canada.

Taylor D A (2007). Growing Green Roofs, City by City. *Environmental Health Perspectives* 115, A306-A311.

The Green Roof Centre (2010). Sheffield Green Roof Audit 2010. The University of Sheffield, Sheffield City Council and Groundwork Sheffield, Sheffield, UK.

Tung Y-K (1985). River flood routing by nonlinear Muskingum method. *Journal of Hydraulic Engineering* 111 (12), 1447-1460.

Uhl M and Schiedt L (2008). Green roof storm water retention – monitoring results. *11th International Conference on Urban Drainage*, Edinburgh, UK, 31st August – 5th September 2008.

United States Department of Agriculture (1957). *Use of storm and watershed characteristics in synthetic hydrograph analysis and application*. United States Department of Agriculture, Soil Conservation Service, Washington, DC.

United States Department of Agriculture (1992). *SCS Engineering Handbook*. Unted States Department of Agriculture, Soil Conservation Service, Washington, DC.

US Army Corps of Engineers (1998). HEC-5. Simulation of Flood Control and Conservation Systems. User's Manual Version 8.0. US Army Corps of Engineers, Hydrologic Engineering Center. Davis, CA. 66 pp.

van Genuchten M Th (1980) A closed-form equation for predicting the hydraulic conductivity of unsaturated soils. *Soil Science Society of America Journal* 44(5), 892-898

Van Renterghem T and Botteldooren D (2008). Numerical evaluation of sound propagating over green roofs. *Journal of Sound and Vibration* 317 (3–5), 781-799.

Van Seters T, Rocha L and MacMillan G (2007). Evaluation of the Runoff Quantity and Quality Performance of an Extensive Green Roof in Toronto, Ontario. *5th North American Green Roof Conference – Greening Rooftops for Sustainable Communities*, Minneapolis, MN, 29th April-1st May 2007.

VanWoert N D, Rowe D B, Andresen J A, Rugh C L, Fernandez R T and Xiao L (2005). Green roof stormwater retention: Effects of roof surface, slope, and media depth. *Journal of Environmental Quality* 34 (3), 1036-1044.

Vesuviano G (2011). A hydrological runoff model for a green roof drainage layer. *1st National Green Roof Student Conference*, Sheffield, UK, 16-17th May 2011.

Vesuviano G and Stovin V (2011). The hydrological performance of a green roof test bed under UK climatic conditions. *SUDSnet/CIWEM National & International Conference*, Dundee, UK, 11-12th May 2011.

Vesuviano G and Stovin V (2012). A generic hydrological model for a green roof drainage layer. *9th International Conference on Urban Drainage Modelling*, Belgrade, Serbia, 4-6th September 2012.

Vesuviano G (2013). A green roof runoff detention model. *Marie-Curie IAPP 'Green Roof Systems' Project, The Green Roof Research Conference*, Sheffield, 18-19th March 2013.

Vesuviano G, Sonnenwald F and Stovin V (2013). A two-stage storage routing model for green roof runoff detention. *8th International Conference Novatech*, Lyon, France, 23-27th June 2013.

Vesuviano G and Stovin V (2013). A generic hydrological model for a green roof drainage layer. *Water Science and Technology* 68 (4), 769-775.

Vesuviano G, Sonnenwald F and Stovin V (in press). A two-stage storage routing model for green roof runoff detention. *Water Science and Technology*.

Vijayaraghavan K, Joshi U M and Balasubramanian R (2012). A field study to evaluate runoff quality from green roofs. *Water Research* 46 (4), 1337-1345.

Vila A, Pérez G, Solé C, Fernández A I and Cabeza L F (2012). Use of rubber crumbs as drainage layer in experimental green roofs. *Building and Environment* 48 (1), 101-106.

Villarreal E L and Bengtsson L (2005). Response of a Sedum green-roof to individual rain events. *Ecological Engineering* 25 (1), 1-7.

Vogel T and Císlerová M (1988) On the reliability of unsaturated hydraulic conductivity calculated from the moisture retention curve. *Transport in Porous Media* 3, 1-15

Voyde E, Fassman E and Simcock R (2010). Hydrology of an extensive living roof under sub-tropical climate conditions in Auckland, New Zealand. *Journal of Hydrology* 394 (3-4), 384-395.

Water UK (2009). Combined Sewer Overflows: Background briefing (Online). Water UK, London, UK. Available from: http://www.water.org.uk/home/policy/positions/combined-seweroverflows/csos-sept-09.pdf (accessed 17th July 2012).

Welch B L (1947). The Generalization of 'Student's' Problem when Several Different Population Variances are Involved. *Biometrika* 34 (1/2), 28-35.

Wittenberg H (1999). Baseflow recession and recharge as nonlinear storage processes. *Hydrological Processes* 13 (5), 715-726.

Woods Ballard B, Kellagher R, Martin P, Jefferies C, Bray R and Shaffer P (2007). *The SUDS Manual (C697)*. The Construction Industry Research and Information Association, London, UK.

Yang J, Yu Q and Gong P (2008). Quantifying air pollution removal by green roofs in Chicago. *Atmospheric Environment* 42 (31), 7266-7273.

Yio H N M (2011). Green Roof Rainfall-Runoff Performance Under Design Storm Events (3rd Year Thesis). University of Sheffield, Department of Civil and Structural Engineering. Sheffield, UK. 80 pp.

Yio H N M, Stovin V, Werdin J and Vesuviano G (2012). Experimental analysis of greeen roof substrate detention characteristics. *9th International Conference on Urban Draiange Modelling*, Belgrade, Serbia, 4-6th September 2012.

Yio H N M, Stovin V, Werdin J and Vesuviano G (2013). Experimental analysis of greeen roof substrate detention characteristics. *Water Science and Technology* 68 (7), 1477-1486.

Young P, Jakeman A and McMurtrie R (1980). An instrumental variable method for model order identification. *Automatica* 16, 281-294.

Zimmer U and Geiger W F (1997). Model for the design of multilayered infiltration systems. *Water Science and Technology* 36 (8-9), 301-306.

Appendix A: Quantifying Moisture Fluxes of a Green Roof Drainage Layer and Protection Mat during Dry Weather Periods

A.1 Introduction and Objectives

Storm water that has percolated through the substrate layer of a green roof may be retained by a profiled-board drainage layer and/or fibrous protection mat below. However, retention in either component is only possible up to a finite maximum capacity. If some runoff from one storm event is stored in either synthetic layer, then the capacity for that layer to store runoff resulting from the next storm event is reduced. When both layers are at capacity, runoff that has passed through the substrate is only temporarily detained by the drainage layer and protection mat. In order for these components to retain runoff from future storms, their storage capacities must be recharged between storms. Except in the rare cases where the drainage layer is filled with granular infill or the profiled storage cups hold water for the full depth of the drainage component (e.g. type A-20 in Miller, 2003) and are full, an air gap exists immediately below the filter sheet, separating the substrate from the stored water. Hence, water stored below the substrates in the synthetic layers cannot be accessed by capillary action. Plant roots are also extremely unlikely to grow across this air gap into the drainage layer. As a result, the only mechanism by which plants can access the water stored in the synthetic layers is through evaporation of that water into the air gap, followed by adsorption of that water to the lower surface of the substrate. This recharges the storage capacities of the synthetic layers in the process. As the evaporative process is slow, the water stored in the synthetic layers is theoretically available to plants for a longer period of time than the water which is stored in the substrate. A long-term source of water may be useful during periods of extended droughts.

Before the focus of the PhD was changed to include hydrological modelling of substrates during storm events, it was planned to focus entirely on the hydrological processes occurring in the synthetic layers, both during and between storm events. It was intended to quantify the rate of upward water transfer, from the synthetic layers into the substrate. The eventual application of this research would have been to determine optimal planting densities for certain species to maximize survival during extended droughts, or to design irrigation regimes for these plants, if deemed necessary. Two experiments were performed in 2010; planning for a third experiment took place throughout late 2010 and early 2011, but it has not been undertaken. Part of the experimental setup proposed for the third experiment was used in a different experimental programme, designed and undertaken by staff at ZinCo GmbH in 2012. The thesis author was not involved in these experiments.

Within a plant-free green roof system build-up (i.e. substrate and synthetic layers only), five moisture fluxes can be assumed to occur during dry weather periods (Figure A.1):

1.   Evaporation of water from the moisture mat into the air gap below the substrate.

2.   Evaporation from the cups of the drainage layer into the air gap below the substrate.

3.   Adsorption of the moisture from the air gap below the substrate onto the lower surface of the substrate.

4.   Capillary rise of moisture through the substrate to the upper surface.

5.   Evaporation from the upper surface of the substrate to the atmosphere.

The focus of this incomplete experimental programme was to quantify the rate at which water transfers from the synthetic layers to the substrate i.e. the combined rate of Processes 1 and 2, and the rate at which water evaporates from the entire system i.e. Process 5, by mass balance of a small section of an extensive green roof system. Factors affecting the rates of these processes include incident solar radiation, ambient air temperature and humidity, all of which change continuously, substrate moisture content (hence moisture gradient from air gap to lower surface of substrate), which varies throughout the experimental programme, and substrate materials and components (i.e. substrate physical properties), which vary between substrates, but are assumed to be constant over short periods for individual substrate samples.
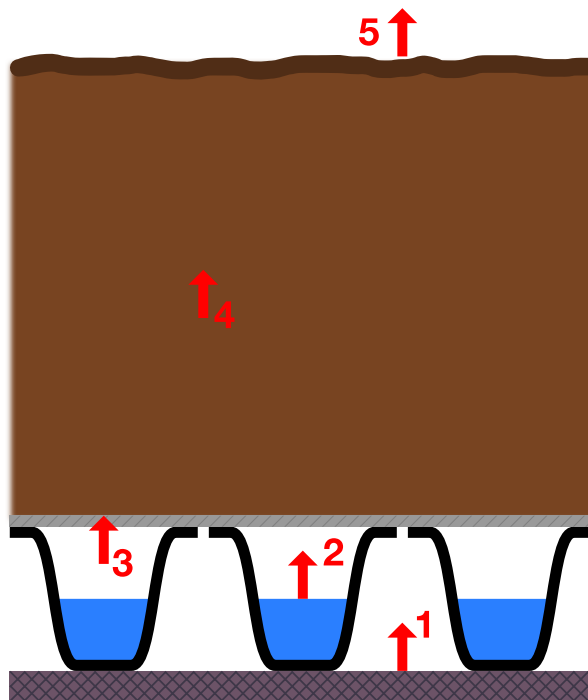

Figure A.1 – Representation of green roof system moisture fluxes.

The rate of Process 3 was assumed to be practically equal to the combined rates of Processes 1 and 2, as the available capacity for moisture storage in the air gap below the drainage layer was minimal (17g of water can be held in 1 m^3 of air at 20°C). The rate of Process 4 could not be measured with any equipment known to the researcher: time-domain reflectometry, for example, would not be able to resolve variations in moisture content at different depths within a sample of only 80 mm total depth.

Both the first and second experiments were conducted in order to determine the rates of Process 3 and Process 5 through mass balance. As the methodology is changed between experiments, the relevant Experimental Procedure sections (A.2.2 and A.3.3) should be referred to for detailed explanations.

A.2   First Experiment

The first experiment aimed at quantifying the upward flux of moisture from the drainage layer and protection mat began on 22nd February 2010 and ended on 1st April 2010. The observed rates of moisture transfer were very low. However, a number of possible improvements were identified, most of which were designed into the second experiment.

A.2.1   Experimental Setup

Two small replicas of a green roof system were produced (Figure A.2), each housed in an impermeable clear acrylic box of internal dimension 200×200 mm base and 112 mm height. At the base of each box was placed a 200×200 mm sample of ZinCo Protection Mat SSM 45. Above this was a 200×200 mm sample of ZinCo Floradrain FD 25-E. A steel mesh basket, of 196×196 mm base and 80 mm height, was lined on the outside of the base and all four sides
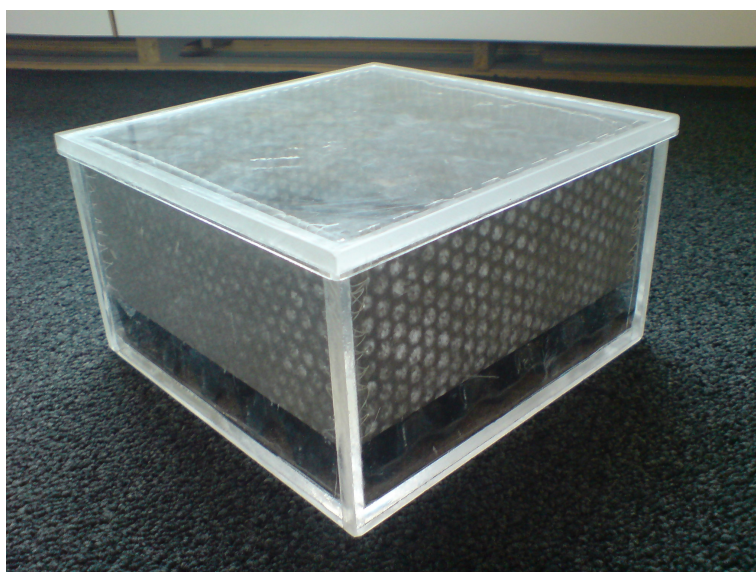

Figure A.2 – Complete system used in first experiment.

with ZinCo Systemfilter SF filter sheet. The basket was filled with ZinCo Heather with Lavender substrate to an even depth of 80 mm and installed above the drainage layer. A clear acrylic lid was placed over the top of one box, while the top of the other box was left open.

The purpose of running two simultaneous tests, one closed with a lid and one without, was to allow evaporation (Process 5) in only one green roof replica system. The change in mass of the open system reflected the rate of evaporation from the green roof. In the closed system, water also transferred from the synthetic layers to the substrate, but was prevented from evaporating from the upper surface of the substrate to the atmosphere. The purpose of monitoring the closed system was to determine the maximum volume of water that the substrate could absorb from the synthetic layers, while the open system was used to determine the rate at which the synthetic layers could recharge their storage capacity.

The experiment was designed to maximize the likelihood of detecting an upward moisture flux (Process 3) by increasing the moisture gradient across the air gap to its maximum. Prior to the start of the experiment, both samples of protection mat were oven-dried at 110°C for 72 hours, fully immersed in water for 24 hours and left to drip-dry to field capacity for two hours. The substrate used in both systems was taken from the same source and oven-dried for 72 hours prior to the start of the experiment. A drying temperature of 80°C was used, to avoid permanently damaging the organic component of the substrate. At the start of the experiment, both drainage layer samples were filled to their maximum storage capacity with water.

A.2.2   Experimental Procedure

Measurements were taken for the mass of the following components in each system: acrylic box, box lid, mesh basket and lining (without, then with, dry substrate), drainage layer (dry), moisture mat (dry). Additionally, the mass of the moisture mat at field capacity for each system was derived by weighing the box with the wetted moisture mat in it. Similarly, the mass of the filled drainage layer was derived by weighing the box, after placing into it the wet moisture mat and dry drainage layer, then filling the drainage layer with water. From these measurements, the masses of the substrate and available water were calculated for each box. The components were then assembled as shown in Figure A.2.

Over the course of the experiment, the masses of both green roof systems were measured at approximately 24 hour intervals using an UWE Geniweigher GW-30K bench scale with a resolution of 2 grams. The water levels in the synthetic layers were visually observed through the clear sides of the box.

The experiment was performed in a non-temperature controlled laboratory in the University of Sheffield's Civil and Structural Engineering department, which for the duration of the experiment

was at a temperature of 18-20°C. Atmospheric humidity was not measured, but was assumed to be within safe working conditions (40-70% RH or 7.1 to 12.5 g water/m^3 air).

At the end of the experiment, it was intended to compare the change in mass of the substrate basket in the closed system (assumed to result from Process 3) to the change in mass experienced by the complete open system (assumed to result from Process 5, itself dependent on Process 3). It was also intended to compare the final mass of the substrate basket in the open system to the final mass of the substrate basket in the closed system. As the observed rates of Processes 3 and 5 during the experiment were very low (see Section A.2.3) and improvements to the setup and methodology were identified for future tests (see Section A.2.5), this was forgotten.

A.2.3   Results and Discussion

Measurement was stopped after 38 days, during which time the mass of the open system had reduced significantly. Over the course of the experimental programme, both green roof systems reduced in total mass (Figure A.3). Unsurprisingly, the reduction was greatest for the open system.

For the first three days, the open system actually gained mass, increasing from 4732 g to 4740 g. This is likely explained by water vapour in the atmosphere adsorbing onto the initially dry substrate. Following this initial mass gain, the open system lost mass at an average rate of 2.7 g, equivalent to only 0.0675 mm, per day. Considering that the listed retention capacities of FD 25 and SSM 45 are 3 and 5 l/m^2 respectively (Alumasc, 2012a), a dry weather period of approximately 119 days is implied for full storage recharge of these two synthetic layers together. However, the test procedure specifically excluded regular measuring of the mass of the substrate basket. One implication of this decision is that moisture may have been transferred
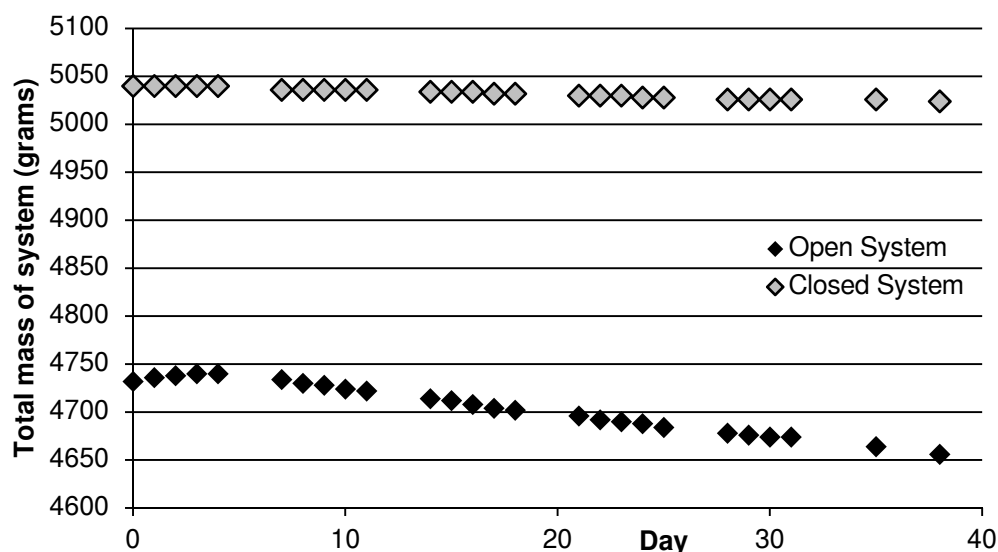

Figure A.3 – Total mass of green roof systems over measuring period.

from the synthetic layers to the substrate at a much faster rate than it was being transferred from the substrate to the atmosphere. As the substrate used in both experiments is initially dry and its moisture holding capacity is approximately 50% by volume (Alumasc, 2012b), or 1.5 kg per system, each system's substrate layer could theoretically hold all of the water stored in the synthetic layers in its lower quarter. However, it is likely that this water would rise to the surface by capillary action, where it would evaporate.

Interestingly, the closed system also reduced in mass, albeit very gradually, over the course of the 39 day monitoring period. A total of 16 grams (equivalent to 0.4 mm) was lost, 10 of these over weekends, including 4 grams over the first weekend. As some pressure was required to push the lid into place, it is possible that the airtight seal may have been broken by a slightly overfilled substrate basket pushing back against the lid. As the lid was pushed down every time the mass was recorded, the longest the airtight seal could have been broken was around 24 hours on a weekday, but up to 72 hours over a weekend.

A.2.4   Conclusions

As the open system lost mass despite beginning with a dry substrate, it is confirmed that water must be lost from the synthetic layers during simulated dry weather periods. However, the rate of loss appears to be too small to have a significant recharging effect on the retention capacity of the synthetic layers, except in the case of dry weather periods lasting for weeks or months. As the substrate basket was not weighed, it is possible that the substrate gained water over the course of the experiment, implying that the rate of Process 3 was higher than the measured rate of Process 5. In this case, the combined rate of recharge of the synthetic layers would be greater than the measured 0.0675 mm/day rate of water loss from the whole system.

A.2.5   Recommendations for Second Experiment

This first experiment was performed with substrate that had been dried at 80 °C for 72 hours. The temperature chosen was lower than the 105°C specified by the FLL for determining the dry density of a substrate sample (FLL, 2008), in order to avoid burning the organic content of the substrate before the start of the experiment. However, the drying regime may still have destructively affected the moisture holding capability of the substrate. It was therefore proposed to start any future experiments with substrate at an unknown, equilibrium moisture content. The moisture content of each substrate sample at every point in time would be back-calculated after the experiment, by subjecting each sample to an intense drying regime at 80°C. The lowest mass reached by each sample would be that sample's mass at zero moisture content. Although the substrate's water holding properties may still be affected, this would be irrelevant as the experiment would already have taken place. A temperature of 80°C would still be used, to avoid burning off any organic content that was present as substrate mass during the experiment.

While the temperature in the laboratory was reasonably comparable to the air temperature surrounding a green roof in a British summer, the roof itself would be expected to reach much higher temperatures in direct sunlight (without plants, the surface of the system is more similar to a gravel-ballasted roof). As the lights in the laboratory were almost always off, the green roof systems were almost never in direct radiation. It was proposed to more closely match the temperature and direct radiation conditions of an installed green roof by performing future experiments in an unshaded greenhouse. If the greenhouse is temperature controlled, uncertainties and variations in temperature are removed and comparative studies at a range of temperatures become possible, depending on the accessibility of the control system. However, the effects of wind, which would be expected to increase the rate of evaporation, would necessarily be absent from, or simulated in, any experiments performed indoors. For use with the greenhouse, a pyranometer was proposed, to measure incident solar radiation at one-hour intervals, as it was believed that the periods of greatest evaporation would coincide with periods of direct, intense solar radiation.

One major physical difference between a real green roof and the small replicas used in this study was the presence of the substrate basket. In an installed green roof, the substrate is directly above the filter sheet, so 100% of the lower surface of the substrate is separated from the drainage layer by only a filter sheet. In this study, both baskets used metal mesh with relatively small holes, such that a large proportion (over half) of the lower surface of the substrate was separated from the synthetic layers by a sheet of metal. It was proposed that future experiments would use baskets made primarily of filter sheet with only a thin wire frame to maintain the basket shape. Care would have to be taken when re-inserting the baskets after weighing, as the sides would likely bulge outwards when removed from the boxes.

It is plausible that including plants in the green roof system would greatly increase the rate of Process 5, by providing the two driving forces of growth and transpiration. A more rapidly drying substrate may also increase the rate of Process 3, as the moisture gradient between the substrate and air gap becomes steeper. However, it was not recommended to include plants in any future experimental setups until the processes of the system without plants were fully understood.

A.3   Second Experiment

The second experiment aimed at quantifying the upward flux of moisture from the drainage layer and protection mat began on 21st July 2010 and ended on 10th August 2010. Most of the possible improvements identified from the first experiment were implemented into the second. Consequently, significantly higher evaporation rates were observed.

A.3.1   Recommendations Implemented

The first experiment was performed in a laboratory with no external windows and therefore no direct solar radiation. Norton Nursery, a greenhouse approximately 6 kilometres south of the original laboratory site, was used as the site of the second experiment. The green roof systems were not shaded at any time during the experiment, hence they received direct solar radiation whenever the sun was not obscured. However, a pyranometer, to record the incidences of direct solar radiation, could not be found and so was not used. Furthermore, the greenhouse was initially believed to be temperature and humidity controlled, but was later discovered to be neither.

To avoid adversely affecting the moisture holding capabilities of the substrate, either by burning off the organic content or through another unidentified mechanism, the substrate was not heated at all prior to the experiment. However, it was equilibrated with its surroundings prior to the start of the experiment, to ensure than any changes in mass were due to moisture processes inherent to the green roof system. This was achieved by spreading the substrate to be used in the green roof systems to a depth of no more than 5 cm in trays and leaving it in Norton Nursery for a week before the start of the experiment. It was intended for any transfers of moisture not inherent to the green roof system to take place before the start of the monitoring programme.

It was suspected during the first experiment that the low open area of the mesh used to contain the substrate may have impeded the uptake of water from the synthetic layers. A wire frame construction was proposed in Section A.2.5, in which the lower surface of the substrate basket would consist entirely of filter sheet. However, the risk of basket deformation was considered too high to implement this proposal. A compromise solution was therefore implemented, in which new substrate baskets were produced with a more open mesh, consisting of 1.6 mm wires at 12.5 mm spacing (visible in Figure A.4), giving an open area at the interface between the filter sheet and drainage layer of approximately 76%.

Two other improvements were made to the experimental setup: the first being that the system boxes were increased in size to $304 \times 304 \times 115$ mm internal dimension. This more than doubled the quantities of water involved, such that the evaporation of a certain depth of water, in millimetres, would be measured as more than double the change in mass. Increasing the size of the boxes also reduced the significance of edge effects. The second improvement was to use four systems, allowing duplicate measurements to be taken for two configurations.

A.3.2   Experimental Setup

Four small replicas of a green roof system were produced, each housed in an impermeable clear acrylic box of internal dimension 304×304 mm base and 115 mm height. At the base of each

Figure A.4 – Staged construction of complete system used in second experiment.

box was placed a 304×304 mm sample of ZinCo Protection Mat SSM 45. Above this was a 304×304 mm sample of ZinCo Floradrain FD 25-E. A steel mesh basket, of 300×300 mm base and 80 mm height, lined on the inside of the base and all four sides with ZinCo Systemfilter SF filter sheet, was filled with ZinCo Heather with Lavender substrate to an even depth of 80 mm and installed above the drainage layer. No lid was used on any box, due to the changed methodology for measuring and separating Process 5 from Process 3.

Prior to the start of the experiment, two samples of protection mat were fully immersed in water for 24 hours and left to drip-dry to field capacity for two hours. The other two samples remained at their equilibrium moisture content, which was close to zero. The substrate was not oven-dried, but was left for a week to equilibrate with the atmospheric conditions of the greenhouse, as described in Section A.3.1.

A.3.3   Experimental Procedure

For the second experiment, two systems were intended to start with maximum water stored in the synthetic layers (S1 and S2), and two were intended to start with no water stored in the synthetic layers (E1 and E2). The rates of whole-system evaporation could then be compared between the two configurations, to determine the rate at which water was transferred to the substrate from the synthetic layers.

Figure A.5 – Norton Nursery.

Measurements were taken for the mass of the following components in each system: acrylic box, mesh basket and lining (without, then with substrate), drainage layer (dry), moisture mat (dry). Additionally for S1 and S2, the mass of the moisture mat at field capacity was derived by weighing the box with the wet moisture mat in it. Similarly, the mass of the filled drainage layer was derived by weighing the box, after placing into it the wet moisture mat and dry drainage layer, and then filling the drainage layer with water. From these measurements, the mass of available water in the synthetic layers was calculated for S1 and S2. The components were then assembled as shown in Figure A.4.

All four green roof systems were kept next to each other, elevated approximately one metre above the ground, at Norton Nursery, a horticultural facility in the south of Sheffield (Figure A.5). The masses of all four green roof systems were measured at approximately 4 day intervals using the same UWE Geniweigher GW-30K bench scale that was used in the first experiment. Starting on day 4 of the experiment, each substrate basket was temporarily and briefly lifted out of the system box to be weighed, immediately after the masses of the entire systems were recorded. The change in mass of an entire green-roof system was assumed to correspond with that system's Process 5, whereas the difference between the change in mass of the system and its corresponding basket was assumed to correspond to Process 3. The reason for the reduction in measuring frequency was due to the inaccessible location of the greenhouse.

A.3.4 Results and Discussion

The experiment was started on 22nd July and ended 19 days later on 10th August. For each system, the entire assembly was weighed on day 0 (i.e. at the beginning of the experiment), 1, 4, 8, 12, 14 and 19. The mass of the substrate basket was measured on day 4, 8, 12, 14, 19 and the day before

the start of the experiment (day -1). For boxes E1 and E2, the change in mass of the substrate basket was, as would be expected, extremely similar to the change in mass of the entire system build-up. The mass of water remaining in the synthetic layers of S1 and S2, on days 4, 8, 12, 14 and 19, was found by subtracting the mass of the substrate, basket and "structure" (the acrylic box, the empty mass of the drainage layer and the dry mass of the moisture mat) from the mass of the entire system.

Figure A.6 shows that, from day 4 onwards, all four systems lost mass at an approximately constant rate, which was higher for S1 and S2 than for E1 and E2. The highly linear trend appears to suggest that variations in uncontrolled factors such as temperature, incident solar radiation and relative humidity, are insignificant, at least within the ranges experienced by the systems over the period between consecutive measurements. As well as the linear reduction in total system mass, each substrate basket was found to lose mass at a linear rate (Figure A.7). However, the substrate baskets in systems E1 and E2 lost mass at a faster constant rate than the substrate baskets in systems S1 and S2. The rates at which water is lost from the substrate baskets and whole systems demonstrate that in systems S1 and S2, water is transferred upwards from the synthetic layers to the substrate (Process 3) at a constant rate, also unaffected by the variations in temperature, humidity and solar radiation occurring over the course of this experiment.

The full equations describing, from day 4 onwards, the rate change in mass of the systems and substrate baskets are presented in Table A.1, where m is mass in grams on day d.

It is worth noting that the gradient constants for system E1 and substrate E1 are not identical, neither are they identical for system E2 and substrate E2. Consequently, the masses recorded in
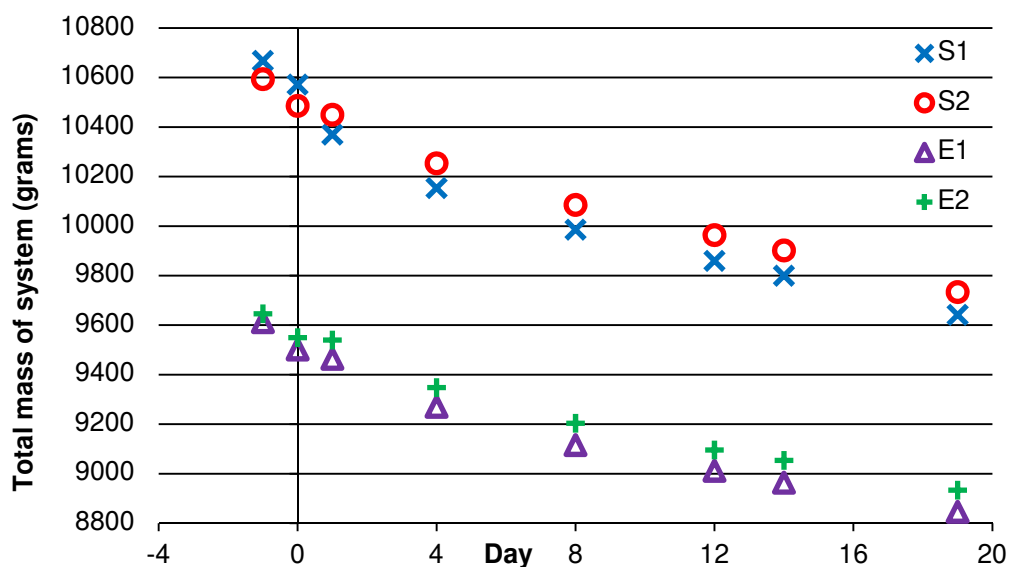

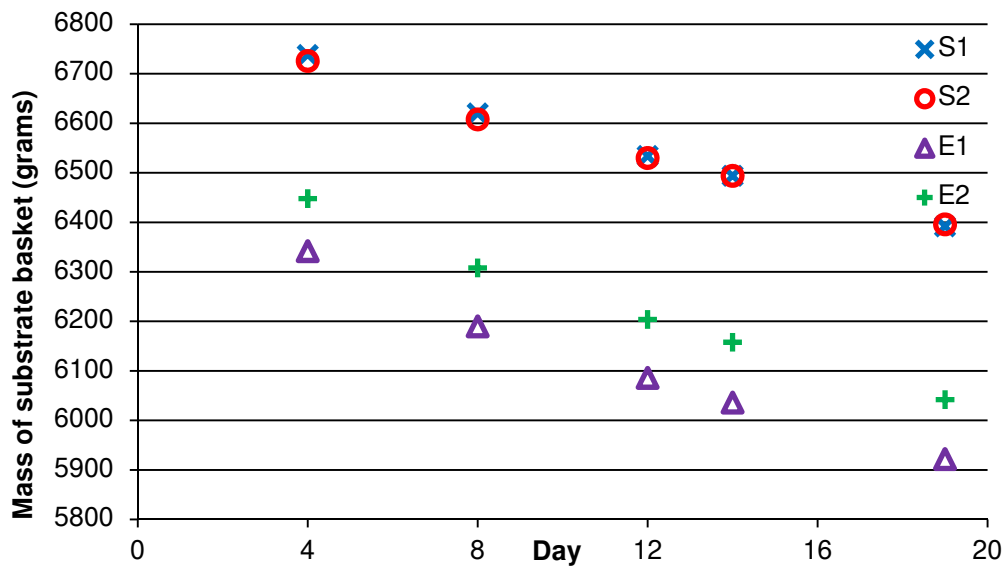**Figure A.6 – Plot of system mass vs. day of experiment.**

Figure A.7 – Plot of mass of substrate basket vs. day of experiment.

Figures A.6 and A.7 are likely to be reasonably accurate, though subject to some error. It is also clear from these two figures that the gradient constants given in Table A.1 are not valid for the first days of the experiment, as the rate of loss during this time appeared to be greater for all systems and substrate baskets.

Finally, the quantity of water remaining in the synthetic layers was found, for day 4 onwards. The results are presented in Figure A.8. Equations describing the linear best-fit are presented in Table A.2, where *m* is the mass of remaining water at day *d*, in grams.

The straight-line equations produced to model the rate of Process 3 are extremely accurate, with coefficients of determination (R^2) of almost 1. However, noting that the directly-measurable "structural" mass of systems E1 and E2 appeared to vary slightly throughout the experiment, and assuming that the same is true of the "structural" mass of systems S1 and S2, each point plotted in Figure A.8, used to build the equations in Table A.2, may be slightly in error. The magnitude of the error is unlikely to affect the gradient coefficients (hence the actual rates of evaporation)

Table A.1 – Equations describing Process 5.

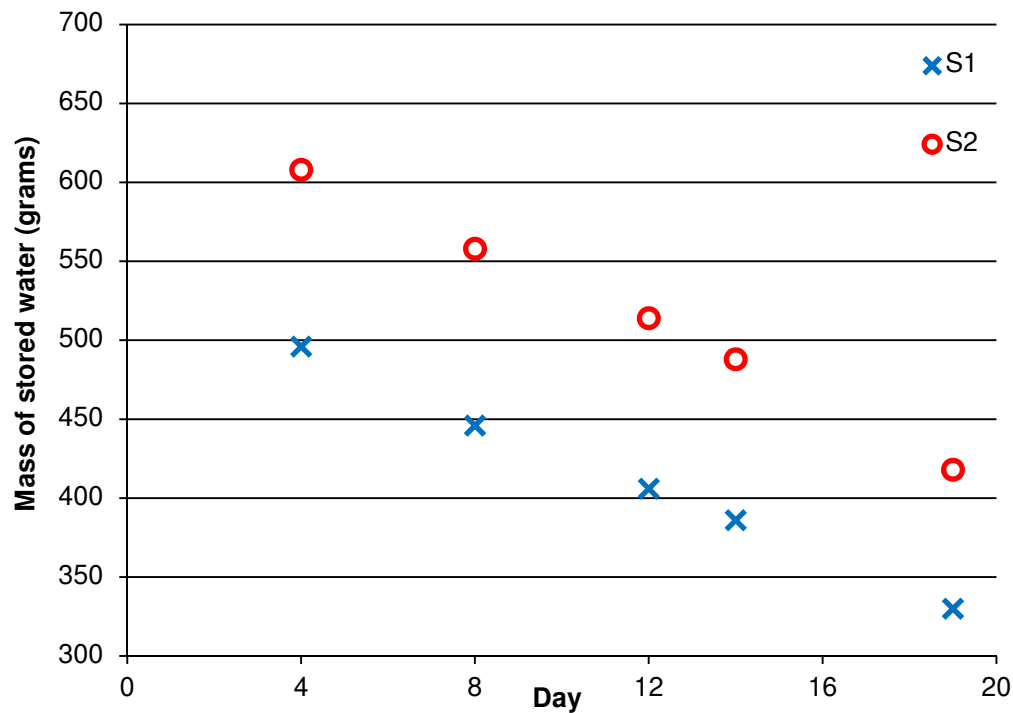| Series	Equation	R^2
System S1	$m = 10272 - 33.665d$	0.9952
System S2	$m = 10376 - 34.070d$	0.9964
System E1	$m = 9358.7 - 27.814d$	0.9868
System E2	$m = 9437.6 - 27.229d$	0.9895
Substrate S1	$m = 6815.0 - 22.753d$	0.9924
Substrate S2	$m = 6796.5 - 21.552d$	0.9895
Substrate E1	$m = 6430.1 - 27.625d$	0.9866
Substrate E2	$m = 6537.0 - 26.753d$	0.9906

Figure A.8 – Plot of stored water in Systems S1 and S2 vs. day of experiment.

by any significant amount. It is therefore shown that the rate of Process 3 for a green roof system without plants is around 120-140 g/m^2 per day. The results of this experiment imply that an initially full FD 25 drainage layer coupled with an initially saturated SSM 45 protection mat (storing 8 mm of water) will continue to provide moisture to the substrate for 57-67 days after the end of the last storm event, assuming that the rates of transfer remain constant. However, the author was unable to store the stated 8 mm in a saturated SSM 45 mat and filled FD 25 drainage layer. Dividing the initial quantity stored by the author by the rate of loss, for synthetic layers S1 and S2, gives slightly shorter transfer periods of 52 and 49 days respectively.

A.3.5   Conclusions

As the rate of moisture loss from the entire systems was greatest for S1 and S2, but the rate of moisture loss from the substrate only was greatest for systems E1 and E2, it is clear that water held in the synthetic layers of S1 and S2 was transferred to the substrate over the course of the monitoring period. The mean rate of transfer was found to be 0.13 mm/day, approximately twice that of the first experiment. This increased rate reflected the implementation of various modifications that were proposed to increase the rate of evaporation from the synthetic layers

Table A.2 – Equations describing Process 3.

Series	Equation	R^2
Synthetic Layers S1	$m = 659.91 - 12.518d$	0.9974
Synthetic Layers S2	$m = 537.19 - 10.912d$	0.9985

and the adsorption of evaporated water to the substrate layer. However, the rate of evaporative losses from whole systems S1 and S2 was approximately 0.37 mm/day; the synthetic layers could only replenish the substrate at approximately one-third the rate at which water was lost to the atmosphere from the surface of the substrate. This resulted in a net mean daily loss of 0.25 mm/day for the substrates in systems S1 and S2. For comparison, the mean daily rate of loss from the substrates in systems E1 and E2 was 0.3 mm/day.

This experiment did not appear to show any relation between the rate of moisture fluxes and the three main factors that were hypothesized to affect them (temperature, humidity and solar radiation), as rates of all processes were found to be linear. However, this may have been a consequence of the time-scale of the monitoring regime. It is possible that with continuous monitoring, variations relating to temperature, humidity and solar radiation would become apparent, these variations still smoothing to a linear trend over a period of days.

A.4 Recommendations for Further Work

A.4.1 Recommendations for Experimental Design

The substrate in this experiment was pre-conditioned to the atmospheric conditions of Norton Nursery over the course of a week. However, it was clear when filling the substrate baskets that a moisture gradient still existed within the sample. As a result, moisture was lost from systems E1 and E2 over the course of the experiment, during which time ambient conditions did not vary significantly. It was decided that any future pre-conditioning regimes would require the substrate to be spread to a thinner depth and, if necessary, given more time for equilibration.

As the interface between the substrate basket and air gap below the substrate was, by area, almost one-quarter metal, it was considered possible that this may have been a restriction to the adsorption of moisture on the filter sheet. Additionally, there were concerns that the continuous filter sheet running from the base to the top of the substrate basket, coupled with a 2 mm gap all around to allow for easy removal, may have provided a preferential pathway for evaporation. To address these problems, the box and substrate basket were redesigned. The sides of the substrate holder were proposed to be produced from the same plastic as the system box; a layer of filter sheet would be glued to the ends of the plastic panels, forming the bottom of the basket. The inside of the system box would be stepped: a double wall thickness would be used lower in the system build up, creating a shelf just above the top of the drainage component, on which the plastic sides of the substrate holder would sit, sandwiching the filter sheet between the shelf and the base of the substrate holder. The drainage layer pushing against the filter sheet would help maintain the shape of the substrate, as it does in an installed green roof. This re-designed system box is shown in Figure A.9, where it is coupled to a redesigned monitoring system. A white
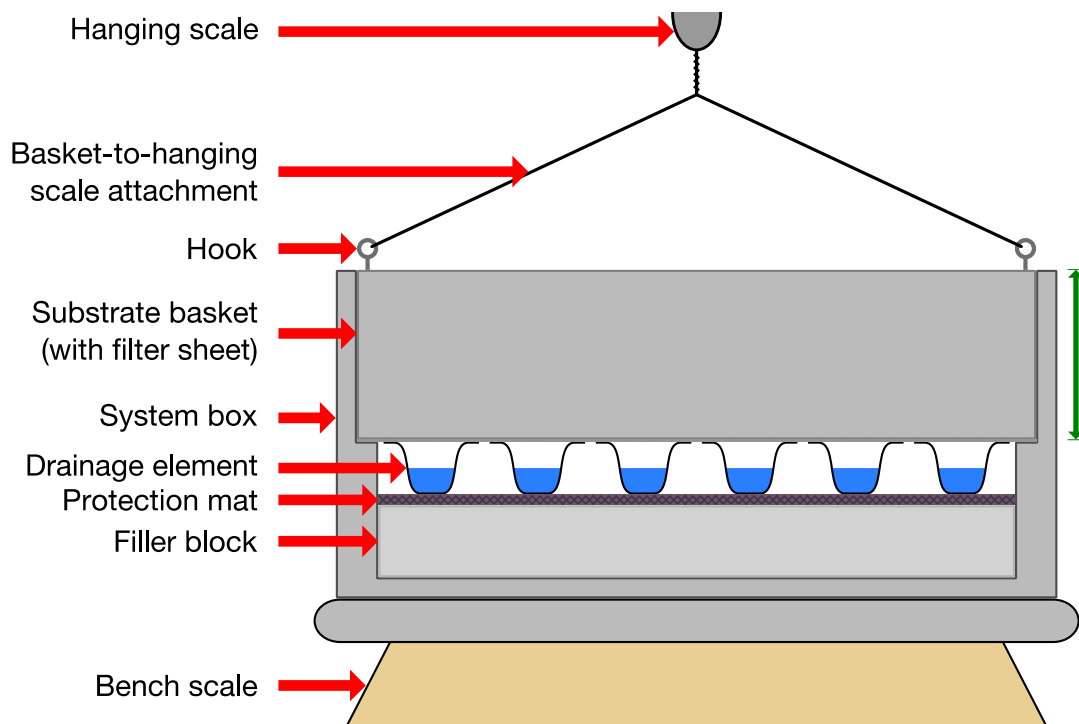
Figure A.9 – Redesigned system box and monitoring setup.

plastic was intended to be used for the system box and substrate holder, to prevent the green roof system housing from absorbing heat and re-emitting it into the test green roof system.

The greenhouse at Norton Nursery was initially believed to be temperature and humidity controlled, but was later found out to be neither. Though the rates of the measured processes appeared to be linear, it is entirely possible that this was the consequence of an infrequent monitoring regime, over which random variations in temperature, incident solar radiation and atmospheric humidity would have occurred between two measurement samples, which were spaced four days apart on average. Using a climate chamber, all three of these variables could be specified and controlled, reducing climatic uncertainties to near-zero and allowing comparisons of process rates to be made between otherwise identical systems in different climates.

In addition to controlling climatic variables, it would be extremely advantageous to increase the frequency of the monitoring regime. The first experiment was monitored more frequently, every weekday, but following the conclusion of the second experiment, a continuous monitoring system was designed. This made use of a hanging scale in addition to a bench scale. Figure A.9 shows this new experimental setup, which has a further advantage over manual weighing: as the boxes are never handled during the experiment, they remain perfectly horizontal throughout. It was believed that, during the first and second experiments, water was transferred from the drainage layer to the protection mat as a result of the system boxes not being kept perfectly horizontal during transport to and from the scale. In order to utilize a continuous monitoring

system, bench and hanging scales with a finer resolution than the bench scale used in the first and second experiments would be required, as the mass change of any monitored component over an hour is much smaller than the mass change of the same component over one or four days.

A.4.2   Possible Recommendations for Future Experiments

Although it is unlikely that further significant resources will be committed, some opportunities for subsequent research were identified while it was still envisioned that a full research programme would be developed and at least partly implemented.

The experiments previously conducted had started with the synthetic layers either both empty or both at maximum capacity. While these experiments were useful for determining the availability of water during dry weather periods, it was impossible to separate the moisture flux from the drainage layer and the moisture flux from the protection mat. There was therefore no way of knowing if the provision of water to the substrate was primarily due to one component or the other. It was proposed that future experiments should be conducted to separately quantify the moisture fluxes resulting from Processes 1 and 2. This would be achieved by comparing two otherwise identical system configurations, one with an initially saturated moisture mat and dry drainage layer, the other with an initially full drainage layer and dry protection mat. Hence, either Process 1 or 2, but not both, would be possible and monitored (via Process 3) in each system configuration.

As real green roof systems are built with a variety of substrate depths and compositions, it was intended for future experiments to investigate the effects of these variables on moisture fluxes occurring within and out of green roof systems. To successfully test different depths of substrate, one design of system box and substrate holder would be required for each depth to be tested; the dimension marked by a green arrow on Figure A.9 would always need to equal the substrate depth.

In order to complete a comprehensive programme in a reasonable timeframe, separating Processes 1 and 2 while also exploring the effects of substrate depth, substrate composition, drainage components and climatic factors, many duplicate sets of experimental equipment would be required, greatly increasing the cost and complexity of performing these experiments. To simultaneously investigate three substrate depths, three substrate mixes and three combinations of drainage layer and protection mat, separating Processes 1 and 2, in one climate, would require 162 systems to be set up for triplicate tests of each configuration. It is likely that two months would be required for all activity in each climate to stop. Hence, it would be both extremely labour-intensive and costly to complete a comprehensive experimental programme of the type speculated upon here.

A.5 Conclusions

Two experiments were performed to attempt to quantify the processes that would recharge the water storage capacity of the synthetic layers (i.e. drainage layer and/or protection mat) in a green roof during dry weather periods. The results and observations made during the first experiment were used to inform improvements in the design of the second experiment. The second experiment found the rate of moisture flux from the synthetic layers to the substrate to be approximately 0.12-0.14 mm/day in the absence of plants. However, it was concluded that the design of the second experiment was too imprecise to provide definitive, repeatable results to quantify these rates. A greatly improved experimental design was developed for a third experiment, theoretically eliminating all deficiencies that had been encountered in the two previous experiments. Due to the changed priorities of both this thesis and the wider green roof project, and the cost and labour involved in performing a comprehensive experimental programme, the author did not procure the new equipment required for this experiment. It is noted in Section A.1 that work has been conducted by ZinCo, aimed at quantifying evapotranspiration rates of green roof systems, including plants. This work did not involve the thesis author, and so discussion of it is outside the scope of this thesis. In the absence of further discussion, it is concluded from the two experiments discussed in this appendix that all upward flux processes are ignored when runoff response of a green roof is modelled during a rainfall event and that existing evapotranspiration calculations are used to determine the storage recharge rate of the green roof system as a whole between storms, and during long dry periods within storms.

A.6 References

Alumasc (2012a). Alumasc Waterproofing | Product Datasheets (Online). Alumasc Exterior Building Products Ltd, St. Helens, UK. Available from: http://www.alumascwaterproofing .co.uk/downloads/product-datasheets (accessed 19th July 2012).

Alumasc (2012b). Product Data Sheet. Substrate "Heather with Lavender" (Online). Alumasc Exterior Building Products Ltd, St. Helens, UK. Available from: http://www.alumascwaterproofing.co.uk/media/68072/pd-zinco-substrate-heatherlavender .pdf (accessed 1st August 2012).

FLL (2008). *Guidelines for the Planning, Execution and Upkeep of Green-roof sites.* Forschungsgesellschaft Landschaftsentwicklung Landschaftsbau e.V., Bonn, Germany.

Miller C (2003). How to assess retention/drainage sheets. (Online). Roofscapes, Inc., Philadelphia, PA. Available from: http://www.roofmeadow.com/wp-content/uploads/How _to_Assess_Retention_Drainage_Sheets.pdf (accessed 17th July 2012).

Appendix B: Example Matlab Code

The programs given below are provided as "examples" of the Matlab code used in the analysis sections of this thesis. The function of the example code is identical to the function of the code actually used. However, the examples given below contain explanatory comments not present in the code employed in this thesis. In addition, most variables in the example code have been given more logical names that aid in understanding the function of the code.

The command "textread" is used in various example codes to read data from individual test records into column vectors of time, rain and runoff. This command is valid as of Matlab 7.12.0 (R2011a), but is scheduled for removal in a future release, according to the warning bar in Matlab's editor window. To continue to load test data after the "textread" command is removed, a replacement code construct employing the command "textscan" will be required.

List of Example Codes

B.1 Optimization_Storage.m – code to call *lsqcurvefit* to find optimal values of *a*, *b* and *delay* for nonlinear storage routing.

B.2 Storoute.m – nonlinear storage routing function, called by *lsqcurvefit* from within B.1.

B.3 Optimization_Storage_b.m – adaptation of B.1 for specified values of *a*.

B.4 Storoute_b.m – adaptation of B.2 for specified values of *a*.

B.5 Optimization_Musk.m – code to call *lsqcurvefit* to find optimal values of *K*, *x* and *delay* for Muskingum routing.

B.6 Musk.m – Muskingum routing function, called by *lsqcurvefit* from within B.5.

B.7 Systemroute.m – nonlinear storage routing model comprising a substrate reservoir in series with a drainage layer reservoir, receiving parameter values from an external source.

B.8 Profiler.m – code to redistribute total rainfall into net rainfall depth (equal to runoff depth) permanent retention and evaporative losses.

B.1   Optimization_Storage.m

```
tic                                               %Start timer

max_delay = 81;
no_of_tests = 300;
global vd                                         %Allow vd (variable delay)
                                                  %to pass to Storoute
Locala = zeros(max_delay,1);                       %Pre-allocate memory space
Localb = zeros(max_delay,1);
LocalRt2 = zeros(max_delay,1);
loc = zeros(300,1);
a = zeros(300,1);
b = zeros(300,1);
delay = zeros(300,1);
Rt2 = zeros(300,1);
test_time = zeros(300,1);

%Loop to sequentially process all records
for test_no = 1:no_of_tests

    FileName = ['TEST' int2str(test_no) '.txt'];        %Open test data
    [time,rain,runoff] = textread(FileName, '%f %f %f'); %Read    data    into    three
vectors

    lb = [0.00001, 1];                                %Lower bounding values
    ub = [1, 6];                                      %Upper bounding values
    options = optimset('MaxFunEvals', 50000, 'MaxIter', 2000,'Display','off');

    %Optimize a and b for vd (variable delay) from 0 to max_delay-1
    for vd = 1:max_delay
        Params = [0.01;2.5];                          %Starting estimates
        [OptParams,resnorm]                                                    =
lsqcurvefit(@Storoute,Params,rain,runoff,lb,ub,options);
        Params = [OptParams(1);OptParams(2)];
        RoutedRunoff = Storoute(Params,rain);
        Locala(vd) = OptParams(1);
        Localb(vd) = OptParams(2);
        LocalRt2(vd) = 1 - sum((RoutedRunoff-runoff).^2/sum(runoff.^2));
    end

    loc(test_no) = find(LocalRt2 == max(LocalRt2));
    a(test_no) = Locala(loc(test_no));
    b(test_no) = Localb(loc(test_no));
    delay(test_no) = loc(test_no) - 1;
    Rt2(test_no) = LocalRt2(loc(test_no));

    if test > 1                                       %Time for optimization
        test_time(test_no) = toc - sum(test_time(1:test_no-1));
    else
        test_time(test_no) = toc;
    end

    avg_time = toc/(test_no);
    est_rem = ((no_of_tests - test_no) * avg_time)/60;   %Estimate remaining time
    fprintf('Test  %d  finished.  Approximately  %0.1f  minutes  remain.\n',  test_no,
est_rem)
end

m=[a b delay Rt2 test_time];
dlmwrite('RESULTS_STOR.csv',m,'precision',10);        %Output results in file

toc                                                %Report total time
```

B.2 Storoute.m

```matlab
function F = Storoute(Params,rain)
global vd                                     %Receive vd from main code
a = Params(1);
b = Params(2);
d = vd - 1
h = zeros(size(rain,1),1);
RoutedRunoff = zeros(size(rain,1),1);
for row = d+1:size(rain,1)
    if(row>1)
        RoutedRunoff(row,1) = a * h(row-1,1)^b;
        h(row,1) = h(row-1,1) - RoutedRunoff(row,1) + rain(row-d,1);
    end
end
F = RoutedRunoff;
```

B.3 Optimization_Storage_b.m

```matlab
tic                                                     %Start timer

max_delay = 81;
no_of_tests = 300;
global vd a test                                        %Allow variables to pass
a = csvread('opt_a.csv');                               %Read a-values from file

Localb = zeros(max_delay,1);                            %Pre-allocate memory space
LocalRt2 = zeros(max_delay,1);
loc = zeros(300,1);
b = zeros(300,1);
delay = zeros(300,1);
Rt2 = zeros(300,1);
test_time = zeros(300,1);

%Loop to sequentially process all records
for test_no = 1:no_of_tests

    FileName = ['TEST' int2str(test_no) '.txt'];        %Open test data
    [time,rain,runoff] = textread(FileName, '%f %f %f'); %Read   data   into   three
vectors

    lb = [1];                                           %Lower bounding values
    ub = [6];                                           %Upper bounding values
    options = optimset('MaxFunEvals', 50000, 'MaxIter', 2000,'Display','off');

    %Optimize n for vd (variable delay) from 0 to max_delay-1
    for vd = 1:max_delay
        Params = [2.5];                                 %Starting estimate for b
        [OptParams,resnorm]                                                 =
lsqcurvefit(@Storoute_b,Params,rain,runoff,lb,ub,options);
        Params = [OptParams(1)];
        RoutedRunoff = Storoute_b(Params,rain);
        Localb(vd) = OptParams(1);
        LocalRt2(vd) = 1 - sum((RoutedRunoff-runoff).^2/sum(runoff.^2));
    end

    loc(test_no) = find(LocalRt2 == max(LocalRt2));
    b(test_no) = Localb(loc(test_no));
    delay(test_no) = loc(test_no) - 1;
    Rt2(test_no) = LocalRt2(loc(test_no));

    if test > 1                                         %Time for optimization
        test_time(test_no) = toc - sum(test_time(1:test_no-1));
    else
        test_time(test_no) = toc;
    end

    avg_time = toc/(test_no);
    est_rem = ((no_of_tests - test_no) * avg_time)/60;  %Estimate remaining time
    fprintf('Test %d finished. Approximately %0.1f minutes remain.\n', test_no,
est_rem)
end

m=[a b delay Rt2 test_time];
dlmwrite('RESULTS_STOR_b.csv',m,'precision',10);        %Output results in file

toc

                                                        %Report total time
```

B.4   Storoute_b.m

```matlab
function F = Storoute_b(Params,rain)
global vd a test                                    %Receive from main code
b = Params(1);
d = vd - 1
h = zeros(size(rain,1),1);
RoutedRunoff = zeros(size(rain,1),1);
for row = d+1:size(rain,1)
    if(row>1)
        RoutedRunoff(row,1) = a(test) * h(row-1,1)^b;
        h(row,1) = h(row-1,1) - RoutedRunoff(row,1) + rain(row-d,1);
    end
end
F = RoutedRunoff;
```

B.5 Optimization_Musk.m

```matlab
tic                                                 %Start timer

max_delay = 100;
no_of_tests = 300;
global vd                                           %Allow vd to pass to Musk

LocalK = zeros(max_delay,1);                        %Pre-allocate memory space
LocalX = zeros(max_delay,1);
LocalRt2 = zeros(max_delay,1);
loc = zeros(no_of_tests,1);
K = zeros(no_of_tests,1);
X = zeros(no_of_tests,1);
delay = zeros(no_of_tests,1);
Rt2 = zeros(no_of_tests,1);
test_time = zeros(no_of_tests,1);

%Loop to sequentially process all records
for test_no = 1:no_of_tests

    FileName = ['TEST' int2str(test_no) '.txt'];        %Open test data
    [time,rain,runoff] = textread(FileName, '%f %f %f'); %Read   data   into   three
vectors

    lb = [0, 0];                                    %Lower bounding values
    ub = [Inf, 0.5];                                %Upper bounding values
    options = optimset('MaxFunEvals', 50000, 'MaxIter', 2000,'Display','off');

    %Optimize k and X for vd (variable delay) from 0 to max_delay-1
    for vd = 1:max_delay
        Params = [1;0];                                 %Starting estimates
        [OptParams,resnorm] = lsqcurvefit(@Musk,Params,rain,runoff,lb,ub,options);
        Params = [OptParams(1);OptParams(2)];
        RoutedRunoff = Musk(Params,rain);
        LocalRt2(vd) = 1 - sum((RoutedRunoff-runoff).^2/sum(runoff.^2));
        LocalK(vd) = OptParams(1);
        LocalX(vd) = OptParams(2);
    end

    loc(test_no) = find(LocalRt2 == max(LocalRt2));
    K(test_no) = LocalK(loc(test_no));
    X(test_no) = LocalX(loc(test_no));
    delay(test_no) = loc(test_no)-1;
    Rt2(test_no) = LocalRt2(dly2(test_no));

    if test > 1                                     %Time for optimization
        test_time(test_no) = toc - sum(test_time(1:test-1));
    else
        test_time(test_no) = toc;
    end

    avg_time = toc/test;
    est_rem = ((no_of_tests - test) * att)/60;          %Estimate remaining time
    fprintf('Test %d finished. Approximately %0.1f minutes remain.\n', test, est_rem)
end

m=[K X dly Rt2 test_time];
dlmwrite('RESULTS_MUSK.csv',m,'precision',10);          %Output results in file

toc                                                 %Report total time
```

B.6 Musk.m

```matlab
function F = Musk(Params,rain)
global vd                                    %Receive vd from main code
K = Params(1);
X = Params(2);
d = vd − 1;
RoutedRunoff = zeros(size(rain,1),1);
for row = d+2:(size(rain,1) - 1)
    if(row>1)
        RoutedRunoff(row,1) = (((1 - (2 * K * X)) * rain(row-d,1)) + ((1 + (2 * K *
X)) *
        rain(row-d-1,1)) + (((2 * K * (1 - X)) - 1) * RoutedRunoff(row-d-1,1))) / ((2
* K
        * (1 - X)) + 1);
    end
end
F = RoutedRunoff;
```

B.7   Systemroute.m

```matlab
tic                                                    %Start timer

ABDG = ('a_b_delay_values_growing_medium.csv');        %Read in a, b, delay values
for
aG = ABDG(:,1);                                        %growing medium
bG = ABDG(:,2);
dG = ABDG(:,3);

ABDD = ('a_b_delay_values_drainage_layer.csv');        %Read in a, b, delay values
for
aD = ABDD(:,1);                                        %drainage layer
bD = ABDD(:,2);
dD = ABDD(:,3);

no_of_tests = size(aG,1);

%Loop to sequentially process all records
for test_no = 1:no_of_tests

    FileName = ['TEST' int2str(test_no) '.txt'];        %Open test data
    [time,rain,runoff] = textread(FileName, '%f %f %f'); %Read   data   into   three
vectors
    RoutedInflow = zeros(size(rain,1),1);
    RoutedRunoff = zeros(size(rain,1),1);
    hG = zeros(size(rain,1),1);
    hD = zeros(size(rain,1),1);

     Growing medium model
    for row = dG+1:size(rain,1)
        if(row>1)
            RoutedInflow(row,1) = aG * h(row-1,1)^bG;
            hG(row,1) = hG(row-1,1) - RoutedInflow(row,1) + rain(row-dG,1);
        end
    end

    %Drainage layer model
    for row = dD+1:size(rain,1)
        if(row>1)
            RoutedRunoff(row,1) = aD * hD(row-1,1)^bD;
            hD(row,1) = hD(row-1,1) - RoutedRunoff(row,1) + RoutedInflow(row-dD,1);
        end
    end

    Rt2(test) = 1 – sum(RoutedRunoff-runoff).^2/sum(runoff.^2));

    if test > 1                                         %Time for optimization
        test_time(test_no) = toc - sum(test_time(1:test_no-1));
    else
        test_time(test_no) = toc;
    end

    avg_time = toc/(test_no);
    est_rem = ((no_of_tests - test_no) * avg_time)/60;   %Estimate remaining time
    fprintf('Test %d finished. Approximately %0.1f minutes remain.\n', test_no,
est_rem)
end

m=[Rt2 test_time];
dlmwrite('RESULTS_SYSTEM.csv',m,'precision',10);        %Output results in file

toc
                                                        %Report total time
```

B.8 Profiler.m

```matlab
daily_evap = csvread('daily_evap.csv');                %Read in daily evaporation rates
minute_evap = daily_evap/1440;
BP = 3;                                                 %Set "breakpoint" value to 3 mm
no_of_events = 24;

for event = 1:no_of_events

    FileName = ['TEST' int2str(test_no) '.txt'];        %Open test data
    [time,rain,runoff] = textread(FileName, '%f %f %f'); %Read data into three vectors
    evap_rate = minute_evap(event);
    dry_minutes = sum(rain == 0);
    total_evap = dry_minutes * evap_rate;
    init_stor = sum(rain) – (sum(runoff) + total_evap);
    stor = zeros(size(rain,1));

    rain(1)=0;
    reload_rain = rain;

    max_iterations = 500;
    error = zeros(iterations+1,1);
    exitflag = zeros(no_of_events,1);

    for repeat = 1:max_iterations

    rain = reload_rain;

    stor(1) = stor(1) + error(repeat)/2;                %Set initial storage capacity to
                                                        %previous initial capacity plus
        if stor(1) < 0                                  %half of cumulative error from
            stor(1) = 0;                                %previous iteration
        end                                             %Value must be positive

        for i=2:size(rain)
            if rain(i) == 0
                stor(i) = stor(i-1) + minute_evap;      %If no rain, evaporation
            elseif stor(i-1) > BP                       %else
                stor(i) = stor(i-1) - rain(i);          %All rainfall retained if storage
                rain(i) = 0;                            %capacity above "breakpoint"
            else                                        %else
                ramp = 1 - stor(i-1)/BP;                %Retention and runoff shared
                stor(i) = stor(i-1) - rain(i) * ramp;   %according to ramp function
                rain(i) = rain(i) * (1 - ramp);
            end
        end
        error(repeat+1) = sum(rain) - sum(runoff);
        if abs(error(repeat+1)) < 0.00001
            exitflag = 1;                               %Indicate that difference between
        end
                                                        %rainfall and runoff is below
        if exitflag == 1                                %threshold of 0.00001 mm and
            break                                       %stop iterating
        end
    end
end

%Write file with net rainfall in column 2 and total rainfall in column 4
m=[time rain runoff repeat_rain];
dlmwrite([int2str(event) '.csv'],m)
```

Appendix C: Adaptation of Nonlinear Storage Routing Equation for Manning's *n*

The Manning formula (Equation C.1) states that:

$$V = \frac{C}{n} R^{\frac{2}{3}} S^{\frac{1}{2}}$$

Equation C.1

Where V is cross-sectional average velocity, C is a conversion factor, n is Manning's n, R is hydraulic radius and S is channel slope.

Noting that, in a rectangular channel, the volumetric discharge rate, Q, is velocity multiplied by channel width multiplied by water height, $V \times W \times h$, and that for very wide channels, $R \approx h$ gives Equation C.2:

$$\frac{Q(t)}{Wh} = \frac{C}{n} h^{\frac{2}{3}} S^{\frac{1}{2}}$$

Equation C.2

Specifically for the drainage layer, the rate of discharge in units of depth per unit time, q, is equal to the volumetric rate, Q, divided by the plan area of the drainage layer, A. Substituting gives Equation C.3:

$$\frac{Aq(t)}{Wh} = \frac{C}{n} h^{\frac{2}{3}} S^{\frac{1}{2}}$$

Equation C.3

Re-arranging for q gives Equation C.4:

$$q(t) = \frac{CW}{An} h^{\frac{5}{3}} S^{\frac{1}{2}}$$

Equation C.4

Setting C to 1.49 and substituting into the continuity of volume equation, $dh/dt = i(t) - q(t)$, gives the governing equation of the SWMM RUNOFF module (James *et al.*, 2000), as used by She & Pang in their physically-based green roof model (She & Pang, 2010; see also Section 2.6.4.2 of this thesis)

The nonlinear head-discharge relationship used throughout Chapters 5, 6 and 7 is given in Equation C.5:

$$q(t) = ah^b$$

Equation C.5

Where a is the scale parameter and b is the exponent parameter. $q(t)$ is discharge, measured in mm per time unit (either seconds or minutes) and b is dimensionless, so a must take units of

mm^{1-n} per unit time. Substituting Equation C.5 into Equation C.4 with an exponent of 5/3 gives Equation C.6:

$$ah^{\frac{5}{3}} = \frac{CW}{An}h^{\frac{5}{3}}S_R^{\frac{1}{2}}$$

Equation C.6

By dividing through by $h^{5/3}$, a, which can be optimized by the existing *lsqcurvefit* routine, is alone on the left side of Equation C.6. The right side shows the physical interpretation of the optimized a-value. Re-arranging to solve for Manning's n gives Equation C.7:

$$n = \frac{CS_R^{\frac{1}{2}}}{aL}$$

Equation C.7

Where L (drainage length) is substituted for A/W.

In Equation C.1, the constant 1.49 has dimensions of ft$^{1/3}$s, which is equivalent to exactly 1 m$^{1/3}$s. For Manning's n to be dimensionless, C must take the dimension of mm$^{1/3}$ per unit time. As 1 m = 1000 mm and the time unit of a is always 1 (either second or minute), the value of C must be 10. Substituting 10 for the value of C gives Equation C.8. This is identical to the equation for Manning's n that is given as Equation 5.1 in Section 5.5.5.1:

$$n = \frac{10S_R^{\frac{1}{2}}}{aL}$$

Equation C.8

Where S_R is roof slope, a is the scale parameter optimized in *lsqcurvefit*, for nonlinear storage routing when the exponent is set to 5/3 and L is drainage length, in millimetres. If, for convenience, L is input to the equation in metres, the result must obviously be divided by 1000.

References

James W, Huber W C, Dickinson R E and James R C (2000). *Water Systems Models: Hydrology: Users Guide to SWMM4 Runoff and Supporting Modules*. Computational Hydraulics International, Guelph, Canada.

She N and Pang J (2010). Physically based green roof model. *Journal of Hydrologic Engineering* 15 (6), 458-464.